

Univerzitet u Beogradu
Fizički fakultet

Frakcioni kvantni Holov efekat u višekomponentnim sistemima

Zlatko PAPIĆ

doktorska teza

odbranjena na Univerzitetu u Beogradu, 23. septembra 2010. pred Komisijom

Dr. Zoran RADOVIĆ
Dr. Milan KNEŽEVIĆ
Dr. Milica MILOVANOVIĆ
Dr. Marc GABAY
Dr. Mark O. GOERBIG
Dr. Thors Hans HANSSON
Dr. Nicolas REGNAULT



Abstract

We study a number of fractional quantum Hall systems, such as quantum Hall bilayers, wide quantum wells or graphene, where underlying multicomponent degrees of freedom lead to the novel physical phenomena. In the quantum Hall bilayer at the filling factor $\nu = 1$ we study mixed composite boson-composite fermion trial wave functions in order to describe the disordering of the exciton superfluid as the bilayer distance is increased. We propose wave functions to describe the states of the bilayer for intermediate distances and examine their properties. At the bilayer total filling $\nu = 1/2$ and $\nu = 2/5$ we study the quantum phase transition between the multicomponent Halperin states and the polarized, Abelian and non-Abelian, phases as the tunneling term is varied. We use a combination of exact diagonalization and the effective BCS model to study the transitions. Furthermore we introduce a realistic model of the wide quantum well which is used to examine even-denominator quantum Hall states at $\nu = 1/2$ and $\nu = 1/4$ in the lowest Landau level. Finally, we explore some possibilities for the fractional quantum Hall effect in graphene based on the multicomponent picture of spin and valley degrees of freedom.

Apstrakt

U ovoj tezi proučavamo nekoliko primera frakcionog kvantnog Hall-ovog efekta, u sistemima kao što su kvantni Hall-ov dvosloj, široke kvantne jame i grafen, gde višekomponentni sistemi slobode dovode do novih fizičkih fenomena. U slučaju kvantnog Hall-ovog dvosloja na punjenju $\nu = 1$ proučavamo probne talasne funkcije koje opisuju mešavinu kompozitnih bozona i kompozitnih fermiona, sa ciljem da opišemo razuredjenje ekscitonskog superfluida sa povećanjem rastojanja između slojeva. U slučaju dvosloja na punjenju $\nu = 1/2$ i $\nu = 2/5$, proučavamo kvantne fazne prelaze između višekomponentnih Halperin-ovih stanja i polarizovanih, abelijanskih i neabelijanskih, faza koje nastaju sa povećanjem tuneliranja. Prelazi su analizirani pomoću metoda egzaktno dijagonalizacije i efektivnog BCS modela. U nastavku je uveden realistični model za široku kvantnu jamu koji je iskorišćen za ispitivanje kvantnih Hall-ovih stanja sa parnim imeniocem na punjenju $\nu = 1/2$ i $\nu = 1/4$ u najnižem Landau-ovom nivou. Na kraju, ispitivane su mogućnosti za frakcioni kvantni Hall-ov efekat u grafenu na osnovu višekomponentnog opisa koji uključuje stepene slobode koju potiču od spina i rešetke.

Résumé

Nous étudions un certain nombre de manifestations de l'effet Hall quantique fractionnaire dans les bicouches d'effet Hall quantique, des puits quantiques larges ou le graphène, dans lesquels les degrés de liberté multicomposantes produisent des phénomènes physiques insolites. Dans la bicouche d'effet Hall quantique du remplissage total $\nu = 1$, nous examinons les fonctions d'onde mixtes des bosons composites et fermions composites afin de décrire la destruction de la suprafluidité excitonique au fur et à mesure qu'on augmente la distance entre les deux couches. Nous proposons des fonctions d'onde d'essai qui décriraient bien l'état de la bicouche quand il s'agit de distances intermédiaires et nous y étudions leurs propriétés. Dans la bicouche d'effet Hall quantique du remplissage total $\nu = 1/2$ et $\nu = 2/5$, nous étudions la transition de phase quantique entre les états multicomposantes de Halperin et les phases polarisées (abeliennes et non-abeliennes) en fonction des modifications effectuées dans le terme tunnel. Afin d'étudier les transitions, nous utilisons à la fois la diagonalisation exacte et la théorie effective BCS. Nous présentons d'autre part un modèle réaliste du puits quantique large que nous utilisons dans l'examen des états avec un dénominateur pair, à $\nu = 1/2$ et $\nu = 1/4$ dans le plus bas niveau de Landau. Nous proposons enfin quelques états d'effet Hall quantique fractionnaire possibles dans le graphène, celles-ci reposant sur l'image multicomposante qui concerne les degrés de liberté de spin et de vallée.

Acknowledgements

The work presented here began at the Scientific Computing Laboratory in Belgrade, under the supervision of Milica Milovanović. I thank her for the patient guidance throughout the years of my thesis, for being always attentive to my evolving research interests and available to discuss physics. I consider myself fortunate that she gave me the chance to work in the quantum Hall effect, the field I had discovered as an undergraduate student at the Weizmann Institute doing my internship with Moty Heiblum, to whom I am thankful for the best possible introduction to the quantum Hall effect that a theoretician can hope for: through the dirty and complicated experimental work.

I am furthermore indebted to Milica for having the foresight to realize my difficulty in learning the numerical tools necessary for the topic I was working on and sharing her advisorship over my PhD with Mark Goerbig at the Laboratoire de Physique des Solides in Orsay, and Nicolas Regnault at the Laboratoire Pierre Aigrain at Ecole Normale Supérieure in Paris. I feel enriched by having had the possibility of working with all of these three great physicists (whom I equally consider my advisors, should I ever need to quantify that), despite the fact that the numbers of our exchanged emails could be daunting at times. I also relish the fact that I've experienced a new country and a new culture without having to abandon the place I came from.

I would like to thank Mark for being calm and authoritative when it was needed, for being always there for practical issues, discussing physics and doing all that with a unique zest of hedonism. I thank Nicolas for teaching me nearly everything about exact diagonalization and numerics in general - with a light touch!, running some of my codes on his cluster and doing some calculations instead of me ;-), as well as showing me how to be a practical physicist-theoretician.

During the course of my PhD, I attended several great workshops at ICTP Trieste, SFK conference in Vršac, Max Planck institute for complex systems, KITP in Santa Barbara and Nordita in Stockholm, where certain collaborations were initiated. I would like to especially thank Bogdan Andrei Bernevig for countless discussions and inspiration by his inimitable way of doing physics in every situation imaginable. I also thank Sankar Das Sarma for our joint work on wide quantum well problems. I have furthermore benefitted a great deal from discussing numerics with Karel Vyborny and Thierry Jolicoeur.

I thank the Scientific Computing Laboratory, Laboratoire de Physique des Solides and Laboratoire Pierre Aigrain for their hospitality and all the colleagues for making the work and leisure time enjoyable and fun. A personal note of gratitude goes to Aleksandar Belić for his continuous support as the head of SCL, as well as to Hans Hansson and Steve Simon for their proofreading of the manuscript.

This work has been supported in part by the fellowship of the Serbian Ministry of science, the Marie Curie scholarship for early stage research training in Orsay, the CNRS fellowship and the fund of Région Ile-de-France for “cotutelle” programs.

Finally, I would like to dedicate this thesis to my family and dear friends whose support during the last years enabled me to reach this point.

Zlatko Papić



Contents

Nomenclature	ix
Foreword	xv
1 Introduction	1
1.1 Fractional quantum Hall effect	1
1.2 Polarized electrons in the lowest Landau level	5
1.2.1 Laughlin's wave function	6
1.2.2 Effective field theories	7
1.2.3 Composite fermions	9
1.2.4 Compressible state $\nu = 1/2$	9
1.3 Second Landau level	10
1.3.1 The $\nu = 5/2$ state	10
1.3.2 Conformal field theory approach	12
1.4 Multicomponent quantum Hall systems	13
1.4.1 Wide quantum wells	14
1.4.2 Quantum Hall bilayer	14
1.5 Multicomponent systems studied in this thesis	15
1.5.1 Quantum Hall bilayer at $\nu = 1$	15
1.5.2 $\nu = 1/2$	18
1.5.3 $\nu = 2/5$	19
1.5.4 $\nu = 1/4$	20
1.5.5 Graphene	22
2 Numerical studies of the FQHE	25
2.1 Exact diagonalization: Sphere	25
2.1.1 Example: Effect of finite thickness on the Laughlin $\nu = 1/3$ state	27
2.1.2 Entanglement spectrum on the sphere	28
2.1.3 Example: Multicomponent states in the $\nu = 1/4$ bilayer	29
2.2 Exact diagonalization: Torus	30
2.2.1 Example: Abelian vs. non-Abelian states on the torus	32
2.2.2 Example: Torus degeneracy of the 331 multicomponent state	33

2.3	Summary	35
3	Quantum disordering of the quantum Hall bilayer at $\nu = 1$	37
3.1	Chern-Simons theory for the Halperin 111 state	37
3.2	Trial wave functions for the quantum Hall bilayer	40
3.3	Basic response of trial wave functions	42
3.4	Chern-Simons theory for the mixed states	43
3.4.1	Case Ψ_1	43
3.4.2	Case Ψ_2	45
3.4.3	Generalized states	47
3.5	Possibility for a paired intermediate phase in the bilayer	47
3.5.1	First-order corrections to the 111 state	48
3.5.2	Discussion	50
3.5.3	Numerical results	50
3.6	Conclusion	52
4	Transitions between two-component and non-Abelian states in bilayers with tunneling	55
4.1	Transition between 331 Halperin state and the Moore-Read Pfaffian	55
4.1.1	BCS model for half-filled Landau level	56
4.1.2	Exact diagonalization	57
4.1.3	Pfaffian signatures for intermediate tunneling and a proposal for the phase diagram	61
4.1.4	Generalized tunneling constraint	63
4.2	Transition from 332 Halperin to Jain's state at $\nu = 2/5$	65
4.2.1	The system under consideration	65
4.2.2	Exact diagonalizations	66
4.2.3	Intepretation of the results within an effective bosonic model	68
4.3	Conclusions	71
5	Wide quantum wells	73
5.1	Finite thickness and phase transitions between compressible and incompressible states	73
5.2	Two-subband model of the quantum well	78
5.2.1	Connection between the quantum-well model and the bilayer	78
5.3	$\nu = 1/2$ in a quantum well	83
5.4	$\nu = 1/4$ in a quantum well	85
5.5	Conclusion	86
6	Graphene as a multicomponent FQH system	89
6.1	Interaction model for graphene in a strong magnetic field	89
6.1.1	SU(4) symmetry	91

6.1.2	Effective interaction potential and pseudopotentials	92
6.2	Multicomponent trial wave functions for graphene	93
6.2.1	$[m; m, m]$ wave functions	93
6.2.2	$\nu_G = 1/3$ state in graphene	94
6.2.3	$[m; m - 1, m]$ wave functions	95
6.2.4	$[m; m - 1, m - 1]$ wave functions	96
6.3	Conclusions	97
7	Outlook	99
A	DiagHam	101
	References	113

Nomenclature

$-e$ electron charge
 B magnetic field
CF composite fermion
CB composite boson
GS ground state
WF wave function
RPA random phase approximation
ODLRO off-diagonal long-range order
QPT quantum phase transition
(L)LL (lowest) Landau level
 $\hbar\omega_c$ cyclotron energy
FQHE fractional quantum Hall effect
IQHE integer quantum Hall effect
 \mathbf{k} wave vector
 $l_B = \sqrt{\hbar c/eB}$ magnetic length
 L angular momentum
 m_e electron mass
 m_b band mass ($m_b = 0.067m_e$ for GaAs)
 N number of electrons
 N_ϕ number of flux quanta
 ν filling factor
 ϕ_0 flux quantum ($\phi_0 = hc/e$)
 \mathcal{P}_{LLL} projection to the LLL
 R_H, R_{xy} transversal (Hall) resistance
 R_L, R_{xx} longitudinal resistance
 $R_K = h/e^2 = 25813.807\Omega$ unit of resistance
2DEG two-dimensional electron gas
 $z = x - iy$ position in the plane
 Δ_{SAS} tunneling amplitude or the splitting between the symmetric and antisymmetric subband
 $\Delta\rho$ density imbalance in the quantum well
 d distance between the layers
 w width of the quantum well
 a/b aspect ratio of the torus

List of Figures

1.1	Archetype of a quantum Hall experiment: the sample is in a perpendicular magnetic field B while the current I is driven through it. The response of the system is characterized by the longitudinal $R_L \equiv V_L/I$ and the Hall resistance $R_H \equiv V_H/I$.	1
1.2	GaAs heterostructure	2
1.3	Integer and fractional quantum Hall effect. [1]	2
1.4	Quantum well with the two lowest subbands	5
1.5	Chern-Simons transformation to composite bosons	7
1.6	FQHE in the second Landau level. [2]	10
1.7	Quantum Hall bilayer: two decoupled layers for large d (left) and the quantum coherent state for small d (right).	15
1.8	Quantum Hall effect at $\nu = 1$. [3]	15
1.9	Tunneling conductance dI/dV as a function of the interlayer bias voltage at total filling of $\nu = 1$ for several values of d/l_B . [4]	17
1.10	R_{xx} and R_{xy} for the bilayer $\nu = 1$ system at $T = 50\text{mK}$, in the parallel configuration when the currents are flowing in the same direction in both layers (upper panel) and the counterflow configuration with the two layers contacted individually (lower panel). The distance between the layers is $d/l_B = 1.58$. [5]	18
1.11	Coulomb drag resistances at $T = 30\text{mK}$ in the vicinity of $\nu = 1$ for various d/l_B . [6]	19
1.12	Quantum Hall effect at $\nu = 1/2$ in the wide quantum well. [7]	20
1.13	Quantum Hall effect at $\nu = 1/4$ in the presence of parallel magnetic field. [8]	21
1.14	Quantum Hall effect at $\nu = 1/2$ and $\nu = 1/4$ under density imbalance. [9]	21
1.15	Energy bands of graphene.	22
2.1	Overlap $ \langle \Psi_L \Psi_{\text{exact}} \rangle $ between the exact Coulomb state for finite width (ZDS model) at $\nu = 1/3$ and the Laughlin wave function $N = 4 - 12$ particles. [10] Inset: same quantity but in the first excited Landau level i.e. $\nu = 7/3$.	28
2.2	Entanglement spectrum for $N = 20$ electrons on the sphere, Coulomb interaction at the filling factor $\nu = 5/2$. The block A consists of $N_A = 10$ electrons and $l_A = 19$ orbitals, corresponding to the cut [0]0 in Ref. [11].	29
2.3	Overlap between the exact bilayer state with 553 and 771 states for $N = 8$ particles on the sphere. [12]	30
2.4	Low-energy part of the spectrum of the Coulomb interaction on the torus for $N = 10$ electrons at $\nu = 1/3$ and the aspect ratio 0.99. Energies are shown relative to the ground state and, for comparison, we also show the lowest states of the hard-core V_1 potential (2.7).	32

LIST OF FIGURES

2.5	Low-energy part of the spectrum of the three-body Hamiltonian (1.41) on the torus for $N = 12$ electrons at $\nu = 1/2$ and aspect ratio 0.99. The three degenerate zero-energy states are characterized by $\mathbf{k} = (0, N'/2), (N'/2, 0)$ and $(N'/2, N'/2)$.	33
2.6	Energy spectrum of $N = 14$ electrons on the torus at $\nu = 1/2$ (left) and $\nu = 5/2$ (right), for the aspect ratio of 0.99	34
2.7	Quantum Hall bilayer at the filling factor $\nu = 1/2$ on the torus as a function of distance d (negligible tunneling). The energy spectrum for $N = 8$ electrons at the aspect ratio 0.99 is plotted relative to the ground state at each d and the states belonging to relevant momentum sectors are highlighted and connected as a guide to the eye.	35
3.1	Universality classes of the wave functions Ψ_1 (a) and Ψ_2 (b), together with their paired versions, (c) and (d), respectively.	40
3.2	Real part of the pseudospin channel density-density correlation [13] and the Goldstone mode in the case of Ψ_1	45
3.3	Real part of the pseudospin channel density-density correlation [13] in the case of Ψ_2	46
3.4	QH bilayer $\nu = 1$ on the torus, $N = 16, a/b = 0.99$	51
3.5	Ground state energies on the sphere for the QH bilayer at the shift of $\delta = 1$ and 2. We show the system of $N = 8$ (which has a filled CF shell in each layer) and the largest system with $N = 16$ electrons (without filled CF shells). Similar results are obtained for other system sizes.	52
3.6	Critical bilayer distance d_C defined as the crossing point of the ground-state energies at shifts $\delta = 1$ and $\delta = 2$ on the sphere. Linear extrapolation for $N \rightarrow \infty$ yields $d_C \approx 1.6l_B$ and does not involve the smallest system $N = 8$ which shows strong finite-size effects.	52
4.1	Overlaps between the exact ground state of the Coulomb bilayer (left panel) and short range 331 Hamiltonian (right panel) with the 331 state (O_{331}) and the Pfaffian (O_{Pf}), as a function of tunneling Δ_{SAS} . Also shown on the right axis is the expectation value of the S_x component of pseudospin (for $N = 8$ system) which characterizes the two-component to one-component transition.	58
4.2	Ground state energy for $N = 8$ and $N = 10$ electrons on the sphere, $d = l_B$, for shifts of 2 and 3.	59
4.3	Low-energy part of the spectrum (relative to the ground state) of the short-range 331 (left panel) and the long-range Coulomb Hamiltonian (right panel) for $N = 8$ electrons on the torus at $\nu = 1/2$ and aspect ratio $a/b = 0.97$ as a function of tunneling Δ_{SAS} (right axis). Also shown (left axis) is the overlap with the phases we identify as the 331 state and the CFL.	60
4.4	Spectrum of the $N = 14$ electrons in a single layer at $\nu = 1/2$ interacting with $V^+(r)$ ($d = l_B$), as a function of aspect ratio. We highlight the states with quantum numbers of the Moore-Read Pfaffian.	61
4.5	Possible outcomes of tunneling on a twocomponent system such as the direct transition to a Fermi liquid (as expected for the short range interaction on the sphere) or to a critical Moore-Read Pfaffian for long range (Coulomb) interaction, in the context of phase diagram after Read and Green. [14] Note that the value for $\mu_F \sim 1/m^*$ is interaction-dependent due to the renormalized CF mass m^* and we may have different dividing lines $\mu = \mu_F$ depending on the kind of the interaction. [15]	61

4.6	Overlaps between the exact ground state of $N = 10$ electrons on the sphere with the 331 state (O_{331}) and the Pfaffian (O_{Pf}), as a function of tunneling Δ_{SAS} , for the Coulomb bilayer Hamiltonian and $d = 0.4l_B$	62
4.7	Low-energy part of the spectrum (relative to the ground state) of the Coulomb Hamiltonian (with $d = l_B$) for $N = 8$ electrons on the torus at $\nu = 1/2$ and $\Delta_{SAS} = 0.03e^2/\epsilon l_B$, as a function of the aspect ratio. Shaded region represents the tentative phase with the Pfaffian degeneracy.	62
4.8	Generalized tunneling constraint: the decrease of the density of the system evolves the system along the horizontal line in the phase diagram of Read and Green [14] into the non-Abelian phase.	64
4.9	Overlaps between the exact Coulomb bilayer ground state for $d = l_B$ and the 332 (O_{332}) and Gaffnian state (O_{Gaff}), as a function of tunneling Δ_{SAS} . Data shown is for $N_e = 6$ and 8 electrons. Note that O_{332} and O_{Gaff} can not be directly compared due to the difference in shift between the 332 state and the Gaffnian.	66
4.10	Energy spectrum of the SU(2)-symmetric 332 Hamiltonian on torus (in arbitrary units) for $N_e = 8$ and aspect ratio 0.97. The $\mathbf{k} = 0$ levels that cross define regions of fully polarized $\langle S_x \rangle = N/2$ and unpolarized $\langle S_x \rangle = 0$ phases.	67
4.11	Energy spectrum relative to the ground state of the Coulomb bilayer on torus, for $N_e = 8$ electrons, $d = l_B$ and aspect ratio 0.97. An approximate doublet of states with $\mathbf{k} = (0, 0)$ Haldane pseudomomenta is formed around the transition point $\Delta_{SAS} \approx 0.018e^2/\epsilon l_B$	68
4.12	Polarization $N/2 - \langle S_x \rangle$ as a function of tunneling around the transition point for the system of Fig. 4.11.	69
4.13	Energy spectrum of the Coulomb bilayer on torus (in arbitrary units) for $N_e = 8$ and aspect ratio 0.5.	69
5.1	Comparison of the few largest pseudopotentials (normalized by $V_0(w)$) for the Zhang-Das Sarma (ZDS) interaction and those for the infinite square well model (ISQW).	74
5.2	Overlap $ \langle \Psi_{\text{Pf}} \Psi_{\text{exact}} \rangle $ between the exact ZDS ground state for finite width w/l_B at $\nu = 1/2$ and the Pfaffian for $N = 8 - 18$ particles. Inset: same quantity but in the first excited Landau level i.e. $\nu = 5/2$. Only non-aliased states are shown. Note: the critical width of the QPT increases with system size, however for the three available points and $N \rightarrow \infty$, it extrapolates to a value of $4l_B$	75
5.3	Overlap $ \langle \Psi_{\text{Pf}} \Psi_{\text{exact}} \rangle $ between the exact ZDS ground state for finite width w/l_B and the Pfaffian at $\nu = 1/4$	75
5.4	Overlap $ \langle \Psi_{\text{exact}}(w = 0) \Psi_{\text{exact}}(w) \rangle $ between the exact ZDS state for finite width w/l_B at $\nu = 1/2$ and the CF sea state defined to be exact Coulomb ground state for zero thickness. Red circles represent filled CF shells ($N = n^2, n = 3, 4$), blue triangles are the lowest excited states $\Delta N = N - n^2 = \pm 1$ and so on.	76
5.5	CF levels for $N = 8$ and $N = 9$	76
5.6	Entanglement spectrum of the exact ground state for $N = 18$ particles at $\nu = 1/2$ in the LLL, just before ($w/l_B = 0.8$) and after ($w/l_B = 1.0$) the QPT, and the spectrum of Moore-Read Pfaffian for comparison. Vertical axes show the quantity $\xi = -\log \lambda_A$, where λ_A are the eigenvalues of the reduced density matrix of the subsystem A which comprises of 8 particles and 15 orbitals, given as a function of angular momentum L_z^A . Data shown is only for the partitioning denoted by $[0 0]$ in Ref. [11], other sectors give a similar result.	77

LIST OF FIGURES

5.7	Ratio of the few strongest, inter and intra, bilayer pseudopotentials $V_m^{\text{inter}}/V_m^{\text{intra}}$ derived from an underlying quantum well model, as a function of width w . Note the saturation of the ratios for large widths w , illustrating the limit of validity of the quantum well model.	80
5.8	Densities of the single-particle states in the rotated frame, $ \pm\rangle$	81
5.9	Phase diagram in $\Delta\rho - \Delta_{SAS}$ space for the quantum well of $N = 8$ particles on the sphere, $w/l_B = 2.0$ (left) and $w/l_B = 4.0$ (right): overlaps between the exact ground state and Halperin 331 state (a), Moore-Read Pfaffian (b), and the mean value of S_x (c) and S_z (d) operator of pseudospin.	82
5.10	Phase diagram in $\Delta\rho - \Delta_{SAS}$ space for the quantum well of $N = 8$ particles on the sphere at $\nu = 1/2$ in the second LL and width $w/l_B = 4.0$: overlaps between the exact ground state and Halperin 331 state (a), Moore-Read Pfaffian (b), and the mean value of S_x (c) and S_z (d) operator of pseudospin.	83
5.11	Neutral gap for $N = 8$ electrons on the sphere at $\nu = 1/2$ in the LLL and imbalance set to $\Delta\rho = 0.1e^2/\epsilon l_B$, as a function of width w and tunneling Δ_{SAS}	84
5.12	Energy spectrum of the quantum well Hamiltonian (5.3) for $\Delta_{SAS} = \Delta\rho = 0$ and various widths of the well w in the torus geometry ($N = 8$ electrons at $\nu = 1/2$ and aspect ratio 0.97).	84
5.13	Energy spectrum of the quantum well Hamiltonian (5.3) on the torus for $w = 4.0l_B, \Delta = 0.004e^2/\epsilon l_B$ as the imbalance is increased from zero ($N = 8$ electrons at $\nu = 1/2$ in the LLL and aspect ratio 0.97).	85
5.14	Overlap between the exact Coulomb state of the quantum well for $N = 8$ particles on the sphere at $\nu = 1/4$ with the 553 Halperin state (a), the Moore-Read Pfaffian (b) and Haldane-Rezayi (c) state. The expectation value of the S_z component of the pseudospin is plotted in (d).	85
5.15	Overlap between the exact Coulomb state of the quantum well for $N = 8$ particles on the sphere at $\nu = 1/4$ and $w/l_B = 10.5$ with the 553 Halperin state, the Moore-Read Pfaffian and Haldane-Rezayi states (left axis). The expectation value of the S_z component of the pseudospin is given on the right axis. The shaded region denotes where the ground state is no longer rotationally invariant ($L > 0$).	86
6.1	Pseudopotentials for graphene and the 2DEG in $n = 0$ (graphene and 2DEG, circles), $n = 1$ (graphene, squares), and $n = 1$ (2DEG, triangles). The energy is measured in units of $e^2/\epsilon l_B$. The lines are a guide to the eye.	92
6.2	Splitting of the single-particle $SU(4)$ energy levels in the presence of Zeeman field Δ_z , with the remaining $SU(2)$ degeneracy due to the valley index K	94
6.3	Energy spectrum for $N = 22$ electrons at the filling $\nu = 1 + 1/3$ as a function of Δ_z . We highlight the states belonging to particular S_z sectors for comparison.	95
6.4	Energy spectrum relative to the ground state for $N = 22$ electrons at the filling $\nu = 1 + 1/3$ as a function of angular momentum L and for the fixed $\Delta_z = 0.05e^2/\epsilon l_B$. We highlight the states belonging to the particular S_z sectors that define the lowest-lying spin-flip excitations. The magnetoroton branch is shown in green for $2S_z = 10$	95

Foreword

The subject of this thesis are strongly correlated phases in two-dimensional electron systems with an internal symmetry and in the conditions of strong magnetic fields and low temperatures i.e. in the setting of the fractional quantum Hall effect. Before we delve into details on why this field has generated such intense theoretical and experimental endeavours in the last decades (Chapter 1), we would like to state, in broad terms, our interest and motivation for this work in the general context of condensed matter physics.

Fractional quantum Hall effect (FQHE) has evolved in symbiosis with technological advances in the fabrication of the high quality semiconductor heterostructures which harbor the so-called two dimensional electron gases where electrons are characterized by very long mean free paths and mobilities reaching tens of millions cm^2/Vs at the time of writing. Such materials, when probed in the extreme quantum limit of low temperatures and high magnetic fields, give rise to new phases of matter: the topological quantum fluids. These phases of matter present a challenge for the standard paradigms of condensed matter physics. For example, their physics is determined by the Coulomb interaction which cannot be switched off in order to pursue a perturbational approach – there is no “normal” state because in the absence of the interaction the ground state is astronomically degenerate (which would, in itself, render any perturbative approach practically impossible). The gap in the energy spectrum arises as a result of strong correlations to yield a macroscopic quantum phenomenon that is quite distinct from Bose-Einstein condensation or BCS superconductivity. The underlying particles of the FQHE are believed to be the so-called composite fermions [16], which are the bound states of electrons and a discrete number of quantized vortices. Composite fermions are topological entities whose properties (such as mass) are generated solely by the interaction and not via Anderson-Higgs mechanism as in other fields of physics. In fact, FQH states lie completely beyond Landau theory which classifies phases of matter via their symmetries. Order parameters even for the simplest FQH states are non-local and they are better described by the so-called *topological order* [17].

Phases of matter characterized by topological order are insensitive to local perturbations and depend only on the global properties of the manifold on which they reside. In FQH systems, topological ground states emerge from the most basic condensed matter Hamiltonian – the Coulomb interaction between electrons. In the right circumstances, the topological invariance emerges as the symmetry of this Hamiltonian in the low-energy, long-distance limit. The macroscopic manifestation of this emergent symmetry is the quantization of perpendicular resistance R_{xy} and simultaneous vanishing of the longitudinal resistance R_{xx} (up to the exponential terms $\exp(-\Delta/2k_B T)$ that depend on the size of the gap Δ and temperature T).

Apart from their very special ground states, FQH fluids also display excitations with fascinating properties. One of those is the *fractional charge*: adding an electron to the strongly-correlated FQH state e.g. at the filling factor $\nu = 1/3$, will lead to the nucleation of three lumps of charges, $e/3$ each, as a result of strong correlations. Another unprecedented property of FQH excitations is their *anyonic* exchange statistics. In two dimensions, it is topologically allowed that the exchange of two quasiparticles results in the same wave function multiplied by a phase factor $e^{i\alpha}$, where α is neither 0 (bosons) nor π (fermions). Therefore, quasiparticles which control most of the observable properties of a physical system are fundamentally different in FQHE from those in

more common condensed matter systems such as metals, magnets or liquid helium, where they are either bosons or fermions. In fact, FQHE allows for even more exotic kinds of quasiparticles with the so-called *non-Abelian* exchange statistics. Suppose that a system has a g -degenerate ground-state multiplet $\Psi_a, a = 1, \dots, g$. This could be the so-called Moore-Read Pfaffian state at $\nu = 5/2$. [18] Exchanging two quasiparticles can lead to the initial state Ψ_a being mapped to a linear combination of some other states in the multiplet, so that the exchange operation is represented not by a phase, but by a matrix $\Psi_a \rightarrow M_{ab}\Psi_b$. A subsequent exchange would lead (in general) to a different matrix N and, because M and N do not necessarily commute, we refer to this process as the non-Abelian braiding of quasiparticles. If we have in mind the FQH state where the ground-state multiplet is topologically protected by the system's excitation gap, we can use the entangled state of the quasiparticles as a basis for a qubit and perform quantum operations by braiding the quasiparticles. This idea is inherently free of decoherence problems and could be a platform for fault-tolerant *topological quantum computation* [19, 20], the potential practical importance of FQHE. Although recent proposals for TQC (see [21] and references therein) seem more in favor of p -wave superconductors and topological insulators [22, 23], FQH systems remain one of the most important arenas for investigating exotic excitations and establishing non-Abelian statistics in nature.

If spin or some other internal quantum number of the electrons is not completely frozen out, we deal with the *multicomponent* FQH systems. [24] These include electrons with spin, bilayer structures where layer index assumes the role of the spin (Chapter 3 and 4), wide quantum wells (Chapter 5), or graphene (Chapter 6), where valley and spin indices combine into an $SU(4)$ -spin. The most important experimental ramification to date has been the observation of Bose-Einstein condensation of excitons in the $\nu = 1$ quantum Hall bilayer. [25] The exciton in a quantum Hall bilayer is formed by an electron in one layer and a hole opposite to it in the other layer. The idea of exciton condensation has a long tradition, but it has proved elusive in the era before the QH bilayer experiments. The importance of multicomponent degrees of freedom lies in that they allow the formation of FQH states at filling factors which are more difficult to describe or do not exist in polarized systems, such as $\nu = 1/2$. They are also related to the non-Abelian states – the latter can be viewed as the (anti)symmetrized versions of the former. This connection between non-Abelian and multicomponent states and the quantum phase transitions between them is a fundamental, open problem. Although the non-Abelian states in multicomponent systems are likely to be very fragile and not directly useful for applications such as topological quantum computation, the study of the multicomponent systems provides insight also into the polarized states as the two of them share many characteristics in the low-energy description. This is one of the goals of this thesis.

Chapter 1

Introduction

It is now almost thirty years since the discovery of transport phenomena that go under the name of integer [26, 27] and fractional [1, 28] quantum Hall effect. The field has much evolved since those pioneering days, which is also reflected in a number of excellent reviews that now exist on the subject [16, 29, 30, 31, 32, 33, 34, 35, 36]. In the present introduction we will summarize some of the ideas that have been developed in the physics of fractional quantum Hall effect (FQHE) in the past decades in order to pave the way towards the so-called multicomponent quantum Hall systems that are the main subject of this thesis.

1.1 Fractional quantum Hall effect

The Hall effect has long served as a standard tool to characterize the charge carriers in conductors and semiconductors: the motion of free (or more generally, Bloch) electrons in crossed electric and magnetic fields, such as in the setup of Fig. 1.1, leads to a voltage drop in the direction perpendicular to the injected current. Within a semiclassical treatment, this voltage drop is associated with the Hall resistivity ρ_H that depends linearly on the applied magnetic field B , as a simple consequence of Galilean invariance. [29, 30] Some systems, however, show remarkable

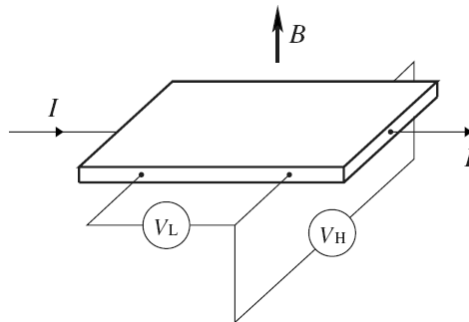


Figure 1.1: Archetype of a quantum Hall experiment: the sample is in a perpendicular magnetic field B while the current I is driven through it. The response of the system is characterized by the longitudinal $R_L \equiv V_L/I$ and the Hall resistance $R_H \equiv V_H/I$.

departure from this kind of behavior. Using molecular beam epitaxy (MBE) and band engineering, it is possible to design systems that effectively act as two-dimensional semiconducting

1. INTRODUCTION

planes, the so-called two-dimensional electron gases (2DEGs). This is conveniently achieved by growing in a controlled way one type of semiconductor, GaAs, over another ($\text{Al}_x\text{Ga}_{1-x}\text{As}$), Fig. 1.2. The choice of these compounds is dictated by their similar lattice constants, but at the same time slightly different band gaps. Upon doping, the electrons are captured on the atomically thin interface between the two sides of the heterostructure, thus effectively moving in two dimensions. In the extreme quantum limit, when magnetic field is strong ($\sim 10\text{T}$) and temperatures very low

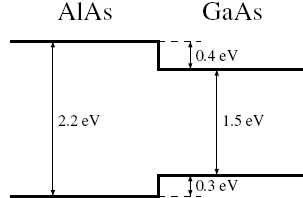


Figure 1.2: GaAs heterostructure

($\sim \text{mK}$), the response of the system is very different from the classical limit: Hall resistance R_H no longer varies smoothly as a function of the magnetic field but is locked around special values given by $R_H = h/\nu e^2$ where $R_K = h/e^2 = 25813.807\Omega$ is the fundamental unit of resistance and ν is an integer or simple fraction ($\nu = p/q$), quantized to an accuracy unprecedented in solid state physics. The law of quantization of R_H is universal, independent of the type of the sample, geometry and disorder. It also persists for a finite range of the control parameter (magnetic field or electron density) around special values – the quantum Hall plateaus. At the same time, in the region of a plateau, the longitudinal resistance displays activated transport $R_{xx} \sim \exp(-\frac{\Delta}{2k_B T})$ in the limit of zero temperature. Any discussion of the fractional quantum Hall effect should begin with the magnificent “skyline” such as the one of Fig. 1.3 [1] that shows the trace of R_H versus B and the consequent vanishing of R_{xx} . How does such an intricate, essentially exact and universal phenomenon arise in systems as different as GaN heterostructures, [37] strained Si quantum wells in Si-SiGe heterostructures [38], graphene [39, 40] or perhaps even organic metals [41]? To answer this question, we begin with the problem of a single nonrelativistic electron

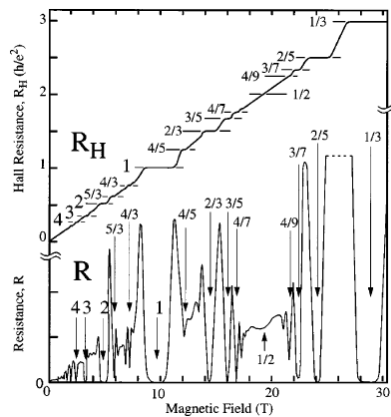


Figure 1.3: Integer and fractional quantum Hall effect. [1]

moving in two dimensions in a perpendicular uniform magnetic field $\nabla \times \mathbf{A} = B\hat{z}$ [42],

$$H = \frac{1}{2m_b} \left(\mathbf{p} + \frac{e\mathbf{A}}{c} \right)^2 \quad (1.1)$$

where m_b is the band mass of the electron ($0.067m_e$ in GaAs) and $-e$ is the charge. This is a standard textbook problem which can be solved in a gauge-invariant manner or by choosing a specific gauge for the vector potential \mathbf{A} . The popular choice for rotationally invariant problems is the symmetric gauge,

$$\mathbf{A} = \frac{1}{2}\mathbf{B} \times \mathbf{r}. \quad (1.2)$$

Here we choose the Landau gauge,

$$\mathbf{A} = (0, Bx, 0), \quad (1.3)$$

which directly casts the Hamiltonian (1.1) into a form analogous to the harmonic oscillator. We obtain the discrete energy spectrum

$$E_n = \left(n + \frac{1}{2} \right) \hbar\omega_c, \quad (1.4)$$

where the quantum number $n = 0, 1, \dots$ labels the equidistant Landau levels separated by the cyclotron energy $\hbar\omega_c = \hbar eB/m_b c$. The associated eigenvectors

$$\phi_{n,X}(\mathbf{r}) = [\pi 2^{2n} (n!)^2]^{-1/4} \exp [ik_y y - (x - k_y l_B^2)^2 / 2l_B^2] H_n [(x - k_y l_B^2) / l_B] \quad (1.5)$$

are expressed in terms of Hermite polynomials H_n and the characteristic *magnetic length*

$$l_B = \sqrt{\frac{\hbar c}{eB}}. \quad (1.6)$$

The eigenstates (1.5) are extended along the y -direction and localized around $k_y l_B^2$ in the x -direction. If we assume that the system is confined to a rectangular cell $L_x \times L_y$, then the periodic boundary condition requires $k_y = 2\pi j / L_y$, with j being an integer. Since the energy (1.4) does not depend on k_y , there is a number of degenerate states N_s inside each Landau level. We enumerate them by the number of allowed values for j that give orbitals localized in the interval $0 < k_y l_B^2 < L_x$ i.e.

$$N_s = \frac{L_x L_y}{2\pi l_B^2} = \frac{\Phi}{\Phi_0}. \quad (1.7)$$

In the above formula we have reexpressed N_s in terms of ratio of the magnetic flux through the system Φ to the flux quantum, $\Phi_0 = hc/e$, which leads us to the definition of the *filling factor* ν ,

$$\nu = \frac{N}{N_s} = 2\pi l_B^2 n, \quad (1.8)$$

as a function of the 2D electron density n . The filling factor ν is the single most important quantity that describes the 2DEG in the extreme quantum limit. First, we focus on the case when ν is an integer number. Due to the single particle spectrum (1.4), the density of states is a sequence of δ -functions with the weight N_s at the energies given by (1.4). This means that the zero-temperature chemical potential $\mu = \left(\frac{\partial E}{\partial N} \right)_B$ has discontinuities at integer filling factors and consequently the isothermal compressibility $\kappa^{-1} = \rho^2 \left(\frac{d\mu}{d\rho} \right)_T$ vanishes. At integer filling factors, compressing the system infinitesimally requires thus a finite amount of energy (sufficient to overcome the cyclotron gap). The incompressibility at integer ν and the vanishing of R_{xx} is a direct consequence of the Landau level structure. The observed plateaus in R_{xy} can

1. INTRODUCTION

be accounted for by disorder in real samples. Disorder modifies the spectrum in the manner that degenerate LL states broaden into bands. The single particle states near the unperturbed energies (1.4) form bands of *extended* states. [43] The extended bands are separated by localized states which do not contribute to the transport (this is called “mobility gap”) and thus the Hall plateaus may form.

Looking back at Fig. 1.3 we notice many cases with $\nu < 1$ that seem to yield the same experimental phenomenology as those with ν integer. If so, let us focus on the case $\nu < 1$ for the time being and ask what is the cause of incompressibility here. A simple combinatorial calculation of how many ways there are for placing N electrons on $N_s > N$ sites (N being a macroscopic number) yields a vast ground state degeneracy. As it was realized and proved in the early 1980s, it is the Coulomb repulsion between electrons that lifts this degeneracy and singles out a unique incompressible ground state for particular values of ν that is identified by the presence of a plateau in transport measurements and, more generally, the minimum in longitudinal resistance. These incompressible states have many intriguing properties that we will describe in more detail in the following Sections. All these properties can in principle be derived from the following master Hamiltonian of a quantum Hall system of N electrons in magnetic field \mathbf{B} :

$$H = \sum_i H_{\text{single}}(\mathbf{r}_i) + \frac{e^2}{\epsilon} \sum_{i < j} \frac{1}{|\mathbf{r}_i - \mathbf{r}_j|} + \sum_i U(\mathbf{r}_i) + g\mu\mathbf{B} \cdot \mathbf{S}. \quad (1.9)$$

The first term represents the single particle Hamiltonians (1.1), followed by two-body Coulomb interaction and one-body interaction with the positive background charges and the disorder, $\sum_i U(\mathbf{r}_i)$. The last term describes the coupling of total spin \mathbf{S} to the magnetic field. Hamiltonian (1.9) has the following typical energy scales for a GaAs heterostructure (Fig. 1.2). The single-particle energy scale is that of the cyclotron energy,

$$\hbar\omega_c \approx 20B [\text{T}] \text{ K}, \quad (1.10)$$

the Coulomb energy scales as

$$\frac{e^2}{\epsilon l_B} \approx 50\sqrt{B [\text{T}]} \text{ K}, \quad (1.11)$$

the Zeeman splitting is

$$2g\mu_B\mathbf{B} \cdot \mathbf{S} \approx 0.3B [\text{T}] \text{ K}, \quad (1.12)$$

with the unit of length being $l_B \approx 25/\sqrt{B [\text{T}]} \text{ nm}$ (1.6). For theoretical discussions, it is often convenient to work in “God’s units” for the FQHE:

$$l_B = 1, \quad \frac{e^2}{\epsilon l_B} = 1, \quad (1.13)$$

and those will be implicitly assumed in this thesis unless stated otherwise. Usually, a number of approximations is made on the Hamiltonian (1.9). We will switch off disorder because we are not interested in the physics of the plateaus, but only in the formation of incompressible states. Furthermore, we assume that the cyclotron energy (1.10) is large enough so that we do not need to explicitly treat more than a single Landau level. This assumption is actually incorrect in the experiments but most calculations would be impossible or very difficult to do without it. Furthermore, it is often customary to assume that the electron’s wave function is a δ -function in the perpendicular direction, so that the dynamics is strictly two-dimensional. This is of course just an approximation but there is no obvious way how the finite-width correction should be implemented. For a heterostructure such as the one in Fig. 1.2, the self-consistent potential experienced by the electrons can often be approximated by a triangular potential well. [44] Although this problem can be solved exactly [42], it is more enlightening to use the variational solution due to Fang and Howard,

$$\phi_{\text{FH}}(z) = \sqrt{\frac{27}{2w^3}} z e^{-3z/2w}, \quad (1.14)$$

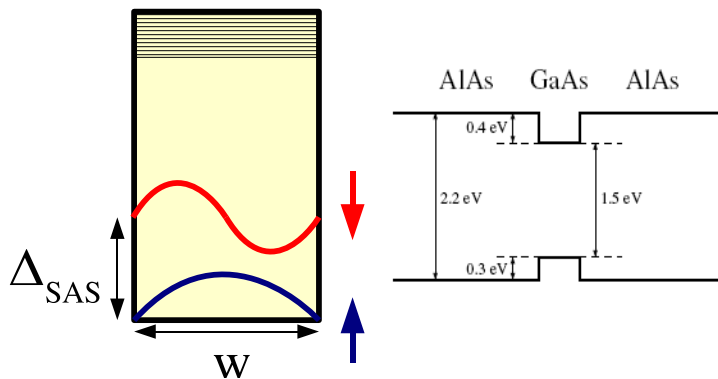


Figure 1.4: Quantum well with the two lowest subbands

which describes the confinement in the perpendicular z -direction in terms of a parameter w related to the width of the 2DEG.

Alternatively, it is possible to produce samples in form of the quantum well, Fig. 1.4. A quantum well device is made out of two nearby AlAs interfaces. Upon doping, the electrons fall into the GaAs region and occupy, depending on the density, one or more subbands. In the simplest case, one can take only the lowest subband which is given by

$$\phi_{\text{ISQW}}(z) = \sqrt{\frac{2}{w}} \sin\left(\frac{\pi z}{w}\right). \quad (1.15)$$

Regardless of the choice of perpendicular confinement, the effective interaction in the plane is given by

$$V^{\text{eff}}(r) = \frac{e^2}{\epsilon l_B} \int dz_1 \int dz_2 \frac{|\phi(z_1)|^2 |\phi(z_2)|^2}{\sqrt{r^2 + (z_1 - z_2)^2}}. \quad (1.16)$$

For large distances $r \gg w$ the effective interaction reduces to pure Coulomb, but for small r it is less repulsive. This effect can be qualitatively captured in a much simpler kind of ansatz for the effective interaction, the so-called Zhang-Das Sarma (ZDS) potential [45]

$$V(r, d) = \frac{e^2}{\epsilon \sqrt{r^2 + d^2}}, \quad (1.17)$$

which is just a Coulomb energy for the two point charges located in two planes separated by the distance d . ZDS potential does not correspond to any obvious wave function in the perpendicular direction, but it leads to the similar softening of the interaction as the realistic confinement models (Chapter 5). It is advantageous to use it because a single parameter can be used to tune directly the interaction potential and simulate the finite thickness of the sample (Fang-Howard or infinite square well model allows one to tweak the single particle wave functions, but it is generally not easy to see directly the effect of such a tweak on the interaction potential because of the difficulty in evaluating the integral (1.16) in the closed form).

1.2 Polarized electrons in the lowest Landau level

Let us assume that $\nu < 1$ so the kinetic energy is an overall constant that can be dropped from the Hamiltonian (1.9). In this section we further assume that the magnetic field is so large that the electron spin is frozen out. In the absence of disorder, the Hamiltonian is then reduced to the form

$$H = \mathcal{P}_{LLL} \sum_{i < j} \frac{1}{|\mathbf{r}_i - \mathbf{r}_j|} \mathcal{P}_{LLL} \quad (1.18)$$

1. INTRODUCTION

i.e. it contains nothing *but* the interaction (explicitly projected to the LLL by the operator \mathcal{P}_{LLL}). This is why the quantum Hall effect is referred to as the paradigm of *strongly correlated systems*. In the case of a partially filled n th LL, one may separate the “low-energy” degrees of freedom, which consist of intra-LL excitations, from the “high-energy” inter-LL excitations. In the absence of disorder, all states within the partially filled LL have the same kinetic energy such that intra-LL excitations may be described by considering only electron-electron interactions,

$$H_n = \frac{1}{2} \sum_{\mathbf{q}} v(q) \rho_n(-\mathbf{q}) \rho_n(\mathbf{q}), \quad (1.19)$$

where $v(q) = 2\pi e^2/\epsilon q$ is the 2D Fourier-transformed Coulomb interaction potential. The Fourier components $\rho_n(\mathbf{q})$ of the density operator are constructed solely from states within the n -th LL. Eq. (1.19) is a Fourier-image of Eq. (1.18) and is valid for 2DEG as well as for other systems such as graphene in the magnetic field (Sec. 1.5.5) if the density operators are appropriately modified (Chapter 6).

1.2.1 Laughlin’s wave function

Since it contains only the interaction, Hamiltonian (1.18) is notoriously difficult to solve because there is no obvious normal state to use as the starting point for the perturbation theory and essentially one has to make an educated guess at what the ground state could possibly be. This was first done by Laughlin [46] who proposed the following wave function for the states at filling factors $\nu = 1/m, m$ – odd integer,

$$\Psi_L = \prod_{i < j} (z_i - z_j)^m \exp\left(-\sum_k |z_k|^2/4\right), \quad (1.20)$$

$z_j = x_j + iy_j$ is the complex coordinate of an electron in the plane ($l_B = 1$) and we will drop the universal Gaussian factor from now on. To understand this wave function, one should use the symmetric gauge (1.2) which yields LLL single particle wave functions that are analytic functions of z and have definite angular momentum l , $\phi_l(z) \sim z^l \exp(-|z|^2/4)$. Using these wave functions and the Jastrow-type variational ansatz known from the physics of liquid He, Laughlin constructed the many-body wave function which captures the correct physics at the filling factor $\nu = 1/3$ which was observed at the time. Namely, he showed that $\nu = 1/m$ states are incompressible fluids with a uniform density. The latter property is nontrivial to establish in the disk geometry and a formal mapping to a 2D plasma is required [47] (in the finite systems, on the contrary, it is very simple to verify this property numerically, see Chapter 2). Using a flux insertion argument, Laughlin also demonstrated that incompressibility at a fractional filling factor implies the existence of fractionally charge excitations [47] that were eventually observed in shot noise experiments. [48, 49] An interesting consequence of the fractional charge of the quasiparticles is their fractional mutual statistics. Based on general arguments [47, 50] (see also Sec. 1.3.2), it is possible to write a wave function for the two quasiholes at u and v

$$\Psi_L^{2qh} = (u - v)^{1/m} \prod_{i,j} (z_i - u)(z_j - v) \Psi_L(\{z\}) \exp[-(|u|^2 + |v|^2)/4m]. \quad (1.21)$$

If we perform an exchange operation on the quasiholes u and v , we notice that the phase of the wave function changes by π/m , instead of the usual π or 2π (for fermions and bosons, respectively). In doing so, we assume that the wave function Ψ_L^{2qh} is properly normalized. [51, 52, 53] Thus, the quasiholes (and similarly, quasiparticles) in the Laughlin state obey *anyonic* (Abelian) statistics. [54] In Sec. 1.3 we will see even more exotic possibilities for the mutual statistics of quasiparticles that are possibly brought by strong correlations in FQHE. The experiments that directly address the statistics of quasiparticles are largely based on interferometry principles and have so far proved difficult to interpret.

Immediate support of Laughlin's theory came however from exact diagonalization studies [55, 56] which, among other things, identified the interaction that produces Laughlin's wave function as a unique zero energy ground state with the smallest angular momentum:

$$V(r) = V\nabla^2\delta(r), \quad (1.22)$$

V being a positive constant that controls the value of the gap. Properly taking care of the short-range correlations makes the Laughlin wave function an excellent description of the generic Coulomb ground state, for fermions as well as for bosons. [57, 58] It was further shown that the Laughlin state possesses a low-energy branch of collective modes called magneto-rotons [59] (in analogy with rotons in liquid helium) and established that there is a hidden, so-called off-diagonal long-range order [60] in the Laughlin ground state. The latter insight was a starting point for the development of the effective Chern-Simons field theories for the fractional quantum Hall states (see the following Section).

To close this brief overview of the Laughlin states, we stress that the Laughlin states are to this day the first experimentally known examples of a new kind of matter which possesses *topological order*. [17] The topological phase of matter is the one canonically characterized by the presence of gap in the excitation spectrum, fractional quantum numbers (such as the quasiparticle charge in the present case) and with a ground state degeneracy on topologically nontrivial manifolds, [17, 61] although some of these may not be the necessary requirements. Not all of these properties are easily proven even for the Laughlin state (e.g. there is no rigorous proof that the Laughlin state is gapped in thermodynamic limit), but there is plenty of numerical evidence and the overall consensus is that this is indeed the case.

1.2.2 Effective field theories

Zhang, Hansson and Kivelson have shown, building on an earlier work by Girvin and MacDonald [60], that applying a singular gauge transformation to the electron coordinates can map them into a system of bosons with an additional gauge interaction. [62, 63] In this representation, an electron is viewed as a composite of a charged boson and a flux tube with an odd number of flux quanta attached to it, Fig. 1.5. The gauge interaction generated this way is given by

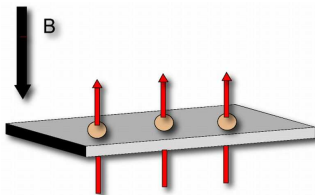


Figure 1.5: Chern-Simons transformation to composite bosons

$$\mathbf{a}(\mathbf{r}_i) = \frac{\Phi_0}{2\pi} \frac{\theta}{\pi} \sum_{j \neq i} \nabla_i \alpha_{ij}, \quad (1.23)$$

where $\theta = (2p+1)\pi$, $2p+1 = \nu^{-1}$ and α_{ij} is the angle between the x -axis and the vector $\mathbf{r}_i - \mathbf{r}_j$. The unitary transformation that connects the electronic and bosonic representations is given by

$$U = \exp \left(-i \sum_{i < j} \frac{\theta}{\pi} \alpha_{ij} \right). \quad (1.24)$$

The Lagrangian which describes the statistical gauge field \mathbf{a} turns out to be the Chern-Simons (CS) term:

$$\mathcal{L}_a = \frac{\pi}{2\theta\Phi_0} \epsilon^{\mu\nu\lambda} a_\mu \partial_\nu a_\lambda. \quad (1.25)$$

1. INTRODUCTION

The fact that all the indices are contracted with the Levi-Civita tensor (which plays the role of the metric tensor) tells about the profound role of topology in these systems. Another hint at this is the fact that the CS action is gauge-invariant only up to the surface terms – therefore there ought to be degrees of freedom that live on the edge of the system and indeed – these are the celebrated edge channels of the quantum Hall effect. [64] In a microscopic theory, they are the zero-energy ground states of the Hamiltonian (1.22) with higher values of the angular momentum compared to the Laughlin ground state.

Putting it all together, we can formulate a path integral description of our system in terms of the bosonic fields ϕ :

$$\mathcal{S} = \int dt \int d^2\mathbf{r} \mathcal{L}_a + \int dt \int d^2\mathbf{r} \mathcal{L}_\phi \quad (1.26)$$

$$\begin{aligned} \mathcal{L}_\phi &= \phi^\dagger(\mathbf{r}) [i\partial_t - e(A_0 + a_0) + \mu] \phi(\mathbf{r}) - \frac{1}{2m} |(-i\nabla + e(\mathbf{A} + \mathbf{a}))\phi|^2 \\ &\quad - \frac{1}{2} \int d^2\mathbf{r}' \rho(\mathbf{r}) V(\mathbf{r} - \mathbf{r}') \rho(\mathbf{r}'). \end{aligned} \quad (1.27)$$

In the remainder of this Section, we present a brief overview of the mean-field solution of the Hamiltonian defined by the action (1.26). More details can be found in the paper of Zhang [63] and the book of Nagaosa. [65] The effective field “seen” by the composite bosons is given by

$$\mathbf{B}_{\text{eff}} = \nabla \times (\mathbf{a} + \mathbf{A}) = -B\mathbf{e}_z + \Phi_0 \frac{\theta}{\pi} \rho(\mathbf{r}) \mathbf{e}_z, \quad (1.28)$$

and is zero when $\nu = 1/(2p+1)$. Therefore, electrons at a filling factor ν with an odd denominator can be understood as CS-transformed bosons without the external field. We will use the following Madelung parametrization that represents a bosonic field $\phi(\mathbf{r})$ in terms of the product of the amplitude $\rho(\mathbf{r})$ and the phase factor $\theta(\mathbf{r})$:

$$\phi(\mathbf{r}) = \sqrt{\rho(\mathbf{r})} e^{i\theta(\mathbf{r})}. \quad (1.29)$$

Substituting this into the action \mathcal{S} , one expands around the stationary point ρ_0 for the bosonic amplitude, performs a Fourier transform and integrates over the remaining degrees of freedom $\delta\rho, \theta$ and a_μ , to arrive at the form

$$\mathcal{L}_{\text{eff}} = \sum_{\mu, \nu} \frac{1}{2} \tilde{\pi}_{\mu\nu}(k) A_\mu(-k) A_\nu(k), \quad (1.30)$$

where $k \equiv (\omega, \mathbf{k})$, from which one can directly read off the response functions $\tilde{\pi}_{\mu\nu}$. For example, the term which couples to A_0^2 represents the compressibility of the system and is given by

$$\kappa = \lim_{k \rightarrow 0} \tilde{\pi}_{00}(k) = \lim_{k \rightarrow 0} \frac{\frac{1}{\tilde{V}(0)} (|\mathbf{k}|/2\theta)^2}{\frac{1}{\tilde{V}(0)} \frac{\rho_0}{m} + (|\mathbf{k}|/2\theta)^2}, \quad (1.31)$$

where $\tilde{V}(\mathbf{k})$ is the Fourier transform of $V(\mathbf{r})$. Assuming that the density ρ_0 is finite, one concludes that compressibility (1.31) tends to zero.

For the usual Bose superfluid, the order parameter is the phase of the wave function of the condensate and the Bose condensation is described in terms of the spontaneous breaking of U(1) symmetry. The ordering can also be described by evaluating the following expectation value

$$\lim_{|\mathbf{r} - \mathbf{r}'| \rightarrow \infty} \langle \phi^\dagger(\mathbf{r}) \phi(\mathbf{r}') \rangle, \quad (1.32)$$

which represents the element of the density matrix. [42] Condensation is manifested in the nonzero value of this quantity when the system is said to display off-diagonal long-range order (ODLRO). We can evaluate (1.32) by going back to the original form of the action \mathcal{S} and eliminate a_μ while setting $A_\mu = 0$. [63] The correlation function follows directly

$$\langle \theta(-k) \theta(k) \rangle = \frac{\frac{2\pi}{\nu} \omega_C \frac{1}{|\mathbf{k}|^2} + \tilde{V}(\mathbf{k})}{\omega^2 - \omega_{\mathbf{k}}^2}, \quad (1.33)$$

where $\omega_{\mathbf{k}}^2 = \omega_C^2 + \frac{\rho_0}{m} |\mathbf{k}|^2 \tilde{V}(\mathbf{k})$ and $\omega_C = \frac{2\pi\rho_0}{m\nu}$. The static correlation function is asymptotically

$$\langle \theta(-\mathbf{k})\theta(\mathbf{k}) \rangle = -i \int \frac{d\omega}{2\pi} \langle \theta(-k)\theta(k) \rangle = -\frac{1}{2\nu} \frac{2\pi}{|\mathbf{k}|^2} + o(1/|\mathbf{k}|). \quad (1.34)$$

Going back to real space, (1.32) becomes

$$\begin{aligned} \lim_{|\mathbf{r}-\mathbf{r}'| \rightarrow \infty} \langle \phi^\dagger(\mathbf{r})\phi(\mathbf{r}') \rangle &= \rho_0 \langle e^{i\theta(\mathbf{r})-i\theta(\mathbf{r}')} \rangle \approx \rho_0 e^{i\langle \theta(\mathbf{r})\theta(\mathbf{r}') \rangle} \\ &\propto \rho_0 |\mathbf{r}-\mathbf{r}'|^{-1/2\nu}, \end{aligned} \quad (1.35)$$

where in the first line we expanded the exponential and used Wick's theorem. The obtained ODLRO (1.35) is algebraic and does not depend on the interaction V .

Magneto-roton excitations are described by topological vortices of this theory and, neglecting their contribution to the ground state, one can derive Laughlin's wave function directly as the ground state description [63, 65] (see also Chapter 3). However, it has proved difficult to generalize the composite boson theory for the non-Laughlin fractions and also to translate it into a microscopic theory which can be tested numerically (some effort in this direction was made in [66]). In Chapter 3 we will use a generalization of this kind of theory to describe the phases of the quantum Hall bilayer at $\nu = 1$.

1.2.3 Composite fermions

A compelling generalization of Laughlin's theory exists for most of the polarized FQH states observed in the LLL due to Jain. [16] This theory can be introduced following a similar transformation as the one outlined in the previous Section, the only difference being that electrons are now capturing an even number $\theta = 2p$ of flux quanta. This means that they preserve their fermionic statistics and therefore are called *composite fermions*. When it happens that composite fermions have just the right number of available (residual) flux quanta left for them to fill the integer number of $\nu^* = n$ LLs, one can readily write down trial wave functions to describe their ground state (the image of this ground state in terms of the original electrons will be a complicated, strongly correlated state). Since the CF ground state is unique being the integer QH state, the incompressibility follows immediately. There is an additional subtlety in that electrons are not capturing flux tubes but rather *vortices*, as it is explained in great detail in Ref. [16]. Here we quote the expression for the wave functions that describe the filling factors $\nu = \frac{n}{2pn \pm 1}$:

$$\Psi_{\nu = \frac{n}{2pn \pm 1}} = \mathcal{P}_{LLL} \Phi_{\pm n} \prod_{i < j} (z_i - z_j)^{2p}, \quad (1.36)$$

where $\Phi_{\pm n}$ is the Slater determinant for n filled CF LLs which are called Λ levels (with a sign depending on the direction of the residual magnetic field). Notice that unless $n = 1$, $\Phi_{\pm n}$ has non-analytic components because it is not a LLL function. Therefore, a projection operator \mathcal{P}_{LLL} is required to explicitly project the whole expression to the LLL. The wave functions (1.36) are remarkable test wave functions as they do not contain any variational parameters, yet they show impressive agreement with the complicated ground states of realistic systems in numerical calculations. The formation of CFs is a nonperturbative outcome of the strongly correlated system, but similarly to the true quasiparticles known in other areas of physics, CFs are mostly weakly interacting. For polarized electrons, the topological properties of their excitations are Abelian.

1.2.4 Compressible state $\nu = 1/2$

A striking feature in Fig. 1.3 is the absence of a plateau at $\nu = 1/2$. Halperin, Lee and Read [15] made a remarkable proposal for the state at $\nu = 1/2$ as a compressible Fermi liquid state of CFs

1. INTRODUCTION

(CFL) that experience zero residual magnetic field. They calculated the response functions in the long-wavelength effective theory and some of these features were verified in surface acoustic wave experiments. [67] On the other hand, Rezayi and Read [68] have formulated a microscopic wave function for such a compressible state at $\nu = 1/2$,

$$\Psi_{\text{RR}} = \mathcal{P}_{\text{LLL}} \mathcal{F}(\{z, \bar{z}\}) \prod_{i < j} (z_i - z_j)^2, \quad (1.37)$$

where multiplication with a Slater determinant of free waves $\mathcal{F} \equiv \det [e^{i\mathbf{k}_i \cdot \mathbf{r}_j}]$ is necessary to ensure a fermionic wave function. The relevance of (1.37) has been numerically demonstrated. [68]

1.3 Second Landau level

In the second Landau level ($2 < \nu < 3$), Fig. 1.6, there is a notable scarcity of FQH states. In principle, the increase in Landau level index favors the compressible phases such as charge density waves, stripes and bubbles [69, 70] (in the third Landau level, e.g. there are no observed FQH states except for weak indications of minima in longitudinal resistance, see Ref. [71]). The curious feature in Fig. 1.6 is the presence of reentrant QH phases and a fully developed plateau at the even-denominator filling $\nu = 2 + 1/2 = 5/2$. [2, 72, 73]

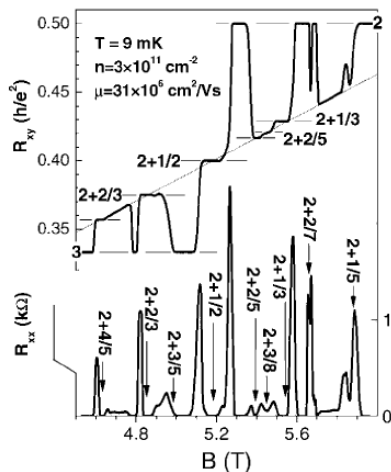


Figure 1.6: FQHE in the second Landau level. [2]

1.3.1 The $\nu = 5/2$ state

The most celebrated 2nd LL state, the $\nu = 5/2$ state, remained enigmatic for some time upon discovery because it was thought to depend crucially on the electron spin [74]. Subsequent studies, as well as exact diagonalization [75], reached the consensus that 5/2 state is likely fully polarized, although the question remains the subject of experimental studies to this day. If the spin is frozen, a way to explain the incompressibility is to postulate that CFs form a p -wave paired state, which is now referred to as the celebrated Pfaffian wave function first given by Moore and Read [18, 76]

$$\Psi_{\text{Pf}} = \text{Pf} \left(\frac{1}{z_i - z_j} \right) \prod_{i < j} (z_i - z_j)^2, \quad (1.38)$$

where ‘‘Pf’’ stands for the Pfaffian

$$\text{Pf } M_{ij} = \frac{1}{2^{N/2}(N/2)!} \sum_{\sigma \in S_N} \text{sgn } \sigma \prod_{k=1}^{N/2} M_{\sigma(2k-1)\sigma(2k)}$$

for an $N \times N$ antisymmetric matrix whose elements are M_{ij} ; S_N is the group of permutations of N objects. The Pfaffian factor guarantees the correct exchange symmetry of the wave function and acts only in the so-called *neutral* sector of the wave function, without affecting the filling factor which is fixed by the Jastrow factor. The latter is referred to as the *charge* part of the wave function. The Pfaffian wave function has a much richer spectrum of excitations than the Laughlin states, its excitations carry charge $e/4$ and obey the so-called *non-Abelian statistics*. [18, 77] If $2n$ quasiholes are introduced above the ground state, it can be shown they give rise to 2^{n-1} linearly independent states. [77] If we set $N = 2$ electrons and look for the wave functions that describe the four quasiholes above the ground state, we obtain two independent states that span the basis proposed by Nayak and Wilczek [78]:

$$\Psi_0^{4\text{qh}} = \frac{(\eta_{13}\eta_{24})^{1/4}}{(1 + \sqrt{1-x})^{1/2}} (\Psi_{(13)(24)} + \sqrt{1-x}\Psi_{(14)(23)}) \quad (1.39)$$

$$\Psi_{1/2}^{4\text{qh}} = \frac{(\eta_{13}\eta_{24})^{1/4}}{(1 - \sqrt{1-x})^{1/2}} (\Psi_{(13)(24)} - \sqrt{1-x}\Psi_{(14)(23)}) \quad (1.40)$$

where η 's denote the positions of the quasiholes, $x = \frac{\eta_{12}\eta_{34}}{\eta_{13}\eta_{24}}$ and $\eta_{12} \equiv \eta_1 - \eta_2$ etc. We have defined $\Psi_{(12)(34)} = \Psi_L^{\nu=1/2}(z_1 - z_2)^{-1} \times [(z_1 - \eta_1)(z_1 - \eta_2)(z_2 - \eta_3)(z_2 - \eta_4) + (z_1 \leftrightarrow z_2)]$ and we assume that all of the quasihole wave functions are normalized [51, 52, 53]. If we focus on the limit $|x| \ll 1$, we have approximately

$$\begin{aligned} \Psi_0^{4\text{qh}} &= 2^{-1/2}(\eta_{13}\eta_{24})^{1/4} (\Psi_{(13)(24)} + \Psi_{(14)(23)}) \\ \Psi_{1/2}^{4\text{qh}} &= 2^{-1/2}(\eta_{13}\eta_{24})^{1/4} (\Psi_{(13)(24)} - \Psi_{(14)(23)}) \end{aligned}$$

It is clear that the exchange e.g. of 1 and 3 leads only to the multiplication by a phase factor. However, the interchange of 2 and 3 gives a rotation in the space $\{\Psi_0^{4\text{qh}}, \Psi_{1/2}^{4\text{qh}}\}$. Therefore, the states $\Psi_0^{4\text{qh}}$ and $\Psi_{1/2}^{4\text{qh}}$ can be used as a basis for a qubit. Braiding of the qubit states can be used to perform quantum operations which are protected from decoherence effects due to the FQH gap. This is the motivation for using FQH states in *topological quantum computation* schemes.

Non-Abelian properties of $\nu = 5/2$ excitations have so far been numerically demonstrated [79] and experiments to test this are under way. [80] Several groups have reported the observation of $e/4$ fractional charges at $5/2$ filling. [81, 82] The key to establishing the non-Abelian statistics in theory, apart from the ground state wave function (1.38), is to identify the Hamiltonian which produces the given wave function as its densest zero-energy ground state, similar to (1.22). In the case of the Pfaffian, this is the Hamiltonian which has no penalty for two electrons approaching each other, but forbids the clustering of three electrons:

$$H_{3b} = - \sum_{i < j < k} \mathcal{S}_{ijk} [\nabla_i^4 \nabla_j^2 \delta(\mathbf{r}_i - \mathbf{r}_j) \delta(\mathbf{r}_j - \mathbf{r}_k)], \quad (1.41)$$

where \mathcal{S}_{ijk} is the symmetrizer. Numerical studies of realistic systems [83] have shown that Pfaffian is a very good trial wave function for the ground state, especially if the interaction is modified with respect to the pure Coulomb by adding some short-range potential of the kind (1.22), and also by particle-hole symmetrizing the Moore-Read wave function. Note that the Moore-Read wave function, being the ground state of 3-body interaction (1.41), is not particle-hole symmetric. The state obtained via particle-hole conjugation of the Pfaffian wave function (1.38) is called *anti-Pfaffian* [84, 85] and has recently received much attention as a viable candidate for the description of the $5/2$ state. [86, 87]

1.3.2 Conformal field theory approach

In this Section we outline the method of conformal field theory (CFT) [88] that historically lead to the construction of the trial wave function (1.38). Conformal field theories have successfully been used to describe two-dimensional statistical mechanics models in the vicinity of critical points, when the correlation length diverges and there is an emergent conformal symmetry. [89] In two dimensions, this emergent symmetry is sufficient to derive critical exponents. FQH systems, on the other hand, are not critical but CFT can nonetheless be used due to the following observation (see [90] for a review of CFT in this context).

Take a free boson theory in 1+1-dimensional Euclidean spacetime, with the correlator given by

$$\langle \phi(z)\phi(z') \rangle = -\ln(z - z'). \quad (1.42)$$

Further defining the normal-ordered *vertex* operators $V_\alpha(z) =: e^{i\alpha\phi(z)} :$, with the help of Wick's theorem, their correlators evaluate to

$$\left\langle \prod_i V_{\alpha_i}(z_i) \right\rangle = \prod_{i < j} (z_i - z_j)^{\alpha_i \alpha_j}, \quad (1.43)$$

if the neutrality condition is assumed $\sum_i \alpha_i = 0$ (or else the correlator identically vanishes). If we choose $\alpha_i = \sqrt{m}$, we obtain precisely the polynomial part of the Laughlin wave function, (1.20). The Gaussian factor can similarly be constructed assuming a uniform background charge. We also get wave functions for n quasipoles (u_1, \dots, u_n) for free if we insert $V_{1/\sqrt{m}}(u_1) \dots V_{1/\sqrt{m}}(u_n)$ into the correlator (1.43). Quasielectron wave functions can also be constructed with some effort. [91]

Thus, CFT correlators have been shown to be a legitimate tool to produce candidate wave functions for FQH states [18, 92, 93, 94, 95] if the latter can be verified by independent means. In particular, Moore and Read [18] in their seminal work combined the chiral boson theory with the Majorana fermion, described by correlator $\langle \chi(z)\chi(z') \rangle = 1/(z - z')$, to arrive at the Pfaffian (1.38)

$$\left\langle \prod_i \chi(z_i) e^{i\sqrt{2}\phi(z_i)} \right\rangle. \quad (1.44)$$

More generally, instead of a Majorana fermion, it is possible to use the \mathbb{Z}_k *parafermion* algebra to construct generalizations of a Pfaffian paired state for the fillings $\nu = k/(k+2)$. [96] These are the states which allow for clustering of k particles and forbid $(k+1)$ -particle clusters, with the excitations having non-Abelian statistics. Case $k = 2$ is the Pfaffian and there are indications that $k = 3$ is also physically relevant, being the particle-hole conjugate of the second LL $\nu = 2/5$ state observed in the experiments. [2] Braiding of the quasiparticles in states with $k = 3$ and $k > 4$ can be used to perform fault-tolerant quantum computation and hence presents an exciting venue for further research. [20]

All of the previously described CFTs are known as *unitary*. There have been attempts [94] that produce wave functions out of *nonunitary* CFTs, such as the so-called ‘‘Gaffnian’’ wave function which is related to the so-called $M(5, 3)$ minimal model [88] and describes a possible state at the filling factor $\nu = 2/5$. In numerical studies, Gaffnian appears as a serious contender for the description of $2/5$ state (the role shared by Jain's CF state), but on general grounds [53, 97] it is expected to describe a critical point rather than a stable incompressible phase. Both Gaffnian and Jain $2/5$ state have an underlying multicomponent structure which we explain in the following Section. Deeper understanding of the role of nonunitary CFTs and related FQH states is the subject of on-going research.

1.4 Multicomponent quantum Hall systems

In this thesis, we understand the term “multicomponent” to loosely refer to FQH systems with an internal degree of freedom. This degree of freedom is most naturally provided by electron spin when the magnetic field is not too strong to completely freeze out its dynamics. Looking at the relative interaction strengths (1.10, 1.11, 1.12), we see that the Zeeman splitting is less than the Coulomb or cyclotron energy in the accessible B range and we need to explicitly take it into account. This was first suggested by Halperin [98] who also wrote down a generalization of the Laughlin wave function for these systems. Halperin’s wave functions in the case of an ordinary $SU(2)$ spin are defined by dividing the electrons into two species (with \uparrow and \downarrow spin projection) and introducing correlations among them, in a manner of Laughlin’s wave function (1.20), so each electron “sees” the same number of flux quanta because they are indistinguishable particles:

$$\Psi_{m_1, m_2, n}^H(\{z_j^\uparrow, z_j^\downarrow\}) = \prod_{k < l}^{N_\uparrow} (z_k^\uparrow - z_l^\uparrow)^{m_1} \prod_{k < l}^{N_\downarrow} (z_k^\downarrow - z_l^\downarrow)^{m_2} \prod_{k=1}^{N_\uparrow} \prod_{l=1}^{N_\downarrow} (z_k^\uparrow - z_l^\downarrow)^n. \quad (1.45)$$

We have dropped the Gaussian factors for simplicity and the set of the exponents (m_1, m_2, n) characterize the wave function. The requirement that each electron “sees” the same number of flux quanta translates into the condition $m_1(N_\uparrow - 1) + nN_\downarrow = m_2(N_\downarrow - 1) + nN_\uparrow$. With the help of the total number of electrons $N = N_\uparrow + N_\downarrow$, the filling factor that this wave function describes is

$$\nu = \nu_\uparrow + \nu_\downarrow = \frac{m_1 + m_2 - 2n}{m_1 m_2 - n^2}, \quad (1.46)$$

except when $m_1 m_2 - n^2 = 0$. The physical realization of the last condition is the Laughlin ferromagnetic wave function $m_1 = m_2 = n$ which does not fix the relative number of \uparrow and \downarrow particles. There is also an additional constraint that (1.45) needs to satisfy if it is to be a proper trial wave function for the spinful system: it must be the eigenstate of the total spin operator \mathbf{S}^2 , which places constraints on the values of m_1, m_2, n . However, as we will see below, this requirement can be lifted in certain situations where the $SU(2)$ symmetry is not fully respected by the Hamiltonian.

It is possible to write down also the generalization of Halperin wave functions for systems with an $SU(K)$ internal symmetry. These are expected to describe quantized states in K -component systems such as graphene (Sec. 1.5.5). In graphene, a valley and spin degree of freedom (for a certain range of interaction strengths) combine into an effective $SU(4)$ degree of freedom ($K = 4$). Generalized Halperin wave functions are given by

$$\psi_{m_1, \dots, m_K; n_{ij}}^{SU(K)}(\{z_{j_1}^{(1)}, z_{j_2}^{(2)}, \dots, z_{j_K}^{(K)}\}) = \Psi_{m_1, \dots, m_K}^L \times \Psi_{n_{ij}}^{\text{inter}} \quad (1.47)$$

which consists of a product of Laughlin wave functions

$$\Psi_{m_1, \dots, m_K}^L = \prod_{j=1}^K \prod_{k_j < l_j}^{N_j} (z_{k_j}^{(j)} - z_{l_j}^{(j)})^{m_j}$$

for each of the components and a term

$$\Psi_{n_{ij}}^{\text{inter}} = \prod_{i < j}^K \prod_{k_i}^{N_i} \prod_{k_j}^{N_j} (z_{k_i}^{(i)} - z_{k_j}^{(j)})^{n_{ij}}$$

that takes into account the correlations between particles of different components. Many properties of these wave functions for general K can be worked out using the usual arguments such as flux counting and plasma analogy to assess their stability and identify those that are viable candidates to describe physical systems. [99]

Besides the intrinsic electron spin, multicomponent GaAs QH systems can be easily fabricated in the experiment in the form of wide quantum wells (Sec. 1.4.1) or bilayers (Sec. 1.4.2), where

the subband or layer index plays the role of the spin-like degree of freedom. In what follows we will introduce these systems and provide an overview of the physical phenomena that are studied in this thesis (Sec. 1.5).

1.4.1 Wide quantum wells

In Section 1.1 we introduced the quantum well structure (Fig. 1.4). It consists of two nearby AlAs interfaces, resulting in a semiconductor quantum well. Upon doping, the electrons fall into the GaAs region and occupy, depending on the density, one or more subbands. The width of the well w is usually between 15 and 50nm, while the depth of the well is on the order of 0.4eV, which is often much larger than other energy scales and therefore can be assumed infinite. The splitting between the subbands, Δ_{SAS} , scales as $1/w^2$, but it is expected to be renormalized in each sample, so it is convenient to think of it as a free parameter. What may happen is that the lowest two subbands are relevant for the low-energy description of the electrons, as indicated on the left side of Fig. 1.4, while we can discard the rest of the higher energy levels. The reason why we can sometimes keep only the two lowest subbands and discard the rest of the energy levels is subtle because, in a single particle picture, the gap between the lowest and the first excited subband is not very different from the one between the first excited and the second excited subband. In Chapter 5 we will quantify the range of validity of the two-subband approximation on the mean-field level. This calculation will show that, at least for some moderate values of the well width, we can restrict the dynamics to the lowest two subbands. For the infinite square well, the lowest two levels happen to be the sine functions, labeled S and A :

$$\phi_{S\equiv\uparrow}(z) = \sqrt{\frac{2}{w}} \sin\left(\frac{\pi z}{w}\right), \quad \phi_{A\equiv\downarrow}(z) = \sqrt{\frac{2}{w}} \sin\left(\frac{2\pi z}{w}\right). \quad (1.48)$$

The two-subband model is often a very good approximation in the experiments and provides a useful mapping of the quantum well system to a multicomponent description (see Chapter 5). The internal symmetry in this case is provided by the *subband* quantum number instead of the usual z -projection of spin. Therefore, we expect that FQH states observed in samples with the geometry of a quantum well can be described by Halperin wave functions (1.45). Note, however, that ϕ_S and ϕ_A have different symmetry regarding the reflection with respect to the center of the well $z = w/2$: the former is symmetric, while the latter is antisymmetric (it possesses a node at the center of the well). This implies that the problem does not have full SU(2) symmetry and therefore we are not obliged to require the $\Psi_{m_1, m_2, n}^H$ to be an eigenstate of \mathbf{S}^2 .

1.4.2 Quantum Hall bilayer

Bilayer semiconductor structure consists of two quantum wells grown by MBE and spatially separated by an insulating barrier that is on the same order of magnitude as the width of each of the wells, Fig. 1.7. The key parameter that describes this system is d/l_B , the ratio of center-to-center distance d to the magnetic length l_B . Applying gate voltage changes the electron density in each layer, which in turns changes the effective magnetic length and therefore also d/l_B . Note that besides the top/bottom gates which control the electron density (and are not in direct contact with the 2DEG), separate Ohmic contacts that are annealed onto the sample can be used to probe electronic transport. Theoretically we describe the quantum Hall bilayer imagining that there are two groups of electrons situated in the \uparrow and \downarrow layer. Electrons within the same layer interact with the unscreened Coulomb interaction $V^{\text{intra}}(r)$, whereas electrons in different groups repel each other by a slightly weaker interaction, $V^{\text{inter}}(r)$

$$V^{\text{intra}}(r) = e^2/\epsilon r, \quad V^{\text{inter}}(r) = e^2/\epsilon\sqrt{r^2 + d^2}. \quad (1.49)$$

Additional energy scale is set by the tunneling between the layers. However, it is possible to fabricate bilayer systems which have negligible tunneling and interesting quantum mechanical

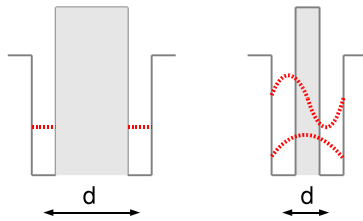


Figure 1.7: Quantum Hall bilayer: two decoupled layers for large d (left) and the quantum coherent state for small d (right).

coherence effects can then be established at sufficiently small d/l_B , even in the lack of any tunneling.

1.5 Multicomponent systems studied in this thesis

1.5.1 Quantum Hall bilayer at $\nu = 1$

Certainly the most spectacular example of a multicomponent QH system is the quantum Hall bilayer at total filling factor $\nu = 1$ i.e. $1/2$ in each layer. Here, one would ordinarily expect to obtain a compressible state (Sec. 1.2.4). Murphy *et al.* [3] reported a vanishing of R_{xx} in such a bilayer system when the distance d is less than $2l_B$, Fig. 1.8, even in the absence of any tunneling between the layers. With nonzero tunneling, the critical distance becomes larger, as shown in the inset of Fig. 1.8. This suggests that bringing the two layers close together establishes quantum mechanical coherence between them, even when there is no explicit tunneling from one layer to the other.

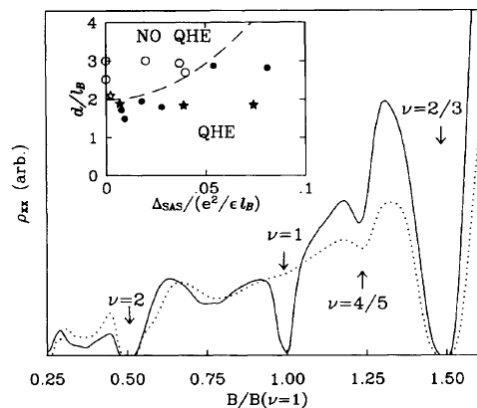


Figure 1.8: Quantum Hall effect at $\nu = 1$. [3]

In the language of Halperin multicomponent states, we have a wave function for this kind of state, called the 111 state: it is Ψ_{111} . Because all the correlation exponents are the same, there is a simple physical picture in Ψ_{111} : it describes an *exciton* condensate where directly across an electron in one layer there is a correlation hole in the opposite layer. This is particularly transparent in the wave function proposed by Fertig [100], $\bar{\Psi}_{111} = \prod_m \frac{1}{\sqrt{2}} (c_{m\uparrow}^\dagger + c_{m\downarrow}^\dagger) |0\rangle$,

1. INTRODUCTION

which can be understood as “grand canonical” generalization of Ψ_{111} . The numbers of particles in \uparrow and \downarrow layer are not sharp in $\bar{\Psi}_{111}$ (i.e. their difference $N_\uparrow - N_\downarrow$ fluctuates, while the sum is fixed), but they are both individually conserved in Ψ_{111} . Because the excitons are neutral, the bilayer for $d = 0$ can also be understood as a composite boson condensate [101] (Sec. 1.2.2).

In $d \rightarrow 0$ limit the $SU(2)$ pseudospin rotation symmetry makes the bilayer system equivalent to the Heisenberg problem, in which spins can rotate freely in three dimensions. At finite d , the intralayer repulsion is stronger than interlayer repulsion. If the pseudospins would order in the z -direction, all of the electrons would be in a single layer and the capacitive charging energy would be large. That would lead to an “easy-plane” anisotropy in which the pseudospins prefer to order in $x - y$ plane and the symmetry is reduced to $U(1)$ (see Ref. [102] for a quick introduction to the physics of spin and pseudospin in quantum Hall systems). This is made explicit by comparing the ground state of the easy-plane ferromagnet [24, 103]

$$\bar{\Psi}_{XY} = \prod_m \frac{1}{\sqrt{2}} \left(c_{m\uparrow}^\dagger + e^{i\phi} c_{m\downarrow}^\dagger \right) |0\rangle. \quad (1.50)$$

to $\bar{\Psi}_{111}$. The phase ϕ represents a global phase difference between \uparrow and \downarrow particles and interpolates between the symmetric ($\phi = 0$) and antisymmetric ($\phi = \pi$) superposition. Similar to the BCS wave function of a superconductor, the phase ϕ is fixed, but the particle number fluctuates. To be precise, the total number of particles is fixed, but the particle number difference between the layers is indefinite. However, contrary to the Cooper-pair order parameter, the order parameter here

$$\langle \psi_\uparrow^\dagger(\mathbf{r}) \psi_\downarrow(\mathbf{r}) \rangle \sim e^{i\phi(\mathbf{r})}$$

is charge-neutral and can condense even in high magnetic fields.

In the absence of tunneling between the layers, the Hamiltonian of the system should not depend on the phase ϕ , but it may nonetheless depend on its gradient

$$\mathcal{H}_{XY} = \frac{\rho_s}{2} \int d^2r |\nabla\phi|^2, \quad (1.51)$$

ρ_s being the pseudospin stiffness which is typically about 0.5K [103] and represents the energy cost of twisting the pseudospins out of their perfect alignment. This low-energy description is known as the Berezinskii-Kosterlitz-Thouless (BKT) model. [65] It displays a topological phase transition at finite temperatures on the order of ρ_s , driven by proliferation of vortices. The transition occurs when the vortices in the phase field ϕ become unbound as a result of entropy gain (although their interaction energy grows logarithmically with distance). In the context of QH bilayer, vortices are known as *merons* and they carry both charge and vorticity. [103] The broken $U(1)$ symmetry in the bilayer at $\nu = 1$ has received a stunning confirmation in the experiments of Spielman *et al.* [4] who studied interlayer transport as a function of bias voltage, Fig. 1.9. At large d/l_B the interlayer conductance is strongly suppressed. As the layers are nearly decoupled for large d/l_B , there is an energy penalty for an electron that tunnels from one correlated state into the other as the latter needs to be reorganized to accommodate the extra electrons. This is not so when d/l_B is below 1.8. As seen in Fig. 1.9, a sharp resonance develops at zero bias voltage which can be accounted for by the excitonic condensation in the 111 state. Opposite to each electron there is now a hole and it is energetically advantageous for an electron to tunnel. The effect is reminiscent of the Josephson effect, although strictly speaking the two “weak links” in this case are parts of the same quantum state.

Further experimental support for the picture of an excitonic superfluid forming in the $\nu = 1$ bilayer came from the so-called *counterflow* experiments. As the excitons are charge neutral and hence do not carry a net current, their presence can be detected in a configuration in which the injected currents in the two layers are equal in magnitude but flow in opposite directions, Fig. 1.10. The fundamental charge carriers can be electrons [5] or holes. [104] As seen in Fig. 1.10, the parallel and counterflow configurations show qualitatively different behaviors at

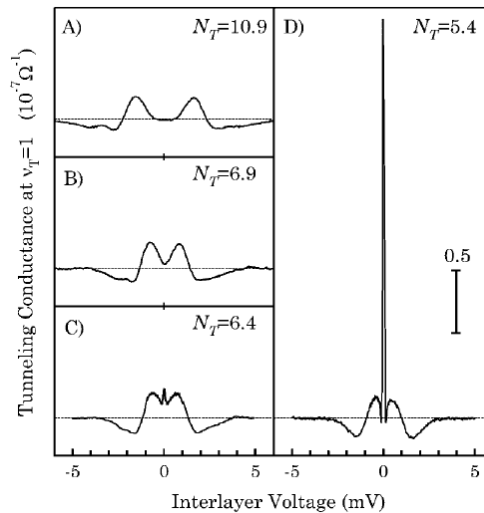


Figure 1.9: Tunneling conductance dI/dV as a function of the interlayer bias voltage at total filling of $\nu = 1$ for several values of d/l_B . [4]

$\nu = 1$: R_{xy} is quantized for the former but has a minimum for the latter. From the temperature dependence, both the Hall and the longitudinal resistances show approximately activated behavior, presumably vanishing in the $T \rightarrow 0$ limit. The counterflow conductivity σ_{xx}^{CF} , which is obtained from the longitudinal and the Hall resistances by matrix inversion, increases rapidly with decreasing temperature. These results are taken to support the formation of excitonic superfluidity at $T = 0$, but they also demonstrate the absence of perfect excitonic superfluidity at nonzero temperatures in these bilayer systems. In spite of a sharp resonance, the height of the interlayer tunneling peak remains finite in the limit of vanishing temperature. Theory predicts a finite temperature Kosterlitz Thouless transition, [103] below which the *Ohmic* resistance in the counterflow channel should vanish, resulting in a non-linear $I - V$ characteristics. No evidence of non-Ohmic behavior has been seen so far.

This points out to the fact that imperfect superfluidity may be attributed to the disordered excitonic superfluid. [105] Further indications of this stem from the *drag* experiments, Fig. 1.11. A current flowing in one layer induces a current in the other one as a result of interlayer momentum relaxation by Coulomb interaction (when d/l_B is not too large) or phonon exchange (for large separations). If no current is being drawn through the other layer, a voltage is eventually established that produces a current to cancel the induced current. The induced voltage in the “passive” layer divided by the current in the “active” layer is called the drag resistance. For simple Fermi liquids, the drag vanishes as T^2 as $T \rightarrow 0$, because of the lack of phase space allowing for inelastic scatterings, and for CFs at $\nu = 1/2$ it vanishes as $T^{4/3}$. [106] The drag of CFs has been investigated by Lilly *et al.* [107] in the weakly coupled region outside the 111 part of the phase diagram in Fig. 1.8. They did not see a clear evidence of $T^{4/3}$ dependence and, more surprisingly, discovered that the drag extrapolates to a nonzero value in the $T \rightarrow 0$ limit. That might suggest that the actual bilayer state in this region might not be weakly coupled. The observation might be related to the work of Bonesteel *et al.* [108], that suggests that the CS gauge field mediated interaction between CFs is attractive and induces an interlayer pairing at any layer separation. This pairing turns out to be very important in theoretical studies of the quantum Hall bilayer at $\nu = 1$. [13, 109, 110, 111, 112]

We close this review of the quantum Hall bilayer by a disclaimer that our discussion was in-

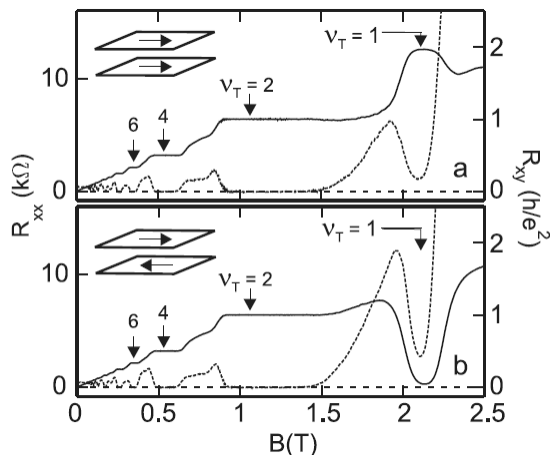


Figure 1.10: R_{xx} and R_{xy} for the bilayer $\nu = 1$ system at $T = 50\text{mK}$, in the parallel configuration when the currents are flowing in the same direction in both layers (upper panel) and the counterflow configuration with the two layers contacted individually (lower panel). The distance between the layers is $d/l_B = 1.58$. [5]

tentionally focused almost exclusively on the fascinating experiments that have been done on this system and are still performed at the time of writing. The field has also witnessed dramatic advances on the theoretical side to which our review cannot do justice. The fundamental problem that the quantum Hall bilayer at $\nu = 1$ poses to the theorist is how to connect the small d limit (characterized by the effective CB quasiparticles, the incompressibility and the Goldstone mode) with the large d limit described by compressible CF $\nu = 1/2$ states. The way to resolve this crossover, which also received compelling quantitative support, [111] is to assume the mixed states which contain a coherent mixture of CFs and CBs with their relative ratio being determined by the distance d . In Chapter 3 we present more details of this theory.

1.5.2 $\nu = 1/2$

As we remarked in Sec. 1.2.4, $\nu = 1/2$ in the LLL is a compressible state. In wide quantum wells, however, an incompressible state is formed [7, 113], Fig. 1.12. For the results in Fig. 1.12, a 68nm wide quantum well was used. It was shown, by a self-consistent Hartree-Fock calculation [7], that this system effectively acts as a bilayer system i.e. the charge distribution forms two maxima close to the sides of the well. The distance between the two maxima is the bilayer distance d . The system is obviously two-component because we have two groups of electrons, one near each side of the well. A $1/2$ plateau is seen in the approximate parameter range $2.6 < d/l_B < 8$ with an activation gap on the order of 200 mK. In contrast, Ref. [113] used a double quantum well geometry with a thin but high barrier to suppress interlayer tunneling. Both experimental systems are two-component, however, and a natural explanation for the incompressibility at $\nu = 1/2$ is the Halperin wave function Ψ_{331} . This wave function is not a good representation of the ground state for small bilayer distances where the $SU(2)$ symmetry approximately holds. Also, if the width of the well is very large, the system is expected to be compressible. There have been a few numerical studies of the problem of $\nu = 1/2$ bilayer [114, 115, 116] and they are generally consistent with each other and agree that Ψ_{331} is at the origin of incompressibility for intermediate d .

We would like to note that Ψ_{331} can be understood as a paired state where the pairing is described by the Cauchy determinant. Using the Cauchy identity [117] (up to the unimportant

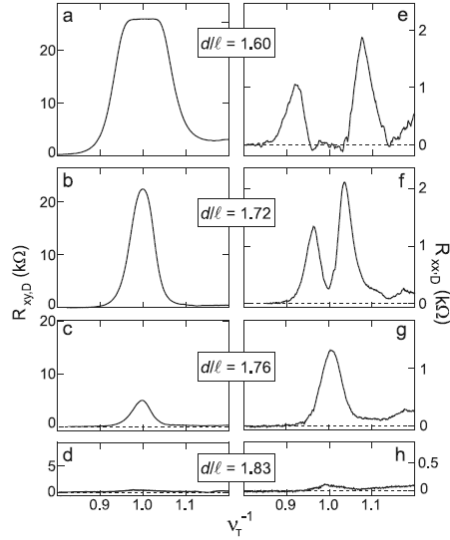


Figure 1.11: Coulomb drag resistances at $T = 30\text{mK}$ in the vicinity of $\nu = 1$ for various d/l_B . [6]

phase factor),

$$\det\left(\frac{1}{z_{i\uparrow} - z_{j\downarrow}}\right) = \frac{\prod_{i<j}(z_{i\uparrow} - z_{j\uparrow}) \prod_{k<l}(z_{k\downarrow} - z_{l\downarrow})}{\prod_{p,q}(z_{p\uparrow} - z_{q\downarrow})}, \quad (1.52)$$

we can rewrite Ψ_{331} in the following way

$$\Psi_{331} = \det\left(\frac{1}{z_{i\uparrow} - z_{j\downarrow}}\right) \Phi_1^2(\{Z\}), \quad (1.53)$$

where $\Phi_1^2 = \prod_{i<j}(Z_i - Z_j)^2$ represents the charge part and Z 's label all particles irrespective of their spin index. Haldane-Rezayi state which also occurs at $\nu = 1/2$ (Sec. 1.3.1) is the 331 state multiplied by a permanent, $\text{per}[1/(z_{i\uparrow} - z_{j\downarrow})]$, a determinant with plus signs. [74, 118]. Using a linear algebra identity, Haldane-Rezayi state can be written in the form (1.53) where the argument of the determinant is $1/(z_{i\uparrow} - z_{j\downarrow})^2$.

Another interesting identity that can be proved using elementary algebra is the following [119]

$$\mathcal{A}\left\{\prod_{i<j}(z_{i\uparrow} - z_{j\uparrow})^3 \prod_{k<l}(z_{k\downarrow} - z_{l\downarrow})^3 \prod_{p,q}(z_{p\uparrow} - z_{q\downarrow})\right\} \propto \Phi_1^2(\{Z\}) \text{Pf}\left(\frac{1}{Z_i - Z_j}\right), \quad (1.54)$$

or in other words, antisymmetrizing the 331 state between \uparrow and \downarrow leads to the Pfaffian. This suggests an interesting possibility. Let us imagine a wide quantum well or a bilayer, prepared in an incompressible 331 state. The effect of tunneling between the two layers or subbands in a quantum well is to organize the single particle states into even and odd superpositions, $\uparrow \pm \downarrow$. For large tunneling, the even superposition $\uparrow + \downarrow$ is energetically favored and the particles of the even channel should therefore have the Pfaffian description. This transition is the subject of Chapter 4.

1.5.3 $\nu = 2/5$

Yet another example of the relevance of multicomponent FQH states presents itself at the filling factor $\nu = 2/5$ described by the state Ψ_{332} . It is an eigenstate of the Casimir operator for the

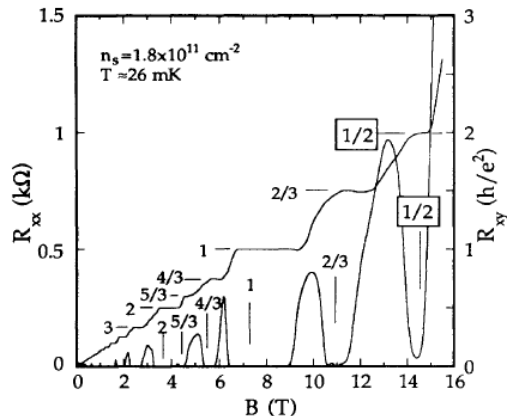


Figure 1.12: Quantum Hall effect at $\nu = 1/2$ in the wide quantum well. [7]

SU(2) group which is easy to prove noting that an overall Laughlin-Jastrow factor $\prod_{i<j}(Z_i - Z_j)^2$ can be factored out of the wave function (Z 's describes electrons of both spins), leaving two Slater determinants for \uparrow and \downarrow which trivially satisfy the Fock cyclic condition. [117] Therefore Ψ_{332} , being a spin-singlet, is an equally valid candidate for an unpolarized spin state (since the populations are balanced, $N_\uparrow = N_\downarrow$), as well as for a bilayer state where SU(2) symmetry is broken at a finite distance between the layers. [114] There exists also a polarized CF state with two filled CF Λ levels, (1.36). [16]

When the SU(2) symmetry is conserved and in the absence of Zeeman effect, the ground state of the single layer is the Halperin 332 wave function (1.45) [120] but the energy splitting between the unpolarized and the first excited polarized state is extremely small, which is also seen in variational calculations. [16] Therefore there is a transition from an unpolarized to the CF state above a critical value of the Zeeman energy Δ_z , which was observed in the experiments. [121, 122]

In Sec. 1.3.2 we mentioned a so-called Gaffnian state which is also realized at the filling factor $\nu = 2/5$. Since this state derives from a nonunitary CFT, it is not likely that it describes the polarized $\nu = 2/5$ state which is one of the strongest experimentally observed fractions. However, both Gaffnian and Jain states are intimately related to the Halperin 332 state. This connection is obvious in the following manner of writing down the wave function of the Gaffnian, [114, 123]

$$\Psi_{\text{Gaff}} = \mathcal{A} \left\{ \text{perm} \left(\frac{1}{z_{i\uparrow} - z_{j\downarrow}} \right) \Psi_{332}(\{z_\uparrow, z_\downarrow\}) \right\}, \quad (1.55)$$

as an antisymmetrized product of a 332 state and a permanent, the determinant with plus signs. Reminiscent of a transition driven by tunneling between the 331 state and the Pfaffian discussed in Sec. 1.5.2, in a bilayer system at $\nu = 2/5$ one can envision a transition between the unpolarized 332 state and the polarized Jain CF state. In principle, there is a possibility for Gaffnian to play a role of a critical state during this transition, as we discuss in Section 4.2.

1.5.4 $\nu = 1/4$

Recently, Luhman *et al.* [8] reported experimental observations of the $\nu = 1/4$ LLL state possibly forming in a wide quantum well when the magnetic field is tilted, Fig. 1.13. This experiment suggests that $\nu = 1/4$ state is of two-component origin because it emerges with the increase of a parallel component of the magnetic field B_{\parallel} that leads to the decrease of Δ_{SAS} . It was seen

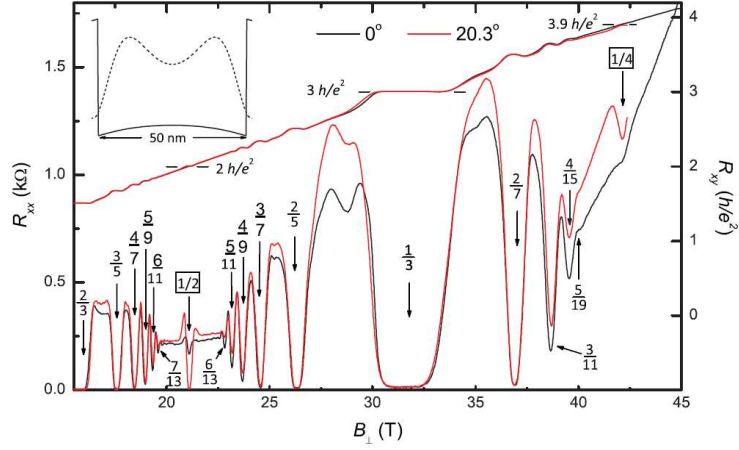


Figure 1.13: Quantum Hall effect at $\nu = 1/4$ in the presence of parallel magnetic field. [8]

that $\nu = 1/2$ behaves in a similar way, presumably due to being described by the 331 Halperin state. However, unlike $\nu = 1/2$, $\nu = 1/4$ does not depend sensitively on the variation of the total density. Increasing the total density is expected to make the system more bilayer-like and thus stabilize the two-component state.

In the experiments of Shabani *et al.* [9], instead of tilting the magnetic field, a charge imbalance was created in a wide quantum well. It was claimed that this mechanism leads generally to the strengthening of even-denominator LLL states, in particular $\nu = 1/2$ and $1/4$, Fig. 1.14.

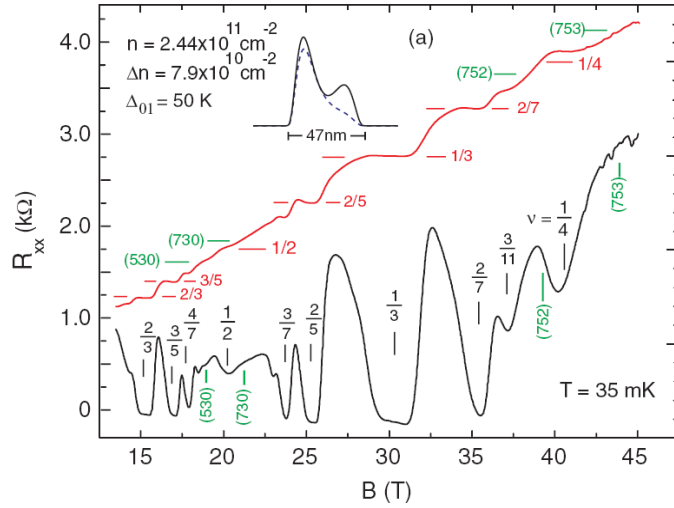


Figure 1.14: Quantum Hall effect at $\nu = 1/2$ and $\nu = 1/4$ under density imbalance. [9]

In wide quantum wells, applying density imbalance leads to the increase of Δ_{SAS} , which enables the tuning of the system between the single-component and two-component regimes. For certain densities, a minimum in R_{xx} was found at $\nu = 1/2$ which disappears with the imbalance, [124] consistent with the behavior expected for the 331 Halperin state. However, a surprising result shown in Fig. 1.14 is that even for densities which do not show evidence of an incompressible state in the balanced case, the extreme imbalance leads to an emerging minimum in R_{xx} . Possible candidates for such a state are the Moore-Read Pfaffian [125] or imbalanced two-component CF

1. INTRODUCTION

states. [126]

At $\nu = 1/4$ one can construct more than one Halperin's wave function. Some likely possibilities would be Ψ_{553} , Ψ_{771} and a state which explicitly breaks the $\uparrow - \downarrow$ symmetry, $\Psi_{5,13,1}$. Because of the very high correlation exponents, the latter two possibilities are very unlikely as they lead to the charge density wave. The upper bound for the stability of bilayer states is determined by the component of the lower filling factor. In these cases, both $1/7$ or $1/13$ are sufficiently low so that Wigner crystal may be favored over the incompressible liquid. Moreover, there is a polarized candidate in analogy to the Moore-Read Pfaffian (1.38), $\Psi_{\text{Pf}}^{1/4} = \text{Pf} [1/(z_i - z_j)] \prod_{i < j} (z_i - z_j)^4$. Thus, the experiments of Luhman *et al.* and Shabani *et al.* implicitly suggest that there may be a possibility to observe non-Abelian FQH states in the LLL if the sample has a special geometry or is subject to especially tuned external fields. Chapter 5 presents a detailed study of $\nu = 1/2$ and $\nu = 1/4$ states in the wide quantum well.

1.5.5 Graphene

As a final example of multicomponent systems, we mention graphene, a one-atom-thick layer of graphite, where "relativistic" QHE was recently seen. [39, 40] Electrons in graphene are described by a relativistic 2D Dirac equation [127] and due to different Landau quantization, the resistance plateaus are found at $n = 2(2n' + 1)$, in terms of an integer n' , i.e. with $n = \pm 2, \pm 6, \pm 10, \dots$ Furthermore, a FQHE with $n = 1/3$ has very recently been observed. [128, 129] From the electronic point of view, graphene is either a zero-overlap semimetal or a zero-gap semiconductor, where the conduction and the valence bands are no longer separated by an energy gap. Indeed, in the absence of doping, the Fermi energy lies exactly at the points where the valence band touches the conduction band and where the density of states vanishes linearly. In order to vary the Fermi energy in graphene, one usually places a graphene flake on a 300nm thick insulating SiO_2 layer which is itself placed on top of a positively doped metallic silicon substrate. In contrast to 2D electron gases in semiconductor heterostructures which have mobilities on the order of 10 million cm^2/Vs , the mobilities achieved in graphene are rather low and typically on the order of $\mu \sim 10^4 - 10^5 \text{cm}^2/\text{Vs}$. Notice, however, that these graphene samples are fabricated in the so-called exfoliation technique, where one "peels" thin graphite crystals, under ambient conditions, whereas the highest-mobility GaAs/AlGaAs laboratory samples are fabricated with a very high technological effort.

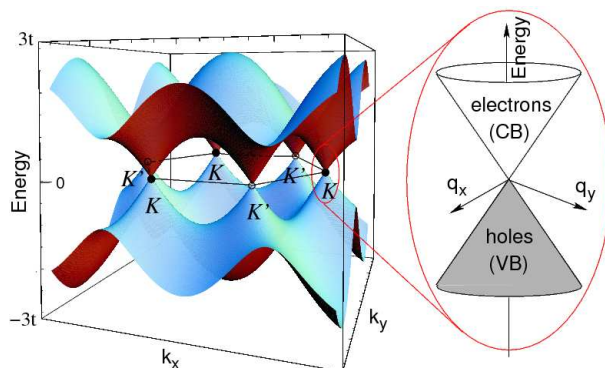


Figure 1.15: Energy bands of graphene.

The band structure of graphene is described by the honeycomb lattice due to the sp^2 hybridization of the valence electrons. It is a triangular Bravais lattice with a two-atom basis $\{A, B\}$. In a tight-binding model, where one considers electronic hopping between nearest-neighbouring sites (for a site A , the nearest neighbors are B sites and *vice versa*) with a hopping amplitude t , the effective Hamiltonian is purely off-diagonal in \mathbf{k} -space and gives rise to two bands labeled by $\lambda = \pm$, plotted in Fig. 1.15. The valence band $\lambda = -$ touches the conduction band ($\lambda = +$) in the two inequivalent corners K and K' of the first Brillouin zone. The Fermi energy lies exactly

in the contact points K and K' of the two bands unless the graphene sheet is doped. The inset in Fig. 1.15 shows the band dispersion in the vicinity of the contact points K and K' , the linearity of which is sufficient to describe the low-energy electronic properties in graphene. The conical form of the two bands is reminiscent of that of relativistic particles, which is also obvious from the Dirac form of the Hamiltonian when it is expressed around K point, $H = v\sigma \cdot \mathbf{p}$. In the continuum description of electrons in graphene we have two electron types, for the K and K' point, which is the *valley* degeneracy. Together with the usual spin degeneracy, graphene is implicitly a four-component system which is therefore characterized by a wave function which is a $SU(4)$ -spinor. The energy scale for lifting the valley/spin degeneracy are similar and much smaller than the one set by the Coulomb interactions. $SU(K)$ internal symmetry (approximately realized in some range of the system parameters) can nonetheless be described with a simple instance of the wave function (1.47) for $K = 4$ that is expected to describe quantized states in four-component systems. Note that the exponents n_{ij} and $n_{jj} \equiv m_j$ define a symmetric 4×4 matrix $M = (n_{ij})$, which determines the component densities ρ_j – or else the component filling factors $\nu_j = \rho_j/n_B$,

$$\begin{pmatrix} \nu_1 \\ \nu_2 \\ \nu_3 \\ \nu_4 \end{pmatrix} = M^{-1} \begin{pmatrix} 1 \\ 1 \\ 1 \\ 1 \end{pmatrix}. \quad (1.56)$$

Eq. (1.56) is only well-defined if the matrix M is invertible. If M is not invertible, some of the component filling factors, e.g. ν_1 and ν_2 , remain unfixed, but not necessarily the sum of the two ($\nu_1 + \nu_2$). This is a particular feature of possible underlying ferromagnetic properties of the wave function, [130] as we discussed in Sec. 1.4. The component filling factors in this context are those that arise naturally in FQHE studies, i.e. they are defined with respect to the *bottom* of the partially filled LL, in contrast to the graphene filling factor, ν_G , defined with respect to the *center* of $n = 0$ level. In order to make the connection between the two filling factors, one needs to choose

$$\nu = \nu_1 + \nu_2 + \nu_3 + \nu_4 = \nu_G + 2. \quad (1.57)$$

In Chapter 6 we consider some particular subclasses of the trial wave functions (1.47), which are natural candidates for a FQHE in graphene.

Chapter 2

Numerical studies of the FQHE

In this Chapter we set up the numerical (exact) diagonalization of the FQH problem in finite geometries. Throughout this thesis, by exact diagonalization (ED) we refer to the procedure where the Hamiltonian of the system, subject to particular boundary conditions, is represented in a convenient (finite) basis and its energy spectrum numerically evaluated using the computer. This method offers the possibility to study the quantum system in an unbiased manner and it was used since the early days of the FQHE, for example in working out the physical properties of the Laughlin wave function. [55] By now it has assumed the status of a standard tool in FQH studies where perturbative approaches are not guaranteed to work and physical properties expected in the thermodynamic limit can be identified already in very small systems. Although the energy spectrum itself offers substantial information about the physical system, it is furthermore possible to make direct comparison between the numerically-obtained eigenvector and the given trial wave function believed to describe the system's state. This amounts to evaluating a simple scalar product between the two vectors and we refer to it as the *overlap* calculation. Knowledge of the eigenvectors also allows one to calculate various operator mean values, propagators etc. The virtue of exact diagonalization is its versatility because it can be applied to any system. However, in practice the computational effort exponentially increases with the size of the system and therefore ED is usually restricted to small systems. Despite this, ED remains a powerful tool of choice for the theoretical studies of the FQHE.

Popular choices of the geometry in the FQH literature have been the disk [56], the sphere [131] and the rectangle with periodic boundary conditions (torus) [132]. In this thesis we focus on the latter two geometries which do not have open boundaries and therefore are particularly useful in examining the bulk properties of incompressible FQH liquids. This Chapter will largely present an overview of the pioneering papers by Haldane [56, 131, 133] and their extensions. [16, 32, 35, 134]

2.1 Exact diagonalization: Sphere

The original insight of Haldane [131] was that the two-dimensional sheet containing electrons can be wrapped around the surface of a sphere, while the perpendicular (radial) magnetic field is generated by a fictitious Dirac magnetic monopole at the sphere's center. The single particle problem had previously been solved by Wu and Yang. [135, 136] We will quote the main results without derivation. A recent pedagogical summary containing some of the derivations is given in [16].

The magnetic flux through the surface of the sphere (measured in units of Φ_0), is quantized to be an integer and denoted by $N_\phi = 2Q$. The position of an electron is given by the spherical coordinates $R = \sqrt{Q}l_B, \theta, \phi$. Because of the rotational symmetry enforced by the choice of

2. NUMERICAL STUDIES OF THE FQHE

the geometry, the orbital angular momentum and its z -component are good quantum numbers, denoted by l and m , respectively. Due to the presence of the monopole, their allowed values are $l = |Q|, |Q| + 1, \dots$ and $m = -l, -l + 1, \dots, l$. Different angular momentum shells correspond to Landau levels in the spherical geometry. The degeneracy of each Landau level is equal to the total number of m values, i.e. $2l + 1$, it is obviously finite and increasing by two units for each successive Landau level. The single particle eigenstates are the monopole harmonics, denoted by Y_{Qlm} , which are a generalization of the familiar spherical harmonics for $Q = 0$. In the lowest Landau level, they reduce to

$$Y_{QQm} = \sqrt{\frac{2Q+1}{4\pi}} \binom{2Q}{2Q-m} (-1)^{Q-m} v^{Q-m} u^{Q+m}, \quad (2.1)$$

where u, v are the spinor variables [131]

$$u = \cos \theta / 2 e^{i\phi/2}, v = \sin \theta / 2 e^{-i\phi/2}. \quad (2.2)$$

The spinor variables are not independent because $|u|^2 + |v|^2 = 1$ and we can transform to a single z complex coordinate by stereographic mapping $z = 2Rv/u$, R being the radius of the sphere. The basis states are given by $z^m / (1 + |z|^2/4R^2)^{1+N_\phi/2}$, where the L_z momentum quantum number is $L_z = N_\phi/2 - m$. Note that if $N_\phi, R \rightarrow \infty$ (with N_ϕ/R^2 fixed), the sphere becomes effectively flat and the single particle states reduce to those on the disk, $z^m e^{-|z|^2/4}$.

For N electrons, the filling factor corresponding to the thermodynamic limit (1.8) is given by

$$\nu = \lim_{N \rightarrow \infty} \frac{N}{2|Q|}, \quad (2.3)$$

but in case of the finite system the relation (2.3) requires a slight modification:

$$N_\phi = \frac{1}{\nu} N - \delta, \quad (2.4)$$

which defines the so-called *shift*, δ . The shift is the topological number that characterizes each FQH state on the spherical surface. It is of order unity (e.g. the Laughlin state at $\nu = 1/3$ has $\delta = 3$) and it is required to specify the system in addition to the filling factor ν . In the thermodynamic limit of an infinite plane, the shift plays no role, but for a finite *sphere* it is a crucial aspect of the ED technique [56] as it can lead to an ‘‘aliasing’’ problem: at a fixed choice of (N_ϕ, N) , more than one quantum Hall state (having different ν, δ and, therefore, different physical properties) may be realized.

We are now in a position to set up the Hilbert space which contains the Slater determinants $|m_1, m_2, \dots, m_N\rangle = c_{m_1}^\dagger \dots c_{m_N}^\dagger |0\rangle$ built from the single-particle states labelled by m_i . It is often advantageous to exploit symmetries in order to reduce the dimension of the Hamiltonian matrix because we only consider translationally/rotationally invariant Hamiltonians. An obvious symmetry which is used in the construction of Hilbert space is the conservation of $L_z = \sum_i m_i$ component. In principle it is possible to demand full rotational symmetry and diagonalize the Hamiltonian in the invariant subspaces of the L^2 operator, but the numerical implementation of this symmetry is difficult. One can also use the symmetry under the discrete parity transformation $L_z \rightarrow -L_z$ in diagonalizing within $L_z = 0$ sector of the Hilbert space.

The general interacting Hamiltonian in the basis of states $|m_1, m_2, \dots, m_N\rangle$, expressed in second-quantized form, is given by

$$H = \frac{1}{2} \sum_{m_1, m_2, m_3, m_4 = -Q}^Q \langle m_1, m_2 | V | m_3 m_4 \rangle c_{m_1}^\dagger c_{m_2}^\dagger c_{m_4} c_{m_3}. \quad (2.5)$$

The interaction V usually is such that it depends solely on the relative coordinate and not the center of mass. This is the case for Coulomb (1.9) and any other physical interaction. Furthermore, if the interaction involves only two particles at a time, it is convenient to express the matrix element $\langle m_1, m_2 | V | m_3, m_4 \rangle$ in the following form

$$\langle m_1, m_2 | V | m_3, m_4 \rangle = \sum_{L=0}^{2Q} \sum_{m=-L}^L \langle Qm_1, Qm_2 | L, M \rangle V_{2Q-L} \langle L, M | Qm_3, Qm_4 \rangle \quad (2.6)$$

where the numbers V_{2Q-L} are called the *Haldane pseudopotentials* and can be directly evaluated (a useful formula for the Coulomb interaction in the LLL is given in [134]). Evaluated on the sphere, V_{2Q-L} represents the energy of two particles in a state with relative angular momentum L in the plane. Apart from geometrical Clebsch-Gordan coefficients $\langle L, M | Qm_i, Qm_j \rangle$, the set of $\{V_L | L = 0, \dots, 2Q\}$ uniquely specifies the interacting Hamiltonian in any one Landau level. If the particles are fermions, the only physically relevant pseudopotentials are those with odd $2Q - L$ because of the exchange antisymmetry. Using the algebra of the harmonic oscillator raising operators, it can be shown that the Fourier transform of the effective interaction V_{eff} of the n th LL projected to the LLL is simply related to the Fourier transform of the LLL interaction V : $V_{\text{eff}}(k) = \left[L_n\left(\frac{k^2}{2}\right) \right]^2 V(k)$. Therefore, as long as we remain in a single Landau level, the problem is uniquely specified by a simple sequence of numbers V_L . Another important insight also due to Haldane [56] was that specifying a few non-zero V_L 's defines special short-range Hamiltonians that uniquely produce certain FQH trial states as their zero-energy modes. The simplest example is the Laughlin state at $\nu = 1/3$ which is the unique, highest density zero mode of the following pseudopotential Hamiltonian:

$$V_1 > 0, V_3 = V_5 = \dots = 0 \quad (2.7)$$

This is the hard-core interaction that is represented by (1.22) in the real space. We can numerically obtain the ground state of the interaction (2.7), inserting (2.7) into the Hamiltonian (2.5) and choosing the proper shift $N_\phi = 3N - 3$. We will recover a unique zero-energy state with a gap controlled by the value of V_1 and a magneto-roton branch in the excitation spectrum, [59] the known facts from the physics of the Laughlin state (Sec. 2.2.1).

2.1.1 Example: Effect of finite thickness on the Laughlin $\nu = 1/3$ state

To illustrate the principle of numerical investigation, let us try to tackle the following simple problem: what is the effect of finite layer width on the $\nu = 1/3$ state. We can model the finite-width FQH system using the effective Zhang-Das Sarma interaction, (1.17). We evaluate the Haldane pseudopotentials for the ZDS interaction, numerically diagonalize the Hamiltonian (2.5) for several values of the width parameter d and obtain the exact eigenvectors $|\Psi_{\text{exact}}\rangle$. On the other hand, the ground state of the interaction (2.7) is just the Laughlin state $|\Psi_L\rangle$. By evaluating the scalar product between the two vectors, $\langle \Psi_L | \Psi_{\text{exact}} \rangle$, we can monitor how well the Laughlin wave function describes the exact ground state. We know that for $d = 0$ the overlap is very large (nearly 1), which means that the Laughlin wave function is an excellent representative of the ground state. More details on the numerical calculations are given in the Appendix. The results for several values of d are given in Fig. 2.1. We see that the overlap decreases with the thickness of the sample, which is consistent with the experiments that see the weakening of the Laughlin state in the samples of very wide width. In the inset to Fig. 2.1 we repeated the calculation for the first excited LL, using the effective interaction V_{eff} as we explained above. Here we may note that the Laughlin state is a much worse description of the exact state for small values of d . Indeed, for $N = 5$ particles we even obtain zero overlap. Small overlap usually means that we have a wrong candidate wave function. Zero overlap, on the other hand, means that we are testing wave functions of different symmetry, e.g. an incompressible $L = 0$ state

2. NUMERICAL STUDIES OF THE FQHE

(such as the Laughlin) against the compressible $L > 0$ state. However, for large d we see that the Laughlin state is stabilized. Thus, we can argue that finite width has the opposite effect on the Laughlin state in the two Landau levels: while it destabilizes the $\nu = 1/3$, it enhances (and may even be necessary for the appearance of) $\nu = 7/3$ state.

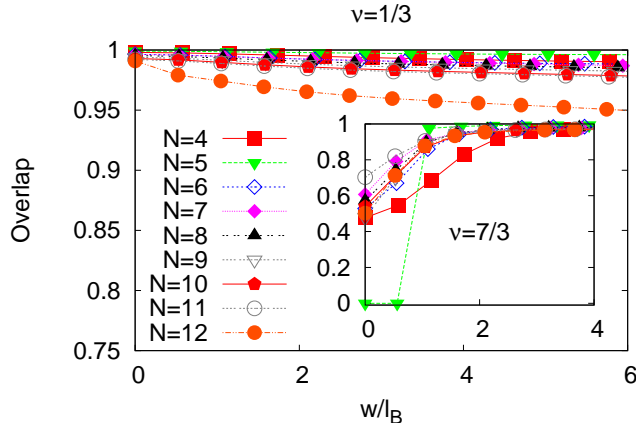


Figure 2.1: Overlap $|\langle \Psi_L | \Psi_{\text{exact}} \rangle|$ between the exact Coulomb state for finite width (ZDS model) at $\nu = 1/3$ and the Laughlin wave function $N = 4 - 12$ particles. [10] Inset: same quantity but in the first excited Landau level i.e. $\nu = 7/3$.

We would like to stress that in order to draw conclusions from the overlap calculations, one needs to assure that a range of system sizes has been studied that would allow at least a minimal finite-size scaling to be performed. The results should also be robust to the slight variation of the interaction parameters in order to be able to identify the phase of the system. Still, examples are known [94] where two fundamentally different trial states both have high overlaps with the exact state and it is not obvious which one is the wrong candidate. In such cases, the study should be complemented with the analysis of excitations, different choice of boundary conditions (Sec. 2.2) and/or alternative tools like the entanglement spectrum.

2.1.2 Entanglement spectrum on the sphere

The idea of entanglement, borrowed from the field of quantum information [137, 138, 139], provides a useful tool to study FQH states on the sphere [11] and torus [140]. Imagine that the sphere is divided at a line of latitude into two regions, A and B , so that $2Q + 1$ orbitals are partitioned into N_{orb}^A around the north pole and N_{orb}^B around the south pole. A general many-body state $|\psi\rangle$ can be decomposed on the product basis $\mathcal{H}_A \otimes \mathcal{H}_B$ involving a sum over the basis of subsystem A and a sum over the basis of subsystem B . We can alternatively perform a Schmidt decomposition (equivalent to the singular value decomposition of a matrix) of $|\psi\rangle$

$$|\psi\rangle = \sum_i e^{-\frac{1}{2}\xi_i} |\psi_A^i\rangle \otimes |\psi_B^i\rangle \quad (2.8)$$

where $\exp(-\frac{1}{2}\xi_i) \geq 0$, $|\psi_A^i\rangle \in \mathcal{H}_A$, $|\psi_B^i\rangle \in \mathcal{H}_B$, and $\langle \psi_A^i | \psi_A^j \rangle = \langle \psi_B^i | \psi_B^j \rangle = \delta_{ij}$, giving $\exp(-\frac{1}{2}\xi_i)$ as the singular values and $|\psi_A^i\rangle$ and $|\psi_B^i\rangle$ the singular vectors. If the state is normalized, $\sum_i \exp(-\xi_i) = 1$. The ξ_i 's can be thought of as the “energy levels” of a system with thermodynamic entropy at “temperature” $T = 1$. The entanglement entropy, $\mathcal{S} = -\sum_i \xi_i \exp(-\xi_i)$ i.e. the von Neumann entropy of the subsystem A , has been shown to contain information on the topological properties of the many-body state. [141] The full structure of the “entanglement spectrum” of levels ξ_i contains much more information than the entanglement entropy \mathcal{S} , a single number. This is analogous to the extra information about a condensed matter system given by its low-energy excitation spectrum rather than just by its ground state energy. For model states, such as Laughlin or Moore-Read, the low-lying part of the entanglement spectrum displays the

structure of the Virasoro levels of the corresponding conformal field theory, up to some limit set by the size of the spherical surface. The counting can be used as a fingerprint of topological order also in the generic states, such as Coulomb, which have much more complicated Slater decomposition than the model states. We illustrate this with the example of the entanglement spectrum for the exact ground state of the Coulomb interaction at $\nu = 5/2$, Fig. 2.2. A very large system of $N = 20$ is split in two parts with the same number of particles and number of orbitals. Because the FQH ground state is translationally and rotationally invariant (with quantum number $L_{tot} = 0$ on the sphere), and the partitioning of Landau-level orbitals conserves both gauge symmetry and rotational symmetry along the z -direction, in either block A or B both the electron number (N_e^A and N_e^B) and the total z -angular momentum (L_z^A and L_z^B) are good quantum numbers constrained by $N_e^A + N_e^B = N_e$, $L_z^A + L_z^B = 0$. The entanglement spectrum splits into distinct sectors labeled by N_e^A and L_z^A . The low-lying part of the entanglement spectrum (with the “banana”-like shape) displays the counting $1, 1, 3, 5, \dots$ which is the same as that of the Moore-Read state (we show the entanglement spectrum of the Moore-Read state in Chapter 5, Fig. 5.6). This result contributes to the belief that the generic $\nu = 5/2$ state is indeed described by the Pfaffian wave function. Furthermore, by changing the location of the cut, one can establish that there are exactly three nonequivalent countings that one may obtain and these correspond to the three topological sectors of the Ising CFT we mentioned in Sec. 1.3.2 (see also Sec. 2.2.1).

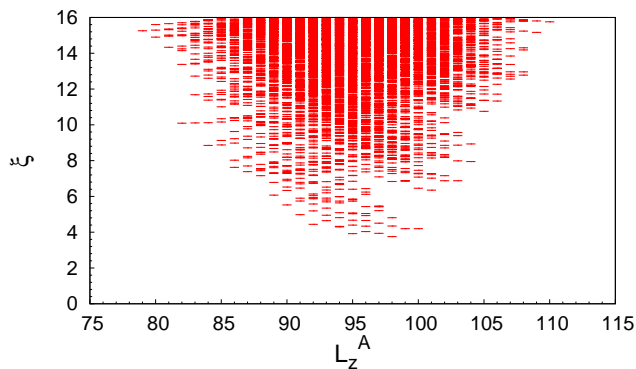


Figure 2.2: Entanglement spectrum for $N = 20$ electrons on the sphere, Coulomb interaction at the filling factor $\nu = 5/2$. The block A consists of $N_A = 10$ electrons and $l_A = 19$ orbitals, corresponding to the cut $[0|0]$ in Ref. [11].

2.1.3 Example: Multicomponent states in the $\nu = 1/4$ bilayer

We consider now a second example to illustrate the extension of ED formalism to the case when there is an internal degree of freedom. This degree of freedom can be represented by an ordinary $SU(2)$ spin or the layer/subband index in bilayer systems or wide quantum wells. The basis states are now specified by pairs of indices $|j_1, \sigma_1; j_2, \sigma_2; \dots; j_{N_e}, \sigma_{N_e}\rangle$, where $\sigma = \uparrow, \downarrow$ is the eigenvalue of the S_z projection of spin. If we are dealing with the physical spin, the Hamiltonian is additionally constrained to be an eigenstate of \mathbf{S}^2 operator of the total spin which acts as a Casimir operator for the $SU(2)$ group. In the application to bilayer systems where the $SU(2)$ symmetry is broken for any nonzero value of d (distance between the layers), \mathbf{S}^2 no longer commutes with the Hamiltonian and the maximal symmetry classification is provided by S_z . In addition, while working in the $S_z = 0$ subspace, it is possible to use the discrete symmetry $S_z \rightarrow -S_z$ to further reduce the dimension of the Hilbert space. Haldane’s pseudopotential formalism is straightforwardly extended to the spinful/bilayer case which yields two sets of interaction coefficients, V_L^{intra} and V_L^{inter} , for the intra and inter-layer interaction, respectively (we assume the layers are identical). We consider the filling factor $\nu = 1/4$ in the LLL, which was the subject of recent experiments [8], and for illustration purpose we analyze to what extent this state can

2. NUMERICAL STUDIES OF THE FQHE

be described by the multicomponent wave functions, $\Psi_{553} \equiv 553$, $\Psi_{771} \equiv 771$, introduced in Sec. 1.4.1. The experiment where $\nu = 1/4$ state was discovered was performed in a single wide quantum well which we will study within a more complete model in Chapter 5. We assume the system is effectively a bilayer, described by the interaction (1.49), and calculate overlap between the exact state and each of the trial states as a function of d , Fig. 2.3. The trial states are defined as the zero mode of the following potentials $V_{553}^{\text{intra}} = \{0, 1, 0, 1, 0, \dots\}$, $V_{553}^{\text{inter}} = \{1, 1, 1, 0, 0, \dots\}$ and $V_{771}^{\text{intra}} = \{0, 1, 0, 1, 0, 1, 0, \dots\}$, $V_{771}^{\text{inter}} = \{1, 0, 0, \dots\}$. 553 displays a familiar maximum [114] in the overlap for intermediate distance between the layers. The 771 overlap starts to increase with larger d , consistent with the large difference in the correlation exponents for intra and inter components. Since our numerics is performed in the spherical geometry, 771 appears as the usual incompressible state, but in the experiment this state would closely compete with the two coupled Wigner crystals. We cannot address this competition in the spherical diagonalization because this geometry is not adapted to assess states with broken translational symmetry. Note also that we cannot make a direct comparison between the Coulomb ground state overlap with each of the trial states, 553 and 771, because the latter are characterized by different shifts (2.4), $\delta = 5$ and $\delta = 7$ respectively. This examples illustrates the fundamental problem of the spherical geometry in describing the competition between different phases realized at the same filling factor, but characterized by different shifts.

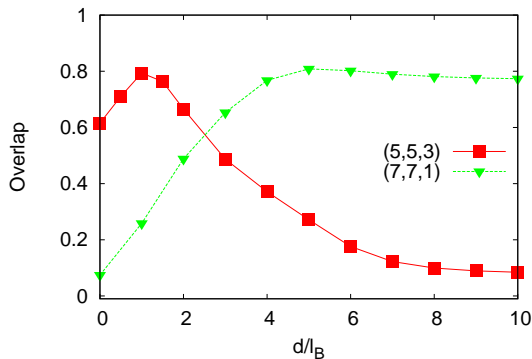


Figure 2.3: Overlap between the exact bilayer state with 553 and 771 states for $N = 8$ particles on the sphere. [12]

2.2 Exact diagonalization: Torus

If we choose to work in the Landau gauge $\mathbf{A} = (0, Bx, 0)$, a more convenient way to compactify the two-dimensional sheet of electrons is to apply the periodic boundary conditions. [32, 56, 132, 133] We assume that a finite number of electrons is placed in a unit cell $a \times b$. The single particle wave functions introduced in (1.5) need to be modified to comply with the magnetic translations along both axes, and they assume the form (setting $l_B = 1$)

$$\phi_j(\mathbf{r}) = \frac{1}{\sqrt{b}\sqrt{\pi}} \sum_{k=-\infty}^{\infty} \exp\{i(X_j + ka)y - (X_j + ka - x)^2/2\}, \quad (2.9)$$

where $X_j = 2\pi j/b$ and j ranges from 0 to $N_\phi - 1$. There are N_ϕ magnetic flux quanta through the surface of the torus defined by the condition we wrote down in (1.7): $N_\phi = ab/2\pi$. Because of this constraint, it is useful to introduce a single number r called the *aspect ratio*, defined as $r = a/b$, which fixes the geometry of the torus. Any two-body interaction depending on the relative distance between particles, $V(\mathbf{r})$, such as the Coulomb interaction, is conveniently made periodic by considering its Fourier transform $v(\mathbf{q})$

$$V(\mathbf{r}) = \frac{1}{ab} \sum'_{\mathbf{q}} v(\mathbf{q}) e^{i\mathbf{q}\mathbf{r}}, \quad (2.10)$$

where \mathbf{q} takes values in the first Brillouin zone $\mathbf{q} = (2\pi s/a, 2\pi t/b)$ (s, t are integers) and where $v(\mathbf{q}) = 2\pi e^2/\epsilon|\mathbf{q}|$ is the Fourier-transformed Coulomb interaction. The prime on the sum in (2.10) indicates that the $\mathbf{q} = 0$ component has been cancelled by the uniform positive background charge. Using (2.10) and (2.9), the matrix elements can be calculated [32] and the interaction part of the Hamiltonian is again defined by (2.5). Apart from the two-body interaction terms, the Hamiltonian contains the one-body terms which result from the interaction of the electrons with their mirror images (a consequence of the periodic boundary condition). These one-body terms depend only on the geometry of the torus and can be dropped from the Hamiltonian as long as the aspect ratio is held fixed.

As in the case of the spherical geometry, it is useful to use symmetries in order to reduce the dimension of the Hamiltonian matrix to be diagonalized, but instead of rotational symmetry one must consider on the torus the magnetic translations along the x and y axes. The full treatment of the magnetic translation symmetry in this context was first given by Haldane. [133] The magnetic translation operator acting on a particle j is defined as

$$T_j(\mathbf{L}) = \exp\left(-\frac{i}{\hbar} \mathbf{L} \cdot \mathbf{K}_j\right), \quad (2.11)$$

where the crystal momentum is $\mathbf{K}_j = -\mathbf{p}_j - eBy_j\mathbf{e}_x$. Consistency requires that encircling the torus around the perimeter of the unit cell produces an identity operation, which yields the condition $\mathbf{e}_z \cdot (\mathbf{a} \times \mathbf{b}) = 2\pi N_\phi$. Let us consider now a many-body system of N_e electrons and N_ϕ flux quanta, so the filling factor $\nu = N_e/N_\phi$ can be expressed in the reduced form $\nu = p/q$, where p, q are coprime numbers. Then we also have $N_e = pN', N_\phi = qN'$, where N' is the greatest common divisor of N_e and N_ϕ . The center of mass translation operator simply translates each of the particles independently, $\bar{T}(\mathbf{L}) = \prod_j T_j(\mathbf{L})$. If the single particle wave functions are to be unaffected by such a transformation, we find that the most general translation is for the vector

$$\mathbf{L} = \frac{1}{N_\phi} \mathbf{L}_{mn},$$

where $\mathbf{L}_{mn} = (ma, nb)$. Center of mass translations give rise to a degeneracy of q for each state at the filling factor $\nu = p/q$. [32, 133] Physical information is contained in the eigenvalues of the *relative* translations

$$\tilde{T}_j(\mathbf{L}) = \prod_i T_j(\mathbf{L}/N_e) T_i(\mathbf{L}/N_e). \quad (2.12)$$

It can be shown that the spectrum of the operators of relative translations \tilde{T}_j consists of N'^2 points in the inverse lattice, labeled by integers $s, t = 0, \dots, N' - 1$. These numbers are the fundamental quantum numbers that classify the physical eigenstates of the Hamiltonian. They are related to the physical momentum via

$$\mathbf{k} = \sqrt{\frac{2\pi}{N_\phi r}} [s - s_0, r(t - t_0)] \quad (2.13)$$

where (s_0, t_0) corresponds to the zero momentum fixed by

$$e^{i2\pi s_0/N'} = e^{i2\pi t_0/N'} = (-1)^{pq(N_e-1)}. \quad (2.14)$$

The incompressible states such as Laughlin's in this notation are characterized by $\mathbf{k} = 0$ ground state and a gap to all excitations. The construction of the symmetry-adapted basis proceeds

2. NUMERICAL STUDIES OF THE FQHE

by noting how the relative translations along the x and y direction act on the many-body state $|j_1, j_2, \dots, j_{N_e}\rangle$:

$$\tilde{T}_j(pmL_y \mathbf{e}_y)|j_1, j_2, \dots, j_{N_e}\rangle = \exp(i2\pi \frac{n}{N'}t)|j_1, j_2, \dots, j_{N_e}\rangle, \quad (2.15)$$

$$\tilde{T}_j(pmL_x \mathbf{e}_x)|j_1, j_2, \dots, j_{N_e}\rangle = |j_1 - qm, j_2 - qm, \dots, j_{N_e} - qm\rangle \quad (2.16)$$

where $t = \sum_i j_i \pmod{N'}$. We see from the above equation that, for each given t , states can be grouped into equivalence classes \mathcal{L} under the action of the x -translation. We therefore arrive at the following set of states, for each value of s and t ($0 \leq s, t \leq N' - 1$), that are the eigenstates of both translation operators:

$$|(s, t); \mathcal{L}\rangle = \frac{1}{\sqrt{|\mathcal{L}|}} \sum_{k=0}^{|\mathcal{L}|-1} \exp(i2\pi sk/N')|j_1 - qk, j_2 - qk, \dots, j_{N_e} - qk\rangle. \quad (2.17)$$

Therefore, we only need to diagonalize the Hamiltonian in each of the subspaces $|(s, t); \mathcal{L}\rangle$. Discrete symmetries relate some of those subspaces to each other and thus further reduce the range of s, t . Finally we stress that, contrary to the sphere, trial states on the torus are uniquely specified by their filling factor and there is no shift ($\delta = 0$).

2.2.1 Example: Abelian vs. non-Abelian states on the torus

We mentioned above that an incompressible state on the torus is characterized by $\mathbf{k} = 0$ pseudomomentum. In Fig. 2.4 we show an example of the low-lying energy spectrum for $N = 10$ electrons on the torus at the filling factor $\nu = 1/3$ and interacting with Coulomb and hard-core V_1 interaction (2.7). The latter interaction produces a unique zero-energy ground state with $\mathbf{k} = 0$, which is described by the Laughlin wave function, along with a characteristic magneto-roton branch of excitations. The high overlap between the ground states of the two interactions, as well as the general similarity of the low-lying spectra, is a convincing evidence that the Coulomb interacting state at $\nu = 1/3$ is the Laughlin state.

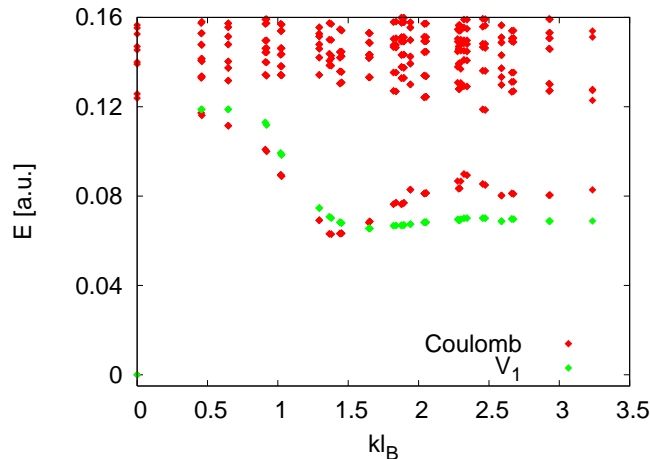


Figure 2.4: Low-energy part of the spectrum of the Coulomb interaction on the torus for $N = 10$ electrons at $\nu = 1/3$ and the aspect ratio 0.99. Energies are shown relative to the ground state and, for comparison, we also show the lowest states of the hard-core V_1 potential (2.7).

Furthermore, it is also possible to translate the Laughlin wave function (1.20) to the torus geometry [142] (see Ref. [143] for the examples of many quantum Hall wave functions translated into torus geometry). The expression for the filling factor $\nu = 1/m$ reads

$$\Psi_{\frac{1}{m}} = \vartheta_{(m-N_\phi)/2}^{\alpha/m+(N_\phi-m)/2m} \left(m \sum_i z_i/a |imb/a \right) \times \prod_{i<j} \vartheta_1((z_i - z_j)/a |ib/a)^m e^{-\frac{1}{2} \sum_i y_i^2}, \quad (2.18)$$

where $\vartheta_b^a(z|\tau) = \sum_n e^{i\pi\tau(n+a)^2 + 2\pi i(n+a)(z+b)}$ (sum over all integers) are the Jacobi theta functions and $\vartheta_1 \equiv \vartheta_{1/2}^{1/2}$ is the standard odd theta function. $\alpha = 0, 1, \dots, m-1$ gives the m degenerate states that differ by a translation of the center of mass only. The relative factor in Eq. (2.18) has been written down using a substitution $1/(z_i - z_j) \rightarrow \vartheta_1(z_i - z_j|\tau)$.

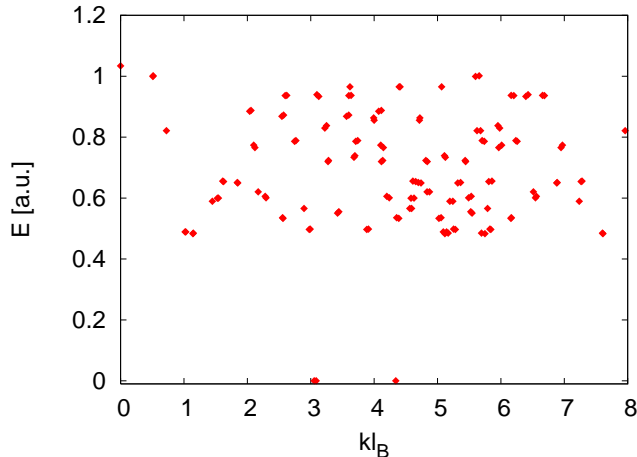


Figure 2.5: Low-energy part of the spectrum of the three-body Hamiltonian (1.41) on the torus for $N = 12$ electrons at $\nu = 1/2$ and aspect ratio 0.99. The three degenerate zero-energy states are characterized by $\mathbf{k} = (0, N'/2)$, $(N'/2, 0)$ and $(N'/2, N'/2)$.

For the non-Abelian states such as the Pfaffian, the construction above needs to be modified because direct substitution in the denominator $1/(z_i - z_j)$ in (1.38) invalidates the periodicity. The correct ansatz involves four Jacobi functions and reads

$$1/(z_i - z_j) \rightarrow \vartheta_\alpha(z_i - z_j|\tau)/\vartheta_1(z_i - z_j|\tau), \quad \alpha = 2, 3, 4 \quad (2.19)$$

which explicitly gives us *three* ground states. This is the topological degeneracy characteristic of the Moore-Read state. We can also recover this degeneracy by diagonalizing the 3-body Hamiltonian (1.41), Fig. 2.5. We find exactly degenerate states in the sectors with pseudo-momenta $\mathbf{k} = (0, N'/2)$, $(N'/2, 0)$ and $(N'/2, N'/2)$, unless we use a square or hexagonal unit cell which can mask the non-Abelian degeneracy because of additional geometric symmetries.

Topological degeneracy therefore can be a useful tool to discriminate between Abelian and non-Abelian trial wave functions in determining the nature of the generic (Coulomb) ground state. If we focus on the filling factor $\nu = 1/2$ or $2 + 1/2$, there are many candidate states including the obvious CFL (1.37), which is very sensitive to the variation of the unit cell shape and has no distinctive ground-state degeneracy. Other compressible phases, such as bubble and stripe phases, [69, 70, 83] are also possible. In Fig. 2.6 we show the energy spectrum of $N = 14$ electrons with the Coulomb interaction, in the LLL and second LL. We indicate the states that are expected to form the topologically degenerate multiplet. In contrast to $\nu = 1/2$ where the presence of other states obscures the degeneracy, at $\nu = 5/2$ we find the correct counting which is a necessary prerequisite for the Pfaffian state. Haldane and Rezayi [83] showed that varying the V_1 component of the Coulomb interaction can lead to further stabilization of this degeneracy and the increase of overlap with the Moore-Read wave function.

2.2.2 Example: Torus degeneracy of the 331 multicomponent state

Analysis of translation symmetry can be immediately generalized to the multicomponent states. We can construct multicomponent Halperin states (1.47) from the Chern-Simons theory using the so-called K -matrix [144] which turns out to be nothing else but a set of wave function

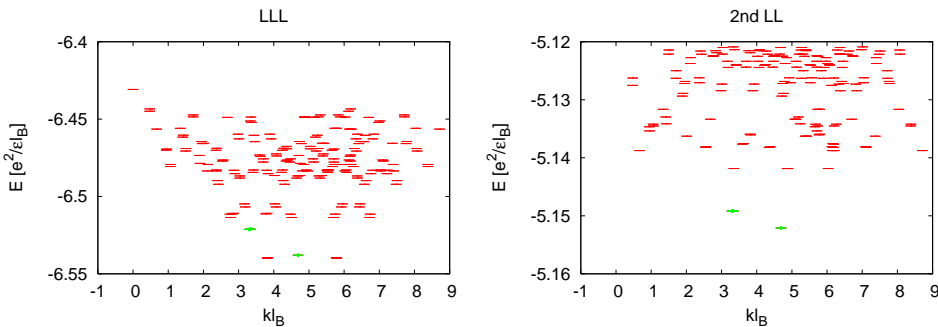


Figure 2.6: Energy spectrum of $N = 14$ electrons on the torus at $\nu = 1/2$ (left) and $\nu = 5/2$ (right), for the aspect ratio of 0.99

exponents $m_1, \dots, m_K; \{n_{ij}\}$. The torus degeneracy of such a state is given by

$$\det K = qN' \quad (2.20)$$

where q is the denominator of the filling factor that describes the overall center-of-mass degeneracy, while N' is an integer that accounts for the different translations of the centers of mass of the different components. The points which have parity invariance are $\mathbf{k} = (0, 0)$, $(0, N'/2)$, $(N'/2, 0)$, $(N'/2, N'/2)$ and therefore we can express N' as the sum of the number of $\mathbf{k} = 0$ states (N_0) and the number of states that lie on the zone boundary N_B . For homogeneous liquids, we have $N' = N_0 + 3N_B$. [145] For the 331 state, we have $q = 2$ and the associated K-matrix is given by

$$K = \begin{bmatrix} 3 & 1 \\ 1 & 3 \end{bmatrix}$$

which gives $\det K = 8$. The explicit form of the 331 wave function in the torus geometry is a straightforward generalization of (2.18) and can be found e.g. in Ref. [145]. Therefore, the multicomponent degeneracy that distinguishes the 331 state is 4 and the degenerate ground states are expected to have momenta $\mathbf{k} = (0, 0)$, $(0, N'/2)$, $(N'/2, 0)$, $(N'/2, N'/2)$. We can verify this fact to numerical precision using the pseudopotential interaction that produces the 331 state as the unique and densest zero mode. For Coulomb interaction, we expect the multiplet of states to be only approximately degenerate. Let us consider the Coulomb bilayer system at the filling factor $\nu = 1/2$ as a function of distance d . We assume that the tunneling between the layers is negligible and the layers are in balance, so $S_z = 0$ is a good quantum number. The Hamiltonian for each d is diagonalized in all the different \mathbf{k} sectors and the energies are plotted relative to the ground state at a given d , Fig. 2.7. We consider $N = 8$ particles and set the aspect ratio to $r = 0.99$, to avoid further degeneracies due to the special symmetry of the Brillouin zone. To track the evolution of the ground state, we highlight the states belonging to the momentum sectors of interest. We see that the tentative quadruplet of states for the 331 begins to form only beyond $d \geq l_B$. The multiplet structure is robust to variation of the aspect ratio of the torus, which eliminates the CFL as the other competing phase at the same filling factor (furthermore, CFL in the same-size system has additional degeneracies which are not seen in the spectrum of Fig. 2.7). This is consistent with the result in the spherical geometry which shows maximum overlap between the Coulomb state and the 331 for this range of d . However, on the sphere the overlap is not very low for smaller d 's and even for $d = 0$. The torus spectra clearly prove that the overlap on the sphere gives an incomplete picture because we also must be in the region of d which gives us the correct ground-state degeneracy. The two geometries, of course, should not give inconsistent results if a range of system sizes is considered and all the competing phases are properly taken into account.

If we are to calculate the overlap on the torus between the trial and an exact state, we must

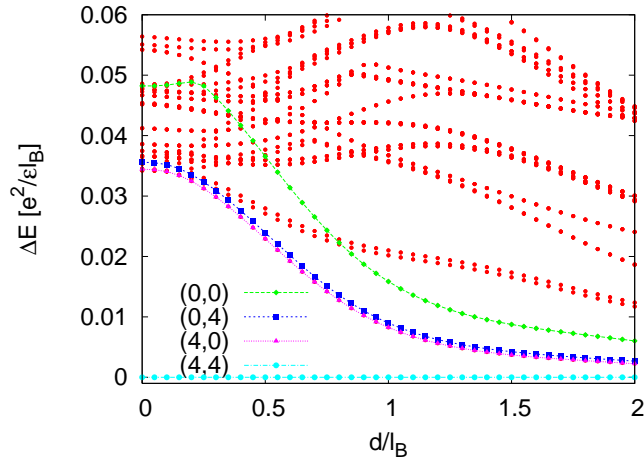


Figure 2.7: Quantum Hall bilayer at the filling factor $\nu = 1/2$ on the torus as a function of distance d (negligible tunneling). The energy spectrum for $N = 8$ electrons at the aspect ratio 0.99 is plotted relative to the ground state at each d and the states belonging to relevant momentum sectors are highlighted and connected as a guide to the eye.

take into account the ground state degeneracy in the following way:

$$|\langle \Psi_{\text{trial}} | \Psi \rangle|^2 \equiv \frac{1}{|\mathcal{S}_{\text{trial}}|} \sum_{\mathbf{k} \in \mathcal{S}_{\text{trial}}} |\langle \Psi_{\text{trial}}(\mathbf{k}) | \Psi(\mathbf{k}) \rangle|^2, \quad (2.21)$$

where $\mathcal{S}_{\text{trial}}$ stands for the degenerate subspace expected for $|\Psi_{\text{trial}}\rangle$. This amounts to adding together the overlap squared for each of the expected members in the ground state multiplet (normalizing the sum by the expected ground state degeneracy $|\mathcal{S}_{\text{trial}}|$ to be 1 at maximum) and the definition is obviously meaningful only in the case where we had previously established the correct level ordering in the spectrum.

2.3 Summary

In this Chapter we have presented an overview of the exact diagonalization procedure adapted to the spherical and torus geometries. Each of these geometries has its advantages and drawbacks. The sphere is particularly suited to establish whether the ground state is a homogeneous $\mathbf{L} = 0$ state and calculate its overlap with the given trial wave function. This task is computationally easier than on the torus because single particle wave functions are simple analytic polynomials, yielding a Hamiltonian matrix which is real and lends itself to the easy implementation of various symmetries. On the other hand, due to the bias of shift, it is not straightforward to compare different candidate wave functions describing the same filling factor on the sphere. One of the main advantages of the torus geometry is the nontrivial ground state degeneracy of non-Abelian and multicomponent states, which can be used as a fingerprint of a phase. The caveat, however, is the existence of an additional geometric parameter, the aspect ratio of the torus. The particular value of this parameter may favor one phase over the other and therefore a complete study should investigate a wide range of values for the aspect ratio, which makes a computational task much more involved.

Chapter 3

Quantum disordering of the quantum Hall bilayer at $\nu = 1$

Quantum Hall bilayer (QHB) at $\nu = 1$ continues to be the subject of many experimental and theoretical studies. Much of the physics has been well established in the extreme cases when the distance between layers, d , is (1) much smaller or (2) much larger than the magnetic length l_B . When $d \ll l_B$, i.e. inter and intra Coulomb interactions are about the same, the good starting point and description is the Halperin state Ψ_{111} (1.45). The physics in Ψ_{111} is of the exciton binding [25, 100]: an electron in one layer and a correlation hole directly opposite to it, in the other layer, are in a coherent quantum-mechanical superposition in the manner of the Ψ_{111} wave function. This exciton description can be a viewpoint of the phenomenon of superfluidity found in these systems [4] and is closely connected to the concept of composite bosons (CBs) [62] that can be used as natural quantum Hall quasiparticles in this system. When $d \gg l_B$ we have the case of the decoupled layers and the ground state (GS) is a product of two Fermi seas (1.37), $\Psi_{RR}(\{z_\uparrow\}) \times \Psi_{RR}(\{z_\downarrow\})$. The underlying quasiparticles are then CFs, the usual quasiparticles of the single layer quantum Hall physics. [16]. To address the range of intermediate d , when the system is a disordered superfluid, one may try to describe the basic physics by interpolating between the two limits or, in other words, to construct mixed states of CBs and CFs. [109] This is a phenomenological approach where we start from the identical electrons, split them into a group of those that correlate as composite bosons and a group of those that correlate as composite fermions. The wave function for the superfluid state at small d will involve mainly composite bosons; the disordering of the CB superfluid is caused by “nucleation” of CF quasiparticles as d is increased. In this Chapter we study such states using Chern-Simons theory. We begin by introducing the Chern-Simons approach for the Halperin 111 state, deriving its basic properties (such as the Goldstone mode and true ODLRO) and pointing out some of its weaknesses (Sec 3.1). We then generalize the theory to the mixed states of CBs and CFs (Sec. 3.2), study their basic response (Sec. 3.3) and investigate possible phases that these wave functions define as representatives of the universality classes, on the basis of analytic considerations and numerics (Sec. 3.4). This Chapter summarizes the main results of Refs. [13] and [112] and presents some new results of the numerical calculations (Sec. 3.4).

3.1 Chern-Simons theory for the Halperin 111 state

We have introduced the 111 Halperin state in (1.45). Here we show how this wave function can be obtained as the ground state of a Chern-Simons theory in a particularly transparent way and derive some of its basic physical properties. These conclusions were previously obtained in more powerful approaches such as the one in Ref. [103].

We begin with the bosonic Lagrangian density

$$\begin{aligned} \mathcal{L}_{111} = & \sum_{\sigma} \{ \phi_{\sigma}^{\dagger} (i\partial_t - a_0 + A_0 + \sigma B_0) \phi_{\sigma} - \frac{1}{2m} |(-i\nabla + \mathbf{a} + \mathbf{A} + \sigma \mathbf{B}) \phi_{\sigma}|^2 \} \\ & + \frac{1}{2\pi} a_0 (\nabla \times \mathbf{a}) - \frac{1}{2} \int d^2\mathbf{r}' \sum_{\sigma, \sigma'} \delta\rho_{\sigma}(\mathbf{r}) V_{\sigma\sigma'}(\mathbf{r} - \mathbf{r}') \delta\rho_{\sigma'}(\mathbf{r}') \end{aligned} \quad (3.1)$$

where ϕ is the bosonic field, $\sigma = \uparrow, \downarrow$ enumerates the layers, \mathbf{a} is a Chern-Simons gauge field, A_{μ} and B_{μ} are the external fields (the former couples to the charge and the latter couples to the pseudospin, e.g. B could be the electric field which is oppositely directed in the two layers). The interaction is defined by $V_{\sigma\sigma'}$ (for symmetry reasons, $V_{\uparrow, \uparrow} = V_{\downarrow, \downarrow}$ and $V_{\uparrow, \downarrow} = V_{\downarrow, \uparrow}$). Introducing $V_C = \frac{V_{\uparrow\uparrow} + V_{\downarrow\downarrow}}{2}$, $V_S = \frac{V_{\uparrow\uparrow} - V_{\downarrow\downarrow}}{2}$, the interaction part becomes diagonal:

$$-\frac{1}{2} \delta\rho V_C \delta\rho - \frac{1}{2} \delta\rho_S V_S \delta\rho_S, \quad (3.2)$$

where $\delta\rho \equiv \delta\rho_{\uparrow} + \delta\rho_{\downarrow}$ and $\delta\rho_S \equiv \delta\rho_{\uparrow} - \delta\rho_{\downarrow}$. Note that the Lagrangian density (3.1) in the limit $d \rightarrow 0$ has the SU(2) symmetry, but the presence of the term V_S breaks the symmetry down to U(1). The main disadvantage of our Lagrangian density is that it neglects the LLL projection.

For technical reasons it is simpler to work in Coulomb gauge [65] and a_0 integration yields the following constraint:

$$\nabla \times \mathbf{a} = 2\pi \delta\rho. \quad (3.3)$$

We treat the bosonic fields by the ansatz

$$\phi_{\sigma} = \sqrt{\bar{\rho}_{\sigma} + \delta\rho_{\sigma}} e^{i\theta_{\sigma}},$$

and introduce further notation $\theta \equiv \theta_{\uparrow} + \theta_{\downarrow}$, $\theta_S \equiv \theta_{\uparrow} - \theta_{\downarrow}$, $\delta\mathbf{a} \equiv \mathbf{a} + \mathbf{A}$, $\bar{\rho} \equiv \bar{\rho}_{\uparrow} = \bar{\rho}_{\downarrow}$. After Fourier transformation, the Lagrangian (3.1) splits into a part which contains only θ (the *charge* channel) and the part involving θ_S (the *pseudospin* channel):

$$\begin{aligned} \mathcal{L}_{111} = & \frac{i\omega}{2} \delta\rho\theta + \delta\rho A_0 - \frac{\bar{\rho}|\mathbf{k}|^2}{4m} \theta^2 - \frac{\bar{\rho}}{m} (\delta a)^2 - \frac{1}{2} \delta\rho V_C \delta\rho \\ & + \frac{i\omega}{2} \delta\rho_S \theta_S - \delta\rho_S B_0 - \frac{\bar{\rho}|\mathbf{k}|^2}{4m} \theta_S^2 - \frac{\bar{\rho}}{m} B^2 - \frac{1}{2} \delta\rho_S V_S \delta\rho_S, \end{aligned} \quad (3.4)$$

including the constraint (3.3). The parameter $\frac{\bar{\rho}}{m}$ is called the pseudospin stiffness (the phase fluctuations are described by an elastic term in the Lagrangian). In Eq. (3.4) we suppressed the dependence on the wave vector $k \equiv (\omega, \mathbf{k})$, so the quadratic terms $[X + Y]^2$ in fact stand for $[X(-k) + Y(-k)][X(k) + Y(k)]$.

As we mentioned above, our starting Lagrangian neglects the LLL projection and, owing to this, it splits into a charge and a pseudospin channel (the two channels would have been coupled had we performed the projection rigorously). For the charge channel only, it is easy to obtain a $\rho - \rho$ correlation function by Gaussian integration over θ and a . From this, similarly to (1.31), it is easy to see that the system is incompressible for $k \rightarrow 0$. The order is of algebraic type, just like in the single layer (1.35), because

$$\mathcal{L}_C = \frac{1}{2} \theta(-k) \frac{1}{4} \frac{\omega^2 - \omega_{\mathbf{k}}^2}{V_C(\mathbf{k}) + \left(\frac{2\pi}{|\mathbf{k}|}\right)^2 \frac{2\bar{\rho}}{m}} \theta(k), \quad (3.5)$$

where $\omega_{\mathbf{k}}^2 = \omega_C^2 + \frac{2\bar{\rho}}{m} |\mathbf{k}|^2 V_C(\mathbf{k})$ and $\omega_C = \frac{4\pi\bar{\rho}}{m}$, and we had set beforehand $A_{\mu} = 0$. The equal-time correlator is therefore

$$\langle \theta(-\mathbf{k}) \theta(\mathbf{k}) \rangle = -2 \times \frac{2\pi}{|\mathbf{k}|^2} + o(1/|\mathbf{k}|), \quad (3.6)$$

which is similar to the result for a single layer (1.34), and therefore the ODLRO

$$\lim_{|\mathbf{r}-\mathbf{r}'|\rightarrow\infty} \langle \phi^\dagger(\mathbf{r})\phi(\mathbf{r}') \rangle \propto \langle e^{i(\theta(\mathbf{r})-\theta(\mathbf{r}'))} \rangle \sim |\mathbf{r}-\mathbf{r}'|^{-2}, \quad (3.7)$$

is also algebraic. In the pseudospin channel the situation is more interesting. The effective Lagrangian in this case is

$$\mathcal{L}_S = \frac{1}{2}\theta_S(-k)\frac{\omega^2 - \frac{2\bar{\rho}}{m}V_S(\mathbf{k})|\mathbf{k}|^2}{4V_S(\mathbf{k})}\theta_S(k), \quad (3.8)$$

assuming that the external field $B_\mu = 0$ to avoid clutter. The correlator is then

$$\langle \theta_S(-\mathbf{k})\theta_S(\mathbf{k}) \rangle = \frac{4V_S(\mathbf{k})}{\omega^2 - \frac{2\bar{\rho}}{m}V_S(\mathbf{k})|\mathbf{k}|^2}. \quad (3.9)$$

From the pole of the correlation function we find the dispersion relation for the pseudospin mode:

$$\omega^0(\mathbf{k}) = \sqrt{\frac{2\bar{\rho}}{m}V_S(\mathbf{k})} \cdot |\mathbf{k}|, \quad (3.10)$$

which is the well-known acoustic mode from the theory of superfluids [65], also derived in Moon *et al.* [103]. In the long-wavelength limit we can estimate $V_S(\mathbf{k}) = \frac{1}{2\epsilon}(\frac{2\pi}{|\mathbf{k}|} - \frac{2\pi}{|\mathbf{k}|}e^{-|\mathbf{k}|d}) \approx \frac{\pi}{\epsilon}d$, plug in $m \approx 0.07m_e$, $\bar{\rho} \approx 2.5 \times 10^{10} \text{cm}^{-2}$, $d/l_B = 1.6$, $\epsilon = 12.6$, to conclude that the Goldstone mode obtained from the Chern-Simons theory exceeds the measured value [4] by as much as an order of magnitude, which illustrates the quantitative weakness of Chern-Simons theory.

The real-space correlation function for θ_S is

$$\langle \theta_S(\mathbf{r})\theta_S(\mathbf{r}') \rangle = \frac{1}{|\mathbf{r}-\mathbf{r}'|} \sqrt{\frac{md}{2\pi\epsilon\bar{\rho}}}, \quad (3.11)$$

which leads to the true ODLRO in the pseudospin channel:

$$\langle \phi^\dagger(\mathbf{r})\phi(\mathbf{r}') \rangle \propto \lim_{|\mathbf{r}-\mathbf{r}'|\rightarrow\infty} e^{(\theta(\mathbf{r})-\theta(\mathbf{r}'))} \longrightarrow \text{const.} \quad (3.12)$$

Therefore, in the pseudospin channel, the system is superfluid, compressible and possesses a linear (acoustic) mode which is the cause of the tunneling resonance in Spielman experiment. [4]

On the other hand, Halperin's 111 wave function also naturally follows from the Lagrangian (3.1). First we focus on the charge channel only. In this channel, θ and $\delta\rho$ are mutually constrained in a Berry-like term, which implies the commutation relation between them $[\theta(\mathbf{k}), \delta\rho(\mathbf{k}')] = 2i\delta(\mathbf{k} + \mathbf{k}')$. The Hamiltonian in the charge sector can be evaluated as [65]

$$\mathcal{H}_C = \frac{\bar{\rho}}{m} \left[\frac{|\mathbf{k}|^2}{4}\theta(-\mathbf{k})\theta(\mathbf{k}) + \left(\frac{2\pi}{|\mathbf{k}|}\right)^2\delta\rho(-\mathbf{k})\delta\rho(\mathbf{k}) \right] + \frac{1}{2}\delta\rho(-\mathbf{k})V_C(\mathbf{k})\delta\rho(\mathbf{k}). \quad (3.13)$$

Upon the substitution $\theta(\mathbf{k}) \rightarrow -2i\frac{\partial}{\partial\delta\rho(-\mathbf{k})}$, one can recognize the harmonic oscillator Hamiltonian and the ground state is therefore

$$\Psi_{\text{gs}} \propto \exp \left[-\frac{1}{2} \sum_{\mathbf{k}} \frac{2\pi}{|\mathbf{k}|^2} \delta\rho(-\mathbf{k})\delta\rho(\mathbf{k}) \right]. \quad (3.14)$$

Using $\delta\rho(\mathbf{r}) = \sum(\mathbf{r} - z_{i\uparrow}) + \sum(\mathbf{r} - z_{i\downarrow}) - \bar{\delta\rho}$, going to the real space (with some subtleties in integration, explained in Ref. [65]), we obtain that Ψ_{gs} is nothing but the modulus of Halperin's 111 wave function:

$$\Psi_{\text{gs}} = |\Psi_{111}|. \quad (3.15)$$

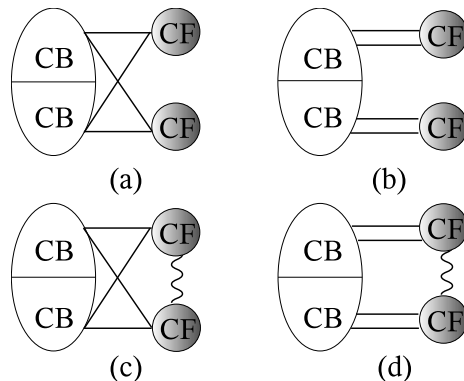


Figure 3.1: Universality classes of the wave functions Ψ_1 (a) and Ψ_2 (b), together with their paired versions, (c) and (d), respectively.

Thus we have obtained the ground state wave function in the bosonic picture. The original fermionic wave function can be obtained by an inverse Chern-Simons transformation, which in this case is given by

$$U = \prod_{i < j} \frac{z_{i\uparrow} - z_{j\uparrow}}{|z_{i\uparrow} - z_{j\uparrow}|} \prod_{k < l} \frac{z_{k\downarrow} - z_{l\downarrow}}{|z_{k\downarrow} - z_{l\downarrow}|} \prod_{m,n} \frac{z_{m\uparrow} - z_{n\downarrow}}{|z_{m\uparrow} - z_{n\downarrow}|}. \quad (3.16)$$

Upon acting by U we recover the full 111 wave function: $U\Psi_{\text{gs}} = \Psi_{111}$. If we take into account also the pseudospin channel, it can be shown [65] that its contribution is a simple constant for $d = 0$. For d nonzero, and especially towards $d \sim l_B$, the system experiences quantum fluctuations and its ground state begins to show significant deviations from the 111 state.

3.2 Trial wave functions for the quantum Hall bilayer

In the previous Section we have seen that the 111 state provides a description of the quantum Hall bilayer for $d = 0$ and perhaps small nonzero d 's. As d is increased towards $d \sim l_B$, the quantum fluctuations grow strong and the superfluid undergoes disordering. To describe the intermediate distances, we may try to, classically speaking, divide electrons into two groups, one in which the electrons are correlated as CBs and the other as CFs. [109] The ratio between the numbers of CBs and CFs would be determined by the distance between layers. The wave function constructed in this way would need an overall antisymmetrization in the end, but also intercorrelations among the groups as each electron of the system “sees” the same number of flux quanta through the system (equal to the number of electrons). This requires that the highest power of any electron coordinate is the same as the number of electrons in the thermodynamic limit. If we denote by a line the Laughlin-Jastrow factor $\prod_{A,B} (z_A - z_B)$ between the two groups of electrons, A and B ($A, B = CB, CF$), the possibilities for the QHB wave functions can be summarized as in Fig. 3.1.

If we ignore the possibility of pairing between CFs, [146] denoted by wiggly lines in Fig. 3.1(c) and Fig. 3.1(d), we have two basic families of the wave functions depicted in Fig. 3.1(a) and Fig. 3.1(b). The requirement that each electron “sees” the same number of flux quanta through the system equal to the number of electrons (as we are at $\nu = 1$) very much reduces the number of possible wave functions in the mixed CB - CF approach. We can consider, for example, the

possibility depicted in Fig. 3.1(a) which stands for the following wave-function in the LLL,

$$\begin{aligned}
 \Psi_1 = & \mathcal{P}_{LLL} \mathcal{A}_\uparrow \mathcal{A}_\downarrow \left\{ \prod_{i<j} (z_{i\uparrow} - z_{j\uparrow}) \prod_{k<l} (z_{k\downarrow} - z_{l\downarrow}) \prod_{p,q} (z_{p\uparrow} - z_{q\downarrow}) \right. \\
 & \times \mathcal{F}(w_\uparrow, \bar{w}_\uparrow) \prod_{i<j} (w_{i\uparrow} - w_{j\uparrow})^2 \times \mathcal{F}(w_\downarrow, \bar{w}_\downarrow) \prod_{k<l} (w_{k\downarrow} - w_{l\downarrow})^2 \\
 & \left. \times \prod_{i,j} (z_{i\uparrow} - w_{j\uparrow}) \prod_{k,l} (z_{k\uparrow} - w_{l\downarrow}) \prod_{p,q} (z_{p,\downarrow} - w_{q,\uparrow}) \prod_{m,n} (z_{m\downarrow} - w_{n\downarrow}) \right\}, \quad (3.17)
 \end{aligned}$$

where \mathcal{A}_\uparrow and \mathcal{A}_\downarrow denote the overall antisymmetrizations, $z_{i\sigma}$ are the coordinates of CBs in the layer $\sigma = \uparrow, \downarrow$ and $w_{i\sigma}$ are the coordinates of CFs in the layer σ . In the thermodynamic limit, the relation between the number of particles and flux quanta reads,

$$\begin{aligned}
 N_\phi^b &= N_{b\uparrow} + N_{b\downarrow} + N_{f\uparrow} + N_{f\downarrow}, \\
 N_\phi^{f\uparrow} &= 2N_{f\uparrow} + N_{b\uparrow} + N_{b\downarrow}, \\
 N_\phi^{f\downarrow} &= 2N_{f\downarrow} + N_{b\uparrow} + N_{b\downarrow}, \quad (3.18)
 \end{aligned}$$

where we denoted by N_ϕ^b and $N_\phi^{f\sigma}$ separately the number of flux quanta which electrons that correlate as CBs and CFs respectively see, $N_{b\sigma}$ and $N_{f\sigma}$ are the number of CBs and CFs inside the layer σ , respectively. The requirement constrains $N_\phi = N_\phi^b = N_\phi^{f\sigma}$, where N_ϕ is the number of flux quanta through the system. This leads to the additional requirement $N_{f\uparrow} = N_{f\downarrow}$ which leaves $N_{b\uparrow} - N_{b\downarrow}$ unconstrained, connected with the Bose condensation phenomenon that this wave function should be part of [13, 25, 100, 103].

The only additional way to introduce the correlations among the electrons is as follows:

$$\begin{aligned}
 \Psi_2 = & \mathcal{P}_{LLL} \mathcal{A}_\uparrow \mathcal{A}_\downarrow \left\{ \prod_{i<j} (z_{i\uparrow} - z_{j\uparrow}) \prod_{k<l} (z_{k\downarrow} - z_{l\downarrow}) \prod_{p,q} (z_{p\uparrow} - z_{q\downarrow}) \right. \\
 & \times \mathcal{F}(w_\uparrow, \bar{w}_\uparrow) \prod_{i<j} (w_{i\uparrow} - w_{j\uparrow})^2 \times \mathcal{F}(w_\downarrow, \bar{w}_\downarrow) \prod_{k<l} (w_{k\downarrow} - w_{l\downarrow})^2 \\
 & \left. \times \prod_{i,j} (z_{i\uparrow} - w_{j\uparrow})^2 \prod_{k,l} (z_{k\downarrow} - w_{l\downarrow})^2 \right\}. \quad (3.19)
 \end{aligned}$$

This wave function is depicted in Fig. 3.1(b). Whereas the intercorrelations in the first family in Fig. 3.1(a) are in the spirit of Ψ_{111} correlations, those in the second family in Fig. 3.1(b), represented by Ψ_2 , are in the spirit of the decoupled states, $\Psi_{RR} \times \Psi_{RR}$, where we correlate exclusively inside each layer. In this case the flux-counting reads:

$$\begin{aligned}
 N_\phi^{b\uparrow} &= N_{b\uparrow} + N_{b\downarrow} + 2N_{f\uparrow}, \\
 N_\phi^{b\downarrow} &= N_{b\uparrow} + N_{b\downarrow} + 2N_{f\downarrow}, \\
 N_\phi^{f\uparrow} &= 2N_{f\uparrow} + 2N_{b\uparrow}, \\
 N_\phi^{f\downarrow} &= 2N_{f\downarrow} + 2N_{b\downarrow}, \quad (3.20)
 \end{aligned}$$

which leads to the constraints $N_{b\uparrow} = N_{b\downarrow}$ and $N_{f\uparrow} = N_{f\downarrow}$.

We can imagine a mixture of both intercorrelations (of Fig. 3.1(a) and Fig. 3.1(b)) in a single wave function but these mixed states, by their basic response [13], fall into one of the universality classes depicted in Fig. 3.1. In Sec. 3.4 we will explicitly consider these possibilities and prove, in the scope of a CS theory, that the case Fig. 3.1(b) does not support a Goldstone (gapless) mode which exists for the state depicted in Fig. 3.1(a). These generalized states therefore belong to the universality class of the state depicted in Fig. 3.1(b) for which in the scope of CS theory we find in the low-energy spectrum only a gapped collective mode.[13]

3.3 Basic response of trial wave functions

A transport theory à la Drude [109] can easily be formulated for the wave functions (3.17) and (3.19) if we consider that CFs bind two quanta of magnetic flux, unlike CBs which bind only one quantum of magnetic flux. As long as we remain in the RPA approximation, they can all be treated as free particles moving in the presence of the effective field which is given by the sum of the external and self-consistently induced electric field. We neglect the projection to the LLL which is the arena where all the physics must be taking place. Nevertheless, we use the field theories established in the works of Zhang *et al.* [62] of CBs and Halperin *et al.* [15] for CFs because even analyses done in the advanced, LLL-projected-type of theories, in the work of Murthy and Shankar [147], came to the conclusion that the usual CS theories are qualitatively accurate. CS theories are known to yield correct physical picture and provide accurate quantum numbers and response functions, whereas they fail when it comes to calculating energies, gaps etc., which we saw in the previous Section in case of the velocity of the Goldstone mode. We furthermore neglect the overall antisymmetrization built in the classes of Fig. 3.1. We can justify this neglect (1) by taking the point of view that stems from similar situations with quantum Hall states like hierarchy and Jain's constructions that in the low-energy sector can be considered as multicomponent systems, [148] or (2) *a posteriori* because the results of the effective description of the classes in Fig. 3.1 are quite sensible and are expected for the states we are familiar with from the numerics (the state in our Fig. 3.1(a) was analyzed in [109]). (We do not ask a CS theory for detailed answers anyhow.)

To set up the Chern-Simons RPA approach, we consider the first case (Ψ_1), when the effective field as seen by particles in the layer σ is given by:

$$\mathcal{E}_f^\sigma = \mathbf{E}^\sigma - 2\epsilon \mathbf{J}_f^\sigma - \epsilon(\mathbf{J}_b^1 + \mathbf{J}_b^2), \quad (3.21)$$

$$\mathcal{E}_b^\sigma = \mathbf{E}^\sigma - \epsilon(\mathbf{J}_b^1 + \mathbf{J}_b^2 + \mathbf{J}_f^1 + \mathbf{J}_f^2), \quad (3.22)$$

where $\mathbf{J}_{f(b)}^\sigma$ denote Fermi- and Bose-currents in the layer σ and $\epsilon = \begin{bmatrix} 0 & R_K \\ -R_K & 0 \end{bmatrix}$, $R_K = \frac{\hbar}{e^2}$.

Transport equations are $\mathcal{E}_{f(b)}^\sigma = \rho_{f(b)}^\sigma \mathbf{J}_{f(b)}^\sigma$ and, as required by symmetry, $\rho_{f(b)}^\uparrow = \rho_{f(b)}^\downarrow$, while the total current is given by $\mathbf{J}^\sigma = \mathbf{J}_b^\sigma + \mathbf{J}_f^\sigma$. We define single layer resistance (ρ^{11}) and drag resistance (ρ^D) as follows:

$$\mathbf{E}^\uparrow = \rho^{11} \mathbf{J}^\uparrow, \quad (3.23)$$

$$\mathbf{E}^\downarrow = \rho^D \mathbf{J}^\uparrow. \quad (3.24)$$

When both layers have the same filling, $\nu_1 = \nu_2 = 1/2$, the tensors ρ_b, ρ_f are diagonal (because the composite particles are in zero net field) and $\rho_b = \text{diag}[\rho_{bxx}, \rho_{bxx}]$, $\rho_f = \text{diag}[\rho_{fxx}, \rho_{fxx}]$. In drag experiments we have additionally $\mathbf{J}^\downarrow = 0, \mathbf{J}^\uparrow$ -finite. Then from (3.21)-(3.24) via elementary algebraic manipulations [13], we can arrive at the following limits for the resistivities. At large d/l_B the number of CBs is small because the condensate is disordered and ρ_{bxx} is large compared to R_K , which is the typical Hall resistance. On the other hand, from the experiments [149] we know that generally $\rho_{fxx} \ll R_K$. Furthermore, even as d/l_B is decreased, we expect ρ_{fxx} to increase only slightly, [109] whereas ρ_{bxx} becomes very small in the superfluid phase. All in all, we have two characteristic limits: (1) the limit of small d/l_B when $\rho_{bxx} \ll \rho_{fxx} \ll R_K$, and (2) the large d/l_B limit when we can assume $\rho_{fxx} \ll R_K \ll \rho_{bxx}$. In the large d/l_B limit, we obtain asymptotically

$$\rho_{xx}^D \approx -\frac{2R_K^2}{\rho_{bxx}}, \quad \rho_{xy}^D \approx 4R_K \left(\frac{R_K}{\rho_{bxx}} \right)^2, \quad |\rho_{xx}^{11}| \approx |\rho_{xx}^D|. \quad (3.25)$$

The semicircle law follows directly from the previous formulas:

$$(\rho_{xx}^D)^2 + \left(\rho_{xy}^D - \frac{R_K}{2} \right)^2 \approx \left(\frac{R_K}{2} \right)^2, \quad (3.26)$$

in agreement with Fig. 1.11 and Ref. [150]. In the opposite limit (when d/l_B is reduced), $\rho_{bxx} \rightarrow 0$ and we obtain the quantization of Coulomb drag, [5, 151] $\rho_{xy}^D \approx R_K, \rho_{xx}^D \approx -\rho_{bxx}^2/(2\rho_{fxx}) \rightarrow 0$, which trivially satisfies the semicircle law. Thus, Ψ_1 can satisfy the semicircle law in the two asymptotic extremes.

Let us turn now to the case of Ψ_2 (3.19). From Fig. 3.1 the formulas for effective fields are modified into [13]:

$$\mathcal{E}_f^\sigma = \mathbf{E}^\sigma - 2\epsilon\mathbf{J}_f^\sigma - 2\epsilon\mathbf{J}_b^\sigma, \quad (3.27)$$

$$\mathcal{E}_b^\sigma = \mathbf{E}^\sigma - \epsilon(\mathbf{J}_b^1 + \mathbf{J}_b^2 + 2\mathbf{J}_f^\sigma). \quad (3.28)$$

In this case as well, there are two physically significant limits depending on the values of ρ_{bxx} and ρ_{fxx} . When $\rho_{bxx} \ll \rho_{fxx} \ll R_K$:

$$\rho_{xx}^D \approx -\frac{\rho_{fxx}}{2}, \quad \rho_{xy}^D \approx \frac{1}{4}\frac{\rho_{fxx}^2}{R_K}, \quad \rho_{xx}^{11} \approx \frac{\rho_{fxx}}{2}, \quad (3.29)$$

and the semicircle law (3.26) follows, whereas $|\rho_{xx}^D| = |\rho_{xx}^{11}|$. On the other hand, in the regime $\rho_{fxx} \ll R_K \ll \rho_{bxx}$, we have asymptotically

$$\rho_{xx}^D \approx -2\frac{\rho_{fxx}^2}{\rho_{bxx}^2}\frac{R_K}{\rho_{bxx}}R_K \ll R_K, \quad \rho_{xy}^D \approx R_K\frac{\rho_{fxx}^2}{\rho_{bxx}^2} \ll R_K, \quad (3.30)$$

which still satisfies the semicircle law, but on the same ‘‘side’’ (small ρ_{xx}^D, ρ_{xy}^D like in (3.29)). Thus in case of Ψ_2 we are able to derive only one limiting case of the semicircle law and we do not obtain the quantization of Hall drag resistance. We are unable to derive the entire semicircle law as e.g. ρ_{bxx} varies, neither for Ψ_1 nor Ψ_2 .

3.4 Chern-Simons theory for the mixed states

In this Section we construct a Chern-Simons theory inspired by the wave functions of the two families, (3.17) and (3.19). This is a phenomenological theory because, unlike the work of Zhang *et al.* [62, 63] and Halperin *et al.* [15], we will divide the electrons (which are of course identical particles) into different groups characterized by different flux attachment (some will correlate as bosons and the others as fermions), dropping the overall antisymmetrization. We expect nonetheless that this approach will yield a qualitatively correct picture when it comes to calculating the basic response of the system, which is the aim of the present Section. This way we will demonstrate, in the RPA approximation, that the states in Fig. 3.1(a) and Fig. 3.1(c) represent superfluids, and the states in Fig. 3.1(b) and Fig. 3.1(d) represent disordered superfluids, compressible and incompressible, respectively.

3.4.1 Case Ψ_1

Because of the flux counting relations (3.18), in formulating the Lagrangian density for the wave function Ψ_1 we need to take into account the following gauge field constraints:

$$\begin{aligned} \frac{1}{2\pi}\nabla \times \mathbf{a}^{F\sigma} &= 2\delta\rho^{F\sigma} + \delta\rho^{B\uparrow} + \delta\rho^{B\downarrow}, \\ \frac{1}{2\pi}\nabla \times \mathbf{a}^{B\sigma} &= \delta\rho^{F\uparrow} + \delta\rho^{F\downarrow} + \delta\rho^{B\uparrow} + \delta\rho^{B\downarrow}. \end{aligned} \quad (3.31)$$

In general we would need four gauge fields $\mathbf{a}^{F\sigma}, \mathbf{a}^{B\sigma}$, but in this particular case it is evident that only two of them are linearly independent: $\mathbf{a}_C = (\mathbf{a}^{F\uparrow} + \mathbf{a}^{F\downarrow})/2 = (\mathbf{a}^{B\uparrow} + \mathbf{a}^{B\downarrow})/2$ and $\mathbf{a}_S = (\mathbf{a}^{F\uparrow} - \mathbf{a}^{F\downarrow})/2$, and (3.31) expressed in the Coulomb gauge reads: $\frac{i|\mathbf{k}|a_C}{2\pi} = \delta\rho_\uparrow + \delta\rho_\downarrow \equiv \delta\rho$ and $\frac{i|\mathbf{k}|a_S}{2\pi} = \delta\rho^{F\uparrow} - \delta\rho^{F\downarrow} \equiv \delta\rho_S^F$ (a_C, a_S are the transverse components of the gauge fields).

3. QUANTUM DISORDERING OF THE QUANTUM HALL BILAYER AT $\nu = 1$

These are the constraints we wish to include into the functional integral via Lagrange multipliers a_0^C and a_0^S :

$$\mathcal{L}_{CS} = \frac{1}{2\pi} \frac{1}{2} a_0^C (\nabla \times \mathbf{a}_C) + \frac{1}{2\pi} \frac{1}{2} a_0^S (\nabla \times \mathbf{a}_S). \quad (3.32)$$

The full Lagrangian density in ‘‘God’s units’’ is given by [152]:

$$\begin{aligned} \mathcal{L} = & \sum_{\sigma} \{ \Psi_{\sigma}^{\dagger} (i\partial_0 - a_0^{F\sigma} + A_0 + \sigma B_0) \Psi_{\sigma} - \frac{1}{2m} |(-i\nabla + \mathbf{a}^{F\sigma} - \mathbf{A} - \sigma \mathbf{B}) \Psi_{\sigma}|^2 \} \\ & + \sum_{\sigma} \{ \Phi_{\sigma}^{\dagger} (i\partial_0 - a_0^{B\sigma} + A_0 + \sigma B_0) \Phi_{\sigma} - \frac{1}{2m} |(-i\nabla + \mathbf{a}^{B\sigma} - \mathbf{A} - \sigma \mathbf{B}) \Phi_{\sigma}|^2 \} \\ & + \mathcal{L}_{CS} - \frac{1}{2} \sum_{\sigma, \sigma'} \int d^2 \mathbf{r}' \delta \rho_{\sigma}(\mathbf{r}) V_{\sigma\sigma'} \delta \rho_{\sigma'}(\mathbf{r}'), \end{aligned} \quad (3.33)$$

where σ enumerates the layers, Ψ_{σ} i Φ_{σ} are composite fermion and composite boson fields in the layer σ and the densities are $\delta \rho_{\sigma} = \delta \rho_{\sigma}^F + \delta \rho_{\sigma}^B$. By \mathbf{A} (and \mathbf{B}) here we mean external fields in addition to the vector potential of the uniform magnetic field, $\mathbf{A}_{\mathbf{B}}$, which is accounted for and included in gauge fields $\mathbf{a}^{F(B)\sigma}$. The external fields \mathbf{A} and \mathbf{B} couple to charge and pseudospin, as before (Sec. 3.1). The interaction part of the Lagrangian is easily diagonalized by introducing $V_C = (V_{\uparrow\uparrow} + V_{\downarrow\downarrow})/2$ and $V_S = (V_{\uparrow\uparrow} - V_{\downarrow\downarrow})/2$. The strategy for integrating out the bosonic functions is the Madelung ansatz $\phi_{\sigma} = \sqrt{\rho_{\sigma} + \bar{\rho}_{\sigma}} e^{i\theta_{\sigma}}$, which expands the wave function in terms of a product of its amplitude and phase factor, while fermionic functions are treated as elaborated in Ref. [15]. After Fourier transformation, within the quadratic (RPA) approximation, and introducing substitutions $\delta \rho_C^i = \delta \rho_{\uparrow}^i + \delta \rho_{\downarrow}^i$, $\delta \rho_S^i = \delta \rho_{\uparrow}^i - \delta \rho_{\downarrow}^i$, $i = F, B$ and $\theta_C = (\theta_{\uparrow} + \theta_{\downarrow})/2$, $\theta_S = (\theta_{\uparrow} - \theta_{\downarrow})/2$, all the terms neatly decouple into a charge C and a pseudospin S channel. [13] This calculation is analogous to the one used for the 111 state in Sec. 3.1 and we obtain (using the compact notation explained there)

$$\begin{aligned} \mathcal{L}_C = & K_{00} (\delta a_0^C)^2 + K_{11} (\delta a_C)^2 + \frac{1}{2\pi} a_0^C i |\mathbf{k}| a_C - \\ & \delta \rho_C^B \delta a_0^C + \frac{i\omega}{2} \delta \rho_C^B \theta_C - \frac{\bar{\rho}_b}{m} \frac{|\mathbf{k}|^2}{4} \theta_C^2 - \frac{\bar{\rho}_b}{m} (\delta a_C)^2 - \frac{1}{2} \frac{|\mathbf{k}|^2 a_C^2}{(2\pi)^2} V_C \end{aligned} \quad (3.34)$$

$$\begin{aligned} \mathcal{L}_S = & K_{00} (\delta a_0^S)^2 + K_{11} (\delta a_S)^2 + \frac{1}{2\pi} a_0^S i |\mathbf{k}| a_S \\ & + \delta \rho_S^B B_0 + \frac{i\omega}{2} \delta \rho_S^B \theta_S - \frac{\bar{\rho}_b}{m} \frac{|\mathbf{k}|^2}{4} \theta_S^2 - \frac{\bar{\rho}_b}{m} B^2 - \frac{1}{2} V_S \left(\delta \rho_S^B + \frac{i|\mathbf{k}|}{2\pi} a_S \right)^2, \end{aligned} \quad (3.35)$$

where $\delta a_0^C \equiv a_0^C - A_0$, $\delta a_C \equiv a_C - A$, $\delta a_0^S \equiv a_0^S - B_0$, $\delta a_S \equiv a_S - B$, $\bar{\rho}_b$ is the mean density of bosons in each layer. $K_{00}(k)$ and $K_{11}(k)$ are the free-fermion correlation functions (density-density and current-current, respectively) in the RPA approximation. [17]

Focusing on the charge channel only, we can extract the density-density correlator defined in Eq. (1.31):

$$\pi_{00}^C(k) = \frac{\left(\frac{|\mathbf{k}|}{2\pi}\right)^2}{\frac{2\bar{\rho}_b}{m} - 2K_{11} + V_C \left(\frac{|\mathbf{k}|}{2\pi}\right)^2 - \frac{\left(\frac{|\mathbf{k}|}{2\pi}\right)^2}{\frac{2\bar{\rho}_b |\mathbf{k}|^2}{m\omega^2} - 2K_{00}}}. \quad (3.36)$$

In the limiting case $x \equiv m\omega/|\mathbf{k}|k_f \ll 1$, where n_f is the fermionic density, the density-density K_{00} and current-current K_{11} correlation functions are $K_{00} \approx \frac{m}{2\pi} (1 + ix)$, $K_{11} \approx -\frac{|\mathbf{k}|^2}{12\pi m} + i\frac{2n_f}{m} x$, and we conclude that as $\omega \rightarrow 0$ (and then $\mathbf{k} \rightarrow 0$) the system is incompressible in the charge channel, so long as there is a thermodynamically significant density of bosons $\bar{\rho}_b$.

In the pseudospin channel, we are primarily looking for the signature of a Bose condensate i.e. whether there exists a Goldstone mode of broken symmetry and what is the long range order of the state. The correlator is

$$\langle \theta_S(-k) \theta_S(k) \rangle = \frac{V_S}{\omega^2 \frac{1}{2} V_S + \alpha - \frac{2\bar{\rho}_b V_S}{m} |\mathbf{k}|^2}, \quad (3.37)$$

where $\alpha = \frac{1}{4}K_{00}^{-1} - K_{11}(\frac{2\pi}{|\mathbf{k}|})^2$. Indeed, there exists a Goldstone mode, albeit with a small dissipative term:

$$\omega^0(\mathbf{k}) = \sqrt{\frac{2\bar{\rho}_b V_S}{m}} |\mathbf{k}| - i \frac{V_S}{16\pi^{3/2} \sqrt{n_f}} |\mathbf{k}|^3. \quad (3.38)$$

In the above we have assumed n_f is nonzero. For $n_f = 0$ we obtain only the real part in Eq. 3.38, which is just the Goldstone mode of the 111 state. Note that introducing pairing among CFs (expected in the real system on the basis of analytical [108] and numerical work [110, 111]) removes the imaginary term [152].

Even for large x , it is easy to check that the pole remains at the same value if we assume $\bar{\rho}_b \gg n_f$ (which is, in fact, the most appropriate assumption in this case). Also, the imaginary term disappears in this case. Such a robust Goldstone mode implies the existence of a true ODLRO and the genuine Bose condensate. Goldstone mode $\omega^0(\mathbf{k})$, (3.38), is easily observed in Fig. 3.2, where we plotted the real part of density-density correlation function of the pseudospin channel $\pi_{00}^S(k)$, [13] in terms of parameters $Q \equiv |\mathbf{k}|/k_f$ and $x \equiv \omega/(|\mathbf{k}|k_f)$. Other (fixed) parameters are: $m = l_B = 1$, $d = 0.5$, $\epsilon = 12.6$, $V_S = \pi d/\epsilon$, $\bar{\rho}_b + n_f = 1/(4\pi)$, $\eta = n_f/\bar{\rho}_b = 1/10$.

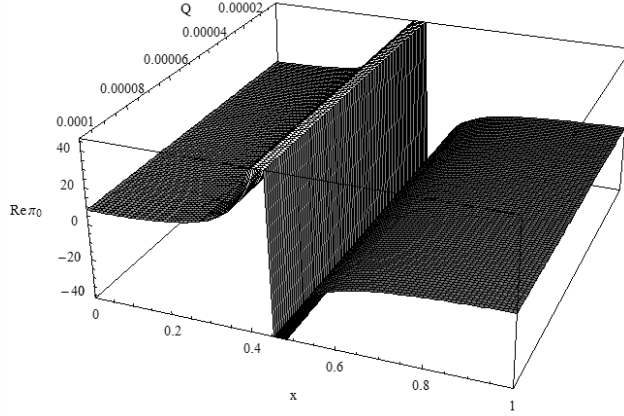


Figure 3.2: Real part of the pseudospin channel density-density correlation [13] and the Goldstone mode in the case of Ψ_1

3.4.2 Case Ψ_2

Let us return to the second case, that of Ψ_2 (3.19) and dominant intracorrelations. According to Fig. 3.1, we now have the following gauge field constraints:

$$\begin{aligned} \frac{1}{2\pi} \nabla \times \mathbf{a}^{F\sigma} &= 2\delta\rho^{F\sigma} + 2\delta\rho^{B\sigma}, \\ \frac{1}{2\pi} \nabla \times \mathbf{a}^{B\sigma} &= 2\delta\rho^{F\sigma} + \delta\rho^{B\uparrow} + \delta\rho^{B\downarrow}. \end{aligned} \quad (3.39)$$

It is obvious that in this case we have only 3 linearly independent gauge fields, namely $a_C = \frac{a^{F\uparrow} + a^{F\downarrow}}{2} = \frac{a^{B\uparrow} + a^{B\downarrow}}{2}$, $a_S = \frac{a^{F\uparrow} - a^{F\downarrow}}{2}$ and $a_{FS} = \frac{a^{B\uparrow} - a^{B\downarrow}}{2}$. The full Lagrangian is given by (3.33) where \mathcal{L}_{CS} is now

$$\mathcal{L}_{CS} = \sum_{i=C,S,FS} \frac{1}{2\pi} \frac{1}{2} a_0^i (\nabla \times \mathbf{a}_i).$$

Once again, the Lagrangian decouples into a charge and a pseudospin channel. The charge channel of Ψ_2 is incompressible. [13] In the pseudospin channel, the calculation of the density-density correlator leads to the conclusion that in this channel the system is compressible (see

also Fig. 3.3). The $\theta - \theta$ correlator is

$$\langle \theta_S(-k)\theta_S(k) \rangle = \frac{\frac{1}{|\mathbf{k}|^2}\beta\gamma}{\left(\frac{\omega}{2\pi}\right)^2(\beta + \gamma) - \frac{2\bar{\rho}_b}{m}\beta\gamma}, \quad (3.40)$$

where $\beta = \frac{1}{2K_{00}}\left(\frac{|\mathbf{k}|}{2\pi}\right)^2 + \frac{2\bar{\rho}_b}{m}$, $\gamma = V_S\left(\frac{|\mathbf{k}|}{2\pi}\right)^2 - 2K_{11}$. For small $|\mathbf{k}|/k_f$ and x , the correlator diverges for $\omega^0 = \frac{4\pi\bar{\rho}_b}{m} = \text{const}$, which obviously contradicts the original assumption for the range of x and hence we reject this pole. For $x \gg 1$ (and still $|\mathbf{k}| \ll k_f$) we obtain two poles:

$$\omega^0(\mathbf{k}) = \frac{4\pi n_f}{m} \sqrt{\frac{1}{2} + \eta - \frac{1}{2}\sqrt{1 + 4\eta}}, \quad (3.41)$$

$$\Omega^0(\mathbf{k}) = \frac{4\pi n_f}{m} \sqrt{\frac{1}{2} + \eta + \frac{1}{2}\sqrt{1 + 4\eta}}, \quad (3.42)$$

where $\eta = \bar{\rho}_b/n_f$ is the ratio of boson to fermion density. (3.41) and (3.42) hold for any η , although in the physical limit that we are presently interested in, η may be regarded as small. In Fig. 3.3 we plotted the real part of the density-density correlation function for the pseudospin channel of Ψ_2 . [13] In contrast to Fig. 3.2, here we opt for ω and Q as free parameters and set $d = 1.5$ and $\eta = \bar{\rho}_b/n_f = 1/10$ as the more likely values in this case. The distinctive feature of Fig. 3.3 at $\omega \cong 1$ is the plasma frequency Ω^0 and the smaller singularity at $\omega \cong 1/10$ corresponds to ω^0 . There is also a striking absence of Goldstone mode in this case.

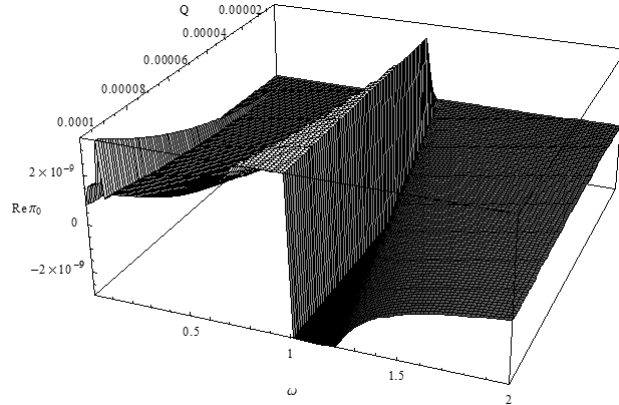


Figure 3.3: Real part of the pseudospin channel density-density correlation [13] in the case of Ψ_2

We now proceed to calculate the ODLRO in the pseudospin channel of Ψ_2 . As it turns out, ODLRO will be nontrivially modified and assume algebraic form. We expect that interaction does not affect the value of the characteristic exponent [63] and therefore set $V_S \equiv 0$. Bearing in mind that we work in the long wavelength limit, we arrive at the following expression for the correlator:

$$\langle \theta_S(-k)\theta_S(k) \rangle = \frac{(2\pi\omega_P/|\mathbf{k}|^2) [\omega^2 - \omega_P^2\eta]}{[\omega^2 - \omega^0(\mathbf{k})^2] [\omega^2 - \Omega^0(\mathbf{k})^2]}, \quad (3.43)$$

where we introduced $\omega_P = \frac{4\pi n_f}{m}$. After contour integration over ω [63], one obtains:

$$\langle \theta_S(-\mathbf{k})\theta_S(\mathbf{k}) \rangle = -\frac{2\pi}{|\mathbf{k}|^2} f(\eta)$$

where $f(\eta) = \frac{1}{\sqrt{1+4\eta}}$, which leads to the following expression for the ODLRO:

$$\langle e^{i\theta_S(\mathbf{r})} e^{-i\theta_S(\mathbf{r}')} \rangle \propto \frac{1}{|\mathbf{r} - \mathbf{r}'|^{f(\eta)}}. \quad (3.44)$$

For $\eta \rightarrow \infty$ when there are no CFs, the correlator (3.44) is a constant. However, Ψ_2 is expected to represent the system when η is small. In that case, even at $T = 0$, we obtain the algebraic ODLRO

$$\langle e^{i\theta_S(\mathbf{r})} e^{-i\theta_S(\mathbf{r}')}\rangle \approx |\mathbf{r} - \mathbf{r}'|^{-(1-2\eta+o(\eta^2))},$$

which indicates that Ψ_2 represents a disordered fluid, although possibly with some remaining intercorrelation.

3.4.3 Generalized states

We can imagine that, apart from Ψ_1 and Ψ_2 , we may have a state that contains a combination of both. We can analyze the response of the state which, in addition to Ψ_2 , includes (in each layer) a different kind of CFs that connect to the CB in the manner of Ψ_1 . This gives us the following gauge field constraints:

$$\frac{1}{2\pi} \nabla \times a^{B\sigma} = \delta\rho_{B\uparrow} + \delta\rho_{B\downarrow} + \delta\rho_{F\uparrow}^{(1)} + \delta\rho_{F\downarrow}^{(1)} + 2\delta\rho_{F\sigma}^{(2)}, \quad (3.45)$$

$$\frac{1}{2\pi} \nabla \times a_1^{F\sigma} = \delta\rho_{B\uparrow} + \delta\rho_{B\downarrow} + 2\delta\rho_{F\sigma}^{(1)} + 2\delta\rho_{F\sigma}^{(2)}, \quad (3.46)$$

$$\frac{1}{2\pi} \nabla \times a_2^{F\sigma} = 2\delta\rho_{B\sigma} + 2\delta\rho_{F\sigma}^{(1)} + 2\delta\rho_{F\sigma}^{(2)}, \quad (3.47)$$

where the superscripts (1), (2) indicate CF species in each layer. CS theory easily follows from the above gauge field equations and yields incompressible behavior in the charge channel. In the pseudospin channel [13] we can derive the following correlation function:

$$\langle \theta_S(-k) \theta_S(k) \rangle = \frac{V_S + \frac{2n_{f2}}{m} \left(\frac{2\pi}{|\mathbf{k}|}\right)^2}{\omega^2 - \left(\frac{2\bar{\rho}_b V_S}{m} |\mathbf{k}|^2 + \left(\frac{4\pi}{m}\right)^2 \bar{\rho}_b n_{f2}\right)} \quad (3.48)$$

to see that the low-energy spectrum is dominated by the plasma frequency:

$$\omega^0(k) = \frac{4\pi}{m} \sqrt{\bar{\rho}_b n_{f2}}, \quad (3.49)$$

where n_{f2} is the density of the CFs which bind exclusively within the layer they belong to. We conclude that the mixed state fall into the universality class of Ψ_2 .

3.5 Possibility for a paired intermediate phase in the bilayer

The classes of wave functions (3.17) and (3.19) (and their paired versions) represent possible outcomes of superfluid disordering in the quantum Hall bilayer before the system is in the phase of decoupled Fermi liquids. We now explain how these wave functions generalize the concept of superfluid disordering of the more traditional theories for small d/l_B (Sec. 3.5.1). The connection will be established on the basis of the predicted first-order (phonon) correction to the 111 state, which is expected to be universal at small d/l_B . In doing so, we identify a simple possibility for the pairing function at small d/l_B in our mixed state approach. Furthermore, a question can be asked whether, for larger $d \sim l_B$, the superfluid disordering in the bilayer can lead to an intermediary paired phase before the layers decouple and each forms a CF liquid. We discuss this question in Sec. 3.5.2 where we present one of the many candidate wave functions for such a phase. This wave function is singled out because it incorporates a pairing with the same angular momentum as the one we derived for small d/l_B (this form of pairing is also supported by numerical studies [110, 111]), but we argue that the phase it describes is likely compressible. We conclude by showing several numerical results for the transition which give some support to the scenario of a direct transition between the 111 phase and the CFL (Sec. 3.5.3).

3.5.1 First-order corrections to the 111 state

As we mentioned, for small d/l_B we expect our construction Ψ_1 to yield the same first-order correction to the 111 state as the other theories that evaluated this correction from the phonon contribution. As we start from the small d/l_B limit, the physical interpretation of the correction in our approach is the inclusion of CFs into the CB condensate.

The traditional [63] CS field theory in the RPA approximation [153] of the bilayer problem at $\nu = 1$ (which in the neutral channel reduces just to the problem of an ordinary superfluid with the phonon contribution) finds the following correction to the Ψ_{111} state [154]:

$$\Psi_{\text{ph}} = \exp \left\{ -\frac{1}{2} \sum_{\mathbf{k}} \frac{\sqrt{\frac{V_S(\mathbf{k})}{\bar{\rho}/m}}}{|\mathbf{k}|} \rho_{\mathbf{k}}^S \rho_{-\mathbf{k}}^S \right\} \Psi_{111} \quad (3.50)$$

where $\rho_{\mathbf{k}}^S \equiv \rho_{\mathbf{k}}^\uparrow - \rho_{\mathbf{k}}^\downarrow$, $V_S(\mathbf{k})$ is the interaction in the neutral channel, m is the electron mass and $\bar{\rho}$ is the uniform total density. The form of the correction in the pseudospin sector in Eq.(3.50) is easily derived along the same lines as in the case of Ψ_{111} , which belongs to the charge sector, in Eqs.(3.13,3.14). In the small d limit $V_S(\mathbf{k}) = \pi d$ and we can expand the expression Ψ_{ph} as

$$\Psi_{\text{ph}} = \Psi_{111} - \left(\sum_{\mathbf{k}} \frac{c\sqrt{d}}{|\mathbf{k}|} \rho_{-\mathbf{k}}^S \rho_{\mathbf{k}}^S \right) \Psi_{111} + \dots \quad (3.51)$$

where c is a positive constant. The terms after the first one represent corrections, in the order of importance, to the Ψ_{111} ansatz as d increases. The form of the correction is fixed by the basic phenomenology and sum rules for a superfluid in two dimensions. [155]

To show how the wave function Ψ_1 (3.17) generalizes the expansion (3.51), let us rewrite the unprojected wave function Ψ_1 in the following way:

$$\begin{aligned} \Psi_1 = & \mathcal{A}_\uparrow \mathcal{A}_\downarrow \left\{ \Psi_{111}(z_\uparrow, z_\downarrow) \Psi_{\text{RR}}(w_\uparrow) \Psi_{\text{RR}}(w_\downarrow) \right. \\ & \left. \prod_{i,j} (z_{i\uparrow} - w_{j\uparrow}) \prod_{k,l} (z_{k\uparrow} - w_{l\downarrow}) \prod_{p,q} (z_{i\downarrow} - w_{q\uparrow}) \prod_{m,n} (z_{m\downarrow} - w_{n\downarrow}) \right\}, \end{aligned} \quad (3.52)$$

where, as before, z_σ 's and w_σ 's denote coordinates of the electrons belonging to the layer with index σ and \mathcal{A}_\uparrow and \mathcal{A}_\downarrow , as before, stand for the antisymmetrizations. Ψ_{RR} was defined in (1.37).

Using \mathcal{S}_\uparrow and \mathcal{S}_\downarrow , symmetrizers inside each layer, the same function, Ψ_1 , can be written as:

$$\Psi_1 = \mathcal{S}_\uparrow \mathcal{S}_\downarrow \left\{ \frac{\prod_{k<l} (w_{k\uparrow} - w_{l\uparrow}) \prod_{p<q} (w_{p\downarrow} - w_{q\downarrow})}{\prod_{i,j} (w_{i\uparrow} - w_{j\downarrow})} \mathcal{F}(w_\uparrow) \mathcal{F}(w_\downarrow) \right\} \Psi_{111}$$

where Ψ_{111} denotes the Vandermonde determinant (Slater determinant in the LLL) of all coordinates in which all groups equally participate. By using the expressions for the densities of electrons in each layer, $\rho^\sigma(\eta) = \sum_i \delta^2(\eta - z_i^\sigma) + \sum_i \delta^2(\eta - w_i^\sigma)$, we can rewrite the wave function in the following way,

$$\begin{aligned} \Psi_1 = \int d^2\eta_{1\uparrow} \dots \int d^2\eta_{n\downarrow} & \left\{ \frac{\prod_{k<l} (\eta_{k\uparrow} - \eta_{l\uparrow}) \prod_{p<q} (\eta_{p\downarrow} - \eta_{q\downarrow})}{\prod_{i,j} (\eta_{i\uparrow} - \eta_{j\downarrow})} \right. \\ & \left. \mathcal{F}(\eta_\uparrow) \times \mathcal{F}(\eta_\downarrow) \times \rho^\uparrow(\eta_{1\uparrow}) \dots \rho^\downarrow(\eta_{n\downarrow}) \Psi_{111}(z_\uparrow, z_\downarrow) \right\}, \end{aligned} \quad (3.53)$$

where n is the total number of electrons that correlate as CFs. The equality is exact; any time we have in the product of ρ 's the same layer electron coordinate more than once, the Laughlin - Jastrow factors of η 's in the same layer force the wave function to become zero. This expression reminds us of a dual picture in terms of some quasiparticles with η coordinates as in [47]. It can be shown that these quasiparticles have to be fermionic. [112]

Now, by virtue of (3.53), we can see that the wave functions of Fig. 3.1(c) allow for the corrections to the 111 state which are more general than the one used in the expansion (3.51), the only

$g(z) = \text{const}$ (no pairing)	$\sum_{\mathbf{k}} f_1(d) \frac{1}{(k_x + ik_y)} \rho_{\mathbf{k}}^{\uparrow} \rho_{-\mathbf{k}}^{\downarrow}$
$g(z) = 1/z$	no correction when multiplies Ψ_{111}
$g(z) = \sqrt{z/\bar{z}}$	$\sum_{\mathbf{k}} f_2(d) \frac{1}{ \mathbf{k} } \rho_{\mathbf{k}}^{\uparrow} \rho_{-\mathbf{k}}^{\downarrow}$
$g(z) = 1/\bar{z}$	$\sum_{\mathbf{k}} f_3(d) \ln(\mathbf{k} l_B) \rho_{\mathbf{k}}^{\uparrow} \rho_{-\mathbf{k}}^{\downarrow}$

Table 3.1: Phonon correction for different choices of the pairing function. The functions f_1 , f_2 , and f_3 define the weight of each correction in terms of the bilayer distance d . In the first case (no pairing) the correction is proportional to $\sum_{\mathbf{k}} \frac{1}{(k_x + ik_y)} \rho_{\mathbf{k}}^{\uparrow} \rho_{-\mathbf{k}}^{\downarrow}$, but we expect that with no constraint on the number of CFs (as in Eqs.(3.50) and (3.51); see also discussion below Eq.(3.53)), this will correspond to $\sum_{\mathbf{k}} \frac{1}{(k_x + ik_y)} \rho_{\mathbf{k}}^S \rho_{-\mathbf{k}}^S$ i.e. zero (no correction) due to the antisymmetry under $\mathbf{k} \rightarrow -\mathbf{k}$ exchange.

constraint we need to satisfy is the equal number of $\rho_{\mathbf{k}}^{\uparrow}$'s and $\rho_{\mathbf{k}}^{\downarrow}$'s because in writing down the classes of Fig. 3.1 we explicitly distinguished \uparrow 's from \downarrow 's and fixed the number of \uparrow 's and \downarrow 's to be equal.

Let us compare the first phonon corrections in both approaches to find out which possibilities for pairing are allowed among the most simple choices for the weak pairing function. From the usual CS theory, the first phonon correction is $\sim \sum_{\mathbf{k}} \frac{1}{|\mathbf{k}|} \rho_{-\mathbf{k}}^{\uparrow} \rho_{\mathbf{k}}^{\downarrow}$. On the other hand, the mixed wave function in Fig. 3.1(c) suggests the following simplest correction for two CFs:

$$\int d^2\eta_{1\uparrow} \int d^2\eta_{2\downarrow} \frac{1}{(\eta_{1\uparrow} - \eta_{2\downarrow})} g(\eta_{1\uparrow} - \eta_{2\downarrow}) \rho^{\uparrow}(\eta_{1\uparrow}) \rho^{\downarrow}(\eta_{2\downarrow}), \quad (3.54)$$

where g is the pairing function. If we take the ‘‘obvious’’ choice $g(z) = 1/z$, we do not obtain any correction. This is because we need to evaluate

$$\int d^2\eta_{1\uparrow} \int d^2\eta_{2\downarrow} \frac{1}{(\eta_{1\uparrow} - \eta_{2\downarrow})^2} \rho^{\uparrow}(\eta_{1\uparrow}) \rho^{\downarrow}(\eta_{2\downarrow}), \quad (3.55)$$

which, after switching to center of mass/relative coordinate, reduces to solving the following Fourier transform

$$\int d^2\eta \frac{1}{\eta^2} \exp\{i\mathbf{k} \cdot \boldsymbol{\eta}\}. \quad (3.56)$$

This can be evaluated analytically [112] to find that it does not depend on \mathbf{k} :

$$\int d^2\eta \frac{1}{\eta^2} \exp\{i\mathbf{k} \cdot \boldsymbol{\eta}\} = -\pi. \quad (3.57)$$

Therefore the correction in this case is proportional to

$$\left(\sum_{\mathbf{k}} \rho_{\mathbf{k}}^{\uparrow} \rho_{-\mathbf{k}}^{\downarrow} \right) \Psi_{111}, \quad (3.58)$$

and in real (coordinate) space this becomes:

$$\begin{aligned} \int d^2\eta \rho^{\uparrow}(\eta) \rho^{\downarrow}(\eta) \Psi_{111} &= \sum_{i,j} \int d^2\eta \delta^2(\eta - z_{i\uparrow}) \delta^2(\eta - z_{j\downarrow}) \Psi_{111} \\ &= \sum_{i,j} \delta^2(z_{i\uparrow} - z_{j\downarrow}) \Psi_{111} = 0, \end{aligned} \quad (3.59)$$

i.e. no correction at all.

Taking the next choice $g(z) = \sqrt{z/\bar{z}}$ (\bar{z} is the complex conjugate of z), the expression in Eq.(3.54) reduces to the form of the first phonon contribution in the long-distance limit with the $\frac{1}{|\mathbf{k}|}$ singularity, (3.51). Thus $g(z) = \sqrt{z/\bar{z}}$ accommodates the usual (on the level of RPA) superfluid description given in (3.51), which which can lead also to a pseudospin density wave. [153]

Thus, we have shown that $g(z) = 1/z$ does not yield any correction to the 111 state (it can be shown analogously that $g(z) = \text{const}$ i.e. no pairing, also produces a trivial correction), while the choice $g(z) = \sqrt{z/\bar{z}}$ recovers the formula (3.51). We can continue exploring the simple choices for pairing, e.g. the next possibility in the order of weakness of pairing that retains the same angular momentum for the pairing as $g(z) = \sqrt{z/\bar{z}}$ is $g(z) = 1/\bar{z}$. The phonon contribution in this case turns out to be $\sim \sum_{\mathbf{k}} \ln(|\mathbf{k}|l_B) \rho_{\mathbf{k}\uparrow}^\dagger \rho_{-\mathbf{k}\downarrow}^\dagger$. [112] Therefore, we can summarize our results as in Table 3.1.

3.5.2 Discussion

Having identified some simple pairing functions allowed in the bilayer system starting from Ψ_1 and the small d/l_B , we can ask whether any of those may lead to a paired *phase* in the intermediate range of d/l_B . If the translation symmetry remains unbroken as we increase d , one of the viable candidates is a wave function in Fig. 3.1(d) with the pairing $g(z) = 1/\bar{z}$. This pairing has the same angular momentum as $g(z) = \sqrt{z/\bar{z}}$, but it also has an additional amplitude factor. If we take the choice $g(z) = 1/\bar{z}$ and examine the final form of the state of Fig. 3.1(d) when there are no CBs, we are lead to its following forms,

$$\begin{aligned} \tilde{\Psi}_2 &= \det \left(\frac{1}{\bar{z}_{i\uparrow} - \bar{z}_{j\downarrow}} \right) \prod_{i < j} (z_{i\uparrow} - z_{j\uparrow})^2 \prod_{k < l} (z_{k\downarrow} - z_{l\downarrow})^2 \\ &= \det \left(\frac{1}{\bar{z}_{i\uparrow} - \bar{z}_{j\downarrow}} \right) \det \left(\frac{1}{z_{k\uparrow} - z_{l\downarrow}} \right) \Psi_{111}, \end{aligned} \quad (3.60)$$

where we used the Cauchy determinant identity. The neutral part of $\tilde{\Psi}_2$ (i.e. the two determinants which do not carry a net flux through the system as Ψ_{111} does) can be viewed as a correlator of vertex operators of a single *nonchiral* bosonic field. According to [18] CFT correlators not only describe quantum Hall system wave functions, but also can be used to find out about excitation spectrum and connect to its edge and bulk theories. As customary in CFT applications in quantum Hall physics, we can construct (neutral) excitations in terms of vertex operators $e^{i\beta_1\phi(w, w^*)}$ and $e^{i\beta_2\theta(w, w^*)}$, where $\phi(w, w^*) = \phi(w) + \phi(w^*)$, $\theta(w, w^*) = \phi(w) - \phi(w^*)$, and $\phi(w)$ and $\phi(w^*)$ are holomorphic and antiholomorphic parts of the bosonic field respectively (see Ref. [112] for details). The insertion of these vertex operators corresponds to single-valued expressions that multiply Ψ_2 only if $\beta_2 = 1/2$. [112] If the low-lying spectrum were consisting of $\beta_1 = 1/2$ and $\beta_2 = 1/2$ quasiparticle excitations, the system would be described by the so-called BF Chern-Simons theory or the theory of 2D superconductor. [156] The mutual statistics of quasiparticles - quasiparticles and vortices, in this theory is semionic (due to the fact that vortices carry half-flux $h/2ec$ quantum) and that this is also the case with our excitations can be easily checked via CFT correlators. [112] Combining the analysis with the charge part (Ψ_{111}) in which only charge-1 excitations are allowed (half-flux quantum excitations are strongly confined [157]) we may come to the conclusion that the degeneracy of the system GSs on the torus must be 4. [156, 158] However, the expression for the first kind of excitations $e^{i\beta_1\phi(w, w^*)}$ allows a real continuum for the value of β_1 exponent including $\beta_1 = 0$ [112] and therefore we expect a compressible (gapless) behavior of the system despite the incompressibility of the charge channel, despite the seemingly topological behavior in the neutral sector.

3.5.3 Numerical results

There are many comprehensive numerical studies of the QH bilayer at $\nu = 1$. [109, 110, 111, 159, 160, 161] In particular, elaborate studies in Refs. [109, 111] demonstrated the relevance of CB-CF constructions that we introduced in Sec. 3.2 for the clean systems (no impurities). Trial wave functions of this kind describe a continuous crossover between the CB superfluid and the two decoupled CF liquids via an intermediate *p*-wave paired phase that in our analysis of Sec. 3.5.1 corresponds to $\tilde{\Psi}_2$, 3.60. Here we would like to focus on addressing the question whether

such a phase is allowed in numerics. This question is relevant in light of the new experimental results which indicate that the CF liquid phase in the usual samples is partially spin-polarized. [162] Since 111 state is a QH ferromagnet, the experiments appear to preclude the possibility of a smooth crossover and instead suggest a first-order transition. [163] For larger Zeeman fields, the transition becomes smooth and the critical point drifts to larger values of d . [162, 164]

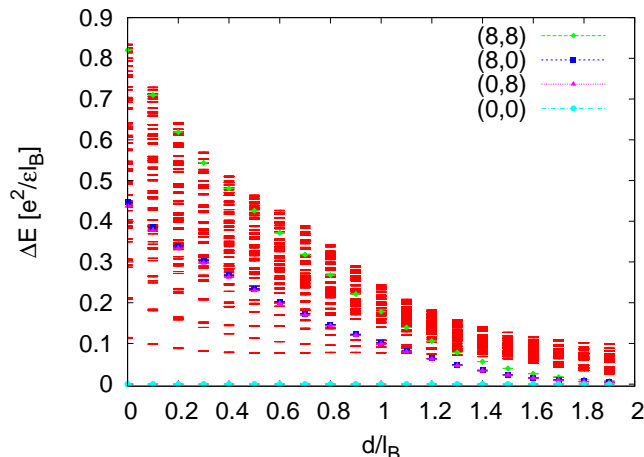


Figure 3.4: QH bilayer $\nu = 1$ on the torus, $N = 16$, $a/b = 0.99$.

The topological content of $\tilde{\Psi}_2$ is the 4-fold ground state degeneracy on the torus. In Ref. [111] this degeneracy was analyzed as a function of d and different shapes of the torus unit cell, but no definite conclusion was drawn due to the strong finite size effects. We corroborate this finding by diagonalizing a larger system of $N = 16$ particles, Fig. 3.4. Four seemingly degenerate states can be identified in the lowest lying spectrum starting from $d = 1.4l_B$, but the gap decreases smoothly with the increase of d , which suggests that these states could be part of the compressible CF liquid. Two decoupled CF liquids are allowed to display a fourfold degeneracy due to their center of mass motion. This degeneracy, contrary to the one of $\tilde{\Psi}_2$, has no topological content, but in a finite system it may nonetheless persist for some variation of the aspect ratio or other parameters.

On the other hand, if we choose to look at the system on the sphere, $\tilde{\Psi}_2$ is characterized by the shift $\delta = 1$, like the 111 state, whereas CF liquid state occurs at $\delta = 2$. Therefore, we are unable to directly compare e.g. the overlaps of the exact ground state with the 111 state and CF liquids. Instead, one must calculate a physical quantity which is meaningful in the thermodynamic limit to discriminate between phases. Ground state energy is an example of such a quantity; it defines the transition point d_C between the 111 state and CF liquids as the value of d/l_B above which the ground state energy is lower at the shift $\delta = 2$ than at $\delta = 1$. We have analyzed the ground state energies as a function of d for a range of system sizes $N = 6$ through $N = 16$, and for both shifts $\delta = 1, 2$, Fig. 3.5. The values for the energy in Fig. 3.5 include the background charge correction and the rescaling of the magnetic length in order to carefully compare the energies of the systems on the two different FQH spheres. We notice that beyond $d \sim 1.4l_B$, which we identified as the critical value for the appearance of 4-fold degeneracy on the torus, we can no longer describe the system at the shift of $\delta = 1$. Nevertheless, the two energies remain very close to each other and the paired wave function such as $\tilde{\Psi}_2$ is not ruled out as a candidate for the description of the system. It may either describe an excited state of the CF liquid or a phase with a tiny gap that would be hard to discern from an ordinary compressible state in the experiment. We obtain a more quantitative estimate of the critical $d_C \approx 1.6l_B$ by linear extrapolation for $N \rightarrow \infty$ (Fig. 3.6).

Therefore it is likely that the 111 phase goes directly into the CF liquids even at this finite value of d and not via the p -wave paired state. Note that we have not proved that we have a direct transition between the shift of the ground state ($\delta = 1$ vs. $\delta = 2$). In order to do that, one would

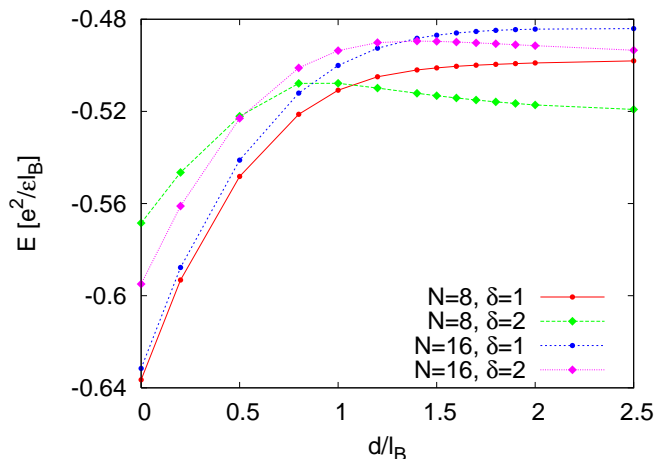


Figure 3.5: Ground state energies on the sphere for the QH bilayer at the shift of $\delta = 1$ and 2. We show the system of $N = 8$ (which has a filled CF shell in each layer) and the largest system with $N = 16$ electrons (without filled CF shells). Similar results are obtained for other system sizes.

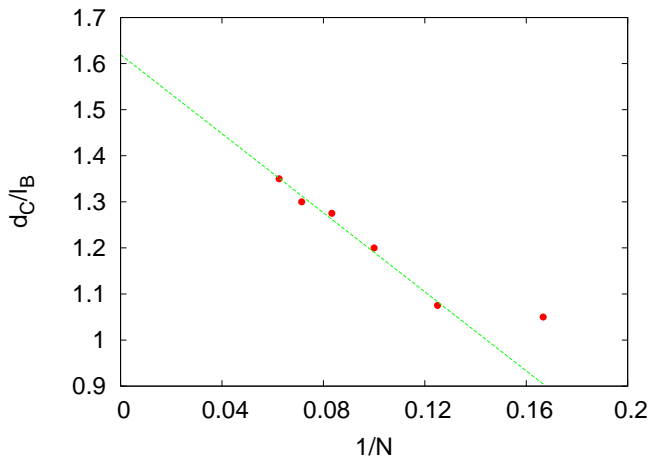


Figure 3.6: Critical bilayer distance d_C defined as the crossing point of the ground-state energies at shifts $\delta = 1$ and $\delta = 2$ on the sphere. Linear extrapolation for $N \rightarrow \infty$ yields $d_C \approx 1.6l_B$ and does not involve the smallest system $N = 8$ which shows strong finite-size effects.

want, for each fixed d , to diagonalize the Hamiltonian for all the available system sizes and make the thermodynamic extrapolation of the energies (with the appropriate corrections) as a function of $1/N$. While this works nicely for the shift of $\delta = 1$, in case of CF shift $\delta = 2$ the ground state energy has a nontrivial dependence on $1/N$ which reflects the shell-filling effect. The dependence of energy on $1/N$ is somewhat similar to Ref. [165], except that the energy minima occur for $N/2 = n^2, n = 2, 3, \dots$. In between the minima, the energy has a local maximum. Therefore, in order to perform a reliable extrapolation, a few minima/maxima would be required, but since we are only able to diagonalize up to $N = 16$, that gives us a single minimum $n = 2$. However, the fact that for all the available systems we consistently obtain lower ground state energy for sufficiently large d strongly suggests that the transition involves a change in shift at finite d .

3.6 Conclusion

In conclusion, we have introduced the model states Ψ_1, Ψ_2 and their paired versions to describe the superfluid disordering in the quantum Hall bilayer. The key question in this analysis is:

what is the nature of the compressible phase at larger d/l_B that still harbors some of the intercorrelation present at smaller d/l_B [6]?

The answer to this question cannot be given by looking at simple transport properties as both Ψ_1 and Ψ_2 (in certain regimes) recover the semicircle law. [6] On the other hand, our picture is certainly incomplete because it does not explicitly include the effects of disorder (which must be very relevant for the physics of bilayer in the regimes $d \sim l_B$ - a simple way to see this is to look at the behavior of measured counterflow resistances [5, 104] ρ_{xx}^{CF} , ρ_{xy}^{CF} that enter the insulating regime very quickly after passing through $\nu = 1$). Fertig and Murthy [105] provided a realistic model for the effects of disorder and in their disorder-induced coherence network in the incompressible phase of the bilayer, merons (vortices) are able to sweep by hopping across the system, causing the activated behavior of resistance (dissipation) in counterflow. This finding is consistent with our scenario based on the first family of wave functions (without weak pairing). [112]

Quantum Hall bilayer was also probed using resonant Rayleigh scattering [166] for samples with different tunneling amplitudes and when the in-plane magnetic field is present. They detected a nonuniform spatial structure in the vicinity of the transition, suggesting a phase-separated version of the ground state. If we think in terms of the phase-separated description, our picture must be in the spirit of the Stern and Halperin proposal [150] but instead of the 1/2 compressible phase coexisting in a phase separated picture with the superfluid phase (Ψ_1), we assume the existence of Ψ_2 .

On the other hand, in a translatory invariant system, the analysis on the basis of mixed states does not preclude an intercorrelated, paired liquid state for the neutral sector. Numerical studies give some evidence for a paired phase (Sec. 3.5.3) which is likely to be masked by the Fermi liquid state appearing at a finite critical d .

Chapter 4

Transitions between two-component and non-Abelian states in bilayers with tunneling

In this Chapter we explore the possibility of creating non-Abelian states out of two-component ones in the quantum Hall bilayer via tunneling mechanism. In particular we focus on the two problems: (a) whether it is possible to create the Moore-Read Pfaffian in the LLL by applying tunneling to the two-component 331 state at $\nu = 1/2$ in the LLL, and (b) we analyze the transition from the 332 Halperin state to the Jain $\nu = 2/5$ polarized state and examine whether critical states, presumably gapless, such as Gaffnian or the permanent state, may play a role in the transition region. Note that we neglect the electron spin in the present discussion. These two problems represent two classes of transitions: in the first case, as we will show later, we have an incompressible-compressible transition, whereas in the second case we have a transition between the two incompressible states. Tunneling as a perturbation that drives the transition from the two-component to a one-component FQH system was studied previously by analytical [167] and numerical [168] means. Current Chapter summarizes the results of Refs. [125] and [169].

4.1 Transition between 331 Halperin state and the Moore-Read Pfaffian

As we saw in Sec. 1.5.2, owing to a mathematical identity, antisymmetrizing the neutral (Cauchy determinant) part of Ψ_{331} between \uparrow and \downarrow leads to the Moore-Read Pfaffian. [123, 170] However, such a procedure is a complex mathematical entity because it creates a state with different physical properties (non-Abelian statistics out of the Abelian), while we are interested in a physical mechanism that mimics the antisymmetrization in an experimental situation. We restrict our discussion to the Coulomb bilayer system, as a generic two-component system with the antisymmetrization mechanism provided by the tunneling term $\sim -\Delta_{SAS}S_x$. The tunneling term favors the even superposition (channel) where one expects to find a weakly paired (Moore-Read) phase. We establish that this route towards the Moore-Read state is complicated by the presence of the compressible CFL, which is the resulting phase for large tunneling. The results obtained within the present bilayer model are relevant also in the study of wide quantum wells [8, 9, 124] as the latter can, with moderate approximations, effectively be described by a bilayer Hamiltonian, where the tunneling term mimics the effective confinement gap between the lowest and the first excited electronic sublevel (see Chapter 5). [12] The remainder of this Section is organized as

4. TRANSITIONS BETWEEN TWO-COMPONENT AND NON-ABELIAN STATES IN BILAYERS WITH TUNNELING

follows. We first introduce the BCS model due to Read and Green; this is an effective theory which hides many subtleties of the physical system inside a few parameters such as the single particle dispersion or the pairing function. These parameters will likely be modified with the change in tunneling, but we will, nevertheless, verify that despite its crudeness, BCS predictions are in agreement with exact diagonalization calculations, so that combining the two approaches we can obtain a complete picture of the transition. At the end, we will discuss an extension of the BCS model in a way that surpasses the exact diagonalization capabilities, but which can give us a clue as to how one can engineer the Pfaffian state in bilayers exclusively in the LLL.

4.1.1 BCS model for half-filled Landau level

At $\nu = 1/2$ (or $\nu = 2 + 1/2$), the CFs experience a zero net magnetic field, [15, 171] and if we limit ourselves to the neutral part of $|\Psi_{\text{Pf}}\rangle$ (1.38), they may be described within the framework of the effective BCS model introduced in the seminal work of Read and Green. [14] We consider the system to be at zero temperature and neglect fluctuations in the Chern-Simons gauge field that are related to the charge part of $|\Psi_{\text{Pf}}\rangle$. [172] The Hamiltonian which describes the Cauchy pairing between \uparrow and \downarrow particles with tunneling Δ_{SAS} reads

$$H = \sum_{\mathbf{k}} \left[\tilde{\epsilon}_{\mathbf{k}} (c_{\mathbf{k}\uparrow}^\dagger c_{\mathbf{k}\uparrow} + c_{\mathbf{k}\downarrow}^\dagger c_{\mathbf{k}\downarrow}) + \left(\Delta_{\mathbf{k}} c_{\mathbf{k}\uparrow}^\dagger c_{-\mathbf{k}\downarrow}^\dagger + \text{H.c.} \right) - \frac{\Delta_{SAS}}{2} (c_{\mathbf{k}\uparrow}^\dagger c_{\mathbf{k}\downarrow} + c_{\mathbf{k}\downarrow}^\dagger c_{\mathbf{k}\uparrow}) \right], \quad (4.1)$$

where $\tilde{\epsilon}_{\mathbf{k}} = \epsilon_{\mathbf{k}} - \mu$, in terms of the putative CF dispersion relation $\epsilon_{\mathbf{k}}$ and the chemical potential μ , which is assumed positive $\mu > 0$. Notice that because of the vanishing net magnetic field, the 2D wave vector $\mathbf{k} = (k_x, k_y)$ is again a good quantum number. The order parameter $\Delta_{\mathbf{k}} = \Delta_0(k_x - ik_y)$ is chosen to describe p -wave pairing and Δ_0 is a constant. This may seem like a drastic simplification, but it leads to the physical conclusions [14] which agree with exact diagonalization results, as we show below. Furthermore, there is a number of assumptions implicit to the effective model defined by (4.1), such as that $\Delta_{\mathbf{k}}$ and μ are not renormalized by the tunneling (while they should be evaluated self-consistently from the Bogoliubov-de Gennes equations) and that CFs have a single-particle-like dispersion relation with a well-defined mass. For fixed tunneling, $\Delta_{\mathbf{k}}$ is also expected to depend on the interaction and the well width or bilayer distance. Note also that as it stands, Hamiltonian (4.1) does not distinguish between Landau levels i.e. it has the same form for the LLL and first excited LL and detailed microscopic theory is needed to model $\Delta_{\mathbf{k}}$ and $\tilde{\epsilon}_{\mathbf{k}}$ to account for their difference. All of these effects are outside the scope of the treatment in this Chapter.

With the help of the even, $c_{\mathbf{k},e} = (c_{\mathbf{k},\uparrow} + c_{\mathbf{k},\downarrow})/\sqrt{2}$, and odd spin combinations $c_{\mathbf{k},o} = (c_{\mathbf{k},\uparrow} - c_{\mathbf{k},\downarrow})/\sqrt{2}$, the Hamiltonian (4.1) decouples into an even and odd channel, [14] $H = H^e + H^o$, where (the index τ denotes the even and odd channel, $\tau = e, o$)

$$H^\tau = \sum_{\mathbf{k}} \left[(\epsilon_{\mathbf{k}} - \mu^\tau) c_{\mathbf{k},\tau}^\dagger c_{\mathbf{k},\tau} + \left(\Delta_{\mathbf{k}}^\tau c_{\mathbf{k},\tau}^\dagger c_{-\mathbf{k},\tau}^\dagger + \text{H.c.} \right) \right], \quad (4.2)$$

in terms of the chemical potentials $\mu^e = \mu + \Delta_{SAS}/2$ and $\mu^o = \mu - \Delta_{SAS}/2$ for the even and odd channels, respectively. Furthermore, the even/odd p -wave order parameters read $\Delta_{\mathbf{k}}^e = \Delta_{\mathbf{k}}/2 = (\Delta_0/2)(k_x - ik_y)$ and $\Delta_{\mathbf{k}}^o = \Delta_{-\mathbf{k}}/2 = -(\Delta_0/2)(k_x - ik_y)$.

For moderate tunnelings, it is instructive to view the effective chemical potential μ^{eff} of the whole system as the weighted sum of the two channels, $\mu^{\text{eff}} = P\mu^e + (1-P)\mu^o$. In this crude approximation P measures the population of the even channel ($1/2 \leq P \leq 1$) and may have a complicated dependence on Δ_{SAS} . In particular, for some values of Δ_{SAS} we may be below the critical line $\mu^{\text{eff}} = P\Delta_{SAS}$ defined by $\mu^o = 0$ and inside the non-Abelian (Pfaffian) phase. However, in the limit of large tunneling, the system is dominated by the even channel and the chemical potential of the whole system is $\mu^{\text{eff}} = \mu^e$ because $P = 1$. Remember that the associated BCS wave function in the even channel reads

$$|\psi_{BCS}\rangle = \prod_{\mathbf{k}} \left(1 + g_{\mathbf{k}} c_{\mathbf{k},e}^\dagger c_{-\mathbf{k},e}^\dagger \right) |\text{vacuum}\rangle, \quad (4.3)$$

in terms of the pairing function $g_{\mathbf{k}} = v_{\mathbf{k}}/u_{\mathbf{k}} = -(E_{\mathbf{k},e} - \tilde{\epsilon}_{\mathbf{k},e})/\Delta_{\mathbf{k}}^{e*} \sim \mu^e/\Delta_0$ (see below). One notices then that an increase of the chemical potential μ^{eff} controlled by the large value of the tunneling parameter Δ_{SAS} is equivalent to a reduction of the order parameter Δ_0 . Therefore the BCS system will eventually be transformed into the one of the Fermi liquid. We can see this more explicitly by examining the relevant excitations of the even channel, [14]

$$E = \sqrt{(\epsilon_{\mathbf{k}} - \mu^e)^2 + \Delta_0^2 k^2}, \quad (4.4)$$

in the limit of large μ^e around $k = |\mathbf{k}| = 0$. They become unstable and $\mathbf{k} = 0$ becomes a point of local maximum. The minimum is expected to move to $|\mathbf{k}| = k_F$, the Fermi momentum. [14] Therefore if Δ_0 does not “renormalize” with increasing Δ_{SAS} , the net effect of the strong tunneling ($\mu^e \gg \mu$) on the Cauchy pairing is to drive the system into a Fermi liquid. This is not unexpected because one retrieves an effective one-component system in this limit, where all particles are “polarized” in the even channel. However, even if the system becomes compressible in order to find a minimum at $|\mathbf{k}| = k_F$, the wave function (4.3) still describes its excited state. Therefore, Pfaffian in this system may arise either as an excited state of the CFL or as an intermediate state before complete polarization. We revisit the BCS approach in Sec. 4.1.4, with a slightly different perspective in which the antisymmetrization is imposed, in a functional formalism, with the help of a Lagrangian multiplier which plays a similar role as the present tunneling term Δ_{SAS} .

As we pointed out earlier, the population of the even channel P may be a complicated function of tunneling. In the following section we use exact diagonalization of small finite systems in order to get a hint of the form of this dependence $P = P(\Delta_{SAS})$ and determine the nature of possible phases as P increases from 1/2 to 1.

4.1.2 Exact diagonalization

Here we study the full interacting quantum Hall bilayer Hamiltonian for small finite systems in the presence of tunneling, [116, 173]

$$H = -\Delta_{SAS} S_x + \sum_{i < j, \sigma \in \uparrow, \downarrow} V^{\text{intra}}(\mathbf{r}_{i\sigma} - \mathbf{r}_{j\sigma}) + \sum_{i,j} V^{\text{inter}}(\mathbf{r}_{i\uparrow} - \mathbf{r}_{j\downarrow}), \quad (4.5)$$

where in coordinate representation we have $2S_x = \int d\mathbf{r} [\Psi_{\uparrow}^{\dagger}(\mathbf{r})\Psi_{\downarrow}(\mathbf{r}) + \text{H.c.}]$, $\Psi_{\sigma}^{\dagger}(\mathbf{r})$ creates a particle at the position \mathbf{r} in the layer σ . We have decomposed the interaction into terms between electrons belonging to the same layer (V^{intra}) and those residing in opposite layers (V^{inter}). We consider a short-range interaction, defined as

$$V_{331}^{\text{intra}}(r) = V_1 \nabla^2 \delta(r), \quad V_{331}^{\text{inter}}(r) = V_0 \delta(r), \quad (4.6)$$

which produces the 331 state as the densest and unique zero energy state when V_0, V_1 are chosen positive. [56, 77] We also consider long-range Coulomb interaction,

$$V_{\text{Coul}}^{\text{intra}}(r) = e^2/\epsilon r, \quad V_{\text{Coul}}^{\text{inter}}(r) = e^2/\epsilon \sqrt{r^2 + d^2}, \quad (4.7)$$

where d is the distance between layers. Note that we are diagonalizing an explicitly lowest Landau level problem. We fix the total number of particles in our calculations to be an even integer and, unless stated otherwise, take $d = l_B$, which merely sets the range for the distance between the layers where the Coulomb ground state is supposed to be fairly well described by the 331 wave function (compare with Sec. 2.2.2). In what follows, we consider spherical and torus geometry for exact diagonalization. When we compare the exact ground state with $|\Psi_{\text{Pf}}\rangle$, it is understood that the latter is defined in the even basis i.e. single-particle states are understood to be even combinations of the original \uparrow, \downarrow states.

In Fig. 4.1 we present results of exact diagonalization on the sphere for the short-range (331) Hamiltonian (4.6) and long-range (Coulomb) Hamiltonian (4.7). 331 and Pfaffian trial states

4. TRANSITIONS BETWEEN TWO-COMPONENT AND NON-ABELIAN STATES IN BILAYERS WITH TUNNELING

occur at the same value of the shift, thus we are able to track their evolution as a function of tunneling simultaneously. We also use $\langle S_x \rangle$, the expectation value of the S_x operator in the ground state, to monitor the two-component to one-component transition, whereas $\langle S_z \rangle$ remains zero throughout, which is due to the weaker interlayer as compared to the intralayer interaction. Starting from the long-range Hamiltonian (Fig. 4.1, left panel), we see that the 331 state gives way to a Pfaffian-like ground state, with the overlap quickly saturating to a value of around 0.92. [116, 173] The transition occurs for $\Delta_{SAS} \simeq 0.1e^2/\epsilon l_B$ which agrees well with the typical experimental value and shows little size dependence when the largest accessible system $N = 10$ is considered (note that the subsequent $N = 12$ system suffers from the aliasing problem). On the other hand, notice that for the short-range Hamiltonian (Fig. 4.1, right panel), the 331 state is much more robust to perturbation by Δ_{SAS} : before it reaches full polarization in the x -direction (maximum $\langle S_x \rangle$), the overlap with both incompressible states drops precipitously beyond some critical Δ_{SAS} which is rather size-sensitive (it also depends on the values of the parameters one chooses in Eq. (4.6), but the qualitative features of the transition are reproduced for many different choices of V_0, V_1).

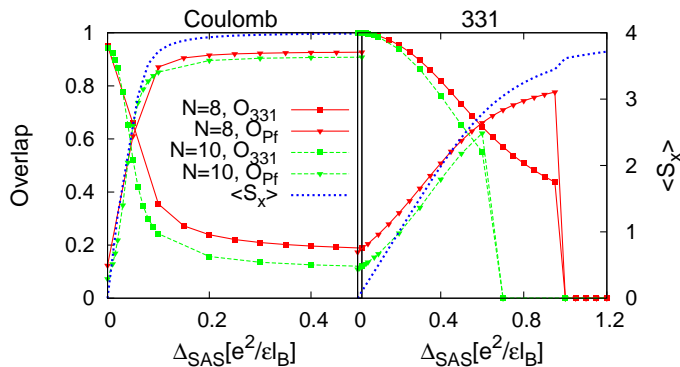


Figure 4.1: Overlaps between the exact ground state of the Coulomb bilayer (left panel) and short range 331 Hamiltonian (right panel) with the 331 state (O_{331}) and the Pfaffian (O_{Pf}), as a function of tunneling Δ_{SAS} . Also shown on the right axis is the expectation value of the S_x component of pseudospin (for $N = 8$ system) which characterizes the two-component to one-component transition.

We see nonetheless that the breakdown of a two-component phase yields a one-component state manifested by $\langle S_x \rangle \rightarrow N/2$ (this is the limit $P \rightarrow 1$ from Sec. 4.1.1). At the transition to the one-component state, $\langle S_x \rangle$ develops a small but visible kink which we show on the right side of Fig. 4.1. Focusing on the large tunneling limit, we find that the nature of the ground state is effectively that of the single layer (polarized) ground state for the symmetric interaction $V^+(r) = [V^{\text{intra}}(r) + V^{\text{inter}}(r)]/2$. This intuitive result was directly verified for all the available system sizes, including very large $N = 10$ system on both sphere and torus. In view of this, it is not surprising that the large-tunneling limit of the short-range Hamiltonian is the compressible CFL: V^+ in this case reduces to the repulsive hard core V_1 pseudopotential which has a tendency to produce the Jain CF state. This is also apparent in the fact that the ground states for large tunneling are obtained in the angular momentum sectors that agree with the predictions for the excitations of the CFL yielding overlap of 0.99 with the excited CF sea ground state. In Chapter 5 we will explain in more detail the non-zero angular momentum excitations of the CFL. In a nutshell, because the CFs at $\nu = 1/2$ are in a zero effective field, they fill a number of shells (the single particle states in the spherical geometry are monopole harmonics (2.1)). When there is an extra flux, such as when the shift is changed to the one of the 331 state, the excited states can be constructed which in a number of cases (though not always) turn out to have the maximum angular momentum, reminiscent of Hund's rule in atomic physics. [16] In the present case, we find the Hund rule to be perfectly satisfied for the large tunneling Δ_{SAS} .

Therefore, the results for the short-range Hamiltonian are suggestive that we may have a direct 331-CFL transition in the thermodynamic limit because the transition point seems to be shifting towards smaller tunnelings as we increase N . In the Coulomb case, on the other hand, we observe a curious saturation of the ground state overlap with the Pfaffian. We attribute this feature to the effect of the long range Coulomb potential on a finite system. One notices that by adding an asymptotic tail to the “intra” component of the short-range pseudopotentials $V_L^{\text{intra}} = V_{L,331}^{\text{intra}} + \alpha/2\sqrt{L}$ (α nonzero for $L \geq 3$), one progressively increases the critical value of Δ_{SAS} for the abrupt drop of the overlaps as $\alpha \rightarrow 1$ (pure Coulomb). In fact, for $N = 8, 10$ it is sufficient to consider only V_3^{intra} to achieve the saturation and push the critical value of Δ_{SAS} to infinity.

Results for the Coulomb interaction in the large Δ_{SAS} limit (Fig. 4.1) are similar to those obtained in Ref. [10] where single-layer Zhang-Das Sarma interaction was used. As long as we are in the large Δ_{SAS} limit, $V^+(r)$ interaction produces numerically the same effect as the Zhang-Das Sarma interaction. In particular, transition to a Moore-Read Pfaffian will be induced if the layer separation d is sufficiently large. [10] Of course, these two interactions are different from each other and the fact that they yield the same phenomenology (phase transitions as d is varied) only means we are probing a critical state where even the slightest perturbation away from pure Coulomb interaction (coupled with the bias of the shift) is sufficient to generate a small gap. However, despite large overlap, the gap remains very small after the transition. As we argued in Sec. 4.1.1, from the BCS model for large tunneling we expect the ground state to be described by a CFL, however the Pfaffian (4.3) can still describe an excited state. This is a low-lying excited state, as the calculation of ground state energies shows, Fig. 4.2. In Fig. 4.2

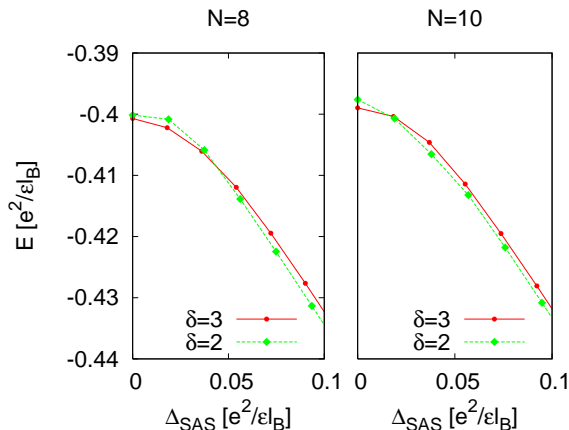


Figure 4.2: Ground state energy for $N = 8$ and $N = 10$ electrons on the sphere, $d = l_B$, for shifts of 2 and 3.

we plotted the ground state energy for two shifts on the sphere which correspond to the Pfaffian and CFL. We included the background charge corrections and rescaled the magnetic length to account for the finite size effects. [16] Because of the availability of only two system sizes, we are unable to perform a more rigorous finite size scaling of the data. If we fix $d = l_B$ as in Fig. 4.2, we notice that large Δ_{SAS} gives the ground state at the shift $\delta = 2$ and the excited state closely above is the Pfaffian. This agrees with the interpretation that the Pfaffian describes an excited state of the CFL. If we increase d , we can recover the ground state at the shift of 3 for the whole range of Δ_{SAS} , which is additional evidence of the critical nature of the Pfaffian phase that we are describing.

In Fig. 4.3 we show the relevant low energy part of the spectrum of the Hamiltonians (4.6) and (4.7) as a function of tunneling, measured relative to the ground state (right axis), for $N = 8$ electrons on the torus and the fixed aspect ratio 0.97 in the vicinity of the square unit cell. We identify the multiplet of 4 states that build up the 331 phase, whose exact degeneracy for the short-range Hamiltonian and small Δ_{SAS} (left panel) is partially lifted in case of the Coulomb

4. TRANSITIONS BETWEEN TWO-COMPONENT AND NON-ABELIAN STATES IN BILAYERS WITH TUNNELING

interaction (right panel). 331 phase is destroyed for sufficiently large Δ_{SAS} when the $\mathbf{k} = (1, 1)$ state (fourfold degenerate) comes down and eventually forms a gapless branch with $(0, 4)$ and $(4, 0)$ members of the 331 multiplet (other excited states not shown). We identify the large-tunneling phase as the CFL phase because exactly the same spectrum is seen in a single layer with Coulomb interaction and the same aspect ratio. This transition is quantitatively reflected also in the overlap with the trial 331 states and CFL as a function of tunneling (Fig. 4.3, left axis). Upon a closer look at Fig. 4.3, one notices that the torus spectra suggest little qualitative

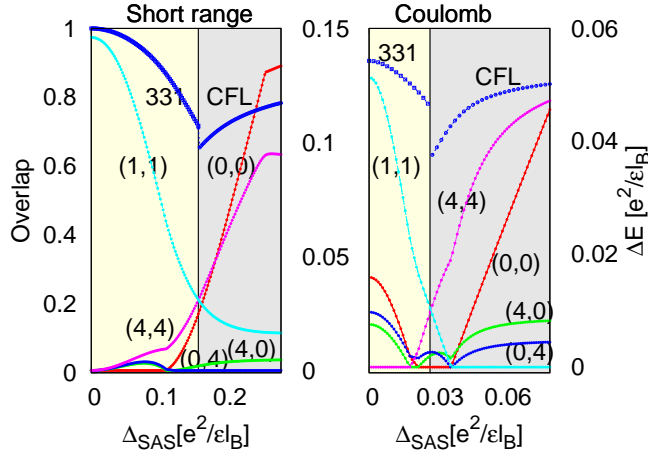


Figure 4.3: Low-energy part of the spectrum (relative to the ground state) of the short-range 331 (left panel) and the long-range Coulomb Hamiltonian (right panel) for $N = 8$ electrons on the torus at $\nu = 1/2$ and aspect ratio $a/b = 0.97$ as a function of tunneling Δ_{SAS} (right axis). Also shown (left axis) is the overlap with the phases we identify as the 331 state and the CFL.

difference between the short-range and the Coulomb Hamiltonian. In particular, we do not see any indication of the Pfaffian threefold ground-state degeneracy for large Δ_{SAS} which could be expected from the large overlap on the sphere (Fig. 4.1). To reconcile these two results, we again focus on the large tunneling limit and vary the aspect ratio of the torus to investigate the possibility of an emergent Pfaffian phase (Fig. 4.4). We assume that in the large tunneling limit, we have effectively a single layer (polarized) ground state for the symmetric interaction $V^+(r)$. In Fig. 4.4 we show the spectrum of the single layer system of $N = 14$ electrons interacting with $V^+(r)$ as a function of aspect ratio and connect the levels that have the quantum numbers of the Moore-Read Pfaffian. We also include the background charge correction. [132, 174] One notices that, with the exception of a very narrow range of aspect ratios around 0.4, there is no evidence of a clear Moore-Read degeneracy. A narrow region where we see the threefold multiplet of states for $N = 14$ also exists for $N = 8$, but is obscured by the presence of higher energy levels in systems of $N = 10$ and 12 electrons. Thus we conclude that it cannot represent a stable phase, but a possibility remains that it is a critical phase which becomes stronger as one approaches the thermodynamic limit or as one changes the interaction away from the pure Coulomb.

We note that varying d (at the fixed aspect ratio) does not lead to any qualitative change in the ground state degeneracy as long as $V^+(r)$ interaction is used. This is clearly different from Zhang-Das Sarma interaction which induces level crossings in the spectrum in such a way that for large d (typically beyond $4l_B$), a Pfaffian degeneracy is seen for big enough systems, [175, 176] such as $N = 12$ and $N = 14$ (it is not visible in systems $N = 8$ and $N = 10$). This is similar to the results in the second Landau level [175], as well as the calculations on the sphere [10], but the prohibitively small gap suggests that such a state, if it exists, is very fragile.

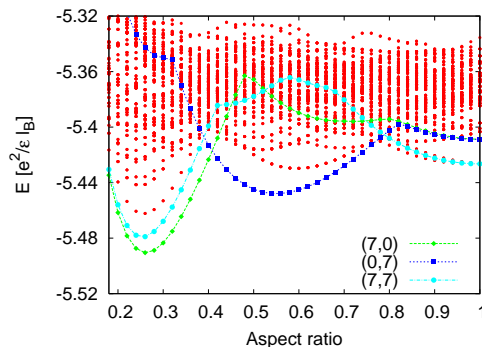


Figure 4.4: Spectrum of the $N = 14$ electrons in a single layer at $\nu = 1/2$ interacting with $V^+(r)$ ($d = l_B$), as a function of aspect ratio. We highlight the states with quantum numbers of the Moore-Read Pfaffian.

4.1.3 Pfaffian signatures for intermediate tunneling and a proposal for the phase diagram

We now summarize our ED results in the two geometries in order to make a connection with the BCS analysis of Sec. 4.1.1 and sketch possible paths of the $\nu = 1/2$ two-component system with tunneling in the phase diagram of Read and Green, [14] see Fig. 4.5. In Fig. 4.5, μ has the meaning of the effective chemical potential μ^{eff} of the whole system as in Sec. 4.1.1, renormalized by Δ_{SAS} , i.e. $\mu = \mu(\Delta_{SAS})$. It is assumed that it can be approximated by the value of the chemical potential of the dominant even channel, $\mu^{\text{eff}} \simeq \mu^e$ and the separation between the Abelian and non-Abelian phases in Fig. 4.5 is defined by setting then the value of the chemical potential of the odd channel to zero, i.e. $\mu^o \simeq \mu(\Delta_{SAS}) - \Delta_{SAS} = 0$. This approximation renders necessary taking into account the renormalization of the parameters in the BCS Hamiltonian (4.1) with tunneling, as in Ref. [14].

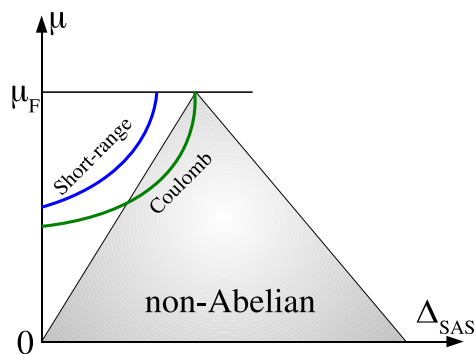


Figure 4.5: Possible outcomes of tunneling on a twocomponent system such as the direct transition to a Fermi liquid (as expected for the short range interaction on the sphere) or to a critical Moore-Read Pfaffian for long range (Coulomb) interaction, in the context of phase diagram after Read and Green. [14] Note that the value for $\mu_F \sim 1/m^*$ is interaction-dependent due to the renormalized CF mass m^* and we may have different dividing lines $\mu = \mu_F$ depending on the kind of the interaction. [15]

On the sphere, we first recall a very large difference in Δ_{SAS}^C , the critical value of tunneling required to fully polarize the system in the x -direction, for the two interactions considered. A much larger value for the short-range 331 Hamiltonian suggests that the chemical potential for the even channel in this case is much more strongly renormalized than for the long-range Coulomb interaction and therefore such a system may directly move from 331 state through the

4. TRANSITIONS BETWEEN TWO-COMPONENT AND NON-ABELIAN STATES IN BILAYERS WITH TUNNELING

Abelian phase and into a CFL, Fig. 4.5.

A question we ask at this point is whether the CFL, a likely phase at $P = 1$, leaves room for other one-component states to form as we increase the tunneling. In particular, is there a possibility for a system to evolve along the trajectory which touches the critical line or briefly transits through the non-Abelian phase in Fig. 4.5? Such an intermediate state could possess significant overlap with the Moore-Read Pfaffian, but it would necessarily have a small gap and we refer to it as “critical Pfaffian”.

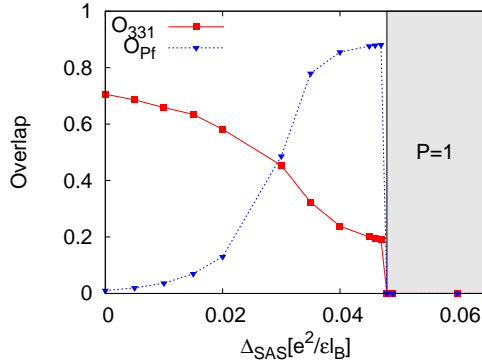


Figure 4.6: Overlaps between the exact ground state of $N = 10$ electrons on the sphere with the 331 state (O_{331}) and the Pfaffian (O_{Pf}), as a function of tunneling Δ_{SAS} , for the Coulomb bilayer Hamiltonian and $d = 0.4l_B$.

On the sphere, a suitable system to detect the signature of the critical Pfaffian is the Coulomb $N = 10$ system where the large-tunneling phase is compressible for $d \lesssim 0.5l_B$. [10] We therefore fix $d = 0.4l_B$ and vary Δ_{SAS} (Fig. 4.6). For $\Delta_{SAS} = 0$, we are still largely in the 331 phase and for large Δ_{SAS} we are in the CFL; however, for intermediate tunnelings we see a developing Pfaffian that establishes in a narrow range around $\Delta_{SAS} = 0.04e^2/\epsilon l_B$. Therefore, despite “weaker” incompressibility for small Δ_{SAS} and full compressibility for large Δ_{SAS} , for intermediate tunneling we find evidence for the Pfaffian, as suggested by the green trajectory in Fig. 4.5).

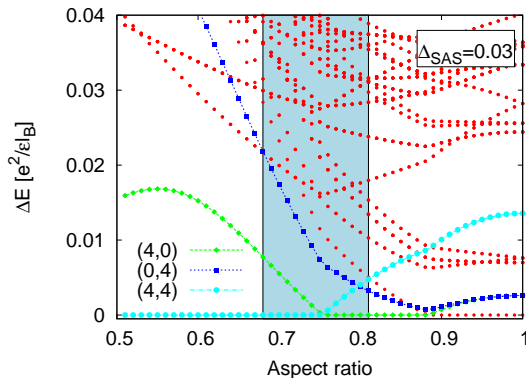


Figure 4.7: Low-energy part of the spectrum (relative to the ground state) of the Coulomb Hamiltonian (with $d = l_B$) for $N = 8$ electrons on the torus at $\nu = 1/2$ and $\Delta_{SAS} = 0.03e^2/\epsilon l_B$, as a function of the aspect ratio. Shaded region represents the tentative phase with the Pfaffian degeneracy.

The effects of CFL physics are rendered more transparent in the torus geometry, where we have identified the dominant phases as 331 and CFL (Fig. 4.3), with a direct transition between the two of them. We choose a value for $\Delta_{SAS} = 0.03e^2/\epsilon l_B$ which places the system in the center of the transition region (compare also with Fig. 4.6) and examine the spectrum of an $N = 8$ system as a function of aspect ratio for an emerging Pfaffian degeneracy, Fig. 4.7. In torus geometry there is no subtle dependence on d , so we take as before $d = l_B$. In agreement with

the results on sphere, we find a region of aspect ratios where the correct Pfaffian degeneracy is visible.

Previous results lend support to the scenario of an intermediate critical phase in a long-range Coulomb system, which has a small gap (Fig. 4.7) but possesses large overlap with the Moore-Read Pfaffian (Fig. 4.6). A stronger indication of topological degeneracy is likely to be found in a model that assumes non-zero thickness of each layer, [175] but that would lead also to a substantial decrease of the gap. [177]

4.1.4 Generalized tunneling constraint

In Sec. 4.1.2 we found that in a system with a fixed number of particles and the tunneling commonly expressed as $-\Delta_{SAS}S_x$, there is no unambiguous evidence for the Pfaffian phase in finite systems that can be studied by ED. This evidence appears most striking when Coulomb overlaps in the spherical geometry are considered (Fig. 4.1), but the torus geometry, which treats both phases on the same footing, suggests that the CFL is the likely outcome of tunneling on the 331 state. By combining the analysis from Read-Green theory with exact diagonalization, we have identified the mechanism leading to this: it is the increase of the effective chemical of the even channel. Therefore, one must find a way to prevent the effective even-channel chemical potential from becoming too large if the weakly-paired phase is to be established in the system. In this Section, we discuss a way to express this requirement formally via “generalized tunneling constraint”. On the level of the BCS model used in Sec. 4.1.1, this constraint leads to a stable weak-pairing phase in the even channel. Experimental implementation of this constraint is feasible in a system which is in contact with a reservoir with which it can exchange particles.

The basic guideline is that we need to find a way to “identify” \uparrow with \downarrow electrons, thereby converting from Cauchy determinant pairing (which describes the p -wave pairing of \uparrow and \downarrow particles) to the the spinless Pfaffian pairing. Within functional formalism, that amounts to adding a term of the form

$$\chi(\mathbf{r})[\Psi_{\uparrow}(\mathbf{r}) - \Psi_{\downarrow}(\mathbf{r})] \quad (4.8)$$

to the Langragian density via Grassmannian Lagrange multiplier $\chi(\mathbf{r})$. We will assume instead that we can alternatively express this via the constraint

$$\lambda(\mathbf{r})[\Psi_{\uparrow}^{\dagger}(\mathbf{r}) - \Psi_{\downarrow}^{\dagger}(\mathbf{r})][\Psi_{\uparrow}(\mathbf{r}) - \Psi_{\downarrow}(\mathbf{r})], \quad (4.9)$$

in terms of the bosonic multiplier $\lambda(\mathbf{r})$. By construction this constraint affects only the odd channel. Within the mean-field approximation of a spatially constant multiplier $\lambda(\mathbf{r}) = \lambda$, one may identify $\lambda = \Delta_{SAS}/2$, i.e. the effect of the multiplier is the same as the tunneling term in Sec. 4.1.1, except for an overall decrease of the chemical potential:

$$\mu \rightarrow \mu - \lambda,$$

which eventually yields a λ -independent chemical potential in the even channel,

$$\mu^e = \mu,$$

as mentioned above. Integration over the Lagrange multiplier projects to $\Psi_o^{\dagger}\Psi_o = 0$, where $\Psi_o^{\dagger} = [\Psi_{\uparrow}^{\dagger}(\mathbf{r}) - \Psi_{\downarrow}^{\dagger}(\mathbf{r})]/\sqrt{2}$ is again the odd spin superposition written in terms of the fermion fields $\Psi_{\sigma}(\mathbf{r})$, i.e. it leaves us with no density in the odd channel.

The BCS Hamiltonian including the constraint (4.9) has the same form as (4.1) except that now $\tilde{\epsilon}_{\mathbf{k}} = \epsilon_{\mathbf{k}} - \mu + \lambda$, as a consequence of the above-mentioned shift in the chemical potential. We can diagonalize it by a Bogoliubov transformation and show [125] that the stationary point for the BCS Hamiltonian is given by $\lambda \rightarrow +\infty$ and we have strong coupling in the odd channel, while the chemical potential of the even channel is constant $\mu^e = \mu$ and it can be weakly paired. [14]

4. TRANSITIONS BETWEEN TWO-COMPONENT AND NON-ABELIAN STATES IN BILAYERS WITH TUNNELING

The previous discussion was on the simplified model of 331 physics in terms of neutral fermions with an additional constraint that leads to the Pfaffian, but seems artificial and hard to implement in an experimental setting. Nevertheless it suggests a possible way to achieve the stable Pfaffian phase. With respect to ordinary tunneling, the generalized constraint can be modeled by strong tunneling and an additional term in the effective description, λN , where N is the total number of particles and λ tunneling strength as before. The chemical potential (of the whole system) depends on the tunneling and changes as $\mu - \lambda$. Then we have the following physical picture in mind: as we take $\lambda > 0$ this decrease of the chemical potential with tunneling will imply the decrease of the density of the system. On the other hand from the solution of the BCS system with the generalized constraint, we see that the effective chemical potential of the even channel stays the same (equal to μ). This means also that the number of particles in the even channel stays the same, so the effects of the tunneling and the additional term cancels, but the polarization P increases with tunneling. Thus we effectively maintain the same effective parameter μ with tunneling, its value will not increase, and we will be able to achieve the stable Pfaffian phase. This will correspond to the evolution along a straight line parallel to Δ_{SAS} -axis in the phase diagram like in Fig. 4.8.

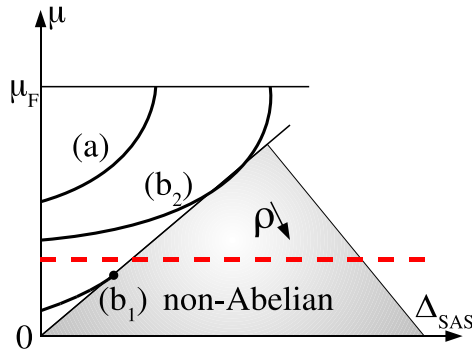


Figure 4.8: Generalized tunneling constraint: the decrease of the density of the system evolves the system along the horizontal line in the phase diagram of Read and Green [14] into the non-Abelian phase.

Therefore, in principle, by changing the density of the system we can achieve a stable Pfaffian phase. We would like to compare the present discussion which is based on the simplified model of neutral fermions (mean field in nature, with the simplifying assumption $\Delta_o = -\Delta_e = \text{constant}$ i.e. independent of tunneling) with exact diagonalization in the LLL in the previous section. The proposal outlined here calls for an open system with adjustable density (which demands also the adjustment of magnetic field B) to achieve the stable Pfaffian phase. Although doing so will preserve the filling factor, in general changing the total density may enhance the role of LL mixing and thus invalidate the LLL assumption in the exact diagonalizations. It will also lead to the renormalization of the parameters of the BCS effective model not taken into account in Sec. 4.1.1. Indeed, when lowering the total chemical potential via the generalized constraint, the density is also decreased. On the other hand the ratio between interaction strength (e^2/l_B) and cyclotron frequency ($\omega_c \sim 1/l_B^2$) is proportional to $1/\sqrt{\rho}$, from which we see that the LLL projection is invalidated if the density is significantly reduced. Therefore to reach and establish the Pfaffian phase it is likely that LL mixing has to be taken into account. This has been discussed in the recent literature [87, 178] as a way to stabilize the Pfaffian phase. Here we seek the Pfaffian in a two-component setting when a parameter of the system λ is varied, which makes the inclusion of higher LLs harder. If we remain in the LLL, changing of the density amounts to simple rescaling of spectra ($e^2/l_B \rightarrow c e^2/l_B$ with $c > 0$), which cannot induce any significant effect such as the change in the nature of (quasi)degeneracy of ground states on the torus. Even if the evidence for a Pfaffian phase is rather weak for the system sizes studied here, one may

hope that the increase of these sizes will improve the case for such a state in the LLL as the odd channel may assume the role of the first excited Landau level before a complete polarization.

4.2 Transition from 332 Halperin to Jain's state at $\nu = 2/5$

In this Section we study the transition from Halperin's two-component 332 state (1.45) to the one-component Jain state at the filling factor $\nu = 2/5$ (1.36) via tunneling. The interest is threefold: we would like to find out (a) about the nature of quantum phase transitions between topological phases which are similar (332 and Jain's state have the same ground state degeneracy [133, 144, 179] but different shift [56, 180]), (b) we would like to find if Gaffnian [94] can be characterized as a critical state in these circumstances when the gap closes, and (c) we explore possible consequences for the effective description of the Jain state due to a better understanding of the transition.

4.2.1 The system under consideration

We consider the bilayer system at the filling factor $\nu = 2/5$ defined by the Hamiltonian (4.5). As we outlined in Sec. 1.5.3, in the small tunneling regime the ground state of the Hamiltonian (4.5) at $\nu = 2/5$ is the 332 Halperin state for two distinguishable species of electrons. Due to the fact that the correlation exponents between electrons of the same layer are bigger than those between electrons of the opposite layers, we expect the 332 wave function (1.45) to be more appropriate for non-zero d e.g. in the range $d \sim l_B$. However, as it possesses the necessary symmetry properties, [56] it can be a candidate also for $d = 0$. The properties of the 332 wave function (1.45) were numerically verified in Ref. [114].

As the tunneling strength Δ_{SAS} is increased, the electrons find it energetically favorable to be in the superposition of two layers, $\uparrow + \downarrow$, and the system loses its two-component character. The effective single-component state is characterized by full polarization in the x -direction. At $\nu = 2/5$ in the LLL, a compelling candidate for the polarized state is Jain's CF state, (1.36). Note that a single index now suffices to label the electron coordinates as the pseudospin index is implicitly assumed to be $\uparrow + \downarrow$. An alternative candidate for the polarized state at $\nu = 2/5$ exists, which is the so-called Gaffnian state, (1.55). In the notation of Eq. (1.55) one can think of the Gaffnian as originating from the two-component 332 state with the additional pairing represented by the permanent. [123, 181] The two-component state is made single-component under the action of the antisymmetrizer \mathcal{A} between \uparrow and \downarrow electron coordinates. Gaffnian (1.55) has generated a surge of interest because in finite size (spherical) exact diagonalization it shows high overlaps with the Coulomb ground state, comparable to those of Jain's state, yet the topological properties of the two states are very different. [94] Moreover, the strong evidence for Gaffnian in numerical calculations is puzzling in view of the fact that it is a correlator of a non-unitary conformal field theory and hence not expected to describe a stable phase. [53] In the spherical geometry, Jain's state and the Gaffnian can only be distinguished by their excitation spectrum [182] or by using advanced tools such as the entanglement spectrum. [183]

Since the antisymmetrizer \mathcal{A} can, to some extent, be mimicked by the tunneling term, [125] and since the Gaffnian incorporates the pairing defined by the permanent, there is an additional natural candidate for $\nu = 2/5$ which we refer to as the permanent state,

$$\Psi_{\text{perm}} = \Psi_{332} \text{ perm}\left\{\frac{1}{z_{\uparrow} - z_{\downarrow}}\right\}. \quad (4.10)$$

This state distinguishes between \uparrow and \downarrow electrons, hence it is expected in the limit of intermediate tunneling Δ_{SAS} before a full x -polarization has been achieved. Like the Gaffnian, the state (4.10) is related to a non-unitary conformal field theory [77] and one may expect that it plays a role of the critical state in the transition region before full x -polarization.

4. TRANSITIONS BETWEEN TWO-COMPONENT AND NON-ABELIAN STATES IN BILAYERS WITH TUNNELING

In the following Sections we study numerically the transitions between two-component and one-component states at the filling factor $\nu = 2/5$ and present a possible interpretation of the results within an effective bosonic BCS model.

4.2.2 Exact diagonalizations

In this Section we study the transition at $\nu = 2/5$ via tunneling Δ_{SAS} using exact diagonalization in the spherical and torus geometries to gain complete insight into topological properties of the different competing trial states. We use Coulomb interaction (1.49), as well as the short-range interaction that defines the 332 state as its unique and densest zero mode, $V^{\text{intra}} = \{0, V_1^a, 0, 0, \dots\}$ and $V^{\text{inter}} = \{V_0, V_1^e, 0, 0, \dots\}$. There is some freedom in choosing $V_0, V_1^{a,e}$ apart from the requirement that they should all be positive and we set them to unity. Values of $V_0, V_1^{a,e}$ control the gap for the 332 state and thereby affect the critical value for the tunneling Δ_{SAS} in the following discussion, but our main conclusions remain unaffected by this choice. In the case of Jain's state we do not have a pseudopotential formulation (a useful ansatz that does not lead to a unique zero-energy eigenstate is $\{0, V_1, 0, 0, \dots\}$).

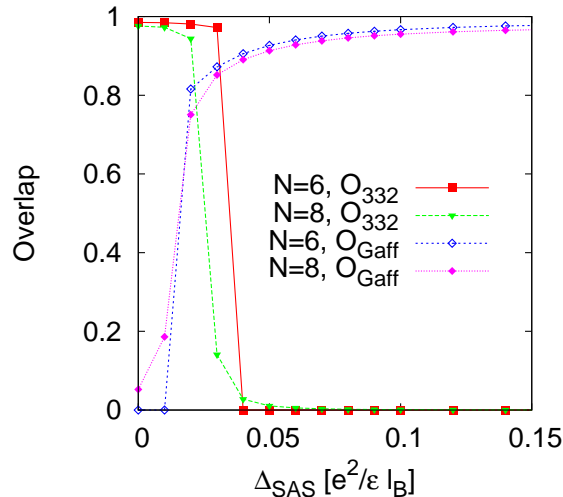


Figure 4.9: Overlaps between the exact Coulomb bilayer ground state for $d = l_B$ and the 332 (O_{332}) and Gaffnian state (O_{Gaff}), as a function of tunneling Δ_{SAS} . Data shown is for $N_e = 6$ and 8 electrons. Note that O_{332} and O_{Gaff} can not be directly compared due to the difference in shift between the 332 state and the Gaffnian.

In Fig. 4.9 we present our results for the case of the Coulomb bilayer on the sphere with the bilayer distance d equal to l_B . Overlaps of the exact ground state with the 332 state and the Gaffnian are calculated as a function of tunneling Δ_{SAS} . Separate diagonalizations have been performed because the two trial states, 332 and Gaffnian, occur in slightly different Hilbert spaces due to the mismatch in shift ($\delta = 3$ and $\delta = 4$, respectively). Following the rapid destruction of the 332 state with the increase of Δ_{SAS} , the overlap with the Gaffnian state rises to the high value known from earlier studies in a single-layer model. [94, 183] This occurs at the point when the system is almost fully x -polarized. Consequently, the overlap with the Jain state for large Δ_{SAS} is also high and virtually indistinguishable from that of the Gaffnian on the scale of this figure.

In the torus geometry, Figs. 4.10 – 4.13, trial states which represent topological phases are uniquely specified by their filling factor $\nu = p/q$. What is then characteristic of the Abelian states such as the 332 and Jain's state, is that on the torus they only possess the ground state degeneracy due to the motion of the center of mass of the system, equal to q , [133] which we will mode out in the data. In the case of Gaffnian the degeneracy of the ground state is expected [94, 184] to be doubled with respect to the trivial one i.e. equal to $2 \times 5 = 10$. In the literature

there is no consensus that Gaffnian is a gapless state, [94, 182] but if we can establish that the nature of the lowest lying states is as expected for the Gaffnian, we could nonetheless claim its presence at the transition from the 332 to the Jain's state.

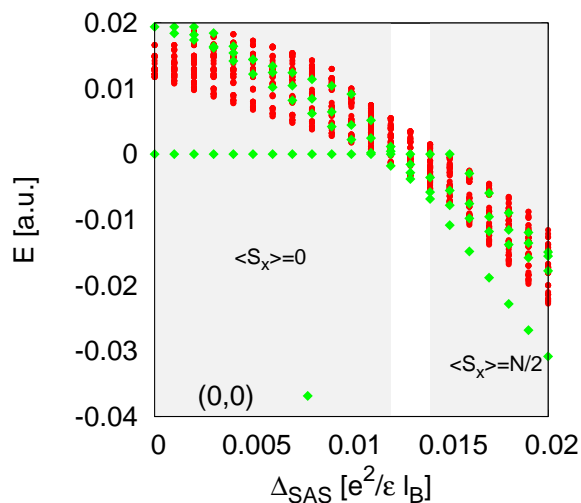


Figure 4.10: Energy spectrum of the SU(2)-symmetric 332 Hamiltonian on torus (in arbitrary units) for $N_e = 8$ and aspect ratio 0.97. The $\mathbf{k} = 0$ levels that cross define regions of fully polarized $\langle S_x \rangle = N/2$ and unpolarized $\langle S_x \rangle = 0$ phases.

In Fig. 4.10 we plot the low energy spectrum of the 332 short-range Hamiltonian on the torus for $N = 8$ electrons and close to the square unit cell (aspect ratio $a/b = 0.97$). We observe the 332 state, distinctly marked by its zero energy, which remains unaffected by Δ_{SAS} until level crossing is induced with the excited polarized state. The state characterized by $\langle S_x \rangle = N/2$ that becomes the ground state for large tunneling develops into a Jain CF state, (1.36). This is expected because the original system defined in terms of $V_c^{\text{intra}}(r), V_c^{\text{inter}}(r)$ (1.49), in the limit of very large tunneling becomes an effective one-component model with the modified interaction $[V_c^{\text{intra}}(r) + V_c^{\text{inter}}(r)]/2$. [125] For the short-range 332 Hamiltonian, this is simply a V_1 pseudopotential which yields a good approximation to Jain's state. Furthermore, as we vary the aspect ratio of the torus, we find the following thin torus configuration ...0 1 0 0 1..., which is that of the Jain state. [185] For an excellent introduct to the thin torus, consult Ref. [186].

Fig. 4.11 shows the energy spectrum of the $N_e = 8$ Coulomb bilayer system on the torus with the same aspect ratio $a/b = 0.97$ (slightly different from unity to avoid accidental geometric degeneracy) and distance between layers is set to $d = l_B$. We identify incompressible states for small and large tunneling as the 332 and the Jain state, with the transition between them occurring for $\Delta_{SAS}^C \approx 0.018e^2/\epsilon l_B$. The states can be identified e.g. with respect to the Fig. 4.10 by calculating overlaps. If we denote the ground state of the short-range and Coulomb Hamiltonian for a given tunneling Δ_{SAS} as $\Psi_{\text{short}}(\Delta_{SAS})$ and $\Psi_C(\Delta_{SAS})$, respectively, we obtain the following overlap $\langle \Psi_{\text{short}}(\Delta_{SAS} = 0) | \Psi_C(\Delta_{SAS} = 0) \rangle \approx 0.95$. This means that for Coulomb bilayer interaction we have the 332 state for zero tunneling. Also, in the large tunneling limit, we obtain e.g. $\langle \Psi_{\text{short}}(\Delta_{SAS} = 0.05) | \Psi_C(\Delta_{SAS} = 0.05) \rangle \approx 0.948$, i.e. Jain's state.

If we define the quantity which describes the density of the odd channel, $N/2 - \langle S_x \rangle$, the transition is characterized by an approximately linear or even step-like discontinuity in the plot of $N/2 - \langle S_x \rangle$ as a function of $\tilde{\Delta}_{SAS} = \Delta_{SAS} - \Delta_{SAS}^C$, Fig. 4.12. In the transition region, an approximate doublet of states with $\mathbf{k} = 0$ Haldane pseudomomenta is formed (Fig. 4.11). Although the doublet has the expected quantum numbers of the Gaffnian, [184] the specific root configurations in the thin torus limit [185] cannot be unambiguously identified as those of the Gaffnian. Both of the members of the doublet share the following thin torus configuration ...0 1 0 0 1..., among other spurious patterns, which is that of the Jain state. Moreover, the member of the doublet higher in energy has a lower polarization $\langle S_x \rangle$ than the ground state.

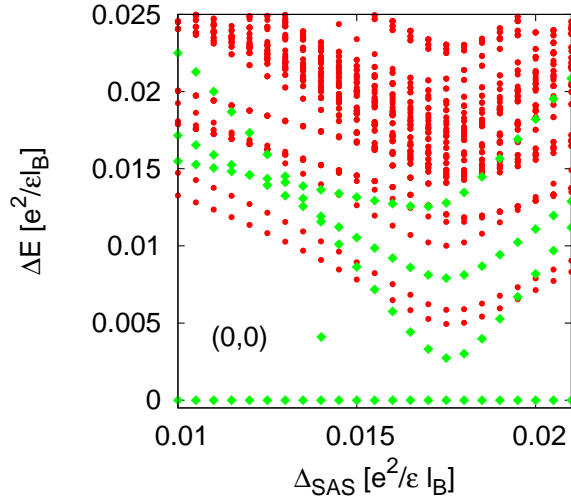


Figure 4.11: Energy spectrum relative to the ground state of the Coulomb bilayer on torus, for $N_e = 8$ electrons, $d = l_B$ and aspect ratio 0.97. An approximate doublet of states with $\mathbf{k} = (0, 0)$ Haldane pseudomomenta is formed around the transition point $\Delta_{SAS} \approx 0.018e^2/\epsilon l_B$.

These facts suggest that the excited $\mathbf{k} = 0$ state in the transition region is a spinful CF state rather than the (polarized) Gaffnian.

For the long-range Coulomb interaction on the torus and the aspect ratio close to 1, the transition between the Jain and 332 state proceeds as an avoided level crossing or a smooth crossover without an obvious closing of the gap. The gap is expected to close in the thermodynamic limit between the two distinct topological phases. On the other hand, for the short-range interaction that defines the 332 state as the zero-energy ground state and for the identical geometry of the torus ($a/b = 0.97$), it appears that the gap closes, Fig. 4.10. This difference between Figs. 4.10 and 4.11 can be attributed to the symmetry of the interaction. For the short range interaction used in Fig. 4.10, $V_1^{\text{inter}} = V_1^{\text{intra}}$, hence it does not break the $SU(2)$ symmetry. In this case, the tunneling part of the total Hamiltonian, being proportional to S_x component, commutes with the interaction part and we expect level crossing which we indeed observe in Fig. 4.10. The interaction in the bilayer with $d = l_B$, on the other hand, breaks $SU(2)$ invariance (Fig. 4.11), but we can nevertheless show that the level crossing persists and can be induced by changing the aspect ratio of the torus away from unity. In Fig. 4.13 we show one such energy spectrum (without the ground state energy subtraction) when the aspect ratio is equal to 0.5. The level crossing is induced by deforming the system towards the crystalline limit, when the Coulomb interaction is increasingly of short range. Note, however, that the states at $\Delta_{SAS} = 0$ and Δ_{SAS} -large are still 332 and Jain's, respectively (verified by the overlaps with the ground state of the short-range interaction and by their thin torus limit).

4.2.3 Interpretation of the results within an effective bosonic model

High overlaps with the Gaffnian on the sphere around and after the transition, as well as the crossover via level repulsion in Fig. 4.11 on the torus, can be a motivation for considering the system of CS-transformed composite bosons [63, 187] (\uparrow and \downarrow) that pair in the way of p -wave in a picture of the underlying neutral sector physics. As we already pointed out in the preceding section, the high Gaffnian overlaps are not to be taken as a proof that we have the Gaffnian phase after the transition, in the thermodynamic limit, but may serve as a motivation for discussing the role for the Gaffnian as a critical state. More generally, as the system is closer to the one-component limit, the theory may inherit the pairing structure built in the Gaffnian state and this is captured in the permanent state, (4.10). As we mentioned in Sec. 4.2.1, the connection

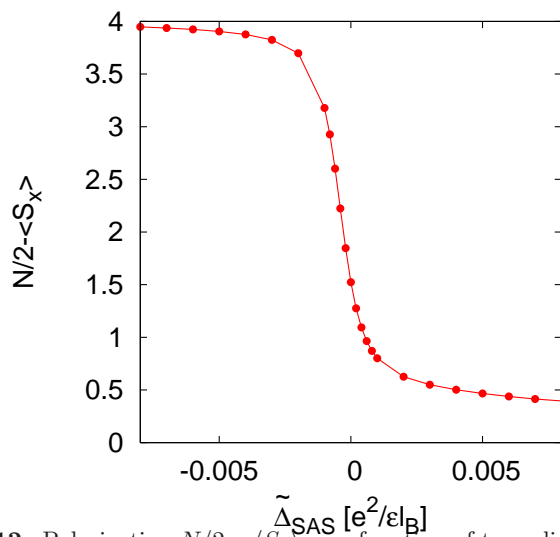


Figure 4.12: Polarization $N/2 - \langle S_x \rangle$ as a function of tunneling around the transition point for the system of Fig. 4.11.

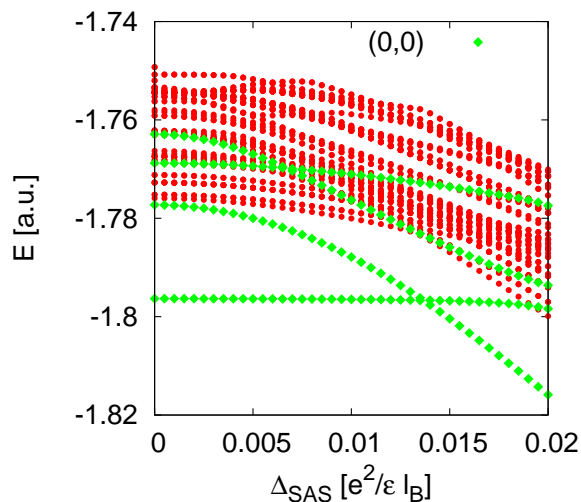


Figure 4.13: Energy spectrum of the Coulomb bilayer on torus (in arbitrary units) for $N_e = 8$ and aspect ratio 0.5.

between the Gaffnian (1.55) and the permanent state (a p -wave state of bosons) (4.10) is the antisymmetrization. We assume that the operation of antisymmetrization corresponds, in the language of effective theory, to a tunneling term. [125]

The effective description in this case is not as clean-cut as in the analysis of Sec. 4.1 and some additional approximations need to be introduced, apart from the ones mentioned before. One first begins with performing the CS transformations in the field-theoretical description of the system (4.5) that leaves, in the mean field, \uparrow and \downarrow bosons that pair in the way of a p -wave. At $\nu = 2/5$, for no tunneling, in the presence of Coulomb or suitable short range interaction, we expect that the bilayer (two-component) system is described by 332 state. We know very well how to define the CS transformation to bosons in these circumstances, for the first time it was given in Ref. [187]. It entails a transformation from electronic Ψ_σ fields to bosonic Φ_σ fields:

$$\Psi_\sigma(\mathbf{r}) = U_\sigma(\mathbf{r})\Phi_\sigma(\mathbf{r}) \quad (4.11)$$

where

$$U_\sigma(\mathbf{r}) = \exp\left\{-i \int d\mathbf{r}' \arg(\mathbf{r} - \mathbf{r}') [3\rho_\sigma(\mathbf{r}') + 2\rho_{-\sigma}(\mathbf{r}')]\right\} \quad (4.12)$$

4. TRANSITIONS BETWEEN TWO-COMPONENT AND NON-ABELIAN STATES IN BILAYERS WITH TUNNELING

where $\arg(\mathbf{r} - \mathbf{r}')$ is the angle the vector $\mathbf{r} - \mathbf{r}'$ forms with the x axis. In the mean field (when the fluctuations of gauge fields are neglected) we, in fact, describe a system of \uparrow and \downarrow bosons that interact. Therefore we have in the first approximation two ordinary Bose condensates. By the virtue of the Anderson-Higgs mechanism i.e. gauge fluctuations, the two Goldstone modes become gapped and the two gapped bosonic systems describe the two-component 332 system.

The complication comes when we consider the tunneling term as an extra perturbation and an extra term in our starting Hamiltonian for the electrons. The tunneling term is

$$H_T = -\lambda \left(\Psi_{\uparrow}^{\dagger}(\mathbf{r})\Psi_{\downarrow}(\mathbf{r}) + \Psi_{\downarrow}^{\dagger}(\mathbf{r})\Psi_{\uparrow}(\mathbf{r}) \right), \quad (4.13)$$

where λ denotes the tunneling amplitude in this section. Due to the CS transformation (4.11) this can not be translated simply into the hopping of bosons because:

$$\Psi_{\sigma}^{\dagger}\Psi_{-\sigma} = \Phi_{\sigma}^{\dagger}U_{\sigma}^{\dagger}U_{-\sigma}\Phi_{-\sigma} \quad (4.14)$$

and only in the mean field approximation for which

$$U_{\sigma}^{\dagger}U_{-\sigma} \approx I \quad (4.15)$$

(where I is the identity) we have a simple tunneling of bosons i.e.

$$H_T \approx -\lambda \left(\Phi_{\uparrow}^{\dagger}(\mathbf{r})\Phi_{\downarrow}(\mathbf{r}) + h.c. \right) \quad (4.16)$$

The necessary assumption in Eq.(4.15) is $\rho_s = \rho_{\uparrow}(\mathbf{r}) - \rho_{\downarrow}(\mathbf{r}) \approx 0$ i.e. that the fluctuations in density in \uparrow parallel the ones in \downarrow , or the fluctuations in the pseudospin density are negligible. This is a crucial approximation that reconciles the CS transformation with the tunneling term and enables the similar analysis as in Sec. 4.1. Unfortunately, this approximation is difficult to quantify, but nonetheless we expect to get the qualitatively correct insight into the transition. Additional justification for the bosonic model arises from numerics. Namely, the results for SU(2) symmetric interaction (4.10) and Coulomb interaction (4.11) both reflect the abrupt change in polarization at the transition. In this case, we may use the SU(2)-invariant interaction as a starting point and the symmetric-antisymmetric basis for the Chern-Simons transformation. This way, the tunneling term will retain the same form as in the fermionic basis.

Treating the residual interaction in a mean field manner i.e. taking the Hartree-Fock and BCS decomposition, we come to the following form of the Hamiltonian for the effective description of \uparrow and \downarrow bosons around the $\mathbf{k} = 0$ point in the momentum space:

$$H = \sum_{\mathbf{k}} \left(\sum_{\sigma} \tilde{\epsilon}_{\mathbf{k}} b_{\mathbf{k}\sigma}^{\dagger} b_{\mathbf{k}\sigma} - \lambda (b_{\mathbf{k}\uparrow}^{\dagger} b_{\mathbf{k}\downarrow} + b_{\mathbf{k}\downarrow}^{\dagger} b_{\mathbf{k}\uparrow}) + \Delta_{\mathbf{k}} b_{\mathbf{k}\uparrow}^{\dagger} b_{-\mathbf{k}\downarrow}^{\dagger} + \Delta_{\mathbf{k}}^* b_{-\mathbf{k}\downarrow} b_{\mathbf{k}\uparrow} \right) \quad (4.17)$$

where $\tilde{\epsilon}_{\mathbf{k}} = \epsilon_{\mathbf{k}} - \mu$, $\sigma = \uparrow, \downarrow$ and $\Delta_{\mathbf{k}}$ is the p -wave order parameter function $\Delta_{\mathbf{k}} \sim k_x - ik_y$. The question of mutual statistics (between \uparrow and \downarrow electrons and the ensuing composite bosons) may be raised but we assume that it is bosonic. In Ref. [169] we show that the Hamiltonian above can be diagonalized by a Bogoliubov transformation to obtain two pairs of eigenvalues:

$$E + \lambda, E - \lambda, \text{ and } -E + \lambda, -E - \lambda, \quad (4.18)$$

where $E = \sqrt{\tilde{\epsilon}_{\mathbf{k}}^2 - |\Delta_{\mathbf{k}}|^2}$. The last two eigenvalues $-E \pm \lambda$ correspond to well-defined excitations of the system. For $\mu > 0$:

$$-E \pm \lambda \approx -\mu + \epsilon_{\mathbf{k}} + \frac{\Delta^2}{2\mu} \pm \lambda \quad (4.19)$$

i.e. we have an ordinary, non-interacting boson description where the tunneling λ defines the transition at $\lambda = \mu$ from the two Bose condensates to a one Bose condensate (one disappears because $\mu^{\text{eff}} = \mu - \lambda < 0$ i.e. we have vacuum for these particles). This motivates to consider that a viable composite boson effective description of the $\nu = 2/5$ Jain's state is with only one

composite boson condensate and a Bose vacuum. This stems as a natural consequence from our analysis and the multicomponent approach to Jain's states. [123] Any effective description of quantum Hall states must encompass the edge physics as the low energy physics of these states happens on the edge. In the effective description based on composite bosons [64] of the $\nu = 2/5$ fractional quantum Hall edge, one encounters both charge and neutral modes that propagate in the same direction as relativistic particles and the discrepancy with respect to experiments [188] has to be resolved [189]. In the effective description based on composite fermions, [190] at $\nu = 2/5$ edge only the charge mode is propagating, in agreement with the experiment, but the reason why the neutral mode does not propagate is not obvious. Here we suggest an effective picture of the multicomponent degrees of freedom of Jain's state at $\nu = 2/5$ via a Bose vacuum. Any time we have to describe an excitation of the system that involves also these, multicomponent, degrees of freedom, we excite a boson in a vacuum that propagates, not relativistically, but according to Schrödinger equation [191], which in an effective description can be neglected with respect to the charge wave propagation along the edge.

Going back to the eigenvalue problem, one may consider the remaining pair of the eigenvalues:

$$E \pm \lambda. \tag{4.20}$$

It is then obvious from (4.19) that these excitations are unstable and hence may relate to the excited states. In fact, it can be shown [169] that these excitations, in the long distance limit, describe a permanent state (4.10), if we assume that the Hamiltonian H is regularized by a phenomenological term $H + \lambda N$. [125] Therefore before reaching the strong tunneling limit and the incompressible FQH state connected with the single BCS condensate in this description at $\nu = 2/5$ (Jain's state), we may find a state at the transition that evolves from an excited state described by the permanent. It may appear mysterious why we choose the theory with pairing to describe a transition which the numerics seem to suggest to occur between two Abelian states. As we pointed out in Sec. 4.1, the formalism of Read and Green [14] also applies to the situation where the pairing structure of the theory is reflected in what turns out to be the excited state (such as the Pfaffian), whereas the ground state (i.e. CFL) has no pairing.

4.3 Conclusions

In Section 4.1 we investigated the possibility of creating the Moore-Read Pfaffian out of the paired two-component 331 state via tunneling. Exact diagonalization, performed under the constraint of the LLL projection and the fixed total number of particles, could not detect a stable Pfaffian phase, but a critical one between 331 and CFL phases. While the short-range interaction is likely to favor a direct transition from the 331 to the CFL phase, long-range Coulomb interactions leave the possibility for a Pfaffian-like phase if the parameters of the system are tuned in a special way. Based on the connection between our numerical results and the effective BCS Hamiltonian theory of paired states, we argue that one way to stabilize the Pfaffian state is to change the density (number of particles) of the system while increasing the tunneling.

The transition at $\nu = 2/5$ is studied in the presence of Coulomb interaction appropriate for the quantum Hall bilayer and a model short-ranged interaction appropriate for the 332 Halperin's state. We established an avoided level crossing in the first case and, in the latter, a first order transition. With respect to the appearance of the Gaffnian state in the transition region between 332 and Jain, we can conclude that in finite systems this is only possible for the interaction that breaks $SU(2)$ invariance, like the Coulomb bilayer interaction, but remains an unlikely possibility because of the difficulty in establishing the thin torus limit for the approximate $\mathbf{k} = 0$ doublet found for the torus with the aspect ratio close to unity (Fig. 4.11). Within the effective bosonic model, we find that the transition in the presence of the Coulomb interaction may be viewed as a transition from two Bose condensates to a Bose condensate and a Bose vacuum, as one type of bosons gradually disappears from the system. The outcome, with the Bose vacuum, can serve

4. TRANSITIONS BETWEEN TWO-COMPONENT AND NON-ABELIAN STATES IN BILAYERS WITH TUNNELING

as an effective description of the Jain state.

Chapter 5

Wide quantum wells

In this Chapter we explore multicomponent and non-Abelian states in wide quantum wells. The first system we analyze in Sec. 5.1 is a single QH layer with finite thickness. We model the thickness by the Zhang-Das Sarma (ZDS) potential and find quantum phase transitions between compressible and incompressible states as the parameter of the ZDS interaction is varied. In particular, we show that incompressible ground states evolve adiabatically under tuning the parameter of ZDS interaction, whereas the compressible ones are driven through a phase transition. Overlap calculations show that the resulting phase is increasingly well described by appropriate analytic model wave functions (Laughlin, Moore-Read, Read-Rezayi). This scenario is shared by both odd ($\nu = 1/3, 1/5, 3/5, 7/3, 11/5, 13/5$) and even denominator states ($\nu = 1/2, 1/4, 5/2, 9/4$). In particular, the Fermi liquid-like state at $\nu = 1/2$ gives way, at large enough value of the width parameter, to an incompressible state identified as the Moore-Read Pfaffian on the basis of its entanglement spectrum. The second system we analyze (Sec. 5.2) is explicitly a two-component model of the quantum well which takes into account the two lowest subbands. We make a direct connection between this model of the quantum well and the effective-bilayer model. We focus on the filling factors $\nu = 1/2$ and $\nu = 1/4$. In the case of former, we explore the transition between the 331 state and the Moore-Read Pfaffian, subject of Chapter 4. At $\nu = 1/4$ we investigate the nature of the ground state examining different multicomponent candidates (553, 771, Haldane-Rezayi state) and the generalized Moore-Read Pfaffian. This Chapter contains some unpublished results and summarizes the main findings of Refs. [10] and [12].

5.1 Finite thickness and phase transitions between compressible and incompressible states

As a warm-up to the realistic quantum well model that is the subject of Sec. 5.2, here we address, via large-scale ED calculations on finite spheres, the important and interesting question of how to tune various FQH ground states between ungapped compressible and gapped incompressible phases by continuously varying the effective electron-electron interaction in a single QH layer. We show that a simple single-parameter parametrization of the effective interaction through the ZDS model (1.17) provides a flexible and powerful method of studying quantum phase transitions (QPTs) between compressible and incompressible phases at both even and odd-denominator FQH states. ZDS interaction (1.17) for the quantum well of width w

$$V(r, w) = \frac{e^2}{\epsilon\sqrt{r^2 + w^2}}, \quad (5.1)$$

possesses a rich structure that can drive the system from parameter regions where it appears to be compressible (manifested by the ground state that breaks rotational invariance i.e. the

5. WIDE QUANTUM WELLS

value of angular momentum $L \neq 0$) towards the incompressible region where the ground state is rotationally invariant ($L = 0$), along with the corresponding overlap with the trial states like Laughlin [46] or paired states (Moore-Read Pfaffian [18], Read-Rezayi [96] etc.) jumping to a value close to unity and an energy gap opening up in the excitation spectrum. In agreement with the experimental phenomenology, we find that the well-known odd-denominator incompressible FQH states (e.g. $1/3$, $1/5$, $7/3$, $11/5$) are robust and usually do not manifest any interaction-tuned QPT whereas the more fragile, even denominator (e.g. $1/2$, $1/4$, $5/2$, $9/4$) FQH states typically exhibit characteristic QPT from a compressible to an incompressible phase as the Coulomb interaction is softened by increasing the ZDS tuning parameter.

We emphasize that the ZDS interaction (5.1) appears to have the same qualitative pseudopotential decomposition as the realistic models (e.g. the Fang-Howard, infinite square well, etc.). In Fig. 5.1 we plot the few strongest pseudopotentials on the sphere, calculated for ZDS and the infinite square well confinement. For each width, we normalize the corresponding pseudopotentials by the value of V_0 . The successive sets of V_m show the softening effect of the perpendicular confinement. We see that, although the parameter w cannot be directly compared between the ZDS and the infinite square well model, the pseudopotential decomposition qualitatively appears the same.

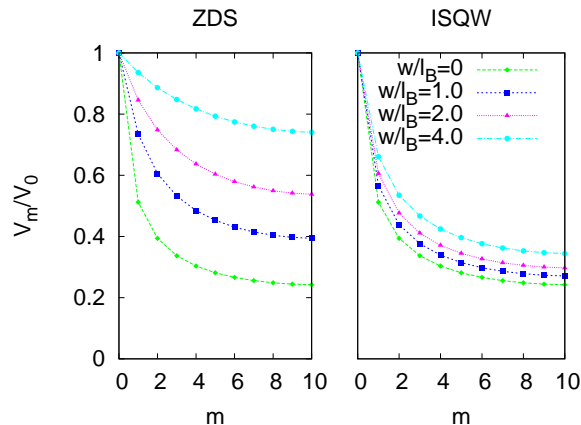


Figure 5.1: Comparison of the few largest pseudopotentials (normalized by $V_0(w)$) for the Zhang-Das Sarma (ZDS) interaction and those for the infinite square well model (ISQW).

However, it was also observed in Ref. [12] that realistic confinement models such as the infinite square well do not always reproduce the QPTs induced by the ZDS interaction, suggesting there may be subtle quantitative differences between ZDS and alternative confinement models which are important in the vicinity of a QPT. In this Section we focus on the ZDS model in carrying out our ED studies since a single parameter enables us to study FQH QPTs in a compact manner because it yields a particularly simple form of the effective interaction. In order to establish the connection with the experiments, we should mention that w in the ZDS model corresponds roughly to the root-mean-square fluctuation in the electron coordinate in the transverse direction, [175] although ZDS interaction (5.1) does not yield any simple wave function for the confinement in the perpendicular direction.

With this choice of the interaction, we use the overlap between the exact, numerically diagonalized finite system, and a candidate analytical wave function (e.g. the Moore-Read wavefunction) to determine the tentative quantum phase of the system. We calculate the overlap as a continuous function of the varying Hamiltonian which is being tuned by w . All the model wave functions studied in this section are Jack polynomials that have squeezable configurations [192] which can be efficiently generated and compared with the exact ground state. In doing so, we disregard the aliased cases [10] from our considerations (we discussed the aliased states below the formula 2.4).

5.1 Finite thickness and phase transitions between compressible and incompressible states

We have already examined the effect of ZDS interaction on the Laughlin states in Sec. 2. It will be shown in what follows that the induced QPT that we have seen earlier for $N = 5, \nu = 7/3$ is not an exceptional case. In Fig. 5.2 we show the overlap results of finite-size calculations on $\nu = 1/2$ in the LLL and $\nu = 5/2$ in the SLL with ZDS interaction. In Fig. 5.3 we present data

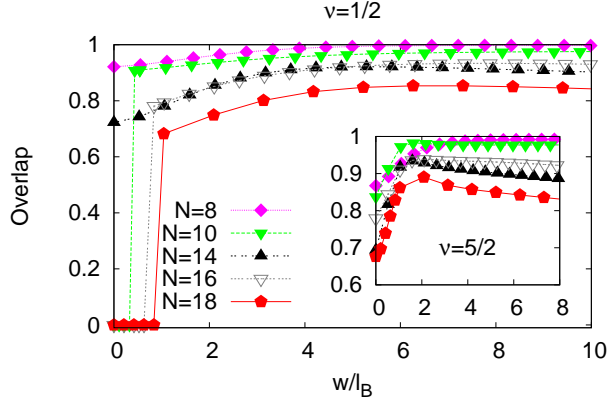


Figure 5.2: Overlap $|\langle \Psi_{\text{Pf}} | \Psi_{\text{exact}} \rangle|$ between the exact ZDS ground state for finite width w/l_B at $\nu = 1/2$ and the Pfaffian for $N = 8 - 18$ particles. Inset: same quantity but in the first excited Landau level i.e. $\nu = 5/2$. Only non-aliased states are shown. Note: the critical width of the QPT increases with system size, however for the three available points and $N \rightarrow \infty$, it extrapolates to a value of $4l_B$.

on $\nu = 1/4$ in the LLL. In this case, the Moore-Read Pfaffian is defined as

$$\Psi_{\text{Pf}}^{1/4}(z_1, \dots, z_N) = \text{Pf} \left(\frac{1}{z_i - z_j} \right) \prod_{i < j} (z_i - z_j)^4. \quad (5.2)$$

We note in passing that, contrary to the finite-width models which change *all* pseudopotentials at once, one may start from the pure Coulomb interaction and vary just a few strongest pseudopotentials. [83] One can vary either V_1 or V_3 (or both), but this procedure does not lead to the phase transitions in all the cases as ZDS interaction does.

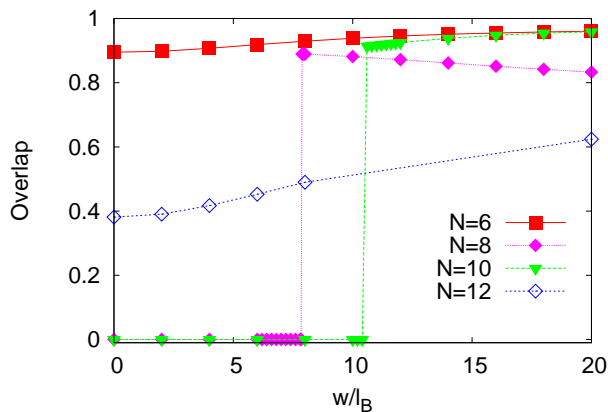


Figure 5.3: Overlap $|\langle \Psi_{\text{Pf}} | \Psi_{\text{exact}} \rangle|$ between the exact ZDS ground state for finite width w/l_B and the Pfaffian at $\nu = 1/4$.

At $\nu = 1/2$ a QPT is induced by increasing the parameter w . Certain particle numbers yield good overlap already for zero thickness and their overlap improves as w increases. Other particle numbers produce ground states with well-defined values of $L > 0$ that undergo a QPT at a critical value of the thickness. For $\nu = 5/2$, the Coulomb ground state for zero thickness is already reasonably well approximated [83, 193] by the Moore-Read Pfaffian and the effect of

5. WIDE QUANTUM WELLS

ZDS interaction is only to increase the overlap in a smooth way. However, the increase is substantial – up to 20% for the largest system amenable to ED. This adiabatic continuity of the Moore-Read description for the SLL $\nu = 5/2$ has been discussed in Refs. [177, 193].

The non-zero values of L that appear at $\nu = 1/2$ in the LLL can be fully understood from the CF theory. [165] Indeed, former work hinted at the possibility of p -wave paired CF state as a result of CF sea being perturbed by ZDS interaction. [194] However, in Ref. [194] only the variational energies of trial states were compared.

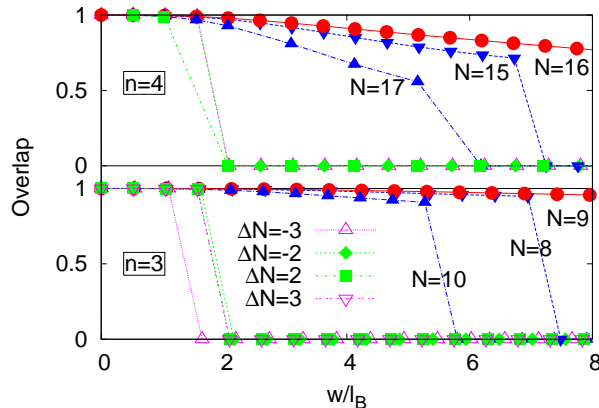


Figure 5.4: Overlap $|\langle \Psi_{\text{exact}}(w=0) | \Psi_{\text{exact}}(w) \rangle|$ between the exact ZDS state for finite width w/l_B at $\nu = 1/2$ and the CF sea state defined to be exact Coulomb ground state for zero thickness. Red circles represent filled CF shells ($N = n^2, n = 3, 4$), blue triangles are the lowest excited states $\Delta N = N - n^2 = \pm 1$ and so on.

In Fig. 5.4 we show that one can establish a connection between the ZDS-induced QPT and the Pfaffian and CF sea states in the LLL at $\nu = 1/2$. Because the CF sea state and the Moore-Read Pfaffian occur at different shifts on the sphere (-2 and -3, respectively), one cannot simultaneously study their evolution with w . However, by analyzing the excitations of CF sea occurring at the Pfaffian shift, one can show (using Hund's rule) that the L values obtained in ED at the Pfaffian shift (Fig. 5.2) are indeed those stemming from the CF sea excitations. Moreover, assuming that the Coulomb ground state in the LLL for zero thickness is exceedingly well approximated by Rezayi-Read wave function (1.37), [68] we define the CF sea state for our purposes as the interacting Coulomb ground state for zero thickness and study its overlap with the $w \geq 0$ ground states, Fig. 5.4. CF theory tells us that (at the shift of -2) the $L = 0$ configurations are obtained when the CF shells are completely filled i.e. for $N = n^2, n = 1, 2, 3, \dots$, Fig. 5.5. These configurations are particularly robust and adding/subtracting electrons from

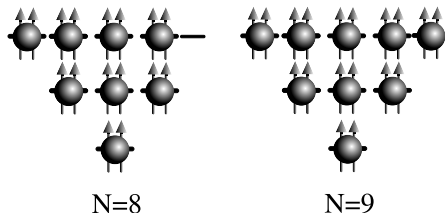


Figure 5.5: CF levels for $N = 8$ and $N = 9$.

them ($\Delta N = N - n^2 = \pm 1, \pm 2, \dots$) creates a configuration that is destroyed at some critical value of the width which depends on how far away the system is from the filled shell. Obviously, there is ambiguity in defining precisely the critical width where the CF sea is destroyed, but this argument nonetheless provides further support for the claim that the ZDS-induced compressible-incompressible transition indeed proceeds via destruction of CF sea towards the Moore-Read Pfaffian. Transition of the same kind can be relevant for the multicomponent candidates [195] at $\nu = 3/8$. We emphasize that the possible finite-width-induced LLL $\nu = 1/2$ FQH

state that we find arising out of the destabilization of the CF sea, even if it exists, is likely to be extremely fragile with a neutral excitation gap smaller than $0.03e^2/\epsilon l_B$. [177] However, numerically extrapolated gap is generally known to be difficult to relate to the experimental value [196] and in our data we cannot rule out the possibility that it goes to zero in thermodynamic limit.

Another way to look at the QPT towards the Moore-Read Pfaffian is to analyze the entanglement spectrum we introduced in Section 2.1.2 (originally proposed in Ref. [11]). This is a powerful way to identify topological order in the given ground state wave function and establish a direct connection with the underlying CFT that produces the given ground state as its correlator and thus offering more information than the simple overlap calculation. [141] In Fig. 5.6 we show the change in the entanglement spectrum for $N = 18$ particles at $\nu = 1/2$ in the LLL, before and after QPT. For $w < l_B$, there is no visible CFT branch in the entanglement spectrum – the generic Coulomb part dominates, leading to a likely compressible ground state. After the QPT, a CFT branch separates from the Coulomb part of the spectrum and the level counting begins to match the first few Virasoro levels of the Ising CFT. This is additional evidence in favor of the possibility of a finite-width-induced QPT to an incompressible half-filled single-layer LLL FQH state.

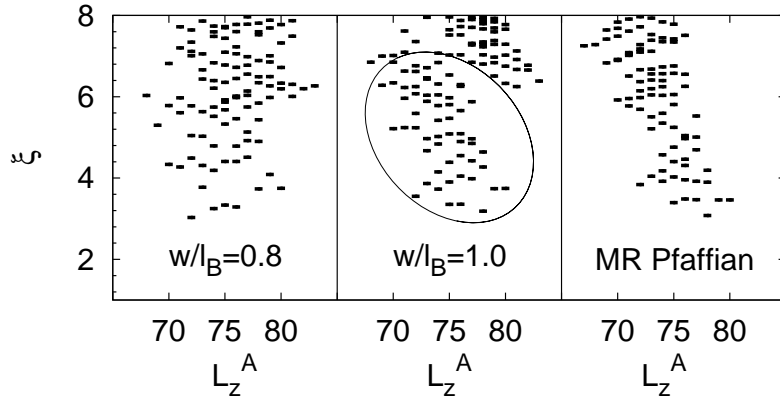


Figure 5.6: Entanglement spectrum of the exact ground state for $N = 18$ particles at $\nu = 1/2$ in the LLL, just before ($w/l_B = 0.8$) and after ($w/l_B = 1.0$) the QPT, and the spectrum of Moore-Read Pfaffian for comparison. Vertical axes show the quantity $\xi = -\log \lambda_A$, where λ_A are the eigenvalues of the reduced density matrix of the subsystem A which comprises of 8 particles and 15 orbitals, given as a function of angular momentum L_z^A . Data shown is only for the partitioning denoted by [0|0] in Ref. [11], other sectors give a similar result.

We have also examined the effect of ZDS potential on other even denominator and paired states. For Read-Rezayi $\nu = 3/5$ state a QPT is induced around $w \sim 4l_B$ and, in the SLL, a $\nu = 9/4$ state is similarly stabilized when ZDS parameter is around $w \sim 3l_B$.

Therefore, we can conclude that the continuous tuning of the interaction through the ZDS Hamiltonian enables a direct study of FQH quantum phase transitions showing that the usual odd denominator states are robust in both the LLL and the SLL, whereas the fragile even denominator FQH states are stable only in a regime of the interaction strength where the bare electron-electron interaction is considerably softer than the pure 2D Coulomb interaction. We find that the ZDS interaction allows for the existence of non-Abelian incompressible FQH states even at unusual even fractions such as $1/2, 1/4$, and $9/4$, raising the intriguing possibility that such exotic non-Abelian states may indeed exist if one can sufficiently soften the interaction along the ZDS prescription. Whether this can be physically achieved in 2D semiconductor systems remains an interesting open question and may require some ‘reverse engineering’ of the quasi-2D samples to achieve a suitable density profile using the fact that the width parameter in the ZDS

model corresponds roughly to the variance of the electron position in the transverse direction.

5.2 Two-subband model of the quantum well

In the preceding Section we used a simple, one-component model of the wide quantum well. In this Section we will introduce a realistic model that takes into account the two lowest subbands as the relevant low-energy degrees of freedom available to the electrons. We consider an infinite square well of width w in the direction $z \in [0, w]$, Fig. 1.4. The electronic motion in the z -direction will then be quantized, yielding an electronic subband structure. Instead of a full description with all the electronic subbands, we only consider the two lowest subbands (we comment on the validity of two-subband approximation in Sec. 5.2.1). We identify the two subbands with the two pseudospin states, $\Psi_{\uparrow,\downarrow} = \phi_{\uparrow,\downarrow}(z)Y_{N_\phi/2, N_\phi/2, m}(\theta, \phi)$, where $\phi_{\uparrow,\downarrow}$ were defined in (1.48) but we now label them as \uparrow and \downarrow , instead of by their reflection symmetry property (symmetric and antisymmetric, respectively). Y 's represent monopole spherical harmonics with $-N_\phi/2 \leq m \leq N_\phi/2$ (we assume that the states are entirely within the LLL). If the energy splitting between the subbands is denoted by Δ_{SAS} , the corresponding second quantized Hamiltonian is given by [197]

$$H = -\Delta_{SAS}S_z - \Delta\rho S_x + \frac{1}{2} \sum_{\{m\}} \sum_{\{\sigma\}} V_{m_1, m_2, m_3, m_4}^{\sigma_1, \sigma_2, \sigma_3, \sigma_4} c_{m_1 \sigma_1}^\dagger c_{m_2 \sigma_2}^\dagger c_{m_4 \sigma_4} c_{m_3 \sigma_3}, \quad (5.3)$$

where the first term stands for the Zeeman splitting between the subbands, followed by the term which represents the density imbalance $\Delta\rho$. For the infinite square well, Δ_{SAS} is directly determined by the width of the well w , however it is expected to be renormalized in each sample, so it is convenient to think of it as a free parameter.

The matrix elements $V_{m_1, m_2, m_3, m_4}^{\sigma_1, \sigma_2, \sigma_3, \sigma_4}$ can be evaluated from the Haldane pseudopotentials for the effective in-plane interaction

$$V_{2D}^{\sigma_1, \sigma_2, \sigma_3, \sigma_4}(\mathbf{r}_1 - \mathbf{r}_2) = \frac{e^2}{\epsilon l_B} \int dz_1 \int dz_2 \frac{\phi_{\sigma_1}^*(z_1) \phi_{\sigma_2}^*(z_2) \phi_{\sigma_3}(z_1) \phi_{\sigma_4}(z_2)}{\sqrt{|\mathbf{r}_1 - \mathbf{r}_2|^2 + (z_1 - z_2)^2}}, \quad (5.4)$$

where the position variables are expressed in units of l_B such that the integral is dimensionless. To evaluate the pseudopotentials for the effective interaction (5.4) we sample the pseudopotentials for the interaction $1/\sqrt{r^2 + z^2}$ for many values of z and then use numerical interpolation scheme to perform the integral over z variables.

As we are interested in the possible phases that may occur and the transitions between them, we expect the model described by the Hamiltonian (5.3) to be qualitatively correct and in agreement with other confinement models (e.g. the Fang-Howard, (1.14)) that assume the lowest subband to be symmetric and the first excited one to have a node. Any difference of the confining potential away from the infinite square well will modify the energy eigenvalues and the associated wave functions $\phi_\sigma(z)$. However, it is expected that the energies are more strongly affected than the wave functions. In particular, the nodal structure of the wave functions is robust, such that the two lowest eigenstates of the infinite well faithfully represent the underlying features. However, we will allow for the general values of the level splitting Δ_{SAS} to account for the variations in the eigen-energies.

5.2.1 Connection between the quantum-well model and the bilayer

The wide quantum well allows the electrons to reduce their mutual Coulomb repulsion by exploring more efficiently the z -direction, and it has been argued that due to this effect, a spontaneous bilayer may be formed, under appropriate conditions. [7, 115] Here, a connection is made between both two-component models, on the basis of the Hamiltonian (5.3). We consider the

quantum well to be symmetric around $w/2$, i.e. the lowest subband (\uparrow) state is symmetric, and the first excited one (\downarrow) is antisymmetric. Furthermore, we consider, in this section, the electrons to be in the 2D plane, for illustration reasons, although the conclusions remain valid also in the spherical geometry.

The interaction part of the Hamiltonian (5.3) may be rewritten in terms of the density and spin-density operators projected to a single Landau level. The Fourier components of the projected density operator of pseudospin- σ electrons reads

$$\bar{\rho}_\sigma(\mathbf{q}) = \sum_{m,m'} \langle m | e^{-i\mathbf{q}\cdot\mathbf{R}} | m' \rangle c_{m\sigma}^\dagger c_{m'\sigma} ,$$

in terms of the 2D wave vector \mathbf{q} and the guiding-center operator \mathbf{R} , the latter acting on the states labeled by the quantum numbers m . It is furthermore useful to define the total (projected) density operator

$$\bar{\rho}(\mathbf{q}) = \bar{\rho}_\uparrow(\mathbf{q}) + \bar{\rho}_\downarrow(\mathbf{q}) \quad (5.5)$$

and the projected pseudospin density operators,

$$\bar{S}^\mu(\mathbf{q}) = \sum_{m,m'} \langle m | e^{-i\mathbf{q}\cdot\mathbf{R}} | m' \rangle c_{m\sigma}^\dagger \frac{\tau_{\sigma,\sigma'}^\mu}{2} c_{m'\sigma'} , \quad (5.6)$$

where $\tau_{\sigma,\sigma'}^\mu$ are the usual 2×2 Pauli matrices with $\mu = x, y, z$.

Using (5.5) and (5.6), we can organize the terms in the Hamiltonian (5.3) into density-density interaction and terms beyond, which may be described as a spin-spin interaction. Indeed, the density-density part consists of the effective interactions (5.4) $V_{2D}^{\uparrow\uparrow\uparrow\uparrow}$, $V_{2D}^{\downarrow\downarrow\downarrow\downarrow}$, and $V_{2D}^{\uparrow\downarrow\uparrow\downarrow} = V_{2D}^{\downarrow\uparrow\downarrow\uparrow}$. Notice that the interactions in the first excited subband (\downarrow) are generally weaker than in the lowest one (\uparrow) because the wave function $\phi_\downarrow(z)$ possesses a node at $w/2$, in the center of the well, i.e. $V_{2D}^{\uparrow\uparrow\uparrow\uparrow} > V_{2D}^{\downarrow\downarrow\downarrow\downarrow}$. With the help of the (spin) density operators (5.5) and (5.6), the density-density part of the interaction Hamiltonian reads

$$H^{\rho-\rho} = \frac{1}{2} \sum_{\mathbf{q}} V_{SU(2)}(\mathbf{q}) \bar{\rho}(-\mathbf{q}) \bar{\rho}(\mathbf{q}) + 2 \sum_{\mathbf{q}} V_{sb}^z(\mathbf{q}) \bar{S}^z(-\mathbf{q}) \bar{S}^z(\mathbf{q}) + \sum_{\mathbf{q}} V_B^z(\mathbf{q}) \bar{\rho}(-\mathbf{q}) \bar{S}^z(\mathbf{q}), \quad (5.7)$$

in terms of the SU(2)-symmetric interaction

$$V_{SU(2)}(\mathbf{q}) = \frac{1}{4} \left[V_{2D}^{\uparrow\uparrow\uparrow\uparrow}(\mathbf{q}) + V_{2D}^{\downarrow\downarrow\downarrow\downarrow}(\mathbf{q}) + 2V_{2D}^{\uparrow\downarrow\uparrow\downarrow}(\mathbf{q}) \right], \quad (5.8)$$

and the SU(2)-symmetry breaking interaction terms

$$V_{sb}^z(\mathbf{q}) = \frac{1}{4} \left[V_{2D}^{\uparrow\uparrow\uparrow\uparrow}(\mathbf{q}) + V_{2D}^{\downarrow\downarrow\downarrow\downarrow}(\mathbf{q}) - 2V_{2D}^{\uparrow\downarrow\uparrow\downarrow}(\mathbf{q}) \right] \quad (5.9)$$

and

$$V_B^z(\mathbf{q}) = \frac{1}{2} \left[V_{2D}^{\uparrow\uparrow\uparrow\uparrow}(\mathbf{q}) - V_{2D}^{\downarrow\downarrow\downarrow\downarrow}(\mathbf{q}) \right]. \quad (5.10)$$

The remaining 12 interaction terms, which cannot be treated as density-density interactions, fall into two different classes; the 8 terms with three equal spin orientations σ and one opposite $-\sigma$ are zero due to the antisymmetry of the integrand in Eq. (5.4). The remaining 4 interaction terms with two \uparrow -spins and two \downarrow -spins are all equal due to the symmetry of the quantum well around $w/2$,

$$V_{sb}^x \equiv V_{2D}^{\uparrow\uparrow\downarrow\downarrow} = V_{2D}^{\downarrow\downarrow\uparrow\uparrow} = V_{2D}^{\uparrow\downarrow\downarrow\uparrow} = V_{2D}^{\downarrow\uparrow\uparrow\downarrow}. \quad (5.11)$$

They yield the term

$$H_{sb}^z = 2 \sum_{\mathbf{q}} V_{sb}^x(\mathbf{q}) \bar{S}^x(-\mathbf{q}) \bar{S}^x(\mathbf{q}), \quad (5.12)$$

which needs to be added to the interaction Hamiltonian (5.7), as well as the term

$$H_{SAS} = -\Delta_{SAS} \bar{S}^z(\mathbf{q} = 0), \quad (5.13)$$

5. WIDE QUANTUM WELLS

which accounts for the electronic subband gap between the \uparrow and the \downarrow levels, and the density-imbalance term

$$H_{\Delta\rho} = -\Delta\rho \bar{S}^x(\mathbf{q} = 0). \quad (5.14)$$

Collecting all terms, the Hamiltonian (5.3) thus becomes

$$\begin{aligned} H = & \frac{1}{2} \sum_{\mathbf{q}} V_{SU(2)}(\mathbf{q}) \bar{\rho}(-\mathbf{q}) \bar{\rho}(\mathbf{q}) + 2 \sum_{\mathbf{q}} V_{sb}^x(\mathbf{q}) \bar{S}^x(-\mathbf{q}) \bar{S}^x(\mathbf{q}) + 2 \sum_{\mathbf{q}} V_{sb}^z(\mathbf{q}) \bar{S}^z(-\mathbf{q}) \bar{S}^z(\mathbf{q}) \\ & + \sum_{\mathbf{q}} V_B^z(\mathbf{q}) \bar{\rho}(-\mathbf{q}) \bar{S}^z(\mathbf{q}) - \Delta_{SAS} \bar{S}^z(\mathbf{q} = 0) - \Delta\rho \bar{S}^x(\mathbf{q} = 0). \end{aligned} \quad (5.15)$$

Several comments are to be made with respect to this result. First, we have checked that for the infinite-square-well model as well as for a model with a parabolic confinement potential there is a natural hierarchy of the energy scales in the Hamiltonian (5.15),

$$V_{SU(2)} > V_{sb}^x \gtrsim V_B^z \gtrsim V_{sb}^z. \quad (5.16)$$

This hierarchy is valid for the interaction potentials in Fourier space and hence as for the pseudopotentials as well.

Whereas the first term of the Hamiltonian describes the SU(2)-symmetric interaction, the second and the third one break this SU(2) symmetry. Because $V_{sb}^x(\mathbf{q}) > V_{sb}^z(\mathbf{q}) > 0$ for all values of \mathbf{q} , states with no polarization in the x - and the z -direction are favored, with $\langle S^x \rangle = 0$ and $\langle S^z \rangle = 0$, respectively. Due to the hierarchy (5.16) of energy scales, a depolarization in the x -direction is more relevant than that in the z -direction. These terms are similar to those one encounters in the case of a bilayer quantum Hall system, where due to the finite layer separation a polarization of the layer isospin in the z -direction costs capacitive energy. [103]

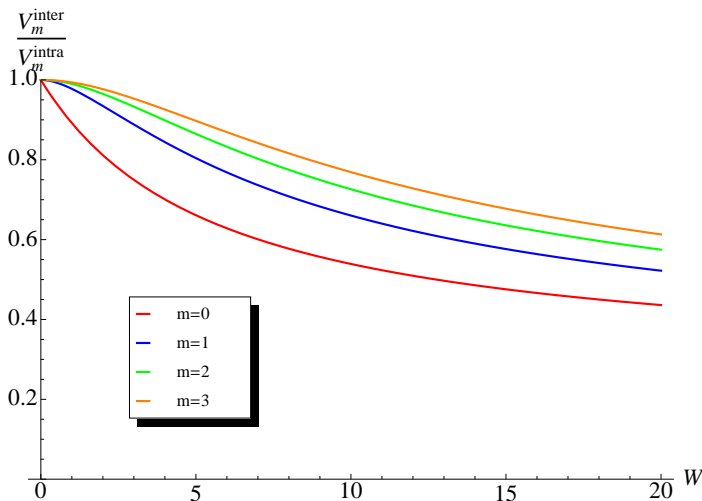


Figure 5.7: Ratio of the few strongest, inter and intra, bilayer pseudopotentials $V_m^{\text{inter}}/V_m^{\text{intra}}$ derived from an underlying quantum well model, as a function of width w . Note the saturation of the ratios for large widths w , illustrating the limit of validity of the quantum well model.

The fourth term of the Hamiltonian (5.15) is due to the stronger electron-electron repulsion in the lowest electronic subband as compared to the first excited one, where the wave function possesses a node at $z = w/2$. In order to visualize its effect, one may treat the density, which we consider to be homogeneous in an incompressible state, on the mean-field level, $\langle \bar{\rho}(\mathbf{q}) \rangle = \nu \delta_{\mathbf{q},0}$, in which case the fourth term of Eq. (5.15) becomes $\nu V_B^z(\mathbf{q} = 0) \bar{S}^z(\mathbf{q} = 0)$ and, thus, has the same form as the subband-gap term (5.13). It therefore renormalizes the energy gap between the lowest and the first excited electronic subbands, and it is natural to define the effective subband

gap as

$$\Delta_{SAS} \rightarrow \tilde{\Delta}_{SAS} = \Delta_{SAS} - \nu V_B^z(\mathbf{q} = 0) = \Delta_{SAS} - \gamma \nu \frac{e^2}{\epsilon l_B} \frac{w}{l_B}, \quad (5.17)$$

where γ is a numerical prefactor that depends on the precise nature of the well model. The expression (5.17) is easy to understand – whereas the subband gap Δ_{SAS} tends to polarize the system in the \uparrow state, namely in narrow samples, the second term in Eq. (5.17) indicates that the interactions are weaker in the \downarrow subband. From the interaction point of view, it is therefore energetically favorable to populate the first excited subband. This effect becomes more pronounced in larger quantum wells. Notice furthermore that this argument also delimits the regime of validity of the two-subband approximation of the wide quantum well; when the term $\gamma \nu (e^2/\epsilon l_B) \times (w/l_B)$ becomes much larger than the bare subband gap Δ_{SAS} , the electrons may even populate higher subbands, which are neglected in the present model, and the system eventually crosses over into a 3D regime.

It is also useful to consider an approximation to the Hamiltonian (5.3)

$$H \simeq \frac{1}{2} \sum_{\mathbf{q}} V_{SU(2)}(\mathbf{q}) \bar{\rho}(-\mathbf{q}) \bar{\rho}(\mathbf{q}) + 2 \sum_{\mathbf{q}} V_{sb}^x(\mathbf{q}) \bar{S}^x(-\mathbf{q}) \bar{S}^x(\mathbf{q}) - \tilde{\Delta}_{SAS} \bar{S}^z(\mathbf{q} = 0). \quad (5.18)$$

The Hamiltonian (5.18) neglects a particular term $\propto \bar{S}^z(-\mathbf{q}) \bar{S}^z(\mathbf{q})$, which turns out to constitute the lowest energy scale in the interaction Hamiltonian (5.3) [see Eq. (5.16)]. Notice that the Hamiltonian (5.18) has the same form as the Hamiltonian which describes a bilayer quantum Hall system, [103] up to a rotation from the z - to the x -axis. In this rotated reference frame, one may define the intra- and inter-layer interactions as

$$V_{\text{intra}}(\mathbf{q}) = V_{SU(2)}(\mathbf{q}) + V_{sb}^x(\mathbf{q}) = \frac{1}{4} \left[V_{2D}^{\uparrow\uparrow\uparrow\uparrow}(\mathbf{q}) + V_{2D}^{\downarrow\downarrow\downarrow\downarrow}(\mathbf{q}) + 2V_{2D}^{\uparrow\downarrow\uparrow\downarrow}(\mathbf{q}) \right] + V_{2D}^{\uparrow\uparrow\downarrow\downarrow}(\mathbf{q}) \quad (5.19)$$

and

$$V_{\text{inter}}(\mathbf{q}) = V_{SU(2)}(\mathbf{q}) - V_{sb}^x(\mathbf{q}) = \frac{1}{4} \left[V_{2D}^{\uparrow\uparrow\uparrow\uparrow}(\mathbf{q}) + V_{2D}^{\downarrow\downarrow\downarrow\downarrow}(\mathbf{q}) + 2V_{2D}^{\uparrow\downarrow\uparrow\downarrow}(\mathbf{q}) \right] - V_{2D}^{\uparrow\uparrow\downarrow\downarrow}(\mathbf{q}). \quad (5.20)$$

As for the case of the true bilayer, the thus defined intra-layer interaction is stronger than the inter-layer interaction, for all values of \mathbf{q} .

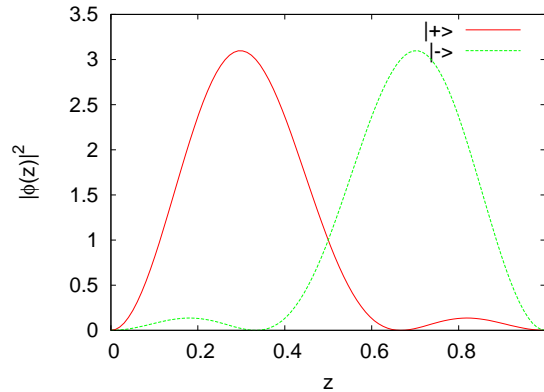


Figure 5.8: Densities of the single-particle states in the rotated frame, $|\pm\rangle$.

The above mapping of the WQW model onto the effective bilayer works best for not too large well widths. As the well width W becomes very large, the effective bilayer distance \tilde{d} saturates. To see this, we can calculate the Haldane pseudopotentials $V_m^{\sigma_1\sigma_2\sigma_3\sigma_4}$, where m is the relative angular momentum of the two electrons. The pseudopotentials for the effective interaction (5.4), written on the disk for simplicity, are

$$V_m^{\sigma_1\sigma_2\sigma_3\sigma_4} = \int \frac{d^2\mathbf{k}}{(2\pi)^2} e^{-k^2} \mathcal{L}_m(k^2) V_{2D}^{\sigma_1\sigma_2\sigma_3\sigma_4}(\mathbf{k}),$$

5. WIDE QUANTUM WELLS

number of particles N	6	8	10	6	8
number of flux $2Q$	9	13	17	19	27
$L_z = 0$ (polarized)	19	151	1514	1242	61731
$L_z = 0, S_z = 0$ (SU(2) spin)	900	39131	2006736	37800	7613345
$L_z = 0$ (SU(2) with tunneling)	2496	123711	7050864	113128	26035319

Table 5.1: Maximum Hilbert space dimensions for some of the systems studied in this Chapter.

where \mathcal{L}_m is the Laguerre polynomial and the Fourier transform $V_{2D}^{\sigma_1\sigma_2\sigma_3\sigma_4}(\mathbf{k})$ can be evaluated analytically. Then, we can construct linear combinations (5.19) and (5.20) of $V_m^{\sigma_1\sigma_2\sigma_3\sigma_4}$ to get the effective bilayer pseudopotentials, V_m^{intra} and V_m^{inter} . We plot the ratios of the few strongest V_m^{intra} and V_m^{inter} in Fig. 5.7 as a function of w . We notice that the limits saturate for large w , indicating that the inter-layer repulsion decreases very slowly with respect to intra-repulsion for larger w , thus suggesting that the model becomes unrealistic in this regime.

Since our ED calculations employ the Hamiltonian (5.3), in order to compare the numerical results with the Halperin states (1.45) which are the native eigenstates of the true bilayer Hamiltonian, we can apply the mapping between the two models described above in a reverse fashion. As Halperin wave functions are commonly labeled by the single particle states $|\uparrow\rangle, |\downarrow\rangle$ (which are the eigenstates of S_z) and defined by interaction potentials $\{V_A, V_E\}$, we can imagine a linear transformation (rotation from z to x) that transforms them into (unnormalized) symmetric $|+\rangle = |\uparrow\rangle + |\downarrow\rangle$ and antisymmetric $|-\rangle = |\uparrow\rangle - |\downarrow\rangle$ combinations. The single-particle densities for the transformed states are shown in Fig. 5.8, thus $|\pm\rangle$ are “bilayer-like” single particle wave functions, localized towards the sides of the well. Then, by inverting the Eqs. (5.19) and (5.20), we obtain the set of interaction potentials that generate the Halperin states (m, m', n) in a quantum well description. In this Chapter, Halperin states (1.45) are understood to be indexed by $|+\rangle, |-\rangle$ instead of the usual notation $|\uparrow\rangle, |\downarrow\rangle$, unless explicitly stated otherwise.

In the remainder of this Chapter we present results of the exact diagonalization of the Hamiltonian (5.3). We consider a range of systems some of which have rather large dimension of the Hilbert space, listed in Tab. 5.1 which illustrates the exponential increase in Hilbert space dimension with the number of particle and number of internal degrees of freedom.

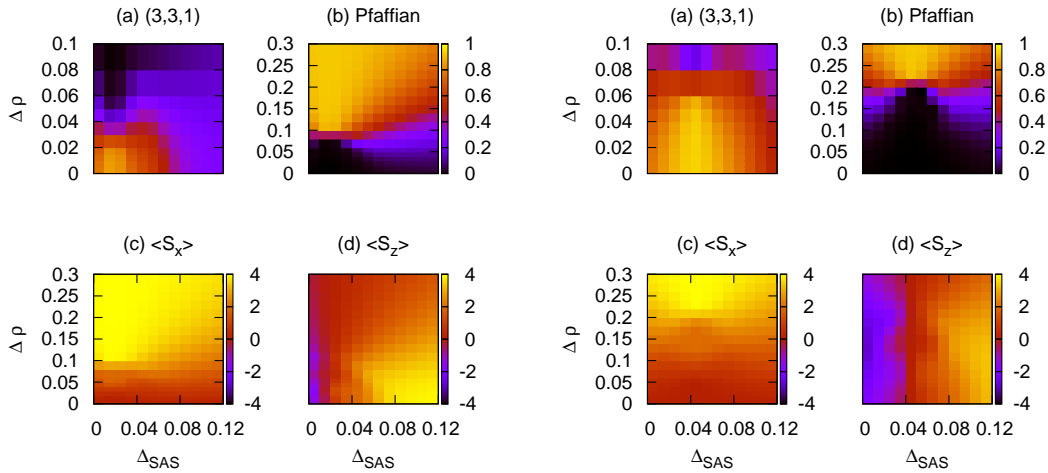


Figure 5.9: Phase diagram in $\Delta\rho - \Delta_{SAS}$ space for the quantum well of $N = 8$ particles on the sphere, $w/l_B = 2.0$ (left) and $w/l_B = 4.0$ (right): overlaps between the exact ground state and Halperin 331 state (a), Moore-Read Pfaffian (b), and the mean value of S_x (c) and S_z (d) operator of pseudospin.

5.3 $\nu = 1/2$ in a quantum well

At the filling factor $\nu = 1/2$ the competing phases we consider here are the 331 Halperin state and the Moore-Read Pfaffian (in Ref. [12] data can be found also for the Haldane-Rezayi state, [74]).

In Fig. ?? we show the overlaps with each of the competing phases, along with the mean values of S_x and S_z operators. The system is $N = 8$ electrons for two values of the quantum well width, $w/l_B = 2.0$ and $w/l_B = 4.0$. Regarding the 331 state, we note that its high overlap is surprisingly robust to variation in either Δ_{SAS} or $\Delta\rho$. On the other hand, the Pfaffian state appears only for large values of the imbalance and in the region where the system is fully x -polarized (maximum $\langle S_x \rangle$). This means that we have effectively a single-component system, although with a more complicated interaction. However, as we have already shown in Chapter 4, the Pfaffian in this kind of system is very fragile. It can describe a phase with a minuscule gap or an excited state of the CFL.

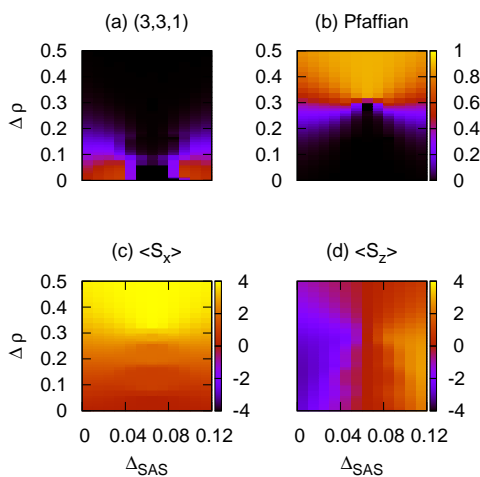


Figure 5.10: Phase diagram in $\Delta\rho - \Delta_{SAS}$ space for the quantum well of $N = 8$ particles on the sphere at $\nu = 1/2$ in the second LL and width $w/l_B = 4.0$: overlaps between the exact ground state and Halperin 331 state (a), Moore-Read Pfaffian (b), and the mean value of S_x (c) and S_z (d) operator of pseudospin.

We also note that the highest overlap with the Pfaffian occurs for the same value of Δ_{SAS} for which the 331 overlap is maximal. This testifies to the transition proceeding via the destruction of the 331 state under the increase of density imbalance. In the experiment, however, imbalancing the quantum well leads also to the increase in Δ_{SAS} , [124] which suggests that in interpreting the plots, our system may be evolving along curved trajectories in the $\Delta_{SAS} - \Delta\rho$ diagram. Note, furthermore, that we have defined our 331 state to be an eigenstate of the S_x operator in the terminology of the true bilayer and not the usual S_z operator (naively defining the Halperin state to be the eigenstate of S_z does not give any appreciable overlap with the exact ground state). There is a simple reason why this needs to be done: because the states of the quantum well possess nodal structure (1.48), the true bilayer states (like the Halperin states) need to be rotated first from z to x direction, in order to match the property of reflection (anti)symmetry, before direct comparison can be made.

If we multiply the interaction with the appropriate form factors to describe the second LL, Fig. 5.10, we notice that 331 state is significantly weaker and the transition to the Pfaffian starts from a compressible state. This is consistent with the expectations for the second LL where Halperin states are generally weak and $\nu = 5/2$ is described by the Moore-Read state.

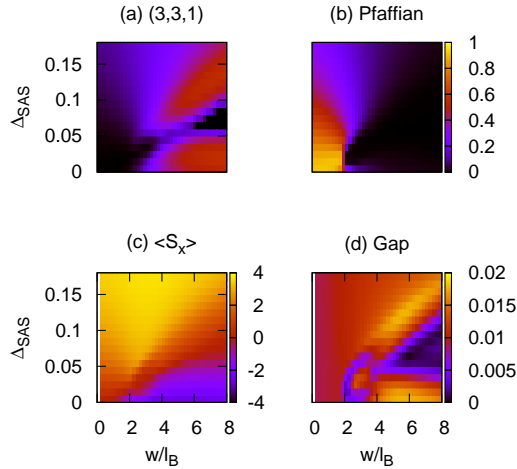


Figure 5.11: Neutral gap for $N = 8$ electrons on the sphere at $\nu = 1/2$ in the LLL and imbalance set to $\Delta\rho = 0.1e^2/\epsilon l_B$, as a function of width w and tunneling Δ_{SAS} .

Another quantity which can give some insight into the stability of a state is the neutral gap for creating a particle-hole excitation, Fig. 5.11. We again work in the LLL and set the imbalance to a value where the Pfaffian state is much stronger than the 331 state, but neither of the overlaps is strictly zero. Even in this “unfavorable” situation for the 331 state, we find that the neutral gap is largest in the regions of the phase diagram that correspond to a nonzero overlap with the 331.

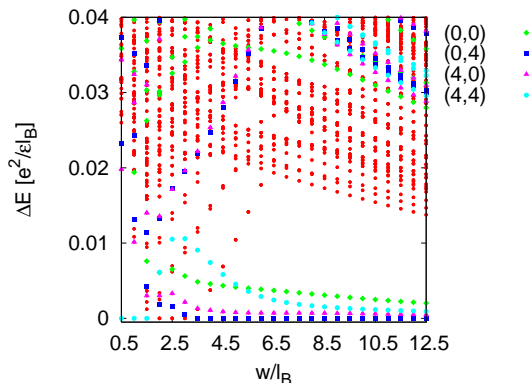


Figure 5.12: Energy spectrum of the quantum well Hamiltonian (5.3) for $\Delta_{SAS} = \Delta\rho = 0$ and various widths of the well w in the torus geometry ($N = 8$ electrons at $\nu = 1/2$ and aspect ratio 0.97).

If we study the quantum well model in the torus geometry, we can distinguish phases by their topological degeneracy (Sec. 2.2.2). In Fig. 5.12 we show the LLL torus spectra for $N = 8$ electrons in the quantum well as a function of width w , when both tunneling and imbalance are set to zero. In this limit, S_z is a good quantum number. For small w there is a complicated structure in the lowest-lying part of the spectrum, but beyond $w = 4.5l_B$ a characteristic four-fold degeneracy emerges, signifying the 331 state.

We know that applying the imbalance to the 331 state, at best, may lead to a “critical” Pfaffian state which has a small gap and is very sensitive to the variation of the interaction parameters. Therefore, we set $w = 4.0l_B$ which places us in the transition region and study the effect of imbalance, Fig. 5.13. Although we see a gap opening up, the ground state multiplet does not

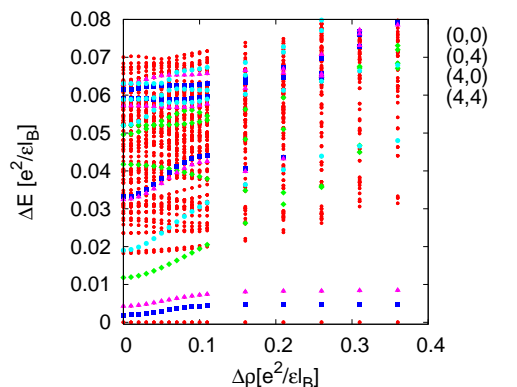


Figure 5.13: Energy spectrum of the quantum well Hamiltonian (5.3) on the torus for $w = 4.0l_B$, $\Delta = 0.004e^2/\epsilon l_B$ as the imbalance is increased from zero ($N = 8$ electrons at $\nu = 1/2$ in the LLL and aspect ratio 0.97).

have the correct topological degeneracy of the Moore-Read state.

5.4 $\nu = 1/4$ in a quantum well

We proceed with analyzing the quantum well at $\nu = 1/4$, Fig. 5.14. The competing phases are the 553, 771 and 5,13,1 Halperin states, the Moore-Read $\nu = 1/4$ Pfaffian and the Haldane-Rezayi state at $\nu = 1/4$. The overlap with the 771 and 5,13,1 state is negligible in the range of widths $w/l_B \lesssim 10.0$, and therefore we will exclude them from the present discussion. Note that, similarly to the 331 state in Sec. 5.3, the 553 state hereinafter is defined as an eigenstate of the S_x operator (if defined as an eigenstate of S_z , the overlap with the exact ground state is negligible). In this Section we also set the imbalance term to zero.

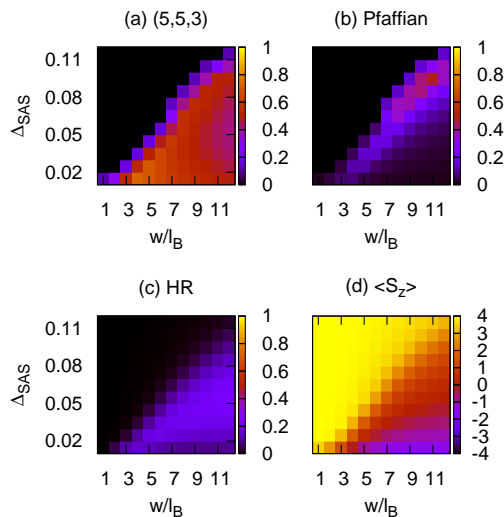


Figure 5.14: Overlap between the exact Coulomb state of the quantum well for $N = 8$ particles on the sphere at $\nu = 1/4$ with the 553 Halperin state (a), the Moore-Read Pfaffian (b) and Haldane-Rezayi (c) state. The expectation value of the S_z component of the pseudospin is plotted in (d).

The 553 state is found in a sizable parameter range, but the maximum overlap is moderate compared to the 331 case previously studied (0.74 for $w/l_B = 4.5$). Haldane-Rezayi state generally has a small overlap (not exceeding 0.2) and the evolution of $\langle S_z \rangle$ is remains smooth,

5. WIDE QUANTUM WELLS

whereas the Moore-Read Pfaffian develops with the increase in Δ_{SAS} but, once the system reaches full polarization, it is destroyed (compare with Fig. 4.6). To shed more light on how this occurs, it is useful to look at the “cross section” of Fig. 5.14 for a fixed value of the width $w/l_B = 10.5$, chosen to represent the region where the Pfaffian phase is most clearly pronounced (Fig. 5.15).

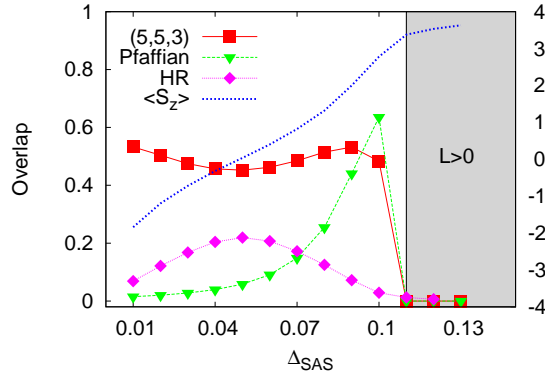


Figure 5.15: Overlap between the exact Coulomb state of the quantum well for $N = 8$ particles on the sphere at $\nu = 1/4$ and $w/l_B = 10.5$ with the 553 Halperin state, the Moore-Read Pfaffian and Haldane-Rezayi states (left axis). The expectation value of the S_z component of the pseudospin is given on the right axis. The shaded region denotes where the ground state is no longer rotationally invariant ($L > 0$).

Although the Pfaffian overlap peaks in the region where that of 553 starts to drop, very abruptly both overlaps fall to zero, and the ground state is no longer rotationally invariant. The fact that $L > 0$ is a hallmark of compressibility. Precisely at the transition point, a small kink is now visible in $\langle S_z \rangle$. A compressible ground state with $L > 0$ may also indicate a phase with modulated charge density, such as the Wigner crystal. Indeed, an insulating behavior, as one would expect for an electron crystal, has been found at filling factors slightly above $\nu = 1/5$. [198] Such a state is not captured in the present ED calculations on the sphere.

5.5 Conclusion

In this Chapter we have presented a realistic model for the wide quantum wells used in the experiments of Luhman *et al.* and Shabani *et al.* Several candidate states, multicomponent Halperin and single-component, non-Abelian states, have been studied systematically within this model of the quantum well in exact diagonalization. Halperin states, as a rule, are generically very robust to perturbation by either tunneling Δ_{SAS} or density imbalance $\Delta\rho$. The non-Abelian states such as the Moore-Read Pfaffian at $\nu = 1/2$ and $\nu = 1/4$ are obtained in the regime when the system is fully x -polarized, but the caveats are the very small gaps and proximity to the compressible CFL state. On the basis of the mapping between a quantum well and a bilayer Hamiltonian, these conclusions agree with our bilayer results in Chapter 4.

Although we believe that our quantum well model takes properly into account the effects of finite thickness, we have entirely neglected the effect of the in-plane magnetic field which may nevertheless prove essential in order to stabilize the incompressible state at $\nu = 1/4$ in the experiment of Luhman *et al.* The existing experimental work [199] on the $\nu = 2/3$ state witnessed that the introduction of an in-plane magnetic field may lead to a strengthening of the minimum in R_{xx} , thus inducing the same one-component to two-component transition as by varying Δ_{SAS} . Similar strengthening occurs for $\nu = 1/2$ if the tilt is not too large. [199] Therefore, the application of the in-plane field may be a likely reason to further stabilize the 553 state at $\nu = 1/4$ if the symmetric-antisymmetric gap Δ_{SAS} is sufficiently small. Including the

effect of an in-plane field is a rather complicated problem, even in the simpler models, because the motion along z -axis is no longer separable from the in-plane motion. Another possibility is that $\nu = 1/2$ state in the wide quantum well is an imbalanced two-component CF state, [126] however there is no such simple candidate for $\nu = 1/4$.

In order to answer without ambiguity which of the possibilities is actually realized in the quantum well under the experimental conditions of Refs. [8, 9], it would be useful to know the dependence of the activation gap as a function of Δ_{SAS} and also as a function of transferred charge from the front to the back of the quantum well using a gate biasing. These results would help to discriminate between the one-component and two-component nature of the ground state.

Chapter 6

Graphene as a multicomponent FQH system

This Chapter explores interacting states in graphene in a strong magnetic field. Due to the valley and spin degrees of freedom, graphene can be described by an internal SU(4) symmetry. We analyze how the four-component structure of graphene may have particular signatures in possible FQHEs. We introduce the interaction model for electrons restricted to a single graphene LL (Sec. 6.1) and concentrate on the spin-valley SU(4) symmetric part of the interaction model, which constitutes the leading energy scale. In Section 6.2 we investigate via the pseudopotential method the possible FQH states in graphene in the LLs $n = 0$ and 1. Recent reviews [200, 201] contain many details on the interaction model for graphene and expectations for a FQHE, as well as the original papers [200] and [202] that this Chapter is based on.

6.1 Interaction model for graphene in a strong magnetic field

From a theoretical point of view, long-range interactions in graphene are expected to be relevant. Let us look at the dimensionless ratio r_s of the characteristic Coulomb energy E_C and the kinetic energy E_{kin} :

$$r_s = \frac{E_C}{E_{\text{kin}}} = \frac{e^2/\epsilon l}{\hbar v_F k_F} \approx \frac{2.2}{\epsilon}, \quad (6.1)$$

where we substituted $E_C = e^2/\epsilon l$ (l being the average inter-electronic distance and ϵ the dielectric constant of the graphene sheet environment) and $E_{\text{kin}} = \hbar v_F k_F \sim \hbar v_F/l$, v_F being the Fermi velocity. Therefore, the ratio r_s places graphene in an intermediate range of correlation strengths (large values of r_s would signal strong coupling). Notice in (6.1) that a convenient way to vary the correlation strength in graphene is via adjustment of the dielectric constant of the substrate. Additionally, we can estimate the Thomas-Fermi wave vector k_{TF}^G which defines the characteristic length $\lambda_{\text{TF}} \sim 1/k_{\text{TF}}^G$ above which the Coulomb interaction potential is screened:

$$k_{\text{TF}}^G \sim r_s k_F \sim \sqrt{n_{el}}, \quad (6.2)$$

which vanishes at the Dirac points where the carrier density n_{el} goes to zero. Therefore, the screening length is very large in graphene and one has to treat the long-range Coulomb interaction directly, instead of attempting to use a Hubbard-like model.

In order to quantify the degree of separation between the energy scales in graphene in the magnetic field, one needs to compare the typical energy for exchange interaction

$$V_C = e^2/\epsilon R_C \simeq 25\sqrt{B[\text{T}]/\epsilon}\sqrt{2n+1} \text{ meV},$$

6. GRAPHENE AS A MULTICOMPONENT FQH SYSTEM

in terms of the cyclotron radius $R_C = l_B \sqrt{2n+1}$, with the magnetic length $l_B = \sqrt{\hbar/eB} = 25/\sqrt{B[\text{T}]} \text{ nm}$, to the LL separation

$$\Delta_n = \sqrt{2}\hbar(v_F/l_B)(\sqrt{n+1} - \sqrt{n}).$$

In spite of the decreasing LL separation in the large- n limit, the ratio between both energy scales remains constant and reproduces the fine-structure constant of graphene,

$$\alpha_G = V_C/\Delta_n = e^2/\hbar v_F \epsilon \simeq 2.2/\epsilon.$$

Notice that the Coulomb interaction respects the fourfold spin-valley degeneracy to lowest order in $a/l_B \simeq 0.005\sqrt{B[\text{T}]}$, where $a = 0.14 \text{ nm}$ is the distance between nearest-neighbour carbon atoms in graphene. [201] This fourfold spin-valley symmetry is described in the framework of the SU(4) group which covers the two copies of the SU(2) spin and the SU(2) valley isospin. Lattice effects break this SU(4) symmetry at an energy scale $V_C(a/l_B) \simeq 0.1B[\text{T}]/\epsilon \text{ meV}$ [203, 204, 205, 206], which is roughly on the same order of magnitude as the expected Zeeman effect in graphene [207]. Other symmetry-breaking mechanisms have been proposed [208, 209, 210, 211] but happen to be equally suppressed with respect to the leading interaction energy scale V_C . An exception may be graphene on a graphite substrate, where the natural lattice commensurability of the substrate and the sample may lead to a stronger coupling than for graphene on a SiO₂ substrate [212]. This yields a mass term in the Dirac Hamiltonian which lifts the valley degeneracy of the zero-energy LL [208].

Based on these considerations, graphene in a strong magnetic field may thus be viewed as a four-component quantum Hall system. An interesting theoretical expectation resulting from this feature is the formation of a quantum Hall ferromagnet at $\nu = \pm 1$ [203, 204, 213, 214] with SU(4)-skyrmion excitations, which may have peculiar magnetic properties [214, 215]. Also for the FQHE, the SU(4) spin-valley symmetry is expected to play a relevant role and has been considered within a CF approach [216] as well as one based on SU(4) Halperin wave functions [99, 130].

In the case of a partially filled LL, we can use the Hamiltonian we defined in (1.19), describing only intra-LL excitations, where the Fourier components $\rho_{\lambda n}(\mathbf{q})$ of the density operator are constructed solely from states within the n -th LL in the band λ ($\lambda = +$ for the conduction and $\lambda = -$ for the valence band). This construction is analogous to that used in the conventional 2DEG, but the density operators $\rho_n(\mathbf{q})$ are now built up from spinor states of the 2D Dirac equation,

$$\psi_{\lambda n, m}^{\xi} = \frac{1}{\sqrt{2}} \begin{pmatrix} |n-1, m\rangle \\ \lambda |n, m\rangle \end{pmatrix} \quad (6.3)$$

for $n \neq 0$ and

$$\psi_{n=0, m}^{\xi} = \begin{pmatrix} 0 \\ |n=0, m\rangle \end{pmatrix} \quad (6.4)$$

for the zero-energy LL $n = 0$, in terms of the harmonic oscillator states $|n, m\rangle$ and the guiding-center quantum number $m = 0$. Here, we have chosen the first component of the spinor to represent at the K point ($\xi = +$) the amplitude on the A sublattice and that on the B sublattice at the K' point ($\xi = -$). Notice that the valley and the sublattice indices happen to be the same in the zero-energy LL $n = 0$ and that, thus, a perturbation that breaks the inversion symmetry (the equivalence of the two sublattices) automatically lifts the valley degeneracy [208, 209, 210, 211]. In terms of the spinor states (6.3) and (6.4), the density operator may be written

$$\rho_{\lambda n}(\mathbf{q}) = \sum_{\xi, m} \left(\psi_{\lambda n, m}^{\xi} \right)^{\dagger} e^{-i\mathbf{q}\cdot\mathbf{r}} \psi_{\lambda n, m'}^{\xi} c_{\lambda n, m; \xi}^{\dagger} c_{\lambda n, m'; \xi}, \quad (6.5)$$

where $c_{\lambda n, m; \xi}^{(\dagger)}$ annihilates (creates) an electron in the state $\psi_{\lambda n, m}^{\xi}$. In Eq. (6.5), we have neglected the contributions that are off-diagonal in the valley index. Indeed, these contributions give rise

to a rapidly oscillating phase $\exp(\pm i\mathbf{K} \cdot \mathbf{r})$ in the matrix elements, where $\pm\mathbf{K} = \pm(4\pi/3\sqrt{3}a)\mathbf{e}_x$ is the location of the K and K' points, respectively, and yield terms in the Hamiltonian (1.19), which break the valley-SU(2) symmetry of the interaction. They are suppressed by a factor a/l_B with respect to the leading interaction energy scale $e^2/\epsilon l_B$ [203] and, for the sake of simplicity and because of their smallness, we neglect these terms here.

Within the symmetric gauge, $\mathbf{A} = (B/2)(-y, x, 0)$, the position operator \mathbf{r} in Eq. (6.5) may be decomposed into the guiding-center position \mathbf{R} and the cyclotron variable $\boldsymbol{\eta}$. Whereas the latter only affects the quantum number n , \mathbf{R} acts on m , and we may therefore rewrite the density operator (6.5), $\rho_{\lambda n}(\mathbf{q}) = \mathcal{F}_n(\mathbf{q})\bar{\rho}(\mathbf{q})$, as a product of the *projected* density operator

$$\bar{\rho}(\mathbf{q}) = \sum_{\xi; m, m'} \langle m | e^{-i\mathbf{q} \cdot \mathbf{R}} | m' \rangle c_{\lambda n, m; \xi}^\dagger c_{\lambda n, m'; \xi} \quad (6.6)$$

and the *graphene form factor*

$$\begin{aligned} \mathcal{F}_n(q) &= \frac{1}{2} (\langle n-1 | e^{-i\mathbf{q} \cdot \boldsymbol{\eta}} | n-1 \rangle + \langle n | e^{-i\mathbf{q} \cdot \boldsymbol{\eta}} | n \rangle) \\ &= \frac{1}{2} \left[L_{n-1} \left(\frac{q^2}{2} \right) + L_n \left(\frac{q^2}{2} \right) \right] e^{-q^2/4} \end{aligned} \quad (6.7)$$

for $n \neq 0$, in terms of Laguerre polynomials, and

$$\mathcal{F}_{n=0}(q) = \langle 0 | e^{-i\mathbf{q} \cdot \boldsymbol{\eta}} | 0 \rangle = e^{-q^2/4} \quad (6.8)$$

for $n = 0$. With the help of the projected density operators, the interaction Hamiltonian (1.19) reads

$$H_{\lambda n} = \frac{1}{2} \sum_{\mathbf{q}} v_n^G(q) \bar{\rho}(-\mathbf{q}) \bar{\rho}(\mathbf{q}), \quad (6.9)$$

where we have defined the effective interaction potential for graphene LLs,

$$v_n^G(q) = \frac{2\pi e^2}{\epsilon q} [\mathcal{F}_n(q)]^2. \quad (6.10)$$

Notice that the structure of the Hamiltonian (6.9) is that of electrons in a conventional 2DEG restricted to a single LL if one notices that the projected density operators satisfy the magnetic translation algebra [59]

$$[\bar{\rho}(\mathbf{q}), \bar{\rho}(\mathbf{q}')] = 2i \sin \left(\frac{\mathbf{q}' \wedge \mathbf{q}}{2} \right) \bar{\rho}(\mathbf{q} + \mathbf{q}'), \quad (6.11)$$

where $\mathbf{q}' \wedge \mathbf{q} \equiv q'_x q_y - q_x q'_y$ is the 2D vector product. This is a remarkable result in view of the different translation symmetries of the zero-field Hamiltonian; whereas the electrons in the 2DEG are non-relativistic and therefore satisfy Galilean invariance, the relativistic electrons in graphene are Lorentz-invariant. However, once submitted to a strong magnetic field and restricted to a single LL, the translation symmetry of the electrons is described by the magnetic translation group in *both* cases.

6.1.1 SU(4) symmetry

The most salient difference between the conventional 2DEG and graphene arises from the larger internal symmetry of the latter, due to its valley degeneracy. This valley degeneracy may be accounted for by an SU(2) valley *isospin* in addition to the physical SU(2) spin, which we have omitted so far and the symmetry of which is respected by the interaction Hamiltonian.

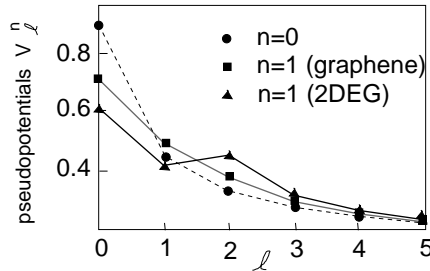


Figure 6.1: Pseudopotentials for graphene and the 2DEG in $n = 0$ (graphene and 2DEG, circles), $n = 1$ (graphene, squares), and $n = 1$ (2DEG, triangles). The energy is measured in units of $e^2/\epsilon l_B$. The lines are a guide to the eye.

Similarly to the projected charge density operator (6.6), we may introduce spin and isospin density operators, $\bar{S}^\mu(\mathbf{q})$ and $\bar{I}^\mu(\mathbf{q})$, respectively, with the help of the tensor products [215]

$$\begin{aligned}\bar{S}^\mu(\mathbf{q}) &= (S^\mu \otimes \hat{1}) \otimes \bar{\rho}(\mathbf{q}), \\ \bar{I}^\mu(\mathbf{q}) &= (\hat{1} \otimes I^\mu) \otimes \bar{\rho}(\mathbf{q}).\end{aligned}\quad (6.12)$$

Here, the operators S^μ and I^μ are (up to a factor 1/2) Pauli matrices, which act on the spin and valley isospin indices, respectively. The operators $(S^\mu \otimes \hat{1})$ and $(\hat{1} \otimes I^\mu)$ may also be viewed as the generators of the $SU(2) \times SU(2)$ symmetry group, which is smaller than the abovementioned $SU(4)$ group. However, once combined in a tensor product with the projected density operators $\bar{\rho}(\mathbf{q})$, the $SU(2) \times SU(2)$ -extended magnetic translation group is no longer closed due to the non-commutativity of the Fourier components of the projected density operators. By commuting $[\bar{S}^\mu(\mathbf{q}), \bar{I}^\nu(\mathbf{q})]$, one obtains the remaining generators of the $SU(4)$ -extended magnetic translation group [215], which is, thus, the relevant symmetry that describes the physical properties of electrons in graphene restricted to a single LL.

6.1.2 Effective interaction potential and pseudopotentials

Another difference, apart from the abovementioned larger internal symmetry, between the 2DEG and graphene in a strong magnetic field arises from the slightly different effective interaction potentials in the n -th LL. The effective interaction for graphene is given by Eq. (6.10) whereas that in the conventional 2DEG reads

$$v_n^{2DEG}(q) = \frac{2\pi e^2}{\epsilon q} \left[L_n \left(\frac{q^2}{2} \right) e^{-q^2/4} \right]^2. \quad (6.13)$$

The difference between the two of them vanishes for $n = 0$, as well as in the large- n limit [203], but leads to quite important physical differences in the first excited LL ($n = 1$) when comparing graphene to the 2DEG.

For the discussion of the FQHE, as we have seen in Chapter 2, it is more appropriate to use Haldane's pseudopotential construction. In the plane, the pseudopotentials of a given interaction potential $v_n(q)$ in Fourier space, such as (6.13) or (6.10), are easily obtained with the help of

$$V_\ell^n = \sum_{\mathbf{q}} v_n(q) L_\ell(q^2) e^{-q^2/2}. \quad (6.14)$$

The pseudopotentials for $n = 0$ and $n = 1$ in graphene and the 2DEG are shown in Fig. 6.1, which allows us to make some qualitative statements about a potential FQHE in graphene as compared to that of the 2DEG. First, apart from the internal symmetry, the polarized FQHE states in the zero-energy LL are expected to be the same in graphene as in the 2DEG because there is no difference in the effective interaction potential. The only difference stems from the larger internal symmetry in graphene, which affects the unpolarised FQHE states in $n = 0$.

Second, the $n = 1$ LL in graphene is much more reminiscent of the $n = 0$ LL than of the $n = 1$ LL in the 2DEG. From an interaction point of view, one would therefore expect that the quantum phases encountered in the $n = 1$ graphene LL are merely a copy of those in $n = 0$. Furthermore, if one considers spin-polarised FQHE states, only pseudopotentials with *odd* angular momentum are relevant due to the fermionic nature of the electrons. It is apparent from Fig. 6.1 that odd- ℓ pseudopotentials are systematically larger in $n = 1$ than in $n = 0$. Therefore, the overall energy scale of FQHE states in $n = 1$ is slightly larger (by $\sim 10\%$) than in $n = 0$, and one would expect, somewhat counterintuitively, that the $n = 1$ FQHE states are more stable than those in $n = 0$, for the same B -field value. These qualitative predictions [203] have been corroborated within ED studies, where only the valley isospin degree of freedom was considered and the physical spin was taken as completely polarized [217, 218].

6.2 Multicomponent trial wave functions for graphene

In the following, we consider some particular subclasses of the trial wave functions (1.47), which are natural candidates for a FQHE in graphene. Explicitly, we label the four spin-valley components as 1 = (\uparrow, K), 2 = (\uparrow, K'), 3 = (\downarrow, K), and 4 = (\downarrow, K'), where the first component denotes the spin orientation (\uparrow or \downarrow) and the second the valley (K or K'). We investigate wave functions, where all intracomponent exponents are identical $m_i = m$, i.e. we consider the same interaction potential for any of the components, as it is the case in graphene. Furthermore, we consider $n_{13} = n_{24} \equiv n_a$ and $n_{12} = n_{14} = n_{23} = n_{34} \equiv n_e$, which makes an explicit distinction between inter-component correlations in the same valley (n_a) and those in different valleys (n_e). This distinction may occur somewhat arbitrary – indeed, it does no longer treat the spin on the same footing as the valley isospin – but it happens to be useful in some cases if one intends to describe states with intermediate polarization, such as for a moderate Zeeman field. The equivalence between spin and valley isospin is naturally restored for $n_e = n_a$. We use the notation $[m; n_e, n_a]$ to describe these subclasses of trial wave functions (1.47), the validity of which we check by ED of N particles on a sphere [56].

6.2.1 $[m; m, m]$ wave functions

If all exponents are identical odd integers m , we obtain a completely antisymmetric orbital wave function, which is nothing other than the Laughlin wave function (1.20). In this case, the distinction between the components vanishes, and the component filling factors are not fixed – one may, without changing the orbital wave function, fill only one particular component as well as another or distribute the particles over all components. Only the total filling factor is fixed at $\nu = 1/m$. The corresponding exponent matrix M (1.56) is indeed not invertible (of rank 1), and the residual freedom of distributing the electrons over the four components may be viewed as the arbitrary orientation of a four-spinor in $SU(4)$ space. The Laughlin wave function in graphene is therefore associated with an $SU(4)$ ferromagnetism, similar to that of the state at $\nu_G = \pm 1$ [203, 204, 213, 214, 215], where a graphene quantum Hall effect has been observed at high magnetic fields [207].

As already mentioned above, the Laughlin wave function has the good property of screening all pseudopotentials with angular momentum $\ell < m$ and has, for $m = 3$, the usual large overlap with the Coulomb ground state [216]. However, states described by the $[m; m, m]$ wave function are ground-state candidates for the filling factors $\nu = 1/m$, which correspond to the graphene filling factors (see Eq. 1.57) $\nu_G = -2 + 1/m$ or hole states at $\nu_G = 2 - 1/m$. These filling factors do not correspond to the FQHE at $\nu_G = \pm 1/3$ observed in the experiments [128, 129].

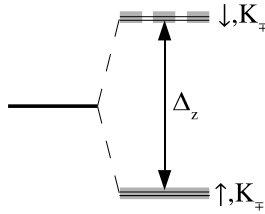


Figure 6.2: Splitting of the single-particle SU(4) energy levels in the presence of Zeeman field Δ_z , with the remaining SU(2) degeneracy due to the valley index K .

6.2.2 $\nu_G = 1/3$ state in graphene

If the spin-valley degeneracy is (at least partially) lifted, e.g. in the manner of Fig. 6.2, we may understand the $\nu_G = 1/3$ state as the $\nu = 2 + 1/3$ FQH state of a 2DEG system with an internal SU(4) symmetry which is broken by a Zeeman field. This would require the Zeeman field to be enhanced, e.g. via a cooperative effect by the formation of a quantum Hall ferromagnetism as the background state at $\nu_G = 0$. If so, the natural trial state for this system would be given by, in the obvious notation,

$$\begin{aligned} \Psi_{\text{SU}(4)} = & \prod_{i < j} (z_i^{K+, \uparrow} - z_j^{K+, \uparrow}) \prod_{k < l} (z_k^{K-, \uparrow} - z_l^{K-, \uparrow}) \\ & \prod_{m < n} (z_m^{K+, \downarrow} - z_n^{K+, \downarrow})^3 \prod_{p < q} (z_p^{K-, \downarrow} - z_q^{K-, \downarrow})^3 \prod_{r, s} (z_r^{K+, \downarrow} - z_s^{K-, \downarrow})^3, \end{aligned} \quad (6.15)$$

where the first line describes a filled \uparrow shell and the remaining part is the effective SU(2) ferromagnet state at $\nu = 1/3$ in the \downarrow shell. If the SU(4) symmetry is not broken by a field such as Zeeman, there will be many more degenerate states and the wave function (6.15) is not expected to represent the ground state. We will present arguments that the wave function (6.15) describes interesting physics beyond the simple Laughlin $\nu = 1/3$ FQH state. Because of the numerical difficulty of treating explicitly the SU(4) case, we focus on the analogous toy model with the broken SU(2) symmetry:

$$\Psi_{\text{SU}(2)} = \prod_{i < j} (z_i^{\uparrow} - z_j^{\uparrow}) \prod_{k < l} (z_k^{\downarrow} - z_l^{\downarrow})^3. \quad (6.16)$$

The spectrum of the SU(2) model as a function of Zeeman field Δ_z is given in Fig. 6.3. The wave function $\Psi_{\text{SU}(2)}$ (6.16) can be shown to occur for the number of flux quanta given by $N_\phi = 3/4N - 3/2$ on the sphere. The data shown is for the largest system $(N, N_\phi) = (22, 15)$ where $\Psi_{\text{SU}(2)}$ is found in the sector with $2S_z = 10$. This is also the largest value of S_z for which an incompressible state can be constructed for the given (N, N_ϕ) . Therefore, in our finite system, as $\Psi_{\text{SU}(2)}$ becomes the ground state for some nonzero Δ_z , it remains the ground state regardless of the how large the Zeeman field becomes. Note that we have shown only one or two lowest lying energies per S_z sector, therefore the upper part of Fig. 6.3 may have additional levels beyond those shown. These, however, are of no importance for our discussion.

We must stress that the system sizes we have considered here are rather small: in the S_z sector that corresponds to $\Psi_{\text{SU}(2)}$, the rotationally invariant $\mathbf{L} = 0$ subspace has dimension 6 for $N = 22$. We believe nevertheless that for a state such as Laughlin's, this is sufficient to uncover the essential physics. The physical picture that emerges from Fig. 6.3 is the following. For zero or very small Δ_z , our trial wave function is not a good description of the ground state. As soon as there is some amount of Zeeman splitting ($\approx 0.01e^2/\epsilon l_B$), it becomes the ground state of the system (with 0.99 overlap). However, the excitation spectrum at that point is still not that of the Laughlin state due to the presence of the low-lying spin-flip excitations.

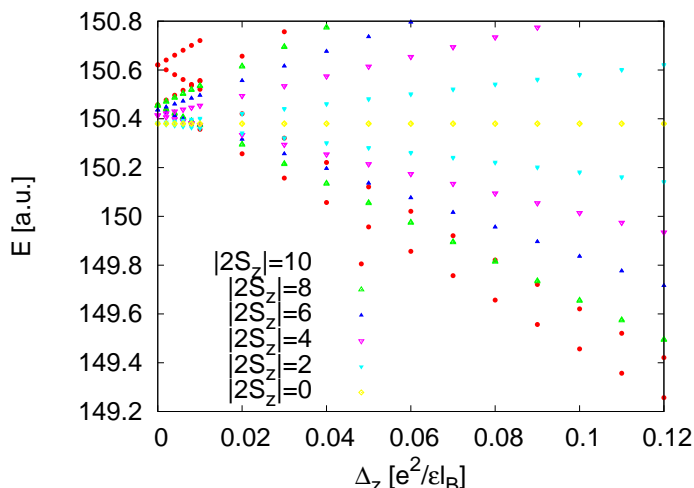


Figure 6.3: Energy spectrum for $N = 22$ electrons at the filling $\nu = 1 + 1/3$ as a function of Δ_z . We highlight the states belonging to particular S_z sectors for comparison.

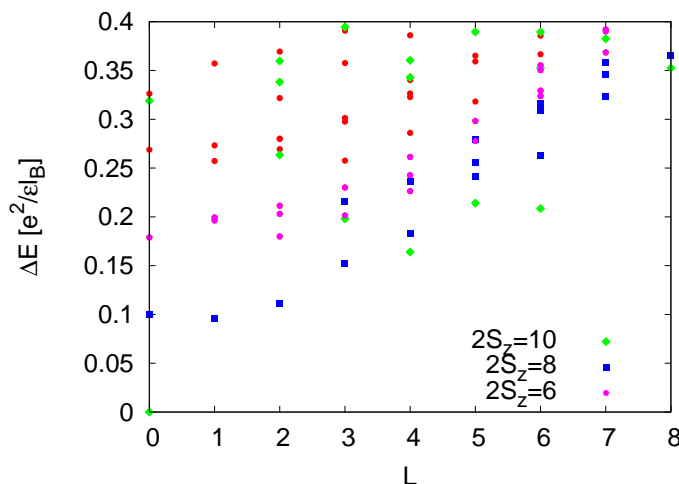


Figure 6.4: Energy spectrum relative to the ground state for $N = 22$ electrons at the filling $\nu = 1 + 1/3$ as a function of angular momentum L and for the fixed $\Delta_z = 0.05e^2/\epsilon l_B$. We highlight the states belonging to the particular S_z sectors that define the lowest-lying spin-flip excitations. The magnetoroton branch is shown in green for $2S_z = 10$.

More specifically, we can study the spectrum as a function of angular momentum L for a fixed value of $\Delta_z = 0.05e^2/\epsilon l_B$ in the middle of this region, Fig. 6.4. The green symbols show the Laughlin ground state and a fully developed magnetoroton branch. The magnetoroton branch is expected to become the lowest excitation for large values of Δ_z (above $0.08e^2/\epsilon l_B$ in Fig. 6.3), when the system displays the complete phenomenology of the Laughlin $\nu = 1/3$ FQH state. For intermediate Zeeman field we predict that, although the ground state is the Laughlin state, there is a possibility for a richer spectrum of excitations involving spin. Additional studies are needed to identify the excitations in this regime of Zeeman fields and determine the critical Δ_z .

6.2.3 $[m; m - 1, m]$ wave functions

Another simple choice for the multicomponent wave function is $[m; m - 1, m]$, where the intervalley-component exponents are decreased by one. It also screens all pseudopotentials $V_{\ell < m}$ in any pair of electrons within the same valley, but an electron pair in two different valleys is affected

6. GRAPHENE AS A MULTICOMPONENT FQH SYSTEM

number of particles N	4	6	8	10
overlap \mathcal{O} in $n = 0$	0.990	0.985	0.979	0.970
overlap \mathcal{O} in $n = 1$	0.965	0.882	0.896	0.876

Table 6.1: Overlap \mathcal{O} between the 332 wave function and the state obtained from exact diagonalization of the effective interaction potential in $n = 0$ and $n = 1$.

by the pseudopotential $V_{\ell=m-1}$. The filling factor, where this wave function may occur, is

$$\nu = \frac{2}{2m-1},$$

i.e. at slightly larger densities as the Laughlin wave function with the same m . The exponent matrix M is still not invertible but of rank 2, and indeed only the filling factors in the two valleys, $\nu_K = \nu_1 + \nu_3$ and $\nu_{K'} = \nu_2 + \nu_4$, respectively, are fixed, $\nu_K = \nu_{K'} = 1/(2m-1)$. The wave function, thus, describes a state with ferromagnetic spin ordering, but which is valley-isospin unpolarized. One may alternatively view this $[m; m-1, m]$ wave function as a tensor product of an SU(2) Halperin $(m, m, m-1)$ isospin-singlet wave function [98] and a completely symmetric (ferromagnetic) two-spinor that describes the physical spin.

We have verified within exact diagonalization calculations that the $[3; 2, 3]$ wave function ($m = 3$) describes indeed, to great accuracy, the ground state in graphene at $\nu = 2/5$. It was shown by ED in Ref. [216] that, for $N = 4$ and 6 particles, the physical properties are indeed governed by an SU(2) symmetry, as suggested by the $[m; m-1, m]$ wave function. The overlap between this trial state and the one obtained by ED with an implemented SU(2) symmetry of the Coulomb interaction in $n = 0$ and 1 is shown in Tab. 6.1 for up to 10 particles. [200] It is above 97% for all studied system sizes in the zero-energy LL $n = 0$, but slightly smaller ($\sim 88\%$) in $n = 1$. We have used the planar pseudopotentials (6.14) in the calculation of the $n = 1$ LL and checked that the difference is less than 1% in $n = 0$ when compared to using the more accurate spherical ones, even for the smallest system sizes $N = 4$ and 6.

It has been shown that the ground state at $\nu = 2/5$ in the conventional 2DEG is well described by an unpolarized 332 SU(2) Halperin wave function once the spin degree of freedom is taken into account [219]. This wave function is identical to the CF wave function when including the SU(2) spin. The energy difference between the polarized and the unpolarized $2/5$ states is, however, relatively small as compared to the Zeeman effect at the corresponding magnetic fields, such that a polarized state is usually favoured. Intriguing spin transitions have furthermore been observed experimentally at $\nu = 2/5$ and hint to even more complex physical properties of the $2/5$ FQHE [220, 221]. Notice that the situation of the $[3; 2, 3]$ state in graphene is remarkably different from that in the 2DEG: even in the presence of a strong Zeeman effect, only the ferromagnetically ordered physical spin is polarized, while the state remains a valley-isospin singlet. Whether such a valley-isospin singlet state is indeed encountered in graphene depends sensitively on the valley-symmetry breaking terms; whereas a possible easy-axis ferromagnetism, as has been proposed for the zero-energy LL $n = 0$ [204], may destroy the $[3; 2, 3]$ state, it is favoured in the case of an easy-plane valley-isospin anisotropy, which may occur in the $n = 1$ graphene LL due to intervalley coupling terms of the order $V_C(a/l_B)$ [203].

We have furthermore studied the 554 wave function ($m = 5$) at $\nu = 2/9$. Its overlap with the state obtained by ED is lower than for the $(3, 3, 2)$ case (with $\mathcal{O} = 0.941$ for $N = 4$ and $\mathcal{O} = 0.892$ for $N = 6$), but remains relatively high.

6.2.4 $[m; m-1, m-1]$ wave functions

Another candidate is the $[m; m-1, m-1]$ wave function [99] which may describe FQHE states at

$$\nu = \frac{4}{4m-3}.$$

The corresponding exponent matrix M is now invertible, and the filling factor of each spin-valley component is $\nu = 1/(4m - 3)$, i.e. the state is an $SU(4)$ singlet. As for the $[m; m, m]$ and $[m; m - 1, m]$ wave functions, all intracomponent correlations are such that the pseudopotentials $V_{\ell < m}$ are screened, but $V_{\ell = m - 1}$ is relevant for all intercomponent interactions.

As an example, we consider the $[3; 2, 2]$ wave function ($m = 3$), which is a candidate for a possible graphene FQHE at $\nu = 4/9$. Our ED calculations with an implemented $SU(4)$ symmetry, for $N = 4$ and 8 particles, indicate that this trial wave function describes indeed to great accuracy the ground state for the Coulomb interaction potential in the $n = 0$ LL, with an overlap of $\mathcal{O} = 0.999$ for $N = 4$ and $\mathcal{O} = 0.992$ for $N = 8$. In $n = 1$, it is $\mathcal{O} = 0.944$ for $N = 8$, for the case where one uses the planar pseudopotentials (6.14). These results indicate that a possible $4/9$ FQHE state in graphene is, remarkably, of a completely different nature than the CF state at $\nu = 4/9$ in a one-component system, such as the conventional 2DEG with complete spin polarization. It is, nevertheless, an open issue to what extent the $SU(4)$ singlet state survives if one takes into account the Zeeman effect at high magnetic fields, which favours a polarization in the spin channel. A complementary CF calculation with an $SU(4)$ symmetry has revealed that, at $\nu = 4/9$, states with intermediate $SU(4)$ isospin polarization – such as a valley-isospin singlet with full spin polarization – may exist, with a slightly higher energy than the CF $SU(4)$ singlet [216], which is indeed identical to the $[3; 2, 2]$ wave function. One may, therefore, expect a transition between two $4/9$ states with different polarization when the Zeeman energy outcasts the energy difference between the two states. This is similar to the abovementioned $2/5$ state in a conventional 2DEG [219].

6.3 Conclusions

In conclusion, we have investigated theoretically some particular features of the FQHE in graphene as compared to the 2DEG. The electrons in graphene lose their relativistic character associated with the Lorentz invariance once they are restricted to a single LL, in which case the translations are governed by the magnetic translation group, as in the 2DEG case. The main difference between the 2DEG and graphene arises from the approximate $SU(4)$ spin-valley symmetry, which is respected in a wide energy range. Another difference arises from the spinor character of the wave functions, which yields a different effective electron-electron interaction in graphene as compared to the 2DEG. The graphene interaction potential in the first excited LL $n = 1$ (in both the valence and the conduction band) is shown to be similar to that in the central zero-energy LL $n = 0$, yet with a slightly larger overall energy scale (roughly 10% larger).

The FQHE at $\nu = 1/3$ is described as a Laughlin state [46] with $SU(4)$ -ferromagnetic spin-valley ordering, similar to the state at $\nu = 1$ [203, 204, 213, 214, 215]. We have presented an additional candidate for the $\nu_G = 1/3$ state with a symmetry broken by the Zeeman field. The latter has the ground state described by the Laughlin wave function and novel spin excitations for the intermediate range of Zeeman fields.

Furthermore, the system may profit from its internal degrees of freedom by choosing a state with partial and full $SU(4)$ -isospin depolarisation at $\nu = 2/5$ and $\nu = 4/9$, respectively. The $[3; 2, 3]$ state at $\nu = 2/5$ is a valley-isospin singlet, but its physical spin is ferromagnetically ordered and may eventually be oriented by the Zeeman effect. The state at $\nu = 4/9$ is described in terms of a $[3; 2, 2]$ Halperin wave function, which is an $SU(4)$ singlet with necessarily zero spin and valley isospin polarisation. A possible FQHE at $\nu = 4/9$ in graphene may therefore be sensitive to the Zeeman effect at high magnetic fields, and one may expect transitions between states with different polarisation, similar to the 2DEG at $\nu = 2/5$ and $2/3$ [220, 221].

Chapter 7

Outlook

In this thesis we have presented studies of a variety of systems where multicomponent degrees of freedom determine the physics or can be used as a proxy towards more exotic, non-Abelian phases of matter. The latter remain one of the most exciting theoretical concepts advanced in condensed matter physics awaiting their experimental confirmation. Such phases include, among others, the p -wave paired phase in the $\nu = 1$ bilayer, the Pfaffian-like states in the wide quantum wells or yet unobserved analogues in graphene, which all represent exciting venues for future studies.

The quantum Hall bilayer at $\nu = 1$ remains the subject of much experimental work. Recent studies point out to the importance of spin physics in the incompressible-compressible transition that was entirely neglected in almost all of the theoretical work including our discussion in Section 3. The question of an intermediate phase between the 111 state and the two Fermi liquids, although an unlikely possibility, remains open. Moreover, the new measurements probe the nature of the critical current in the zero bias anomaly experiments and find that the simple models of a clean, homogeneous bilayer are insufficient and more work is needed to understand the fine details of the disordering of the QH bilayer superfluid.

Understanding of the non-Abelian phases of matter in the context of FQHE has significantly advanced over the last decade, but this knowledge is certainly incomplete because we do not know what kind of physical interaction favors such phases of matter and how they can be potentially engineered in real samples. Is there a $\nu = 5/2$ analogue of the Moore-Read state in graphene? Having a clearer idea of material properties, even outside the usual GaAs structures, that would favor states such as the Moore-Read Pfaffian should also give a definitive answer as to whether the even-denominator states in the wide quantum wells in the LLL are non-Abelian or not. The effect of Landau level mixing which seems to play an important role in the experiment should also prove interesting to study in more detail. Systems such as graphene bilayers could be useful to develop a feeling for the magnitude of its effect because graphene bilayer represents a case of an extreme LL mixing when the zeroth and first excited LL can be brought to coincide.

Finally, there is a fundamental theoretical problem of the role of non-unitary conformal field theories and the wave functions they define as the trial QH states. Can these describe incompressible QH states and, if not, what is the precise nature of gaplessness of their excitations.

7. OUTLOOK

Appendix A

DiagHam

Numerical calculations in this thesis have been performed using DiagHam libraries:

<http://www.nick-ux.org/diagham/>

DiagHam is a set of C++ classes and in-built programs that provide the framework for exact diagonalization of various quantum models, in particular the fractional quantum Hall effect. It is subject to the GPL public license and the source code is most easily obtained from the Subversion repositories:

```
svn checkout https://www.nick-ux.org/diagham/svn/trunk DiagHam
```

The minimal installation assumes that internal DiagHam libraries will be used for full diagonalization. In the root of the checked-out source package one needs to execute

```
./bootstrap.sh
./configure <options>
make
```

where `configure` supports various options that can be listed with the switch `--help`. For FQHE programs, one has to use `--enable-fqhe`. In addition, it is possible to use Lapack libraries for full diagonalization, routines from Gnu Scientific Library (GSL), partial support for MPI etc. DiagHam has been used for very large-scale diagonalization problems (matrices of the order 10^8).

Diagonalization of a given quantum lattice model such as the FQHE proceeds by defining (1) the Hilbert space of the system and (2) the Hamiltonian which acts on the vectors in the given Hilbert space. The Hilbert space of the FQH system depends on the kind of particles (fermions or bosons), the geometry (disk, sphere and torus) and the internal symmetry (fully polarized, SU(2), SU(3), SU(4)). Hamiltonian on the other hand also depends on the kind of interaction (two-body, three-body etc.). We work in the Fock basis where states $|j_1, j_2, \dots, j_{N_e}\rangle$ are understood as binary forms of integer numbers, which makes it easy to manipulate them. This is referred to as the usual *n-body* basis, however DiagHam also allows to define reduced bases such as the squeezed (Haldane) basis, which is useful for Jack polynomial states. Interaction is defined by creation and annihilation operators, c_j and c_j^\dagger , which act like bit operators on the vectors.

In the remainder of this Appendix we will illustrate the typical steps in the standard calculations from Sec. 2. To obtain Fig.2.1 one needs to calculate the ground state of the finite-thickness Coulomb interaction on the sphere for the given number of electrons and flux quanta and compare

A. DIAGHAM

it with the Laughlin state. Any two-body interaction is parametrized by Haldane pseudopotentials and to obtain such a decomposition for the Coulomb interaction on the sphere, one can use the following code:

```
/DiagHam/FQHE/src/Programs/FQHEOnSphere/CoulombPseudopotentials --landau-level
  <LL> --nbr-flux < $N_\phi$ > -d <width or distance> -o <output file>
```

The full list of options for any in-built DiagHam program can be obtained with the switch `-h`. The above will calculate the Haldane pseudopotentials on the sphere for the given number of flux quanta N_ϕ and the thickness or distance parameter d (1.17) in the Landau level $LL=0,1,\dots$. The series of pseudopotentials will be stored in a given output file.

Now we may proceed to the actual diagonalization which is done by `QHEFermionsTwoBodyGeneric` routine:

```
/DiagHam/FQHE/src/Programs/FQHEOnSphere/QHEFermionsTwoBodyGeneric
--nbr-particles < $N$ > --lzmax < $N_\phi$ > --nbr-lz < $N_{L_z}$ > --interaction-file <file>
-interaction-name <interaction name> -S --processors < $N_{\text{processors}}$ > --nbr-eigen
  < $N_{\text{eigen}}$ > --full-diag < $\text{dim}_{\text{max}}$ > --eigenstate -m <memory>
```

The essential parameters are the number of electrons N , flux quanta N_ϕ , the interaction (given in the file e.g. as generated by `CoulombPseudopotentials`), the number of L_z sectors N_{L_z} (for the ground state it is sufficient to consider only $L_z = 0$). The number of sought eigenvalues is controlled by an option `n` and the parameter `full-diag` determines what is the largest size of the Hamiltonian matrix that should be fully diagonalized. If the actual dimension is less than that indicated by `full-diag`, we will obtain all eigenvalues of the matrix; if the dimension is bigger than `full-diag`, Lanczos algorithm will be used for diagonalization. In the latter case, there are additional options which should be understood before blindly calling the program. The switch `eigenvectors` is needed if we seek also the eigenvectors of the Hamiltonian matrix (they will be stored in binary files following the DiagHam naming convention). Finally, there is a range of options which are not essential but are very useful in speeding up the calculation. The switch `S` invokes the symmetric multiprocessing mode which divides the calculation between a few processors whose number is given by `processors`. The amount of RAM memory that can be allocated to store the matrix is defined by the number `-m` (in megabytes). It is always advisable to store the whole matrix in memory if possible. If the matrix requires a larger memory than available, the program will calculate the remaining matrix elements “on the fly”. This is of course much slower than reading them off the RAM, but it is the only choice for very large systems. Lanczos algorithm is fortunate in that it does not require the knowledge of the entire matrix, but only the action of the Hamiltonian H on the given vector \mathbf{v} , $\mathbf{v}' \leftarrow H\mathbf{v}$, which can be calculated at each iteration. The virtue of the Haldane pseudopotential description is that by repeating the same calculation, only with a different interaction (2.7), we can obtain the decomposition of the Laughlin state. After that, we only need to evaluate the scalar product:

```
/DiagHam/src/Programs/GenericOverlap <Coulomb eigenvector> <Laughlin
  eigenvector>
```

which will give us the overlap between the two. DiagHam contains the routines for diagonalization of FQH systems with $SU(K), K = 2, 3, 4$ spin which are straightforward extensions of the one for polarized systems. For $SU(2)$ spin, one needs to specify the S_z projection of the spin and define the interaction via different kinds of Haldane pseudopotentials ($V^{\uparrow\uparrow}, V^{\uparrow\downarrow}, V^{\downarrow\downarrow}$). To diagonalize the Coulomb bilayer on the torus for the given distance d between the layers, one would use the following command line:

```
/DiagHam/FQHE/src/Programs/FQHEOnTorus/FQHETorusFermionsWithSpinAndTranslations
```

```
-p <N> -l <N $\phi$ > -s <S $_z$ > -x <K $_x$ > -y <K $_y$ > --interaction-name coulomb -d <d> -r  
    <aspect ratio>
```

and append the usual Lanczos/full diagonalization options. The above will perform a diagonalization of the bilayer Hamiltonian in the given momentum sector $\mathbf{K} = (K_x, K_y)$.

After obtaining the eigenvectors, various quantities can be calculated e.g. to evaluate the entanglement spectrum on the sphere corresponding to the given state `eigenvector`, one first calculates the reduced density matrix:

```
/DiagHam/FQHE/src/Programs/FQHEOnSphere/FQHESphereFermionEntanglementEntropy  
    <eigenvector> --density-matrix <density matrix file>
```

Using the reduced density matrix stored in `density matrix file`, one can calculate the entanglement spectrum:

```
/DiagHam/FQHE/src/Programs/FQHEOnSphere/FQHESphereEntanglementSpectrum  
<density matrix file> -n <number of particles in subsystem A> -l <number of  
    orbitals in subsystem A> -o <output file>
```

for the given choice of particles and orbitals in the subsystem A .

References

- [1] H. L. Stormer. *Rev. Mod. Phys.*, 71:875, 1999. xi, 1, 2
- [2] J.-S. Xia, W. Pan, C. L. Vicente, E. D. Adams, N. S. Sullivan, H. L. Stormer, D. C. Tsui, L. N. Pfeiffer, K.W. Baldwin, , and K.W.West. *Phys. Rev. Lett.*, 93:176809, 2004. xi, 10, 12
- [3] S. Q. Murphy, J. P. Eisenstein, G. S. Boebinger, L. N. Pfeiffer, and K.W.West. *Phys. Rev. Lett.*, 72:728, 1994. xi, 15
- [4] I. B. Spielman, J. P. Eisenstein, L. N. Pfeiffer, and K. W. West. *Phys. Rev. Lett.*, 84:5808, 2000. xi, 16, 17, 37, 39
- [5] M. Kellogg, J. P. Eisenstein L. N. Pfeiffer, and K. W. West. *Phys. Rev. Lett.*, 93:036801, 2004. xi, 16, 18, 43, 53
- [6] M. Kellogg, J. P. Eisenstein, L. N. Pfeiffer, and K. W. West. *Phys. Rev. Lett.*, 90:246801, 2003. xi, 19, 53
- [7] Y.W. Suen, L.W. Engel, M. B. Santos, M. Shayegan, and D. C. Tsui. *Phys. Rev. Lett.*, 68:1379, 1992. xi, 18, 20, 78
- [8] D. R. Luhman, W. Pan, D. C. Tsui, L. N. Pfeiffer, K. W. Baldwin, and K. W. West. *Phys. Rev. Lett.*, 101:266804, 2008. xi, 20, 21, 29, 55, 87
- [9] J. Shabani, T. Gokmen, Y. T. Chiu, and M. Shayegan. *Phys. Rev. Lett.*, 103:256802, 2009. xi, 21, 55, 87
- [10] Z. Papić, N. Regnault, and S. Das Sarma. *Phys. Rev. B*, 80:201303, 2009. xi, 28, 59, 60, 62, 73, 74
- [11] H. Li and F. D. Haldane. *Phys. Rev. Lett.*, 101:010504, 2008. xi, xiii, 28, 29, 77
- [12] Z. Papić, G. Möller, M. V. Milovanović, N. Regnault, and M. O. Goerbig. *Phys. Rev. B*, 79:245325, 2009. xi, 30, 55, 73, 74, 83
- [13] Z. Papić and M. V. Milovanović. *Phys. Rev. B*, 75:195304, 2007. xii, 17, 37, 41, 42, 43, 44, 45, 46, 47
- [14] N. Read and D. Green. *Phys. Rev. B*, 61:10267, 2000. xii, xiii, 56, 57, 61, 63, 64, 71
- [15] B. I. Halperin, P. A. Lee, and N. Read. *Phys. Rev. B.*, 47:7312, 1993. xii, 9, 42, 43, 44, 56, 61
- [16] J. Jain. *Composite fermions*. Cambridge University Press, 2007. xv, 1, 9, 20, 25, 37, 58, 59
- [17] X. G. Wen. *Quantum Field Theory of Many-Body Systems*. Oxford University Press, 2004. xv, 7, 44

REFERENCES

- [18] G. Moore and N. Read. *Nucl. Phys. B.*, 360:362, 1991. xvi, 10, 11, 12, 50, 74
- [19] S. Das Sarma, M. Freedman, and C. Nayak. *Physics Today*, 49:32, 2006. xvi
- [20] Chetan Nayak, Steven H. Simon, Ady Stern, Michael Freedman, and Sankar Das Sarma. *Rev. Mod. Phys.*, 80:1083, 2008. xvi, 12
- [21] Parsa Bonderson, Sankar Das Sarma, Michael Freedman, and Chetan Nayak. *arXiv:1003.2856*, 2010. xvi
- [22] M. Z. Hasan and C. L. Kane. *arXiv:1002.3895*, 2010. xvi
- [23] Xiao-Liang Qi and Shou-Cheng Zhang. *Physics Today*, 63:33, 2010. xvi
- [24] S. M. Girvin and A. H. MacDonald. Multicomponent quantum Hall systems: The sum of their parts and more. In S. Das Sarma and A. Pinczuk, editors, *Perspectives in Quantum Hall Effects*. New York : Wiley, 1997. xvi, 16
- [25] J.P. Eisenstein and A.H. MacDonald. *Nature*, 432:691, 2004. xvi, 37, 41
- [26] K. von Klitzing, G. Dorda, and M. Pepper. *Phys. Rev. Lett.*, 45:660, 1980. 1
- [27] K. von Klitzing. *Rev. Mod. Phys.*, 58:519, 1986. 1
- [28] D. C. Tsui, H. L. Stormer, and A. C. Gossard. *Phys. Rev. Lett.*, 48:1559, 1982. 1
- [29] Richard E. Prange and Steven M. Girvin. *The Quantum Hall Effect (2nd ed.)*. Springer-Verlag, 1990. 1
- [30] Steven Girvin. The Quantum Hall Effect: Novel Excitations and Broken Symmetries. In A. Comtet, T. Jolicœur, S. Ouvry, and F. David, editors, *Topological Aspects of Low Dimensional Systems*. Addison Wesley, 2000. 1
- [31] A. H. MacDonald. *cond-mat/9410047*, 1994. 1
- [32] T. Chakraborty and P. Pietilainen. *The Quantum Hall Effects, Integral and Fractional*. Springer-Verlag, 1995. 1, 25, 30, 31
- [33] S. Das Sarma and A. Pinczuk. *Perspectives in Quantum Hall Effects*. New York: Wiley, 1997. 1
- [34] O. Heinonen. *Composite fermions: a unified view of the quantum Hall regime*. World Scientific Publishing, 1998. 1
- [35] Daijiro Yoshioka. *The Quantum Hall Effect*. Springer, 2002. 1, 25
- [36] M. O. Goerbig. Quantum Hall Effects. In *Lecture notes for the Singapore session "Ultracold Gases and Quantum Information" of Les Houches Summer School*. 2009. 1
- [37] M. Manfra, L. Pfeiffer, K. West, H. Stormer, S. Syed, K. Baldwin, J. Hsu, D. Lang, and R. Molnar. *APS March meeting*, 2001. 2
- [38] K. Lai, W. Pan, D. C. Tsui, S. Lyon, M. Muhlberger, and F. Schaffler. *Phys.Rev .Lett.*, 93:156805, 2004. 2
- [39] K. S. Novoselov, A. K. Geim, S. V. Morozov, and et al. *Nature*, 438:197, 2005. 2, 22
- [40] Yuanbo Zhang, Yan-Wen Tan, H. Horst, L. Stormer, and P. Kim. *Nature*, 438:201, 2005. 2, 22
- [41] E. Balthes, D. Schweitzer, and P.Wyder. *Solid State Commun.*, 136:238, 2005. 2
- [42] L. D. Landau and L. M. Lifshitz. *Quantum Mechanics*. Pergamon, 1991. 3, 4, 8

-
- [43] B. I. Halperin. *Phys. Rev. B*, 25:2185, 1982. 4
- [44] F. F. Fang and W. E. Howard. *Phys. Rev. Lett.*, 16:797, 1966. 4
- [45] F. C. Zhang and S. Das Sarma. *Phys. Rev. B.*, 33:2903, 1986. 5
- [46] R. B. Laughlin. *Phys. Rev. Lett.*, 50:1395, 1983. 6, 74, 97
- [47] R. B. Laughlin. Elementary theory: The incompressible quantum fluid. In R. E. Prange and S. M. Girvin, editors, *The Quantum Hall Effect*. Springer-Verlag, 1987. 6, 48
- [48] R. de Picciotto, M. Reznikov, M. Heiblum, V. Umansky, G. Bunin, and D. Mahalu. *Nature*, 389:162, 1997. 6
- [49] L. Saminadayar, R. V. Glattli, Y. Jin, and B. Etienne. *Phys. Rev. Lett.*, 79:2526, 1997. 6
- [50] B. I. Halperin. *Phys. Rev. Lett.*, 52:1583, 1984. 6
- [51] V. Gurarie and C. Nayak. *Nucl. Phys. B*, 506:685, 1997. 6, 11
- [52] Steven H. Simon. *Phys. Rev. Lett.*, 100:116803, 2008. 6, 11
- [53] N. Read. *Phys. Rev. B*, 79:045308, 2009. 6, 11, 12, 65
- [54] D. P. Arovas, J. R. Schrieffer, and F. Wilczek. *Phys. Rev. Lett.*, 53:722, 1984. 6
- [55] F. D. M. Haldane and E. H. Rezayi. *Phys. Rev. Lett.*, 54:237, 1985. 7, 25
- [56] F. D. M. Haldane. The hierarchy of fractional states and numerical studies. In R. E. Prange and S. M. Girvin, editors, *The Quantum Hall Effect*. New York: Springer, 1990. 7, 25, 26, 27, 30, 57, 65, 93
- [57] N. K. Wilkin and J. M. F. Gunn. *Phys. Rev. Lett.*, 84:6, 2000. 7
- [58] N. R. Cooper, N. K. Wilkin, and J. M. F. Gunn. *Phys. Rev. Lett.*, 87:120405, 2001. 7
- [59] S. M. Girvin, A. H. MacDonald, and P. M. Platzman. *Phys. Rev. B*, 33:2481, 1986. 7, 27, 91
- [60] S. M. Girvin and A. MacDonald. *Phys. Rev. Lett.*, 58:1252, 1987. 7
- [61] X. G. Wen and Q. Niu. *Phys. Rev. B.*, 41:9377, 1990. 7
- [62] S. C. Zhang, H. Hansson, and S. Kivelson. *Phys. Rev. Lett.*, 62:82, 1989. 7, 37, 42, 43
- [63] S. C. Zhang. *Int. J. Mod. Phys. B*, 6:25, 1992. 7, 8, 9, 43, 46, 48, 68
- [64] X.-G. Wen. *Int. J. Mod. Phys. B*, 6:1711, 1992. 8, 71
- [65] N. Nagaosa. *Quantum Field Theory in Condensed Matter Physics*. Springer, 1999. 8, 9, 16, 38, 39, 40
- [66] Th. Jolicoeur. *Phys. Rev. Lett.*, 99:036805, 2007. 9
- [67] R. L. Willett, R. R. Ruel, K. W. West, and L.N. Pfeiffer. *Phys. Rev. Lett.*, 71:3846, 1993. 10
- [68] E. H. Rezayi and N. Read. *Phys. Rev. Lett.*, 72:900, 1994. 10, 76
- [69] A. A. Koulakov, M. M. Fogler, and B. I. Shklovskii. *Phys. Rev. Lett.*, 76:499, 1996. 10, 33
- [70] R. Moessner and J. T. Chalker. *Phys. Rev. B*, 54:5006, 1996. 10, 33
- [71] G. Gervais, L. W. Engel, H. L. Stormer, D. C. Tsui, K. W. Baldwin, K. W. West, and L. N. Pfeiffer. *Phys. Rev. Lett.*, 93:266804, 2004. 10

REFERENCES

- [72] R. Willett, J. P. Eisenstein, H. L. Stormer, D. C. Tsui, A. C. Gossard, and J. H. English. *Phys. Rev. Lett.*, 59:1776, 1987. 10
- [73] J. P. Eisenstein, K. B. Cooper, L. N. Pfeiffer, and K. W. West. *Phys. Rev. Lett.*, 88:076801, 2002. 10
- [74] F. D. M. Haldane and E. H. Rezayi. *Phys. Rev. Lett.*, 60:956, 1988. 10, 19, 83
- [75] R. H. Morf. *Phys. Rev. Lett.*, 80:1505, 1998. 10
- [76] M. Greiter, X. G. Wen, and F. Wilczek. *Phys. Rev. Lett.*, 66:3205, 1991. 10
- [77] N. Read and E. Rezayi. *Phys. Rev. B*, 54:16864, 1996. 11, 57, 65
- [78] C. Nayak and F. Wilczek. *Nucl. Phys. B*, 479:529, 1996. 11
- [79] Yaroslav Tserkovnyak and Steven H. Simon. *Phys. Rev. Lett.*, 90:016802, 2003. 11
- [80] R. L. Willett, L. N. Pfeiffer, and K. W. West. *arXiv:0911.0345*, 2009. 11
- [81] M. Dolev, M. Heiblum, V. Umansky, A. Stern, and D. Mahalu. *Nature*, 452:829, 2008. 11
- [82] I. P. Radu, J. B. Miller, C. M. Marcus, M. A. Kastner, L. N. Pfeiffer, and K. W. West. *Science*, 320:899, 2008. 11
- [83] E. H. Rezayi and F.D. M. Haldane. *Phys. Rev. Lett.*, 84:4685, 2000. 11, 33, 75
- [84] M. Levin, B. I. Halperin, and B. Rosenow. *Phys. Rev. Lett.*, 99:236806, 2007. 11
- [85] S.-S. Lee, S. Ryu, C. Nayak, and M. P. A. Fisher. *Phys. Rev. Lett.*, 99:236807, 2007. 11
- [86] Hao Wang, D. N. Sheng, and F. D. M. Haldane. *Phys. Rev. B*, 80:241311, 2009. 11
- [87] Edward H. Rezayi and Steven H. Simon. *arXiv:0912.0109*, 2009. 11, 64
- [88] P. Di Francesco, P. Mathieu, and D. Senechal. *Conformal Field Theory*. New York, Springer-Verlag, 1997. 12
- [89] A. A. Belavin, A. M. Polyakov, and A. B. Zamolodchikov. *Nucl. Phys. B*, 241 (2):333, 1984. 12
- [90] E. Ardonne. *A conformal field theory description of fractional quantum Hall states*. 2002. 12
- [91] T. H. Hansson, M. Hermanns, N. Regnault, and S. Viefers. *Phys. Rev. Lett.*, 102:166805, 2009. 12
- [92] M. Flohr and K. Osterloh. *Phys. Rev. B*, 67:235316, 2003. 12
- [93] T. H. Hansson, C.-C. Chang, J. K. Jain, and S. Viefers. *Phys. Rev. B*, 76:075347, 2007. 12
- [94] Steven H. Simon, E. H. Rezayi, N. R. Cooper, and I. Berdnikov. *Phys. Rev. B*, 75:075317, 2007. 12, 28, 65, 66, 67
- [95] Steven H. Simon, E. H. Rezayi, and N. Regnault. *arXiv:0908.0947*, 2009. 12
- [96] N. Read and E. Rezayi. *Phys. Rev. B*, 59:8084, 1999. 12, 74
- [97] N. Read. *Phys. Rev. B*, 79:245304, 2009. 12
- [98] B. I. Halperin. *Helv. Phys. Acta*, 56:75, 1983. 13, 96
- [99] R. de Gail, N. Regnault, and M. O. Goerbig. *Phys. Rev. B*, 77:165310, 2008. 13, 90, 96
- [100] H. A. Fertig. *Phys. Rev. B*, 40:1087, 1989. 15, 37, 41

-
- [101] I. Stanić and M. V. Milovanović. *Phys. Rev. B*, 71:035329, 2005. 16
- [102] S. Girvin. *Physics Today*, 53:39, 2000. 16
- [103] K. Moon, H. Mori, Kun Yang, S. M. Girvin, A. H. MacDonald, L. Zheng, D. Yoshioka, and Shou-Cheng Zhang. *Phys. Rev. B*, 51:5138, 1995. 16, 17, 37, 39, 41, 80, 81
- [104] E. Tutuc, M. Shayegan, and D. A. Huse. *Phys. Rev. Lett.*, 93:036802, 2004. 16, 53
- [105] H. A. Fertig and G. Murthy. *Phys. Rev. Lett.*, 95:156802, 2005. 17, 53
- [106] I. Ussishkin and A. Stern. *Phys. Rev. Lett.*, 81:3932, 1998. 17
- [107] M. P. Lilly, J. P. Eisenstein, L. N. Pfeiffer, and K. W. West. *Phys. Rev. Lett.*, 80:1714, 1998. 17
- [108] N. E. Bonesteel, I. A. McDonald, and C. Nayak. *Phys. Rev. Lett.*, 77:3009, 1996. 17, 45
- [109] Steven H. Simon, E. H. Rezayi, and M. V. Milovanović. *Phys. Rev. Lett.*, 91:046803, 2003. 17, 37, 40, 42, 50
- [110] Gunnar Möller, Steven H. Simon, and Edward H. Rezayi. *Phys. Rev. Lett.*, 101:176803, 2008. 17, 45, 47, 50
- [111] Gunnar Möller, Steven H. Simon, and Edward H. Rezayi. *Phys. Rev. B*, 79:125106, 2009. 17, 18, 45, 47, 50, 51
- [112] M. V. Milovanović and Z. Papić. *Phys. Rev. B*, 79:115319, 2009. 17, 37, 48, 49, 50, 53
- [113] J. P. Eisenstein, G. S. Boebinger, L. N. Pfeiffer, K.W.West, and S. He. *Phys. Rev. Lett.*, 68:1383, 1992. 18
- [114] D. Yoshioka, A. H. MacDonald, and S. M. Girvin. *Phys. Rev. B*, 39:1932, 1989. 18, 20, 30, 65
- [115] S. He, S. Das Sarma, and X. C. Xie. *Phys. Rev. B*, 47:4394, 1993. 18, 78
- [116] K. Nomura and D. Yoshioka. *J. Phys. Soc. Jpn.*, 73:2612, 2004. 18, 57, 58
- [117] I. G. MacDonald. *Symmetric Functions and Hall Polynomials*. Clarendon, Oxford, 1979. 18, 20
- [118] F. D. M. Haldane and E. H. Rezayi. *Phys. Rev. Lett.*, 60:1886, 1988. 19
- [119] M. Greiter, X. G. Wen, and F. Wilczek. *Phys. Rev. B*, 46:9586, 1992. 19
- [120] T. Chakraborty and F. C. Zhang. *Phys. Rev. B*, 29:7032, 1984. 20
- [121] W. Kang, J. B. Young, S. T. Hannahs, E. Palm, K. L. Campman, and A. C. Gossard. *Phys. Rev. B*, 56:R12776, 1997. 20
- [122] I. K. Kukushkin, K. v. Klitzing, and K. Eberl. *Phys. Rev. Lett.*, 82:3665, 1999. 20
- [123] N. Regnault, M. O. Goerbig, and Th. Jolicoeur. *Phys. Rev. Lett.*, 101:066803, 2008. 20, 55, 65, 71
- [124] J. Shabani, T. Gokmen, and M. Shayegan. *Phys. Rev. Lett.*, 103:046805, 2009. 21, 55, 83
- [125] Z. Papić, M. O. Goerbig, N. Regnault, and M. V. Milovanović. *arxiv:0912.3103*, 2009. 21, 55, 63, 65, 67, 69, 71
- [126] V.W. Scarola, C. May, M. R. Peterson, and M. Troyer. *arXiv:1004.1636*, 2010. 22, 87

REFERENCES

- [127] A. H. Castro Neto, F. Guinea, N. M. R. Peres, K. S. Novoselov, and A. K. Geim. *Rev. Mod. Phys.*, 81:109, 2009. 22
- [128] Xu Du, Ivan Skachko, Fabian Duerr, Adina Luican, and Eva Y. Andrei. *Nature*, 462:192, 2009. 22, 93
- [129] Kirill I. Bolotin, Fereshte Ghahari, Michael D. Shulman, Horst L. Stormer, and Philip Kim. *Nature*, 462:196, 2009. 22, 93
- [130] M. O. Goerbig and N. Regnault. *Phys. Rev. B*, 75:241405, 2007. 23, 90
- [131] F. D. M. Haldane. *Phys. Rev. Lett.*, 51:605, 1983. 25, 26
- [132] D. Yoshioka, B. I. Halperin, and P. A. Lee. *Phys. Rev. Lett.*, 50:1219, 1983. 25, 30, 60
- [133] F. D. Haldane. *Phys. Rev. Lett.*, 55:2095, 1985. 25, 30, 31, 65, 66
- [134] G. Fano, F. Ortolani, and E. Colombo. *Phys. Rev. B*, 34:2670, 1986. 25, 27
- [135] T. T. Wu and C. N. Yang. *Nucl. Phys. B*, 107:365, 1976. 25
- [136] T. T. Wu and C. N. Yang. *Phys. Rev. D*, 16:1018, 1977. 25
- [137] A. Kitaev and J. Preskill. *Phys. Rev. Lett.*, 96:110404–1, 2006. 28
- [138] M. Levin and X. G. Wen. *Phys. Rev. Lett.*, 96:110405, 2006. 28
- [139] L. Amico, R. Fazio, A. Osterloh, and V. Vedral. *Rev. Mod. Phys.*, 80:517, 2008. 28
- [140] Andreas M. Läuchli, Emil J. Bergholtz, Juha Suorsa, and Masudul Haque. *arXiv:0911.5477*, 2010. 28
- [141] O. S. Zozulya, M. Haque, and N. Regnault. *Phys. Rev. B*, 79:045409, 2009. 28, 77
- [142] F. D. M. Haldane and E. H. Rezayi. *Phys. Rev. B*, 31:2529, 1985. 32
- [143] M. Hermanns, J. Suorsa, E. J. Bergholtz, T. H. Hansson, and A. Karlhede. *Phys. Rev. B*, 77:125321, 2008. 32
- [144] X.-G. Wen and A. Zee. *Phys. Rev. B*, 46:2290, 1992. 33, 65
- [145] I. A. McDonald. *Phys. Rev. B*, 51:10851, 1995. 34
- [146] N. E. Bonesteel. *Phys. Rev. B*, 48:11484, 1993. 40
- [147] G. Murthy and R. Shankar. *Rev. Mod. Phys.*, 75:1101, 2003. 42
- [148] N. Read. *Phys. Rev. Lett.*, 65:1502, 1990. 42
- [149] R. L. Willett. *Adv. Phys.*, 46:447, 1997. 42
- [150] A. Stern and B. I. Halperin. *Phys. Rev. Lett.*, 88:106801, 2002. 43, 53
- [151] Kun Yang. *Phys. Rev. B*, 58:R4246, 1998. 43
- [152] M. V. Milovanović. *Phys. Rev. B*, 75:035314, 2007. 44, 45
- [153] J. Ye and L. Jiang. *Phys. Rev. Lett.*, 98:236802, 2007. 48, 49
- [154] L. Jiang and J. Ye. *Phys. Rev. B*, 74:245311, 2006. 48
- [155] A. Lopez and E. Fradkin. *Phys. Rev. B*, 51:4347, 1995. 48
- [156] T.H. Hansson, V. Oganesyan, and S.L. Sondhi. *Ann. Phys.*, 313:497, 2004. 50

-
- [157] G.S. Jeon and J. Ye. *Phys. Rev. B*, 71:125314, 2005. 50
- [158] E. Demler, C. Nayak, and S. Das Sarma. *Phys. Rev. Lett.*, 86:1853, 2001. 50
- [159] J. Schliemann, S. M. Girvin, and A. H. MacDonald. *Phys. Rev. Lett.*, 86:1849, 2001. 50
- [160] K. Nomura and D. Yoshioka. *Phys. Rev. B*, 66:153310, 2002. 50
- [161] N. Shibata and D. Yoshioka. *J.Phys.Soc.Jpn*, 75:043712, 2006. 50
- [162] P. Giudici, K. Muraki, N. Kumada, Y. Hirayama, and T. Fujisawa. *Phys. Rev. Lett.*, 100:106803, 2008. 51
- [163] P. Giudici, K. Muraki, N. Kumada, and T. Fujisawa. *Phys. Rev. Lett.*, 104:056802, 2010. 51
- [164] A. D. K. Finck, J. P. Eisenstein, L. N. Pfeiffer, and K. W. West. *Phys. Rev. Lett.*, 104:016801, 2010. 51
- [165] R. Morf and N. d’Ambrumenil. *Phys. Rev. Lett.*, 74:5116, 1995. 52, 76
- [166] S. Luin, V. Pellegrini, A. Pinczuk, B.S. Dennis, L.N. Pfeiffer, and K.W. West. *Phys. Rev. Lett.*, 97:216802, 2006. 53
- [167] X.-G. Wen. *Phys. Rev. Lett.*, 84:3950, 2000. 55
- [168] I. A. McDonald and F. D. M. Haldane. *Phys. Rev. B*, 53:15845, 1996. 55
- [169] M. V. Milovanović and Z. Papić. *Phys. Rev. B*, 82:035316, 2010. 55, 70, 71
- [170] A. Cappelli, L. S. Georgiev, and I. T. Todorov. *Nucl. Phys. B*, 599:499, 2001. 55
- [171] H. W. Jiang, H. L. Stormer, D. C. Isui, L. N. Pfeiffer, and K. W. West. *Phys. Rev. B*, 40:12013, 1989. 56
- [172] N. E. Bonesteel. *Phys. Rev. Lett.*, 82:984, 1999. 56
- [173] Michael R. Peterson and S. Das Sarma. *arXiv:1002.4359*, 2010. 57, 58
- [174] Daijiro Yoshioka. *Phys. Rev. B*, 29:6833, 1984. 60
- [175] M. Peterson, Th. Jolicœur, and S. Das Sarma. *Phys. Rev. B*, 78:155308, 2008. 60, 63, 74
- [176] M. Peterson, Th. Jolicœur, and S. Das Sarma. *Phys. Rev. Lett.*, 101:016807, 2008. 60
- [177] M. Storni, R. H. Morf, and S. Das Sarma. *arXiv:0812.2691*, 2009. 63, 76, 77
- [178] Waheb Bishara and Chetan Nayak. *Phys. Rev. B*, 80:121302, 2009. 64
- [179] X.-G. Wen. *Phys. Rev. B*, 40:7387, 1989. 65
- [180] X.-G. Wen and A. Zee. *Phys. Rev. B*, 69:953, 1992. 65
- [181] D. Yoshioka, A. H. MacDonald, and S. M. Girvin. *Phys. Rev. B*, 38:3636, 1988. 65
- [182] C. Tóke and J. K. Jain. *Phys. Rev. B*, 80:205301, 2009. 65, 67
- [183] N. Regnault, B. A. Bernevig, and F. D. M. Haldane. *Phys. Rev. Lett.*, 103:016801, 2009. 65, 66
- [184] Eddy Ardonne. *Phys. Rev. Lett.*, 102:180401, 2009. 66, 67
- [185] E. J. Bergholtz, T. H. Hansson, M. Hermanns, A. Karlhede, and S. Viefers. *Phys. Rev. B*, 77:165325, 2008. 67

REFERENCES

- [186] E. J. Bergholtz. *One-dimensional theory of the quantum Hall system*. 2009. 67
- [187] Z. F. Ezawa and A. Iwazaki. *Phys. Rev. B*, 48:15189, 1993. 68, 69
- [188] M. Grayson, D. C. Tsui, L. N. Pfeiffer, K. W. West, and A. M. Chang. *Phys. Rev. Lett.*, 80:1062, 1998. 71
- [189] D.-H. Lee and X.-G. Wen. *cond-mat/9809160*, 1998. 71
- [190] Ana Lopez and Eduardo Fradkin. *Phys. Rev. B*, 59:15323, 1999. 71
- [191] S. Sachdev. *Quantum Phase Transitions*. Cambridge University Press, 1999. 71
- [192] B. Andrei Bernevig and F. D. M. Haldane. *Phys. Rev. Lett.*, 100:246802, 2008. 74
- [193] G. Möller and S. H. Simon. *Phys. Rev. B*, 77:075319, 2008. 75, 76
- [194] K. Park, V. Melik-Alaverdian, N. E. Bonesteel, and J. K. Jain. *Phys. Rev. B*, 58:R10167, 1998. 76
- [195] V. W. Scarola, J. K. Jain, and E. H. Rezayi. *Phys. Rev. Lett.*, 88:216804, 2002. 76
- [196] R. Morf and N. d’Ambrumenil. *Phys. Rev. B*, 68:113309, 2003. 77
- [197] M. Abolfath, L. Belkhir, and N. Nafari. *Phys. Rev. B*, 55:10643, 1997. 78
- [198] H. Jiang, R. L. Willet, H. L. Stormer, D. C. Tsui, L. N. Pfeiffer, and K. W. West. *Phys. Rev. Lett.*, 65:633, 1990. 86
- [199] T. S. Lay, T. Jungwirth, L. Smrčka, and M. Shayegan. *Phys. Rev. B*, 56:R7092, 1997. 86
- [200] Z. Papić, M. O. Goerbig, and N. Regnault. *Solid State Commun.*, 149:1056, 2009. 89, 96
- [201] M. O. Goerbig. Electronic properties of graphene in a strong magnetic field. In *arXiv:1004.3396*. 2010. 89, 90
- [202] Z. Papić, M. O. Goerbig, and N. Regnault. *arXiv:1005.5121*, 2010. 89
- [203] M. O. Goerbig, R. Moessner, and B. Douçot. *Phys. Rev. B*, 74:161407, 2006. 90, 91, 92, 93, 96, 97
- [204] J. Alicea and M. P. A. Fisher. *Phys. Rev. B*, 74:075422, 2006. 90, 93, 96, 97
- [205] D. A. Abanin, P. A. Lee, and L. S. Levitov. *Phys. Rev. Lett.*, 98:156801, 2007. 90
- [206] R. L. Doretto and C. Morais Smith. *Phys. Rev. B*, 76:195431, 2007. 90
- [207] Y. Zhang, Z. Jiang, J. P. Small, M. S. Purewal, Y.-W. Tan, M. Fazlollahi, J. D. Chudow, J. A. Jaszczak, H. L. Stormer, and P. Kim. *Phys. Rev. Lett.*, 96:136806, 2006. 90, 93
- [208] F. D. M. Haldane. *Phys. Rev. Lett.*, 61:2015, 1988. 90
- [209] J.-N. Fuchs and P. Lederer. *Phys. Rev. Lett.*, 98:016803, 2007. 90
- [210] I. Herbut. *Phys. Rev. B*, 75:165411, 2007. 90
- [211] I. Herbut. *Phys. Rev. B*, 76:085432, 2007. 90
- [212] G. Li, A. Luican, and E. Y. Andrei. *arXiv:0803.4016*, 2008. 90
- [213] K. Nomura and A. H. MacDonald. *Phys. Rev. Lett.*, 96:256602, 2006. 90, 93, 97
- [214] K. Yang, S. Das Sarma, and A. H. MacDonald. *Phys. Rev. B*, 74:075423, 2006. 90, 93, 97

- [215] B. Douçot, M. O. Goerbig, P. Lederer, and R. Moessner. *Phys. Rev. B*, 78:195327, 2008. 90, 92, 93, 97
- [216] C. Töke and J. K. Jain. *Phys. Rev. B*, 75:245440, 2007. 90, 93, 96, 97
- [217] V. M. Apalkov and T. Chakraborty. *Phys. Rev. Lett.*, 97:126801, 2006. 93
- [218] C. Töke, P. E. Lammert, V. H. Crespi, and J. K. Jain. *Phys. Rev. B*, 74:235417, 2006. 93
- [219] T. Chakraborty and F. C. Zhang. *Phys. Rev. B*, 29:7032, 1984. 96, 97
- [220] W. Kang, J. B. Young, S. T. Hannahs, E. Palm, K. L. Campman, and A. C. Gossard. *Phys. Rev. B*, 56:R12776, 1997. 96, 97
- [221] I. K. Kukushkin, K. v. Klitzing, and K. Eberl. *Phys. Rev. Lett.*, 82:3665, 1999. 96, 97